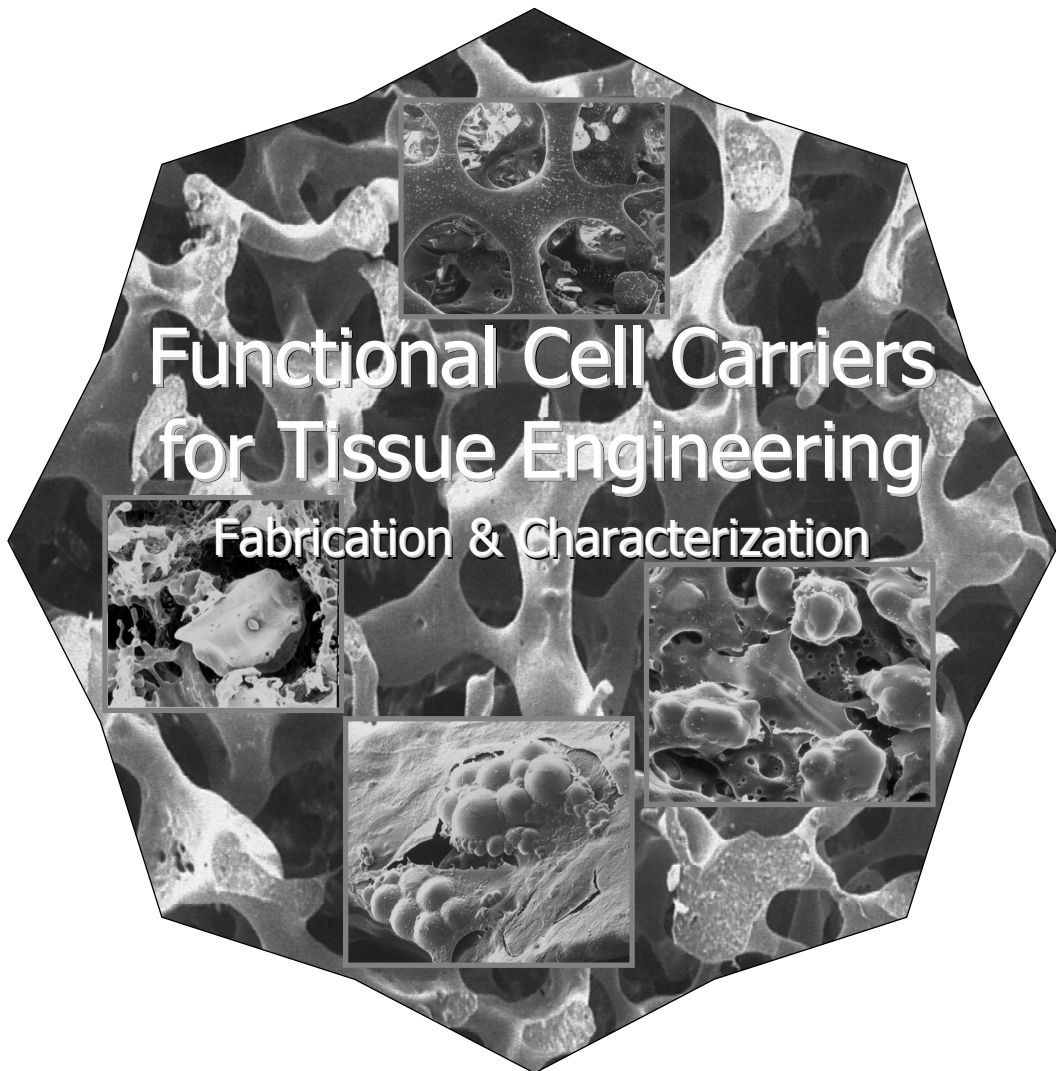


Michael Hacker



Dissertation zur Erlangung des Doktorgrades
der Naturwissenschaften (Dr. rer. nat.)
der Fakultät Chemie und Pharmazie
der Universität Regensburg

Functional Cell Carriers for Tissue Engineering

Fabrication & Characterization

Dissertation zur Erlangung des Doktorgrades der Naturwissenschaften
(Dr. rer. nat.)
der Fakultät Chemie und Pharmazie
der Universität Regensburg



vorgelegt von
Michael Hacker
aus Erlangen
im August 2004

Diese Doktorarbeit entstand in der Zeit von März 2000 bis August 2004 am Lehrstuhl für Pharmazeutische Technologie an der Universität Regensburg.

Die Arbeit wurde von Prof. Dr. Achim Göpferich angeleitet.

Promotionsgesuch eingereicht am: 13. August 2004

Mündliche Prüfung am: 2. September 2004

Prüfungsausschuss:

Prof. Dr. S. Elz	(Vorsitzender)
Prof. Dr. A. Göpferich	(Erstgutachter)
Univ.-Prof. Dr. M.B. Schulz	(Zweitgutachter)
Prof. Dr. A. Kurtz	(Drittprüfer)

Meiner Familie in Liebe und Dankbarkeit gewidmet.

Im Andenken an Ernst Hacker.

Table of Contents

Chapter 1	Introduction and Goals of the Thesis.....	7
Chapter 2	Mediating Specific Cell Adhesion to Low-adhesive Diblock Copolymers by Instant Modification with RGD-peptides	41
Chapter 3	Towards Biomimetic Scaffolds: Anhydrous Scaffold Fabrication from Biodegradable Amine-reactive Diblock Copolymers	59
Chapter 4	Hansen Solubility Parameters as a Means to Replace Halogenated Solvents in Biomaterial Processing	93
Chapter 5	Solubility Parameters of Poly(lactic acid) and its Copolymers - Theoretical and Experimental Considerations.....	117
Chapter 6	Solid Lipid Templating: A Versatile Lab-scale Fabrication Technique for Macroporous Tissue Engineering Scaffolds.....	141
Chapter 7	Synthesis and Characterization of Injectable, Thermogelling Poly(<i>N</i> -isopropylacrylamide)-grafted Gelatin (PNiPAAm-gelatin).....	167
Chapter 8	Summary and Conclusions	191
Appendix	Abbreviations	203
	Hansen Solubility Parameters of common solvents	206
	Solubility Parameter Map.....	209
	Program Listing	210
	Curriculum vitae	217
	List of Publications	218
	Acknowledgements	223

Chapter 1

Introduction
and
Goals of the Thesis

1. Tissue Engineering

At the end of the year 2002, 82,749 patients were registered on the OPTN (Organ Procurement and Transplantation Network) waiting list for organ transplantation (from the OPTN / SRTR Annual report on www.optn.org) with kidney (68%) and liver (22%) being the most required organs followed by lung (5%) and heart (5%). In contrast, a total of only 24,544 organs could be transplanted. Further data provided by the OPTN indicates a death rate of approximately 10% on the waiting list. The active waiting list of Eurotransplant states the need for 12,157 kidneys and 1,841 livers as of July 1, 2004 (from www.eurotransplant.nl). Not only is the need for organs constantly rising, less complex tissues, such as skin, are also required to more efficiently cure the 4.5 million severe burn injuries that are reported each year (from www.medindic.net). Due to the constantly rising life expectancy, the discrepancy between organ donations and patients on the waiting list will become even worse. In the United States, for example, an estimated one person in five reaching 65 years of age will receive temporary or permanent organ-replacement therapy during their remaining life span [1].

These few examples drastically indicate why the replacement of organ functions and living tissue with synthetic substitutes represents one of the most important contributions of 20th century science to clinical medicine [1]. Organ failure and tissue defects resulting from traumatic injury, tumor resection, degenerative diseases, and congenital deformities are the specific problem surgeons have to face with [2-4]. Current strategies to deal with complex tissue defects and organ failure involve surgical reconstruction and organ transplantation. Besides the organ shortage, the risk associated with long-term treatments with immunosuppressive medication is a critical shortcoming in transplantation medicine. Existing methods of tissue replacement therapy rely upon a variety of permanent implants made of metals, ceramics, non-degradable polymers, or composite materials [5-7]. Most of these devices were developed in the 1960s and gradually optimized throughout the following decades. However, such implant devices can only restore tissue form and mechanical function, while their application is limited by finite durability and non-physiological performance as well as a considerable risk of infection or thromboembolism [8]. Surgical tissue reconstruction by the transplantation of autografts, however, is still the ‘gold standard’ in the management of several tissue defects, especially osseous defects. Nevertheless, this

treatment is often constrained by anatomical limitations and associated with donor-site pain and morbidity, extra blood loss and risk of infection [9].

To overcome these limitations, tissue engineering emerged as discovery research in the 1970s [10]. The National Science Foundation (NSF) defined tissue engineering as an interdisciplinary field that applies the principles of engineering and the life sciences to the development of biological substitutes that restore, maintain, or improve tissue function [2]. Work in the field is focused towards replacing tissue defects with living tissue that is ideally generated from autologous cells and designed to meet the specific needs of each individual patient [8]. Generally, two different strategies have been adopted for the *de novo* generation of living tissue from isolated cells. One involves the *in vitro* cultivation of the harvested cells on three-dimensional cell carriers under tailored conditions and biological stimuli. Following this strategy, the cell carrier, which is fabricated from a biomaterial, provides the macroporous architecture on which cells can attach, proliferate and develop into the desired tissue, thus assuming the function of the natural extracellular matrix [11]. The other strategy favors the direct *in vivo* implantation of isolated cells with and without an artificial matrix [2]. Ideally, both strategies lead to a tissue construct that is ultimately indistinguishable from the surrounding or host tissue by histology and radiography. Over the last two decades, promising advances have been made towards the engineering of various types of tissues and organs (Fig. 1) [12].

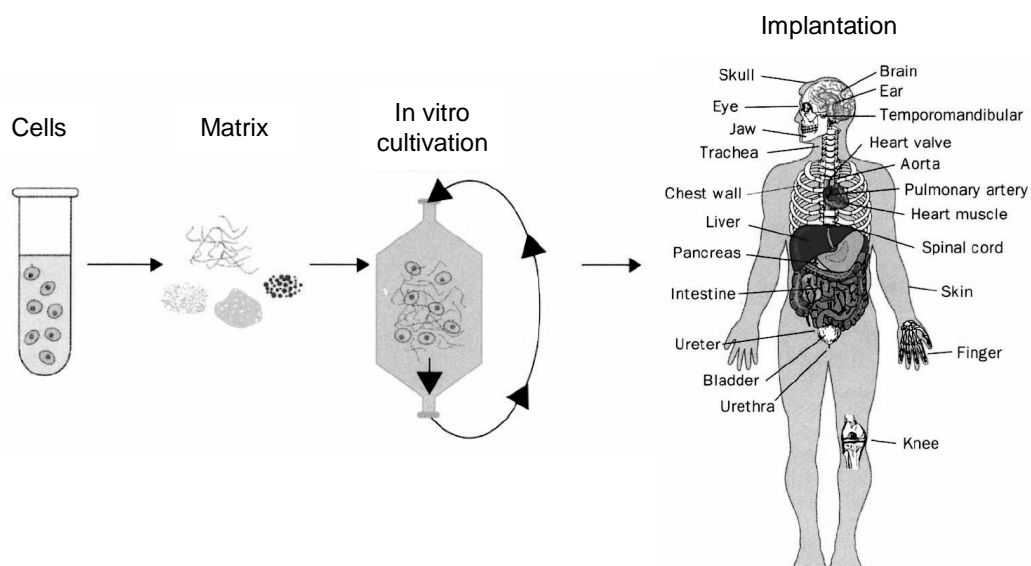


Fig. 1: The Tissue Engineering process (adapted from Vacanti et al. [12]).

By the end of 2002, twenty tissue-engineered products had entered Food and Drug Administration clinical trials, while four were already approved: Apligraf® (Organogenesis; living skin), Carticel® (Genzyme Biosurgery; autologous chondrocytes), Dermagraft® (ATS; living skin), and OrCel® (Ortec; living skin) [13]. Germany's BioTissue Technologies AG has five products in clinical use since the end of 2001 (www.biotissue-tec.com). BioTissue follows the principle of autologous (patient's own) tissue replacement to treat skin (BioSeed®-S), oral mucosa (BioSeed®-M), oral bone (BioSeed®-Oral Bone) and cartilage (BioSeed®-C) defects. The specific cells are taken from the patient as a tissue specimen (biopsy) and then cultured in a GMP-certified laboratory. Once the required quantity of newly cultured cells is reached, combining the cells with a specific, resorbable biomatrix enables the cells to be transplanted into the existing defect.

Generally, the total U.S. health care costs for patients suffering from tissue loss or organ failure exceed \$400 billion per year and approximately 8 million surgical procedures are performed annually to treat these disorders. It has been estimated that the total market for tissue-engineered products is \$80 billion annually in the United States alone [10]. Despite this tremendous economic potential, the field has yet to produce a profitable product [13]. However, the transition from a development state to a successful product has been constrained both by regulatory issues [14-16] and the complexity of tissue biology [17]. Critical issues in creating an entire organ or even a complex functional tissue include enhancing cell survival, maintaining the differentiated function, developing a significant cell mass embedded in its extracellular matrix, and achieving vascularization [10]. Future research has especially to overcome the problems arising from insufficient nutrient supply and the lack of vascularization [18,19]. Furthermore, cell carriers and scaffolding materials have to be designed to mimic natural extracellular matrix design and cell-matrix-interactions, and to support the structural orientation of the developing tissue with regard to the engineering of entire organs [20-23].

2. The cell carrier-based Tissue Engineering concept

The most common approach to tissue regeneration is based on cell-matrix constructs (Fig. 1) [4,24]. This concept is derived from the natural tissue assembly, where cells are embedded in a tissue-specific extracellular matrix that is composed of structural proteins (collagen and elastin), specialized proteins supporting cell matrix-interactions (e.g. fibrillin, fibronectin, and laminin) and hydrophilic proteoglycans (e.g. hyaluronic acid or glycosaminoglycans) [25]. This matrix supports cell proliferation, migration and tissue development [26].

The cell-matrix strategy of tissue engineering generally involves the following components and steps [27-29]: (i) An appropriate cell source, either allogeneic or autologous, must be identified, the cells need to be isolated and produced in sufficient numbers. (ii) A suitable biocompatible material that can be used as a cell substrate (open system) or cell-encapsulation material (closed system) must be isolated or synthesized and manufactured into the desired shape and dimensions, forming an artificial extracellular matrix. (iii) The cells must be uniformly seeded onto or into the material and grown in a bioreactor. (iv) The appropriate biochemical and/or mechanical stimulus must be identified and administered or applied in a controlled manner (amount and time) to improve cell differentiation, extracellular matrix production and tissue formation. (v) Finally, the engineered structure is placed into the *in vivo* site, where, depending on the site and the structure, vascularization may be necessary.

2.1. Cell types and sources

Suitable cells for tissue engineering applications generally include autologous cells from the patient, allogeneic cells from a human donor who is not immunologically identical to the patient, and xenogeneic cells from a different species [17]. The ideal way to obtain cells is to harvest autologous cells directly from the patient, followed by controlled expansion *in vitro* [30]. Although this option is preferred because the cells are acceptable to the recipient's immune system without the need for immunosuppressive therapy, it is limited by the scarcity of available donor tissue and donor site morbidity. Each category, autologous, allogeneic, or xenogeneic, may be further delineated in terms of whether the cells are differentiated (mature cells) or undifferentiated (progenitor or stem cells). In most cases, differentiated cells isolated from adult tissues exhibit a very limited proliferative capacity and tend to lose differentiation within the first passages. Culturing progenitor or stem cells that, by definition, have a higher proliferative capacity is more promising. The differentiation of such cells, however, has to be

obtained *in vitro* by changing the culture conditions after cell expansion or *in vivo* as a consequence of the new microenvironment in the transplant area [31]. The use of stem cells that can be expanded for long periods and finally differentiated into a variety of cell lineages is particularly of interest [31-34]. Despite evidence suggesting that embryonic stem cells might represent a more potent regenerative reservoir than stem cells collected from adult tissues [35,36], ethical considerations have redirected attention to undifferentiated pluripotent cells derived from the bone marrow [37-43], the umbilical cord [44] and cord blood [45,46].

2.2. *Biological stimuli*

The controlled supplementation of biological stimuli, e.g. growth factors, is required to promote cell proliferation, differentiation and tissue maturation in the cell-carrier constructs [28,47].

Various growth factors that induce cell differentiation and tissue maturation have been identified [28]. Cell-matrix constructs that are cultured *in vitro* can be easily supplemented with growth factors, e.g. with every medium exchange. *In vivo*, growth factors are preferably supplemented via drug delivery systems, such as microparticles, implants or even factor-loaded cell carriers to avoid repeated injections. Epidermal growth factor (EGF) was successfully used to improve dermal regeneration [48]. Basic fibroblast growth factor (bFGF) is known to support adipogenesis [49,50] and osteogenesis [51,52], as well as cartilage [53] and nerve regeneration [54,55]. Nerve growth factor (NGF) has also been delivered and demonstrated to improve nerve regeneration. A plethora of studies have been conducted focusing on suitable growth factors for bone [56] and cartilage [57,58] tissue engineering. Transforming growth factor β 1 (TGF- β 1) [59-62] and members of the bone morphogenetic proteins (BMPs) [63-65] proved to be especially potent differentiation factors for orthopedic tissue engineering when applied in the appropriate regimen. BMP-2 turned out as a highly effective factor for bone regeneration, capable of *de novo* bone formation [66,67].

In regard to the engineering of large tissue constructs and organs, angiogenesis and neovascularization, the formation of new blood vessels from existing ones, are key prerequisites to overcome limitations in nutrient and oxygen supply. Acid and basic fibroblast growth factor (aFGF and bFGF), platelet-derived growth factor (PDGF) and vascular endothelial growth factor (VEGF) are the most important factors that have been identified to influence and regulate endothelial cell differentiation and blood vessel formation [19]. Consequently, these proteins have been released from a variety of delivery devices to induce

angiogenesis in engineered tissue constructs [19,68-70]. It was demonstrated that the dual delivery of VEGF-165 and PDGF, each with distinct kinetics, from a single, structural polymer scaffold results in the rapid formation of a mature vascular network [71]. Another study demonstrated that VEGF-121 remained an active and very efficient mitogen for human endothelial cells after immobilization to fibrin. The fibrin-VEGF hydrogels are proposed as a growth matrix for ischemic regions that require an angiogenic response [72]. Recently, a hydrogel system was designed that is capable for the on-demand release of matrix-conjugated VEGF [73].

2.3. Cell carrier (scaffold)

In cell carrier-based tissue engineering attempts, the macroporous three-dimensional cell carriers (scaffolds) play a pivotal role in cell seeding, proliferation, and new tissue formation in three dimensions [74]. Figure 2 summarizes the scaffold characteristics that influence the tissue engineered construct.

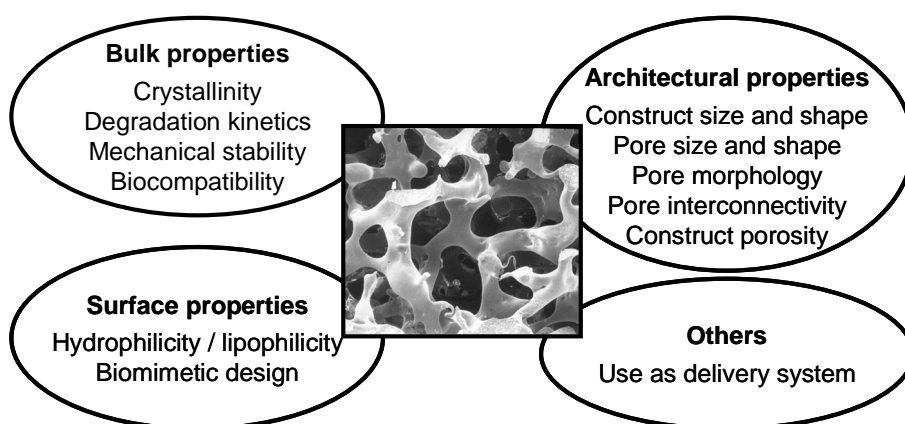


Fig. 2: Critical characteristics of a biodegradable polymer scaffold.

The development of a functional cell carrier that is tailored to the intended application and/or type of engineered tissue involves careful consideration and adaptation of bulk, surface and architectural properties. This is realized by choosing an appropriate scaffold material that mainly determines the bulk and surface characteristics (section 3.1). Control over the architectural properties has to be provided by the scaffold fabrication technique (section 3.2). Ideally, the technique allows for the incorporation of the necessary biological stimuli in a further step.

A functional tissue engineering concept, especially when focused on the engineering of tissues that are naturally vascularized, has to involve an angiogenic strategy.

3. Scaffold materials and fabrication techniques

3.1. *Biomaterials for Tissue Engineering*

A large variety of biomaterials, namely natural and synthetic polymers, ceramics and metals have been employed as scaffold materials [40,75-82]. On the basis of the materials hydrophilicity and mechanical properties, the scaffolding materials can be divided into materials that swell significantly in water forming a hydrogel and materials that only dissolve in organic solvents and are used for the fabrication of macroporous solids. Due to the mechanical properties, hydrogels are the preferred materials for the engineering of soft tissues, nerve fibers and blood vessels [73,83-86]. For the engineering of skeletal tissue, especially bone, the appropriate scaffolds should maintain a rigid structure under physiological conditions.

Hydrogel forming materials

Hydrogels have been increasingly studied as matrices for tissue engineering due to their mechanical similarity to the natural extracellular matrix [75]. Hydrogels are characterized by a high water content and pores that can accommodate living cells. Table 1 gives a survey of the wide and diverse range of hydrogel-forming polymers that are used in biomedical applications. The substances can be categorized into natural polymer hydrogels, synthetic polymer hydrogels and combinations of the two classes. Natural materials, such as collagen, which is a key component of the extracellular matrix, and gelatin, which is denatured collagen, are of special interest as these polymers interact with cells and induce tissue formation [11,87]. While collagen forms gels in physiological environments (pH and temperature), gelatin dissolves in water at body temperature. Therefore, chemical crosslinking with glutaraldehyde, genipin or other crosslinkers is often used to render gelatin insoluble [88-90]. Hydrogel matrices, prepared from crosslinked gelatin, have been comprehensively investigated by Tabata and co-workers in a variety of tissue engineering studies [50,52,61,91]. In these studies, the hydrogel serves not only as cell carrier but also as a growth factor delivery system. Combinations of gelatin with other natural materials, such as alginate or hyaluronic acid, are accepted materials for skin reconstruction [92,93]. Mooney and coworkers have intensively investigated the feasibility of ionically crosslinked alginate hydrogels as cell carriers for tissue engineering experiments [84,94,95].

Table 1: *Hydrophilic polymers used to synthesize hydrogel matrices (adapted from [75])*

Natural polymers and their derivatives (\pm crosslinkers)

Anionic polymers: hyaluronic acid, alginate, pectin, carrageenan, chondroitin sulfate, dextran sulfate

Cationic polymers: chitosan, polylysine

Amphipathic polymers: collagen, gelatin, carboxymethyl chitin, fibrin

Neutral polymers: dextran, agarose, pullulan

Synthetic polymers (\pm crosslinkers)

Polyesters: PEG-PLA-PEG, PEG-PLGA-PEG, PEG-PCL-PEG, PLA-PEG-PLA, PHB, poly(PF-co-EG) \pm acrylate end groups

Other polymers

PEG-bis-(PLA-acrylate), PEG-CDs, PEG-g-poly(AAm-co-vinyl amine), poly(AAm), poly(NiPAAm-co-AAc), poly(NiPAAm-co-EMA), PVAc/PVA, PNVP, poly(MMA-co-HEMA), poly(AN-co-allyl sulfonate), poly(biscarboxy-phenoxy-phosphazene), poly(GEMA-sulfate)

Combinations of natural and synthetic polymers

P(PEG-co-peptides), alginate-g-(PEO-PPO-PEO), P(PLGA-co-serine), collagen-acrylate, alginate-acrylate, poly(HPMA-g-peptide), poly(HEMA/ Matrigel®), hyaluronic acid-g-NiPAAm

Abbreviations: CD, cyclodextrin; EG, ethylene glycol; HEMA, hydroxyethyl methacrylate; AAc, acrylic acid; AAm, acrylamide; AN, acrylonitrile; EMA, ethyl methacrylate; GEMA, glucosylethyl methacrylate; HEMA, hydroxyethyl methacrylate; HPMA, hydroxypropyl methacrylamide; MMA, methyl methacrylate; NiPAAm, N-isopropyl acrylamide; PCL, poly(caprolactone); PEG, poly(ethylene glycol); PEO, poly(ethylene oxide); PF, propylene fumarate; PHB, poly(hydroxy butyrate); PLA, poly(lactic acid); PLGA, poly(lactic-co-glycolic acid); PNVP, poly(N-vinyl pyrrolidone); PPO, poly(propylene oxide); PVA, poly(vinyl alcohol); PVAc, poly(vinyl acetate)

Many different routes have been used to form hydrogels from the polymers listed in Table 1. Gelation is induced either physically or chemically [75]. Physical gels are formed by a change of temperature (e.g. poly(NiPAAm), PEO-PPO-PEO) or pH (e.g. polyAAc, collagen), by mixing polyanions and polycations (e.g. alginate-chitosan), or by crosslinking a polyelectrolyte with multivalent ions (e.g. calcium-alginate). Chemical gels are synthesized by a crosslinking reaction between electron-poor olefins, such as acrylate, vinyl or fumarate groups. In this way a plethora of PEG- or PEO-based hydrogels has been synthesized [96-98]. Recent research has particularly been focused on injectable hydrogel systems, which are liquid at room temperature to enable a comfortable mixing with cells and/or growth factors and form a gel when heated up to body temperature. Promising examples are poly(NiPAAm)-based copolymers exhibiting thermoreversible gelation properties [99-101] and *in situ* polymerizable PEG-based macromers [96,98,102,103]. For instance, injectable PEG-fumarate based hydrogels, like oligo(poly(ethylene glycol)-fumarate) (OPF) and poly(PF-co-EG), have been demonstrated to be biocompatible, biodegradable and suitable biomaterials for the engineering of bone-like tissue [104-109].

Different strategies have been applied to further improve these hydrophilic hydrogels with regard to tissue engineering applications. By covalently attaching adhesion peptides containing the tripeptide Arg-Gly-Asp (RGD), artificial extracellular matrix substitutes have

been developed [22,110-112]. Hubbel and coworkers introduced a fully-synthetic substitute of alginate for cell encapsulation [113] and developed an injectable PEG-based hydrogel for bone regeneration that is proteolytically remodeled by ingrown cells and delivers BMP-2 [114].

The ease with which one may covalently incorporate cell adhesion peptides and the potential to design injectable systems are two significant advantages of using hydrogels as tissue engineering matrices vs. more hydrophobic alternatives. However, a major disadvantage of hydrogels is their low mechanical strength, which poses a significant challenge in their handling. Sterilization issues are also very challenging [75]. A further parameter to consider is the biodegradability of the material. Polyacrylate hydrogels, many polysaccharides, alginates, and polyethers (PEG, PEO, PPO), for example, do not degrade in a physiological environment, but can be excreted if the molecular weight is below the renal threshold barrier [115,116].

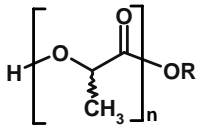
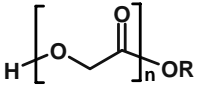
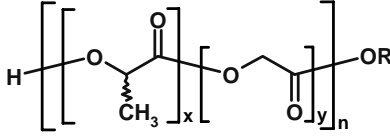
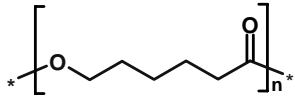
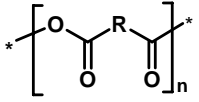
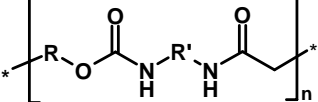
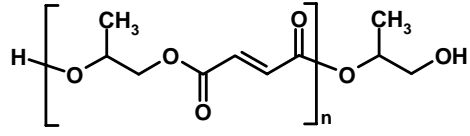
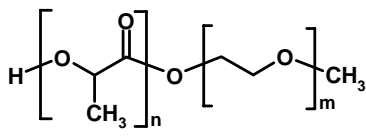
Generally, hydrogels containing cell adhesive components are biodegradable and can be remodeled by encapsulated or invading cells, forming a practical and useful material for biomedical applications that do not require a mechanical stable carrier. We intend to employ a functional hydrogel that delivers angiogenic growth factors and can be injected into rigid scaffolds as an ingrowth matrix for blood vessels.

Materials for the fabrication of rigid scaffolds

Tissue engineering scaffolds have been fabricated from natural and synthetic polymers, ceramics and metals [40,79,117,118]. Biodegradable polymers are the most attractive and widely applied scaffolding materials, often considered superior to ceramics and metals because they degrade as the new tissues are formed [79,119]. In contrast to natural scaffolding materials, such as collagen, chitosan or chitin, these synthetic polymers can be supplied in reproducible quality and free of pathogenic or immunogenic organic residues.

Poly(α -hydroxy acids), namely poly(D,L-lactic acid) (PLA) and copolymers (PLGA) with poly(glycolic acid) (PGA), a polymer that has already been approved by the FDA as a suture material, are probably the most common class of synthetic, biodegradable polymers. Further materials that are under investigation are polyanhydrides [120], polycaprolactones [121] and copolymers with PLA [122], polycarbonates [123], polyurethans [124] and polyfumarates [125]. The polymer structures are summarized in Table 2.

Table 2: Structures of synthetic, biodegradable polymers.

 <p>poly(D,L-lactic acid) (PLA)</p>	 <p>poly(glycolic acid) (PGA)</p>	 <p>poly(lactic-co-glycolic acid) (PLGA)</p>
 <p>Poly(ε-caprolactone) (PCL)</p>	 <p>polyanhydride</p>	 <p>polyurethane</p>
 <p>poly(propylene fumarate) (PPF)</p>	 <p>poly(lactic acid)-<i>block</i>-poly(ethylene glycol) monomethyl ether</p>	

Besides the FDA approval as suture materials, poly(α -hydroxy acids) have other advantages that make them interesting for biomedical applications. By varying the polymer composition, crystallinity and molecular weight, the degradation kinetics and mechanical stability of the polymer can be adapted to the tissue that is to be engineered [79,126-128]. In addition, the polymers are soluble in numerous solvents allowing for lab scale scaffold fabrication.

In tissue engineering approaches with the currently available biodegradable polymers, however, many difficulties arise from the poor control of cell function on the lipophilic polymer surfaces. In a biological environment, proteins non-selectively attach to the polymer surface, which may in turn trigger a number of non-specific cellular responses and lead to uncontrollable tissue development and growth [129]. Strategies to overcome these limitations and to control cell-material-interactions include the covalent grafting of cell type specific adhesion peptides (RGD peptides) to the polymer surfaces [130,131]. The RGD-sequence is the cell attachment site of a large number of adhesive ECM, blood, and cell surface proteins [132,133]. Because cells contain cell adhesion receptors (integrins) that recognize only certain ECM molecules, the use of an appropriate cell-binding sequence leads to cell-selective surfaces [134]. The modification of a lipophilic polymer, however, is often accompanied with laborious chemistry due to the lack of functional groups on the polymer [131]. In addition, surface modification is significantly more efficient when unspecific protein adsorption is suppressed. In this way, recent studies on poly(D,L-lactic acid)-poly(ethylene glycol)-monomethyl ether diblock copolymers (MeO-PEG-PLA) (Table 2) demonstrated the effect of

reduced protein adsorption, caused by the presence of the hydrophilic poly(ethylene glycol) (PEG) [135,136]. The altered surface chemistry also had a significant effect on cell adhesion and cell differentiation compared to unmodified PLA [137]. With the objective of enabling a convenient surface modification with adhesion peptides or growth factors to create a biomimetic surface design, a new class of amine- and thiol-reactive polymers was developed on basis of the PEG-PLA diblock copolymers [138,139]. These reactive copolymers are designed to covalently bind peptides or proteins from aqueous solutions to preformed polymer surfaces during a simple incubation step. As the positive effects of surface-attached adhesion peptides on cell adhesion are thoroughly described [131], the first studies indicate that covalently attached growth factors retained their activity and activated their receptors and downstream signaling proteins [140-142]. Non-diffusional growth factors may allow for localized cell stimulation, surface patterning and a prolonged half-life of the protein. A surface modification concept based on reactive diblock copolymers would allow for an “off the shelf” scaffold or implant coating fabrication, which could be covalently modified with peptides in response to individual needs by incubation with a sterile solution of the required peptide. The general feasibility of this concept has been previously shown in a study on the immobilization of fluorescent dyes or model proteins to preformed films [139]. These polymers are therefore promising scaffold materials for the fabrication of functional or even biomimetic scaffolds.

4. Scaffold fabrication techniques

Several requirements have to be considered in the design of macroporous, polymeric scaffolds for tissue engineering [74,143,144]. First, the scaffold material should be biocompatible and biodegradable. Second, an ideal scaffold is highly porous with an interconnected pore network to accommodate cells, to support cell proliferation and differentiation, and to enhance tissue formation. A high porosity (> 90%) is also important for sufficient oxygen supply and to guarantee unimpaired flow transport of nutrients and metabolic wastes. Third, a suitable surface chemistry is necessary to optimize cell attachment, proliferation, and differentiation. Fourth, the scaffold should have adequate mechanical properties to match those of the tissues at the site of implantation.

A variety of processing technologies have been developed to fabricate polymeric scaffolds. These techniques mainly include textile technologies, solvent casting and particulate leaching, gas foaming, emulsion freeze drying, thermally induced phase separation, electrospinning, and rapid prototyping.

Fiber meshes / fiber bonding

Fibers, produced by textile technology, have been used to fabricate non-woven meshes from PGA and PLLA [24] (Fig. 3a). Fiber meshes represent the ‘gold standard’ in permeability and are still the standard scaffolds for many applications, but lack the necessary structural stability. To improve the mechanical properties of the meshes, the PGA fibers were bound together with solutions of other polymers [145]. In detail, PLLA is dissolved in methylene chloride, which is not a solvent for PLA, and cast over the PGA mesh. After solvent evaporation, the construct is heated above the melting point of PGA. Finally, the PLLA is removed by dissolving in methylene chloride again. This treatment results in a mesh of PGA fibers joined at the cross-points.

Electrospinning

Electrospinning is a fabrication process that uses an electric field to control the formation and deposition of polymer fibers onto a target substrate [146-149]. The electrospinning technique can fabricate fibrous scaffolds from polymer solutions or melts with fiber diameters ranging from several microns down to several hundred nanometers [146] (Fig. 3b).

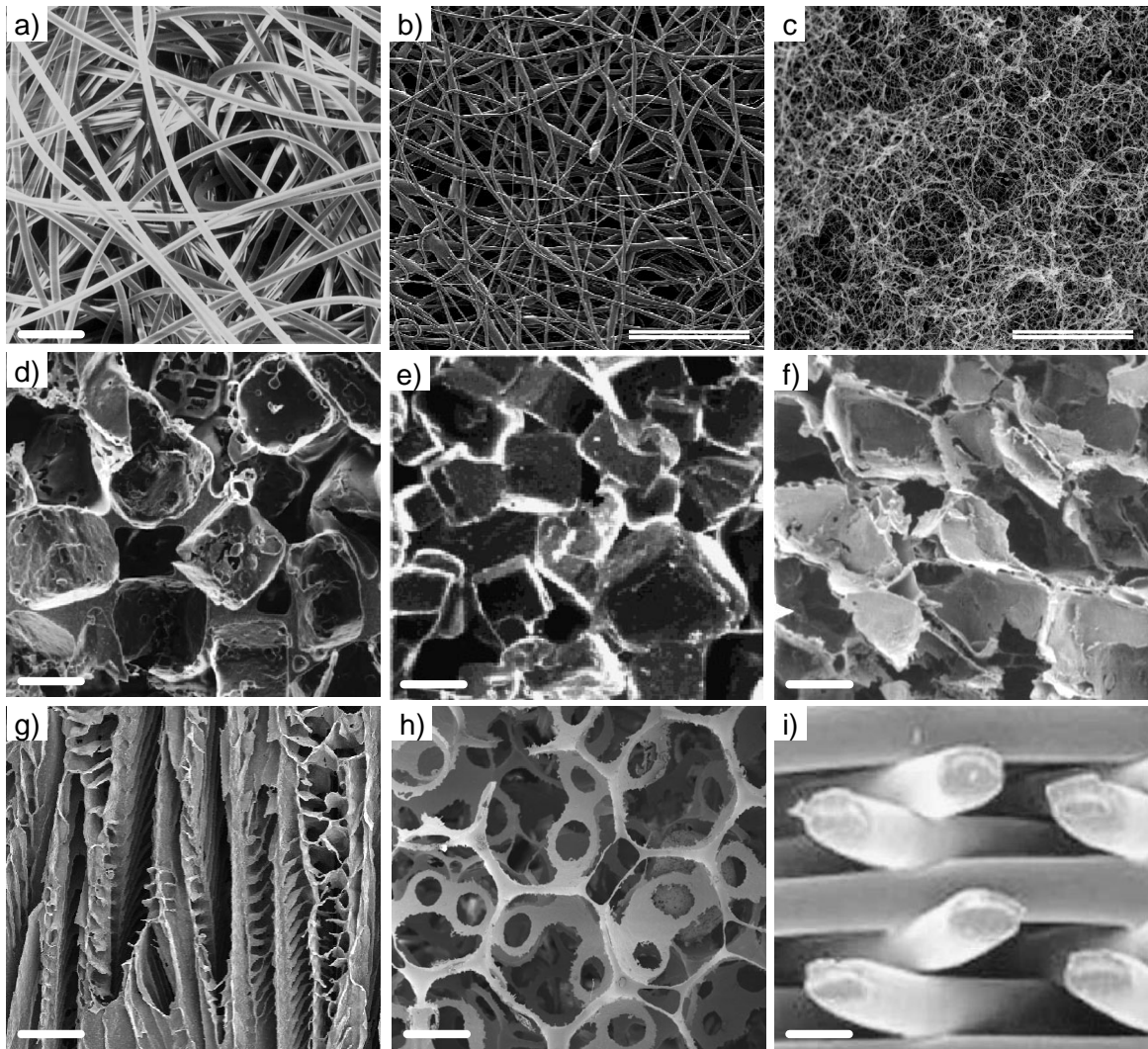


Fig. 3: Scaffold microstructures. Scale bars represent 200 μ m; except in image b and c: 100 μ m. a) Non-woven fiber mesh prepared from crystalline PLLA. b) Electrospun PCL scaffold [148]. c) PLLA fibrous matrix prepared by phase separation [150] d) PLGA scaffold fabricated by salt leaching [151]. e) Scaffold prepared by salt leaching from injectable PPF [152]. f) PLGA scaffold as obtained from gas foaming / salt leaching [153]. g) PLLA scaffold prepared by phase separation [154]. h) PLLA scaffolds prepared with a hydrocarbon porogen [155]. i) PCL scaffold fabricated by fused deposition modeling [156].

Solvent-casting and particulate-leaching

Solvent casting and particulate leaching is a simple and the most commonly used method for the lab-scale fabrication of scaffolds [157]. This method involves mixing water-soluble salt particles into a solution of a biodegradable polymer. After solvent evaporation, the salt particles are leached out with large amounts of water to obtain a porous structure (Fig. 3d,e). The advantages of this method include adequate control of pore size and porosity by the size of the pore-forming salt particles and the salt to polymer ratio, respectively. However, most of the porous materials prepared by solvent casting are characterized by a low pore

interconnectivity that is disadvantageous for uniform cell seeding, tissue growth and fluid flow. Furthermore, the difficulty of removing soluble particles from the interior of a polymer matrix limits the scaffold thickness to 2 mm. Larger constructs were built from thin porous discs by compression molding or lamination techniques.

Strategies to improve the pore interconnectivity of scaffolds prepared by salt leaching involve the use of salt particles in combination with gas foaming agents, e.g. ammonium carbonate [158] or sodium bicarbonate / ascorbic acid [159]. In another attempt, the salt particles were partially fused via treatment in 95% humidity to create a continuous polymer matrix [160]. Despite these improvements, scaffolds prepared by a solvent-casting salt-leaching technique still lack sufficient permeability for homogeneous cell distribution, nutrient and oxygen supply, and tissue development [161].

Recently, water insoluble paraffin microparticles were used as pore forming devices. To generate interconnected scaffolds, the paraffin spheres were bonded together through a heat treatment to form a three-dimensional assembly in a mold. Biodegradable polymers such as PLLA and PLGA were dissolved in a solvent and cast onto the paraffin sphere assembly. After dissolving the paraffin in a non-solvent for the polymer, a porous polymer scaffold was formed (Fig. 3h) [155].

Gas foaming

The gas foaming process can be used to fabricate highly porous polymer foams without the use of organic solvents [162]. In this approach, solid polymer discs are saturated with carbon dioxide (CO₂) at high pressures. The solubility of the gas in the polymer is then rapidly decreased by releasing the excess CO₂ and bringing the pressure back to atmospheric level. This results in thermodynamic instability followed by the nucleation and growth of gas bubbles in the material with sizes ranging between 100 - 500 μm. The disadvantage of this method is that it mostly yields a nonporous surface and closed-pore structure, with only 10 - 30% of interconnected pores. The porosity and pore interconnectivity can be significantly improved by combining the gas-foaming process with the salt leaching technique [163] (Fig. 3f). Nonetheless, completely eliminating closed pores remains challenging.

Melt molding

Melt molding, another process free of organic solvents, involves filling a mold with polymer powder and gelatin microspheres of specific diameter [164]. By heating the mold above the glass transition temperature of the polymer while applying pressure to the mixture, the

polymer particles are bound together. Once the mould is removed, the gelatin component is leached out in water and porous scaffolds are produced in the shape of the mold. Again, this technique is commonly combined with the salt-leaching technique. Like other particulate-leaching techniques, scaffolds fabricated by melt molding often lack sufficient pore interconnectivity and porosity.

Freeze drying

Low-density polymer foams have been produced from several polymers including PLGA and PLGA/PPF using a freeze-drying technique [165,166]. The polymers are first dissolved in a solvent such as glacial acetic acid or benzene. The solution is then frozen and the solvent is removed by lyophilization. The foams have either leaflet or capillary structures depending on the polymer and solvent used in fabrication. These foams are generally not suitable as scaffolds for cell transplantation.

Scaffolds from natural polymers, such as collagen and gelatin, were similarly prepared [82,91,167,168]. Freezing a swollen hydrogel from crosslinked gelatin or collagen results in the formation of ice crystals that cause the collagen molecules to aggregate in the interstitial spaces. The ice crystals are then removed by freeze-drying. The pore size can be controlled by the freezing rate and pH [169-171]. With regard to the mechanical stability, it was shown that the incorporation of PGA fiber is a promising way to reinforce collagen sponge without impairing biocompatibility [172].

Phase separation / emulsification

Instead of the incorporation of a porogen, additional techniques proposed for the fabrication of porous polymer scaffolds are based on the concepts of phase separation. They include emulsion freeze-drying and thermally induced phase separation.

Emulsion freeze-drying

Emulsion freeze-drying creates porous scaffolds by adding water to an organic polymer solution [173]. The two immiscible layers are then homogenized to form a water-in-oil emulsion, which is then quenched in liquid nitrogen and freeze-dried to produce the porous structure. Scaffolds with porosity greater than 90% and low pore sizes (typically below 50 μm) can be fabricated with this method. Again, the major disadvantage of this technique is the closed pore structure in the resulting matrix [174].

Thermally Induced Phase Separation

The controlled thermally induced phase separation (TIPS) process, developed for the preparation of porous membranes, was recently utilized to fabricate biodegradable polymer scaffolds from PLLA and PLGA [122,174-180]. In this approach, the polymer is first dissolved in a solvent with a low melting point and that is easy to sublime, such as naphthalene, phenol, 1,4-dioxane or tetrahydrofuran. In some cases, small amounts of water are added as a non-solvent to induce phase separation [174,178,181]. Liquid-liquid or solid-liquid phase separation is induced by lowering the solution temperature below the melting point of the solvent (polymer poor phase). Subsequent removal of the solidified solvent-poor phase by sublimation leaves a porous polymer scaffold. The pore morphology of the scaffolds varies depending on the polymer, solvent, concentration of the polymer solution and phase separation temperature [174] (Fig. 3c,g). Scaffolds fabricated by TIPS often have good mechanical properties and interconnected pore structures but control of architectural properties and the generation of non-oriented pore structures are difficult.

Rapid-Prototyping Techniques

Rapid prototyping is a technology that has developed from advances in computer science and manufacturing industry [182]. The main advantage of these techniques is their ability to produce complex products for the individual patient from a computer-aided design (CAD) model. The reader is referred to literature reviews on the advantages and benefits, and limitations and shortcomings of current RP techniques [182,183]. Common techniques use established lipophilic polymers for scaffold fabrication. Recently, a technique was developed that allows for the fabrication of hydrogel scaffolds [184,185]. However, all rapid prototyping techniques require a complex instrumental setup and resulting scaffolds often suffer from insufficient resolution and high fiber thickness.

In conclusion, each of the described techniques exhibits several limitations. Fiber meshes lack mechanical stability and salt leached scaffolds are short of interconnected pores and exposed to aqueous media over several days, which constrains the processing of water soluble proteins and polymers containing water-sensitive functions. Phase separation or freeze drying techniques are often anhydrous and generate interconnected pores, but the control of pore size and shape is considerably limited. Several techniques, such as rapid prototyping or fiber fabrication, are limited to polymers that offer distinct physicochemical properties and are not suitable for the processing of small batches of new, functional polymers.

5. Goals of the Thesis

A functional cell carrier design concept involves a biodegradable material that allows for a tailored interaction with cells in terms of adhesion and differentiation. Furthermore, a suitable scaffold fabrication technique is required to process lab-scale amounts of the polymer into macroporous, biocompatible and biodegradable cell carriers with controlled architectural properties. Last but not least, a concept to induce neovascularization of the tissue engineered construct has to be established.

The work presented in this thesis aims at the fabrication of cell carriers following the functional design concept described above. The intention was to model the microstructure of the cell carriers on the load-bearing structure of spongy bone that is shown in Figure 4. The spongy structure is characterized by a high permeability and a pore diameter of approximately 400 μm .

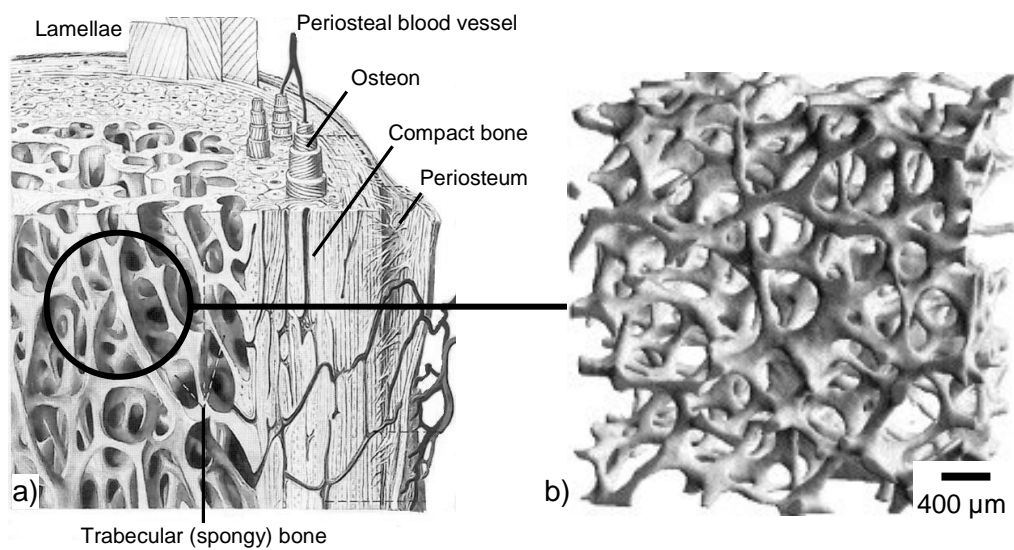


Fig. 4: Structure of bone. a) Compact and trabecular (spongy) bone (from Sobotta/Welsch, textbook of histology) b) Structure of trabecular bone as determined by micro-computed tomographic imaging (adapted from [186]).

We started this work by investigating the ability of a recently developed class of reactive and low adhesive diblock copolymers [138,139] to bind RGD peptides. To this end, reactive polymer films were incubated with a RGD peptide solution in order to create a cell adhesive polymer film surface (**Chapter 2**). These polymers hold great potential for the fabrication of biomimetic surfaces and represent a promising material for the fabrication of functional cell carriers.

Chapter 3 aims at the processing of amine-reactive diblock copolymers into macroporous cell carriers with a spongy microstructure. To this end, a technique was developed (solid lipid templating) on the basis of an anhydrous processing concept [187] that employs triglycerides as biocompatible porogen materials and a non-halogenated solvent mixture to process the block copolymers into appropriate cell carriers. The technique combines the advantages of a particulate leaching technique, namely control of pore size, pore shape, and scaffold porosity, with a phase separation concept to obtain a highly interconnected pore structure. Insulin was used as a model protein that was bound to the surface of a prefabricated surface to demonstrate the preservation of polymer reactivity during processing.

Typical solvents for the processing of biodegradable polymers are chloroform and methylene chloride. In the development stages of the solid lipid templating technique, an azeotropic mixture from acetone and chloroform was employed and suitable processing parameters that result in the desired scaffold microstructure were established. In order to replace the halogenated solvent mixture with a less toxic (according to the ICH guideline on residual solvents [188]) solvent or solvent mixture without the need for the laborious adaptation of processing parameters, we followed a thermodynamic approach. The Hansen solubility parameters (HSPs) of the established solvent mixture were determined and a thermodynamically similar solvent or solvent mixture was systematically searched by solubility parameter comparison (**Chapter 4**).

Based on the promising results of the solvent replacement study, which indicated the usefulness of the HSPs as predictive parameters in polymer processing, we aimed at the determination of the HSPs of poly(lactic acid), poly(lactic-*co*-glycolic acid) and monomethyl ether-poly(ethylene glycol)-*block*-poly(lactic acid) using theoretical and experimental methods (**Chapter 5**).

Since the architectural properties of a scaffold influence fluid flow and tissue development within the scaffold, the processing parameters to vary these architectural parameters are determined in a further study (**Chapter 6**). To this end, rheological measurements are conducted to assess the required adaptation of polymer concentration to varied porogen particle properties. In addition, several polymers characterized by different molecular weights and compositions are processed using the solid lipid templating technique to demonstrate the versatility of this lab-scale process.

Finally, an injectable hydrogel matrix was developed from gelatin and PNiPAAm (**Chapter 7**). The conjugate contains gelatin, which is denatured collagen, a key component of the natural ECM, to attract blood vessel ingrowth. Due to the gelatin backbone, the hydrogel can

be proteolytically remodeled by ingrown cells, because the peptide is a substrate for matrix metalloproteinases. Since gelatin dissolves in aqueous media under physiological conditions, PNiPAAm chains are grafted to the peptide to trigger gelation at body temperature. Rheological measurements are performed to demonstrate and characterize the thermogelling of the conjugate. Cell culture experiments are performed to assess cell viability in the gels. This hydrogel is the first step towards an ingrowth matrix to support neovascularization of tissue engineered constructs. To this end, angiogenic growth factors will be incorporated in the hydrogel in future studies.

6. References

- (1) Lysaght MJ, Nguy NA, Sullivan K. 'An economic survey of the emerging tissue engineering industry'. *Tissue Eng* (1998); **4**: 231-238.
- (2) Langer R, Vacanti JP. 'Tissue engineering'. *Science* (1993); **260**: 920-926.
- (3) Bruder SP, Fox BS. 'Tissue engineering of bone. Cell based strategies'. *Clin Orthop* (1999); S68-S83.
- (4) Freed LE, Vunjak-Novakovic G. 'Culture of organized cell communities'. *Adv Drug Delivery Rev* (1998); **33**: 15-30.
- (5) Spector M. 'Historical review of porous-coated implants'. *J Arthroplasty* (1987); **2**: 163-177.
- (6) Pilliar RM. 'Porous-surfaced metallic implants for orthopedic applications'. *J Biomed Mater Res* (1987); **21**: 1-33.
- (7) Simon JP, Fabry G. 'An overview of implant materials'. *Acta Orthop Belg* (1991); **57**: 1-5.
- (8) Fuchs JR, Nasser BA, Vacanti JP. 'Tissue engineering: a 21st century solution to surgical reconstruction'. *Ann Thorac Surg* (2001); **72**: 577-591.
- (9) Kenley RA, Yim K, Abrams J, Ron E, Turek T, Marden LJ, Hollinger JO. 'Biotechnology and bone graft substitutes'. *Pharm Res* (1993); **10**: 1393-1401.
- (10) Langer R. 'Tissue Engineering'. *Mol Ther* (2000); **1**: 12-15.
- (11) Kleinman HK, Philp D, Hoffman MP. 'Role of the extracellular matrix in morphogenesis'. *Curr Opin Biotechnol* (2003); **14**: 526-532.
- (12) Vacanti JP, Langer R. 'Tissue engineering: the design and fabrication of living replacement devices for surgical reconstruction and transplantation'. *Lancet* (1999); **354**: SI32-SI34.
- (13) Lysaght MJ, Hazlehurst AL. 'Tissue engineering: the end of the beginning'. *Tissue Eng* (2004); **10**: 309-320.
- (14) Indech B. 'The international harmonization of human tissue regulation: Regulatory control over human tissue use and tissue banking in select countries and the current state of international harmonization efforts'. *Food Drug Law J* (2000); **55**: 343-372.
- (15) Ward SM. 'Global harmonization of regulatory requirements for premarket approval of autologous cell therapies'. *Food Drug Law J* (2000); **55**: 225-243.
- (16) Lloyd-Evans M. 'Regulating tissue engineering'. *Mater Today* (2004); **7**: 48-55.
- (17) Griffith LG, Naughton G. 'Tissue engineering - Current challenges and expanding opportunities'. *Science* (2002); **295**: 1009-1014.

- (18) Nomi M, Atala A, Coppi PD, Soker S. 'Principals of neovascularization for tissue engineering'. *Mol Aspects Med* (2002); **23**: 463-483.
- (19) Bouhadir KH, Mooney DJ. 'Promoting angiogenesis in engineered tissues'. *J Drug Targeting* (2001); **9**: 397-406.
- (20) Hubbell JA. 'Biomaterials in tissue engineering'. *Biotechnology (N Y)* (1995); **13**: 565-576.
- (21) de Groot K, Wen HB, Liu Y, Layrolle P, Barrere F. 'Biomimetic coatings on orthopedic implants: a review'. *Mat Res Soc Proc* (2000); **599**: 109-116.
- (22) Shin H, Jo S, Mikos AG. 'Biomimetic materials for tissue engineering'. *Biomaterials* (2003); **24**: 4353-4364.
- (23) Drotleff S, Lungwitz U, Breunig M, Dennis A, Blunk T, Tessmar J, Gopferich A. 'Biomimetic polymers in pharmaceutical and biomedical sciences'. *Eur J Pharm Biopharm* (2004); **58**: 385-407.
- (24) Cima LG, Vacanti JP, Vacanti C, Ingber D, Mooney D, Langer R. 'Tissue engineering by cell transplantation using degradable polymer substrates'. *J Biomed Eng* (1991); **113**: 143-151.
- (25) Bosman FT, Stamenkovic I. 'Functional structure and composition of the extracellular matrix'. *J Pathol* (2003); **200**: 423-428.
- (26) Lukashev ME, Werb Z. 'ECM signalling: orchestrating cell behaviour and misbehaviour'. *Trends Cell Biol* (1998); **8**: 437-441.
- (27) Langer R, Folkman J. 'Polymers for the sustained release of proteins and other macromolecules'. *Nature* (1976); **263**: 797-800.
- (28) Tabata Y. 'The importance of drug delivery systems in tissue engineering'. *Pharm Sci Technol Today* (2000); **3**: 80-89.
- (29) Tabata Y. 'Tissue regeneration based on growth factor release'. *Tissue Eng* (2003); **9**: S5-15.
- (30) Heath CA. 'Cells for tissue engineering'. *Trends Biotechnol* (2000); **18**: 17-19.
- (31) Cancedda R, Dozin B, Giannoni P, Quarto R. 'Tissue engineering and cell therapy of cartilage and bone'. *Matrix Biol* (2003); **22**: 81-91.
- (32) Pittenger MF, Mackay AM, Beck SC, Jaiswal RK, Douglas R, Mosca JD, Moorman MA, Simonetti DW, Craig S, Marshak et al. 'Multilineage potential of adult human mesenchymal stem cells'. *Science* (1999); **284**: 143-147.
- (33) Vats A, Tolley NS, Polak JM, Buttery LD. 'Stem cells: sources and applications'. *Clin Otolaryngol* (2002); **27**: 227-232.

- (34) Cancedda R, Bianchi G, Derubeis A, Quarto R. 'Cell therapy for bone disease: a review of current status'. *Stem Cells (Miamisburg, OH, United States)* (2003); **21**: 610-619.
- (35) Szilvassy SJ. 'The biology of hematopoietic stem cells'. *Arch Med Res* (2003); **34**: 446-460.
- (36) Henningson J, Stanislaus MA, Gewirtz AM. '28. Embryonic and adult stem cell therapy'. *J Allergy Clin Immunol* (2003); **111**: 745-753.
- (37) Ishaug SL, Crane GM, Miller MJ, Yasko AW, Yaszemski MJ, Mikos AG. 'Bone formation by three-dimensional stromal osteoblast culture in biodegradable polymer scaffolds'. *J Biomed Mater Res* (1997); **36**: 17-28.
- (38) Jensen GS, Drapeau C. 'The use of in situ bone marrow stem cells for the treatment of various degenerative diseases'. *Med Hypotheses* (2002); **59**: 422-428.
- (39) Mauney JR, Blumberg J, Pirun M, Volloch V, Vunjak-Novakovic G, Kaplan DL. 'Osteogenic Differentiation of Human Bone Marrow Stromal Cells on Partially Demineralized Bone Scaffolds in Vitro'. *Tissue Eng* (2004); **10**: 81-92.
- (40) van den Dolder J, Farber E, Spauwen PHM, Jansen JA. 'Bone tissue reconstruction using titanium fiber mesh combined with rat bone marrow stromal cells'. *Biomaterials* (2003); **24**: 1745-1750.
- (41) Kruyt MC, Van Gaalen SM, Oner FC, Verbout AJ, De Bruijn JD, Dhert WJA. 'Bone tissue engineering and spinal fusion: The potential of hybrid constructs by combining osteoprogenitor cells and scaffolds'. *Biomaterials* (2004); **25**: 1463-1473.
- (42) Derubeis AR, Cancedda R. 'Bone marrow stromal cells (BMSCs) in bone engineering: limitations and recent advances'. *Ann Biomed Eng* (2004); **32**: 160-165.
- (43) Buma P, Ramrattan NN, van Tienen TG, Veth RPH. 'Tissue engineering of the meniscus'. *Biomaterials* (2004); **25**: 1523-1532.
- (44) Kadner A, Hoerstrup SP, Tracy J, Breymann C, Maurus Ch, Melnitchouk S, Kadner G, Zund G, Turina M. 'Human umbilical cord cells: a new cell source for cardiovascular tissue engineering'. *Ann Thorac Surg* (2002); **74**: 1422-1428.
- (45) Perry TE, Roth SJ. 'Cardiovascular tissue engineering: constructing living tissue cardiac valves and blood vessels using bone marrow, umbilical cord blood, and peripheral blood cells'. *J Cardiovasc Nurs* (2003); **18**: 30-37.
- (46) Barker JN, Wagner JE. 'Umbilical-cord blood transplantation for the treatment of cancer'. *Nat Rev Cancer* (2003); **3**: 526-532.
- (47) Babensee JE, McIntire LV, Mikos AG. 'Growth factor delivery for tissue engineering'. *Pharm Res* (2000); **17**: 497-504.
- (48) Hong SR, Lee SJ, Shim JW, Choi YS, Lee YM, Song KW, Park MH, Nam YS, Lee SI. 'Study on gelatin-containing artificial skin IV: a comparative study on the effect of

- antibiotic and EGF on cell proliferation during epidermal healing'. *Biomaterials* (2001); **22**: 2777-2783.
- (49) Kimura Y, Ozeki M, Inamoto T, Tabata Y. 'Adipose tissue engineering based on human preadipocytes combined with gelatin microspheres containing basic fibroblast growth factor'. *Biomaterials* (2003); **24**: 2513-2521.
- (50) Tabata Y, Miyao M, Inamoto T, Ishii T, Hirano Y, Yamaoki Y, Ikada Y. 'De novo formation of adipose tissue by controlled release of basic fibroblast growth factor'. *Tissue Eng* (2000); **6**: 279-289.
- (51) Yamada K, Tabata Y, Yamamoto K, Miyamoto S, Nagata I, Kikuchi H, Ikada Y. 'Potential efficacy of basic fibroblast growth factor incorporated in biodegradable hydrogels for skull bone regeneration'. *J Neurosurg* (1997); **86**: 871-875.
- (52) Tabata Y, Yamada K, Hong L, Miyamoto S, Hashimoto N, Ikada Y. 'Skull bone regeneration in primates in response to basic fibroblast growth factor'. *J Neurosurg* (1999); **91**: 851-856.
- (53) Fujisato T, Sajiki T, Liu Q, Ikada Y. 'Effect of basic fibroblast growth factor on cartilage regeneration in chondrocyte-seeded collagen sponge scaffold'. *Biomaterials* (1996); **17**: 155-162.
- (54) Aebischer P, Salessiotis AN, Winn SR. 'Basic fibroblast growth factor released from synthetic guidance channels facilitates peripheral nerve regeneration across long nerve gaps'. *J Neurosci Res* (1989); **23**: 282-289.
- (55) Sakiyama ES, Hubbell JA. 'Development of fibrin derivatives for controlled release of heparin-binding growth factors'. *J Control Release* (2000); **65**: 389-402.
- (56) Schliephake H. 'Bone growth factors in maxillofacial skeletal reconstruction'. *International Journal of Oral and Maxillofacial Surgery* (2002); **31**: 469-484.
- (57) Blunk T, Sieminski AL, Gooch KJ, Courter DL, Hollander AP, Nahir AM, Langer R, Vunjak-Novakovic G, Freed LE. 'Differential effects of growth factors on tissue-engineered cartilage'. *Tissue Eng* (2002); **8**: 73-84.
- (58) Holland TA, Mikos AG. 'Advances in drug delivery for articular cartilage'. *J Control Release* (2003); **86**: 1-14.
- (59) Holland TA, Tessmar JKV, Tabata Y, Mikos AG. 'Transforming growth factor- β 1 release from oligo(poly(ethylene glycol) fumarate) hydrogels in conditions that model the cartilage wound healing environment'. *J Control Release* (2004); **94**: 101-114.
- (60) Vehof JWM, Fisher JP, Dean D, Van der Waerden J-P, Spauwen PHM, Mikos AG, Jansen JA. 'Bone formation in transforming growth factor β 1-coated porous poly(propylene fumarate) scaffolds'. *J Biomed Mater Res* (2002); **60**: 241-251.
- (61) Yamamoto M, Tabata Y, Hong L, Miyamoto S, Hashimoto N, Ikada Y. 'Bone regeneration by transforming growth factor β 1 released from a biodegradable hydrogel'. *J Control Release* (2000); **64**: 133-142.

- (62) Fuchs JR, Hannouche D, Terada S, Vacanti JP, Fauza DO. 'Fetal tracheal augmentation with cartilage engineered from bone marrow-derived mesenchymal progenitor cells'. *J Pediatr Surg* (2003); **38**: 984-987.
- (63) Hughes FJ, Collyer J, Stanfield M, Goodman SA. 'The effects of bone morphogenetic protein-2, -4, and -6 on differentiation of rat osteoblast cells in vitro'. *Endocrinology* (1995); **136**: 2671-2677.
- (64) Valcourt U, Ronziere MC, Winkler P, Rosen V, Herbage D, Mallein GF. 'Different effects of bone morphogenetic proteins 2, 4, 12, and 13 on the expression of cartilage and bone markers in the MC615 chondrocyte cell line'. *Exp Cell Res* (1999); **251**: 264-274.
- (65) Nakashima M, Reddi AH. 'The application of bone morphogenetic proteins to dental tissue engineering'. *Nat Biotechnol* (2003); **21**: 1025-1032.
- (66) Geiger M, Li RH, Friess W. 'Collagen sponges for bone regeneration with rhBMP-2'. *Adv Drug Delivery Rev* (2003); **55**: 1613-1629.
- (67) Whang K, Tsai DC, Nam EK, Aitken M, Sprague SM, Patel PK, Healy KE. 'Ectopic bone formation via rhBMP-2 delivery from porous bioabsorbable polymer scaffolds'. *J Biomed Mater Res* (1998); **42**: 491-499.
- (68) Soker S, Machado M, Atala A. 'Systems for therapeutic angiogenesis in tissue engineering'. *World J Urol* (2000); **18**: 10-18.
- (69) Elcin YM, Dixit V, Gitnick G. 'Extensive in vivo angiogenesis following controlled release of human vascular endothelial cell growth factor: implications for tissue engineering and wound healing'. *Artif Organs* (2001); **25**: 558-565.
- (70) Lokmic Z, Thompson EW, Morrison WA, Mitchell GM. 'Angiogenesis in Tissue Engineering'. *Cardiovasc Pathol* (2004); **13**: 181-181.
- (71) Richardson TP, Peters MC, Ennett AB, Mooney DJ. 'Polymeric system for dual growth factor delivery'. *Nat Biotechnol* (2001); **19**: 1029-1034.
- (72) Zisch AH, Schenk U, Schense JC, Sakiyama-Elbert SE, Hubbell JA. 'Covalently conjugated VEGF-fibrin matrices for endothelialization'. *J Control Release* (2001); **72**: 101-113.
- (73) Zisch AH, Lutolf MP, Ehrbar M, Raeber GP, Rizzi SC, Davies N, Schmokel H, Bezuidenhout D, Djonov V, Zilla et al. 'Cell-demanded release of VEGF from synthetic, biointeractive cell ingrowth matrices for vascularized tissue growth'. *FASEB J* (2003); **17**: 2260-2262.
- (74) Liu X, Ma PX. 'Polymeric scaffolds for bone tissue engineering'. *Ann Biomed Eng* (2004); **32**: 477-486.
- (75) Hoffman AS. 'Hydrogels for biomedical applications'. *Adv Drug Delivery Rev* (2002); **54**: 3-12.

- (76) Karp JM, Dalton PD, Shoichet MS. 'Scaffolds for tissue engineering'. *MRS Bull* (2003); **28**: 301-306.
- (77) Piskin E. 'Biodegradable polymers as biomaterials'. *J Biomater Sci , Polym Ed* (1995); **6**: 775-795.
- (78) Seal BL, Otero TC, Panitch A. 'Polymeric biomaterials for tissue and organ regeneration'. *Mat Sci Eng R* (2001); **34**: 147-230.
- (79) Agrawal CM, Ray RB. 'Biodegradable polymeric scaffolds for musculoskeletal tissue engineering'. *J Biomed Mater Res* (2001); **55**: 141-150.
- (80) Li SH, de Groot K, Layrolle P. 'Bioceramic scaffold with controlled porous structure for bone tissue engineering'. *Key Eng Mater* (2002); **218-220**: 25-30.
- (81) Li JP, Li SH, de Groot K, Layrolle P. 'Preparation and characterization of porous titanium'. *Key Eng Mater* (2002); **218-220**: 51-54.
- (82) Tabata Y. 'Scaffolds for tissue regeneration'. *Bone (Osaka, Japan)* (2003); **17**: 29-34.
- (83) Francis Suh J-K, Matthew HWT. 'Application of chitosan-based polysaccharide biomaterials in cartilage tissue engineering: a review'. *Biomaterials* (2000); **21**: 2589-2598.
- (84) Drury JL, Mooney DJ. 'Hydrogels for tissue engineering: scaffold design variables and applications'. *Biomaterials* (2003); **24**: 4337-4351.
- (85) Schmedlen R, Mann B, West J. 'Photopolymerized hydrogels as scaffolds for tissue engineered vascular grafts'. *Ann Biomed Eng* (2000); **28 Supplement 1**: S-118.
- (86) Gingras M, Paradis I, Berthod F. 'Nerve regeneration in a collagen-chitosan tissue-engineered skin transplanted on nude mice'. *Biomaterials* (2003); **24**: 1653-1661.
- (87) Yamamoto M, Yamato M, Aoyagi M, Yamamoto K. 'Identification of Integrins Involved in Cell Adhesion to Native and Denatured Type I Collagens and the Phenotypic Transition of Rabbit Arterial Smooth Muscle Cells'. *Exp Cell Res* (1995); **219**: 249-256.
- (88) Sung HW, Huang DM, Chang WH, Huang RN, Hsu JC. 'Evaluation of gelatin hydrogel crosslinked with various crosslinking agents as bioadhesives: in vitro study'. *J Biomed Mater Res* (1999); **46**: 520-530.
- (89) Matsuda S, Iwata H, Se N, Ikada Y. 'Bioadhesion of gelatin films crosslinked with glutaraldehyde'. *J Biomed Mater Res* (1999); **45**: 20-27.
- (90) Butler MF, Ng YF, Pudney PDA. 'Mechanism and kinetics of the crosslinking reaction between biopolymers containing primary amine groups and genipin'. *Journal of Polymer Science, Part A: Polymer Chemistry* (2003); **41**: 3941-3953.
- (91) Kang HW, Tabata Y, Ikada Y. 'Fabrication of porous gelatin scaffolds for tissue engineering'. *Biomaterials* (1999); **20**: 1339-1344.

- (92) Choi YS, Hong SR, Lee YM, Song KW, Park MH, Nam YS. 'Study on gelatin-containing artificial skin: I. Preparation and characteristics of novel gelatin-alginate sponge'. *Biomaterials* (1999); **20**: 409-417.
- (93) Choi YS, Hong SR, Lee YM, Song KW, Park MH, Nam YS. 'Studies on gelatin-containing artificial skin: II. Preparation and characterization of cross-linked gelatin-hyaluronate sponge'. *J Biomed Mater Res* (1999); **48**: 631-639.
- (94) Eiselt P, Yeh J, Latvala RK, Shea LD, Mooney DJ. 'Porous carriers for biomedical applications based on alginate hydrogels'. *Biomaterials* (2000); **21**: 1921-1927.
- (95) Alsberg E, Anderson KW, Albeiruti A, Rowley JA, Mooney DJ. 'Engineering growing tissues'. *Proc Natl Acad Sci U S A* (2002); **99**: 12025-12030.
- (96) Nguyen KT, West JL. 'Photopolymerizable hydrogels for tissue engineering applications'. *Biomaterials* (2002); **23**: 4307-4314.
- (97) Hubbell JA. 'Hydrogel systems for barriers and local drug delivery in the control of wound healing'. *J Control Release* (1996); **39**: 305-313.
- (98) Temenoff JS, Mikos AG. 'Injectable biodegradable materials for orthopedic tissue engineering'. *Biomaterials* (2000); **21**: 2405-2412.
- (99) Ohya S, Nakayama Y, Matsuda T. 'Thermoresponsive artificial extracellular matrix for tissue engineering: Hyaluronic acid bioconjugated with poly(N-isopropylacrylamide) grafts'. *Biomacromolecules* (2001); **2**: 856-863.
- (100) Ibusuki S, Fujii Y, Iwamoto Y, Matsuda T. 'Tissue-engineered cartilage using an injectable and in situ gelable thermoresponsive gelatin: fabrication and in vitro performance'. *Tissue Eng* (2003); **9**: 371-384.
- (101) Cho JH, Kim SH, Park KD, Jung MC, Yang WI, Han SW, Noh JY, Lee JWJ. 'Chondrogenic differentiation of human mesenchymal stem cells using a thermosensitive poly(N-isopropylacrylamide) and water-soluble chitosan copolymer'. *Biomaterials* (2004); **25**: 5743-5751.
- (102) Cruise GM, Hegre OD, Lamberti FV, Hager SR, Hill R, Scharp DS, Hubbell JA. 'In vitro and in vivo performance of porcine islets encapsulated in interfacially photopolymerized poly(ethylene glycol) diacrylate membranes'. *Cell Transplant* (1999); **8**: 293-306.
- (103) Burdick JA, Anseth KS. 'Photoencapsulation of osteoblasts in injectable RGD-modified PEG hydrogels for bone tissue engineering'. *Biomaterials* (2002); **23**: 4315-4323.
- (104) Suggs LJ, Shive MS, Garcia CA, Anderson JM, Mikos AG. 'In vitro cytotoxicity and in vivo biocompatibility of poly(propylene fumarate-co-ethylene glycol) hydrogels'. *J Biomed Mater Res* (1999); **46**: 22-32.
- (105) Shin H, Quinten Ruhe P, Mikos AG, Jansen JA. 'In vivo bone and soft tissue response to injectable, biodegradable oligo(poly(ethylene glycol) fumarate) hydrogels'. *Biomaterials* (2003); **24**: 3201-3211.

- (106) Shin H, Temenoff JS, Mikos AG. 'In vitro cytotoxicity of unsaturated oligo[poly(ethylene glycol) fumarate] macromers and their cross-linked hydrogels'. *Biomacromolecules* (2003); **4**: 552-560.
- (107) Fisher JP, Lalani Z, Bossano CM, Brey EM, Demian N, Johnston CM, Dean D, Jansen JA, Wong MEK, Mikos et a. 'Effect of biomaterial properties on bone healing in a rabbit tooth extraction socket model'. *J Biomed Mater Res* (2004); **68A**: 428-438.
- (108) Temenoff JS, Shin H, Conway DE, Engel PS, Mikos AG. 'In vitro cytotoxicity of redox radical initiators for cross-linking of oligo(poly(ethylene glycol) fumarate) macromers'. *Biomacromolecules* (2003); **4**: 1605-1613.
- (109) Temenoff JS, Park H, Jabbari E, Conway DE, Sheffield TL, Ambrose CG, Mikos AG. 'Thermally cross-linked oligo(poly(ethylene glycol) fumarate) hydrogels support osteogenic differentiation of encapsulated marrow stromal cells in vitro'. *Biomacromolecules* (2004); **5**: 5-10.
- (110) Stile RA, Burghardt WR, Healy KE. 'Synthesis and characterization of injectable poly(N-isopropylacrylamide)-based hydrogels that support tissue formation in vitro'. *Macromolecules* (1999); **32**: 7370-7379.
- (111) Hern DL, Hubbell JA. 'Incorporation of adhesion peptides into nonadhesive hydrogels useful for tissue resurfacing'. *J Biomed Mater Res* (1998); **39**: 266-276.
- (112) Shin H, Jo S, Mikos AG. 'Modulation of marrow stromal osteoblast adhesion on biomimetic oligo[poly(ethylene glycol) fumarate] hydrogels modified with Arg-Gly-Asp peptides and a poly(ethyleneglycol) spacer'. *J Biomed Mater Res* (2002); **61**: 169-179.
- (113) Cellesi F, Tirelli N, Hubbell JA. 'Towards a fully-synthetic substitute of alginate: development of a new process using thermal gelation and chemical cross-linking'. *Biomaterials* (2004); **25**: 5115-5124.
- (114) Lutolf MP, Weber FE, Schmoekel HG, Schense JC, Kohler T, Muller R, Hubbell JA. 'Repair of bone defects using synthetic mimetics of collagenous extracellular matrices'. *Nat Biotechnol* (2003); **21**: 513-518.
- (115) Domurado D, Fournie P, Braud C, Vert M, Guerin P, Simonnet F. 'In vivo fates of degradable poly(-malic acid) and of its precursor, malic acid'. *J Bioact Compat Polym* (2003); **18**: 23-32.
- (116) Hoste K, Schacht E, Seymour L. 'New derivatives of polyglutamic acid as drug carrier systems'. *J Control Release* (2000); **64**: 53-61.
- (117) Madihally SV, Matthew HWT. 'Porous chitosan scaffolds for tissue engineering'. *Biomaterials* (1999); **20**: 1133-1142.
- (118) Pilliar RM, Filiaggi MJ, Wells JD, Grynepas MD, Kandel RA. 'Porous calcium polyphosphate scaffolds for bone substitute applications -- in vitro characterization'. *Biomaterials* (2001); **22**: 963-972.

- (119) Freed LE, Vunjak NG, Biron RJ, Eagles DB, Lesnoy DC, Barlow SK, Langer R. 'Biodegradable polymer scaffolds for tissue engineering'. *Biotechnology (N Y)* (1994); **12**: 689-693.
- (120) Langer R. 'Biomaterials in drug delivery and tissue engineering: One laboratory's experience'. *Acc Chem Res* (2000); **33**: 94-101.
- (121) Kweon H, Yoo MK, Park IK, Kim TH, Lee HC, Lee HS, Oh JS, Akaike T, Cho CS. 'A novel degradable polycaprolactone networks for tissue engineering'. *Biomaterials* (2003); **24**: 801-808.
- (122) Crane GM, Ishaug SL, Mikos AG. 'Bone tissue engineering'. *Nat Med* (1995); **1**: 1322-1324.
- (123) Choueka J, Charvet JL, Koval KJ, Alexander H, James KS, Hooper KA, Kohn J. 'Canine bone response to tyrosine-derived polycarbonates and poly(L-lactic acid)'. *J Biomed Mater Res* (1996); **31**: 35-41.
- (124) Grad S, Kupcsik L, Gorna K, Gogolewski S, Alini M. 'The use of biodegradable polyurethane scaffolds for cartilage tissue engineering: potential and limitations'. *Biomaterials* (2003); **24**: 5163-5171.
- (125) Peter SJ, Miller MJ, Yasko AW, Yaszemski MJ, Mikos AG. 'Polymer concepts in tissue engineering'. *J Biomed Mater Res* (1998); **43**: 422-427.
- (126) Gopferich A. 'Mechanisms of polymer degradation and erosion'. *Biomaterials* (1996); **17**: 103-114.
- (127) Gopferich A. 'Erosion of composite polymer matrices'. *Biomaterials* (1997); **18**: 397-403.
- (128) Wu L, Ding J. 'In vitro degradation of three-dimensional porous poly(,-lactide-co-glycolide) scaffolds for tissue engineering'. *Biomaterials* (2004); **25**: 5821-5830.
- (129) Lu L, Kam L, Hasenbein M, Nyalakonda K, Bizios R, Gopferich A, Young JF, Mikos AG. 'Retinal pigment epithelial cell function on substrates with chemically micropatterned surfaces'. *Biomaterials* (1999); **20**: 2351-2361.
- (130) Cima LG. 'Polymer substrates for controlled biological interactions'. *J Cell Biochem* (1994); **56**: 155-161.
- (131) Hersel U, Dahmen C, Kessler H. 'RGD modified polymers: biomaterials for stimulated cell adhesion and beyond'. *Biomaterials* (2003); **24**: 4385-4415.
- (132) Pierschbacher MD, Ruoslahti E. 'Cell attachment activity of fibronectin can be duplicated by small synthetic fragments of the molecule'. *Nature* (1984); **309**: 30-33.
- (133) Ruoslahti E. 'RGD and other recognition sequences for integrins'. *Annual Review of Cell and Developmental Biology* (1996); **12**: 697-715.
- (134) Giancotti FG, Ruoslahti E. 'Integrin signaling'. *Science* (1999); **285**: 1028-1032.

- (135) Gopferich A, Peter SJ, Lucke A, Lu L, Mikos AG. 'Modulation of marrow stromal cell function using poly(D,L-lactic acid)-block-poly(ethylene glycol)-monomethyl ether surfaces'. *J Biomed Mater Res* (1999); **46**: 390-398.
- (136) Lucke A, Tessmar J, Schnell E, Schmeer G, Gopferich A. 'Biodegradable poly(,-lactic acid)-poly(ethylene glycol)-monomethyl ether diblock copolymers: structures and surface properties relevant to their use as biomaterials'. *Biomaterials* (2000); **21**: 2361-2370.
- (137) Lieb E, Tessmar J, Hacker M, Fischbach C, Rose D, Blunk T, Mikos AG, Gopferich A, Schulz MB. 'Poly(D,L-lactic acid)-Poly(ethylene glycol)-Monomethyl Ether Diblock Copolymers Control Adhesion and Osteoblastic Differentiation of Marrow Stromal Cells'. *Tissue Eng* (2003); **9**: 71-84.
- (138) Tessmar JK, Mikos AG, Gopferich A. 'Amine-Reactive Biodegradable Diblock Copolymers'. *Biomacromolecules* (2002); **3**: 194-200.
- (139) Tessmar J, Mikos A, Gopferich A. 'The use of poly(ethylene glycol)-block-poly(lactic acid) derived copolymers for the rapid creation of biomimetic surfaces'. *Biomaterials* (2003); **24**: 4475-4486.
- (140) Ito Y, Zheng J, Imanishi Y, Yonezawa K, Kasuga M. 'Protein-free cell culture on an artificial substrate with covalently immobilized insulin'. *Proc Natl Acad Sci U S A* (1996); **93**: 3598-3601.
- (141) Ito Y. 'Tissue engineering by immobilized growth factors'. *Mat Sci Eng C* (1998); **6**: 267-274.
- (142) Kuhl PR, Griffith-Cima LG. 'Tethered epidermal growth factor as a paradigm for growth factor-induced stimulation from the solid phase'. *Nat Med* (1996); **2**: 1022-1027.
- (143) Hutmacher DW. 'Scaffold design and fabrication technologies for engineering tissues - State of the art and future perspectives'. *J Biomater Sci , Polym Ed* (2001); **12**: 107-124.
- (144) Hutmacher DW. 'Scaffolds in tissue engineering bone and cartilage'. *Biomaterials* (2000); **21**: 2529-2543.
- (145) Mikos AG, Bao Y, Cima LG, Ingber DE, Vacanti JP, Langer R. 'Preparation of poly(glycolic acid) bonded fiber structures for cell attachment and transplantation'. *J Biomed Mater Res* (1993); **27**: 183-189.
- (146) Li WJ, Laurencin CT, Cateson EJ, Tuan RS, Ko FK. 'Electrospun nanofibrous structure: A novel scaffold for tissue engineering'. *J Biomed Mater Res* (2002); **60**: 613-621.
- (147) Boland ED, Simpson DG, Wnek GE, Bowlin GL. 'Electrospinning of biopolymers (natural and synthetic) for tissue engineering scaffolds'. *Polym Prepr (Am Chem Soc Div Polym Chem)* (2003); **44**: 92-93.

- (148) Yoshimoto H, Shin YM, Terai H, Vacanti JP. 'A biodegradable nanofiber scaffold by electrospinning and its potential for bone tissue engineering'. *Biomaterials* (2003); **24**: 2077-2082.
- (149) Kidoaki S, Kwon IKI, Matsuda T. 'Mesoscopic spatial designs of nano- and microfiber meshes for tissue-engineering matrix and scaffold based on newly devised multilayering and mixing electrospinning techniques'. *Biomaterials* (2005); **26**: 37-46.
- (150) Ma PX, Zhang R. 'Synthetic nano-scale fibrous extracellular matrix'. *J Biomed Mater Res* (1999); **46**: 60-72.
- (151) Kim H, Kim HW, Suh H. 'Sustained release of ascorbate-2-phosphate and dexamethasone from porous PLGA scaffolds for bone tissue engineering using mesenchymal stem cells'. *Biomaterials* (2003); **24**: 4671-4679.
- (152) Fisher JP, Holland TA, Dean D, Mikos AG. 'Photoinitiated cross-linking of the biodegradable polyester poly(propylene fumarate). Part II. In vitro degradation'. *Biomacromolecules* (2003); **4**: 1335-1342.
- (153) Sheridan MH, Shea LD, Peters MC, Mooney DJ. 'Bioabsorbable polymer scaffolds for tissue engineering capable of sustained growth factor delivery'. *J Control Release* (2000); **64**: 91-102.
- (154) Ma PX, Zhang R. 'Microtubular architecture of biodegradable polymer scaffolds'. *J Biomed Mater Res* (2001); **56**: 469-477.
- (155) Ma PX, Choi JW. 'Biodegradable polymer scaffolds with well-defined interconnected spherical pore network'. *Tissue Eng* (2001); **7**: 23-33.
- (156) Huang Q, Goh JCH, Huttmacher DW, Lee EH. 'In vivo mesenchymal cell recruitment by a scaffold loaded with transforming growth factor beta1 and the potential for in situ chondrogenesis'. *Tissue Eng* (2002); **8**: 469-482.
- (157) Mikos AG, Thorsen AJ, Czerwonka LA, Bao Y, Langer R, Winslow DN, Vacanti JP. 'Preparation and characterization of poly(-lactic acid) foams'. *Polymer* (1994); **35**: 1068-1077.
- (158) Nam YS, Yoon JJ, Park TG. 'A novel fabrication method of macroporous biodegradable polymer scaffolds using gas foaming salt as a porogen additive'. *J Biomed Mater Res* (2000); **53**: 1-7.
- (159) Behravesch E, Jo S, Zygourakis K, Mikos AG. 'Synthesis of in situ cross-linkable macroporous biodegradable poly(propylene fumarate-co-ethylene glycol) hydrogels'. *Biomacromolecules* (2002); **3**: 374-381.
- (160) Murphy WL, Dennis RG, Kileny JL, Mooney DJ. 'Salt Fusion: An Approach to Improve Pore Interconnectivity within Tissue Engineering Scaffolds'. *Tissue Eng* (2002); **8**: 43-52.
- (161) Holy CE, Fialkov JA, Davies JE, Shoichet MS. 'Use of a biomimetic strategy to engineer bone'. *J Biomed Mater Res* (2003); **65A**: 447-453.

- (162) Mooney DJ, Baldwin DF, Suh NP, Vacanti JP, Langer R. 'Novel approach to fabricate porous sponges of poly(-lactic-co-glycolic acid) without the use of organic solvents'. *Biomaterials* (1996); **17**: 1417-1422.
- (163) Harris LD, Kim BS, Mooney DJ. 'Open pore biodegradable matrices formed with gas foaming'. *J Biomed Mater Res* (1998); **42**: 396-402.
- (164) Thomson RC, Yaszemski MJ, Powers JM, Mikos AG. 'Fabrication of biodegradable polymer scaffolds to engineer trabecular bone'. *J Biomater Sci, Polym Ed* (1995); **7**: 23-38.
- (165) Hsu YY, Gresser JD, Trantolo DJ, Lyons CM, Gangadharam PRJ, Wise DL. 'Low-density poly(-lactide-co-glycolide) foams for prolonged release of isoniazid'. *J Control Release* (1996); **40**: 293-302.
- (166) Hsu YY, Gresser JD, Trantolo DJ, Lyons CM, Gangadharam PR, Wise DL. 'Effect of polymer foam morphology and density on kinetics of in vitro controlled release of isoniazid from compressed foam matrices'. *J Biomed Mater Res* (1997); **35**: 107-116.
- (167) Hanthamrongwit M, Grant MH, Wilkinson R. 'Confocal laser scanning microscopy (CLSM) for the study of collagen sponge microstructure'. *J Biomed Mater Res* (1994); **28**: 213-216.
- (168) Shapiro L, Cohen S. 'Novel alginate sponges for cell culture and transplantation'. *Biomaterials* (1997); **18**: 583-590.
- (169) Dagalakis N, Flink J, Stasikelis P, Burke JF, Yannas IV. 'Design of an artificial skin. Part III. Control of pore structure'. *J Biomed Mater Res* (1980); **14**: 511-528.
- (170) Doillon CJ, Whyne CF, Brandwein S, Silver FH. 'Collagen-based wound dressings: control of the pore structure and morphology'. *J Biomed Mater Res* (1986); **20**: 1219-1228.
- (171) Schoof H, Apel J, Heschel I, Rau G. 'Control of pore structure and size in freeze-dried collagen sponges'. *J Biomed Mater Res* (2001); **58**: 352-357.
- (172) Hiraoka Y, Kimura Y, Ueda H, Tabata Y. 'Fabrication and Biocompatibility of Collagen Sponge Reinforced with Poly(glycolic acid) Fiber'. *Tissue Eng* (2003); **9**: 1101-1112.
- (173) Whang K, Thomas CH, Healy KE, Nuber G. 'A novel method to fabricate bioabsorbable scaffolds'. *Polymer* (1995); **36**: 837-842.
- (174) Nam YS, Park TG. 'Porous biodegradable polymeric scaffolds prepared by thermally induced phase separation'. *J Biomed Mater Res* (1999); **47**: 8-17.
- (175) Lo H, Ponticello MS, Leong KW. 'Fabrication of controlled release Biodegradable foams by phase separation'. *Tissue Eng* (1995); **1**: 15-28.
- (176) Lo H, Kadiyala S, Guggino SE, Leong KW. 'Poly(L-lactic acid) foams with cell seeding and controlled-release capacity'. *J Biomed Mater Res* (1996); **30**: 475-484.

- (177) Schugens C, Maquet V, Grandfils C, Jerome R, Teyssie P. 'Biodegradable and macroporous polylactid implants for cell transplantation 1.Preparation of macroporous polylactide supports by solid-liquid phase separtion'. *Polymer* (1996); **37**: 1027-1038.
- (178) Schugens C, Maquet V, Grandfils C, Jerome R, Teyssie P. 'Polylactide macroporous biodegradable implants for cell transplantation. II. Preparation of polylactide foams by liquid-liquid phase separation'. *J Biomed Mater Res* (1996); **30**: 449-461.
- (179) Nam YS, Park TG. 'Biodegradable polymeric microcellular foams by modified thermally induced phase separation method'. *Biomaterials* (1999); **20**: 1783-1790.
- (180) Lee D, Hua FJ, Kim GE. 'Preparation of macroporous biodegradable poly(L-lactic acid) scaffolds via thermally induced phase separation'. *Polym Mater Sci Eng* (2001); **85**: 399-400.
- (181) Ma PX, Zhang R. 'Synthetic nano-scale fibrous extracellular matrix'. *J Biomed Mater Res* (1999); **46**: 60-72.
- (182) Yang S, Leong KF, Du Z, Chua CK. 'The Design of Scaffolds for Use in Tissue Engineering. Part II. Rapid Prototyping Techniques'. *Tissue Eng* (2002); **8**: 1-11.
- (183) Sachlos E, Czernuszka JT. 'Making tissue engineering scaffolds work. Review on the application of solid freeform fabrication technology to the production of tissue engineering scaffolds'. *Eur Cell Mater* (2003); **5**: 29-40.
- (184) Landers R, Pfister A, Hubner U, John H, Schmelzeisen R, Mulhaupt R. 'Fabrication of soft tissue engineering scaffolds by means of rapid prototyping techniques'. *J Mater Sci* (2002); **37**: 3107-3116.
- (185) Landers R, Hubner U, Schmelzeisen R, Mulhaupt R. 'Rapid prototyping of scaffolds derived from thermoreversible hydrogels and tailored for applications in tissue engineering'. *Biomaterials* (2002); **23**: 4437-4447.
- (186) Nazarian A, Muller R. 'Time-lapsed microstructural imaging of bone failure behavior'. *J Biomech* (2004); **37**: 55-65.
- (187) Shastri VP, Martin I, Langer R. 'Macroporous polymer foams by hydrocarbon templating'. *Proc Natl Acad Sci U S A* (2000); **97**: 1970-1975.
- (188) International Conference on Harmonisation of technical requirements for registration of pharmaceuticals for human use. *ICH harmonized Tripartite Guideline (Q3C) Impurities: Residual solvents*. Draft 4 (1997). Available from <http://www.ich.org>

Chapter 2

Mediating Specific Cell Adhesion to Low-adhesive Diblock Copolymers by Instant Modification with RGD-peptides

M. Hacker^{1*}, E. Lieb^{1*}, J. Tessmar², J. Fiedler³, L.A. Kunz-Schughart⁴, C. Dahmen⁵,
U. Hersel⁵, H. Kessler⁵, M.B. Schulz^{1,6}, A. Göpferich¹

¹ Department of Pharmaceutical Technology, University of Regensburg,
Universitaetsstrasse 31, 93040 Regensburg, Germany

² Department of Bioengineering, Rice University, 6100 Main, Houston,
Texas 77005-1892, USA

³ Department of Orthopedics, Division for Biochemistry of Joint and Connective Tissue
Diseases, University of Ulm, Oberer Eselsberg 45, 89081 Ulm, Germany

⁴ Institute of Pathology, University of Regensburg, Franz-Josef-Strauss-Allee 11,
93053 Regensburg, Germany

⁵ Department of Organic Chemistry / Biochemistry, Technical University Munich,
Lichtenbergstrasse 4, 85747 Garching, Germany

⁶ Department of Pharmaceutical Technology, University of Graz, Schubertstrasse 6,
8010 Graz, Austria

* These authors contributed equally to the paper

Abstract

One promising strategy to control the interactions between biomaterial surfaces and attaching cells involves the covalent grafting of adhesion peptides to polymers on which protein adsorption, which mediates unspecific cell adhesion, is essentially suppressed. This study demonstrates a surface modification concept for the covalent anchoring of RGD peptides to reactive diblock copolymers based on monoamine poly(ethylene glycol)-block-poly(D,L-lactic acid) (H₂N-PEG-PLA). Films of both the amine-reactive (ST-NH-PEG₂PLA₂₀) and the thiol-reactive derivative (MP-NH-PEG₂PLA₄₀) were modified with cyclic α v β 3/ α v β 5 integrin subtype specific RGD peptides simply by incubation of the films with buffered solutions of the peptides. Human osteoblasts known to express these integrins were used to determine cell-polymer interactions. The adhesion experiments revealed significantly increased cell numbers and cell spreading on the RGD-modified surfaces mediated by RGD-integrin-interactions.

1. Introduction

The surface design of biomaterials applied in implant technology and tissue engineering is a key element in controlling the interaction with attaching cells and the surrounding tissue [1-4]. Cell adhesion to a material is primarily mediated by integrins, with a plethora of integrin subtypes providing selective interactions with different proteins of the extracellular matrix [5,6]. A number of integrin subtypes recognize the simple tripeptide sequence Arg-Gly-Asp (RGD) as their ligand, but show specific interactions depending on the amino acids flanking the RGD motif as well as on the conformation of the peptide [7-9]. The covalent linking of these adhesion peptides to biomaterials is a widely accepted approach to improve a material's biocompatibility, biological activity and its interactions with cells [9-15]. Biomaterials used in such attempts preferably suppress protein adsorption and the accompanying unspecific cell adhesion on their surfaces in order to provide undisturbed peptide dependent cell-biomaterial interactions [16]. Additionally, these materials need to provide a functional group to allow for the attachment of RGD peptides. Some hydrogels have been shown to be capable of fulfilling both specifications [12,17-19], but lack the mechanical strength and macroporous structure necessary for many tissue engineering applications. Alternatively, non-swelling, lipophilic polymers have been investigated as materials for the fabrication of implants or scaffolds in the engineering of hard tissue. They provide higher mechanical strength and insolubility in water, allowing for defined geometries, macroporosity and permeability [20,21]. However, the covalent modification with RGD peptides is often a laborious procedure since most of these lipophilic polymers lack the required functional groups for surface modification [9]. To address the problem of unspecific protein adsorption and cell adhesion to lipophilic polymer surfaces, diblock copolymers, such as poly(D,L-lactic acid)-poly(ethylene glycol)-monomethyl ether (MeO-PEG-PLA), were developed. These polymers consist of both a hydrophilic and lipophilic chain and therefore combine mechanical stability and water insolubility with low adhesive properties. MeO-PEG-PLAs that contain high ratios of PEG, making them non-conductive for protein and peptide adsorption, have been particularly effective as 'stealth' biomaterials in numerous applications [22,23]. We have recently shown that protein adsorption and cell adhesion can be controlled via the length and content of the MeO-PEG block in these diblock copolymers [23,24]. To enable the convenient modification of these materials with adhesion peptides, mono amine derivatives (H₂N-PEG-PLA) of the MeO-PEG-PLA diblock copolymers have been synthesized and subsequently functionalized by the covalent attachment of disuccinimidyl tartrate or *N*-succinimidyl-3-maleimido

propionate, resulting in amine- (ST-NH-PEG-PLA) and thiol-reactive polymers (MP-NH-PEG-PLA), respectively [25,26]. These reactive copolymers (Fig. 1) are designed to covalently bind peptides or proteins from aqueous solutions to preformed polymer surfaces during a simple incubation step. This concept would allow for an “of the shelf” scaffold or implant coating fabrication, which could be covalently modified with peptides in response to the individual needs by incubation with a sterile solution of the required peptide. The general feasibility of this concept has been shown in previous studies on the immobilization of fluorescent dyes or model proteins to preformed films and scaffolds [26,27]. In the present study, we aimed at surface modification of reactive polymer films with $\alpha v\beta 5/\alpha v\beta 3$ integrin subtype specific cyclic RGD peptides via a free amine or thiol group (Fig. 2) [14,28]. The success of the procedure was demonstrated in a cell adhesion study, since cell adhesion to and spreading on the modified low-adhesive surfaces requires a high density of integrin-binding sites [1,29].

Two polymers were investigated in this study, ST-NH-PEG₂PLA₂₀, an amine-reactive copolymer composed of a 20 kDa PLA chain and a 2 kDa PEG chain, and MP-NH-PEG₂PLA₄₀, a thiol-reactive copolymers with a 40 kDa PLA chain. Polymer films were cast on glass object slides and subsequently modified with cyclic RGD peptides [14]. According to the polymer design concept, the RGD peptide was attached to the polymer surface by an instant procedure. This means that the prefabricated polymer films were simply incubated with a buffered solution of the peptide in a procedure adjusted to the chemistry of the polymers functional groups and to solid phase modification. The adhesion of human osteoblasts on the modified films was investigated, since this cell type is known to strongly express the corresponding $\alpha v\beta 5/\alpha v\beta 3$ integrin [5,15]. This study demonstrates a surface modification concept based on low-adhesive, amine- and thiol-reactive copolymers, to which cell adhesion is mediated by covalently attached integrin subtype specific RGD peptides.

2. Materials and Methods

2.1. Polymer synthesis and characterization

The amine-reactive polymer ST-NH-PEG₂PLA₂₀ (Mw: 22 kDa) (α -Hydro- ω -[3-succinimidyl-oxycarbonyl-2,3-hydroxy-propyl-amido]-poly(oxy-1-oxopropane-2,1-diyl-block-oxyethylene)) (Fig. 1a) was synthesized from H₂N-PEG₂PLA₂₀ and disuccinimidyl tartrate. Synthesis and analytical characterization were performed as described in the literature [25]. The synthesis and characterization of the thiol-reactive diblock copolymer MP-NH-PEG₂PLA₄₀ (Mw: 42 kDa) (α -Hydro- ω -[3-maleimido-propylamido]-poly(oxy-1-oxopropane-2,1-diyl-block-oxy-ethylene)) (Fig. 1b) have been recently presented in [26].

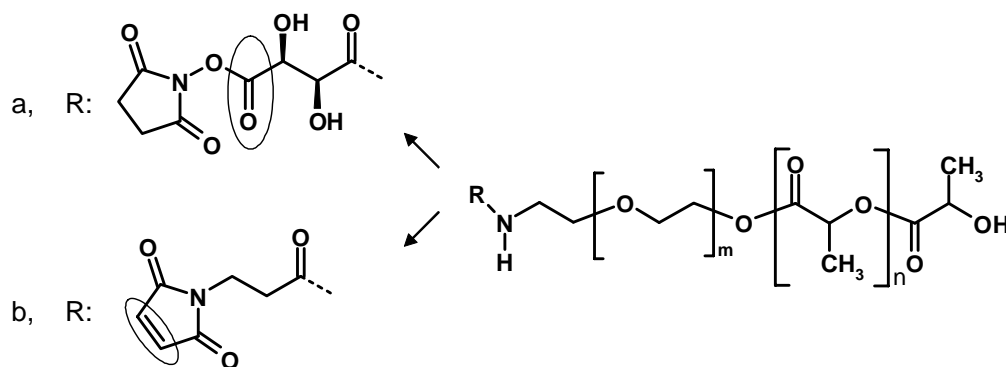


Fig. 1: Polymer structures. a, Amine-reactive ST-NH-PEG-PLA. b, Thiol-reactive MP-NH-PEG-PLA. Circles mark the amine-reactive functionality of the N-hydroxysuccinimide ester and the thiol-reactive double bond of the maleimide.

2.2. RGD peptides and RAD analoges

The α β 5/ α β 3-integrin subtype specific cyclic RGD peptide cyclo(-Arg-Gly-Asp-D-Phe-Lys-) (cyclo(-RGDfK-)) (Fig. 2a) and its non-binding analogue cyclo(-Arg-Ala-Asp-D-Phe-Lys-) (cyclo(-RADfK-)) were synthesized as described by Haubner et al. [28,30]. These peptides were used to modify the amine-reactive copolymer surfaces. The thiol-reactive copolymer was modified with cyclo(-RGDfE-)-spacerAA-C-OH (Fig. 2b), another α β 5/ α β 3-integrin subtype specific cyclic RGD peptide, which contains a spacer amino acid (spacerAA: 20-amino-3,6,9,12,15,18-hexaoxaicosanoic acid) and a free thiol group on the amino acid cysteine [30]. A non-binding RAD-derivative was used as a control.

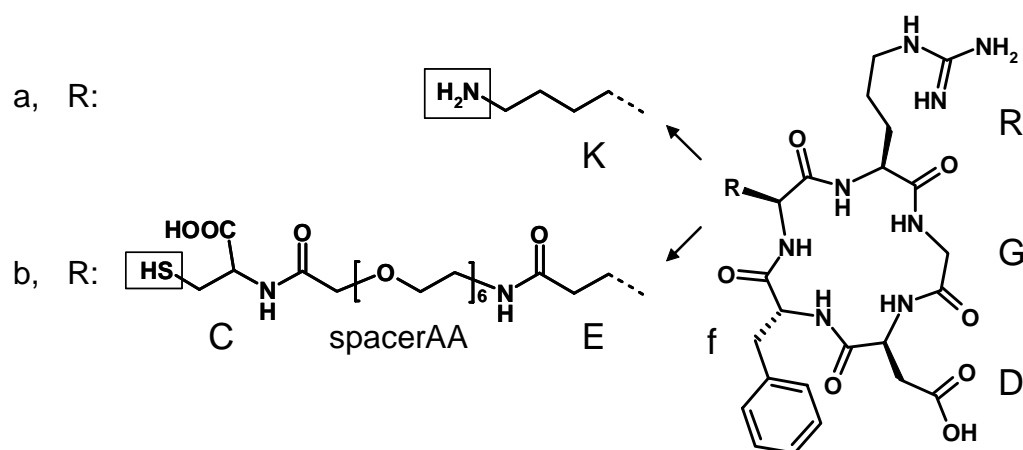


Fig. 2: Chemical structures of the cyclic RGD peptides. a, *cyclo(-RGDfK-)* and b, *cyclo(-RGDfE-)-spacerAA-C-OH* (spacerAA: 20-amino-3,6,9,12,15,18-hexaoxaicosanoic acid). The boxed functional groups were used for a chemoselective ligation of the peptides to the reactive polymer surfaces.

2.3. Human osteoblasts

Osteoblasts were harvested from cancellous human bone fragments derived from routine surgical procedures (during total hip or knee replacement) with informed consent and in accordance with the terms of the ethics committee of the University of Ulm. Cell isolation was done following the published standard protocol [31,32]. Further cultivation was performed in DMEM with 10% fetal bovine serum (FBS, Gemini Bio-Products Inc., Calabasas, California, USA), 1% penicillin/streptomycin (Sigma, Taufkirchen, Germany) and ascorbic acid 50 mg/l (Sigma). For cell adhesion experiments, cells were used following the third passage.

2.4. Experimental setup

An experimental setup (Fig. 3), which allows for easy handling, for direct observation of attaching cells and which requires only low amounts of RGD peptides, has been developed. Glass object slides (Super-Frost Plus, Menzel-Gläser, Braunschweig, Germany) were used as carriers for the cell adhesion experiments. To create a defined area, two rings (diameter: 1.5 cm each) were engraved on the glass object slides using a diamond drill. Before polymer film casting, the glass object slides were aminated to improve polymer adhesion. For this process, the glass object slides were carefully washed using a detergent followed by intensive rinsing with water and finally acetone to remove any lipids. All slides were autoclaved. For amination, the slides were submerged in a stirred solution of 2% (v/v)

3-aminopropyltriethoxysilane (ABC R GmbH & Co. KG, Karlsruhe, Germany) in absolute ethanol for 30 min. After careful rinsing with absolute ethanol, the slides were annealed in an oven for another 30 min at 90°C. After amination the enclosed areas were coated with polymer films. For film casting, solutions of 50 mg diblock copolymer in 1 mL acetone (Merck, Darmstadt, Germany) were prepared and subsequently 20 μL of the polymer solution, corresponding to a mass of 1 mg polymer, were distributed on each marked area of 1.77 cm^2 . Polymer films were fabricated from ST-NH-PEG₂PLA₂₀ and MP-NH-PEG₂PLA₄₀. The slides were dried under a petri-dish for the first 5 min. Covering the slides decelerated the solvent evaporation and ensured the formation of a smooth polymer film surface. Afterwards, the surrounding groove on the slides was covered with a lipophilic barrier (Dako-Pen, Dako, Glostrup, Denmark) so that fluids remained in the engraved area during the incubation and cell adhesion study. Finally, the polymer films were vacuum-dried for 12 hours.

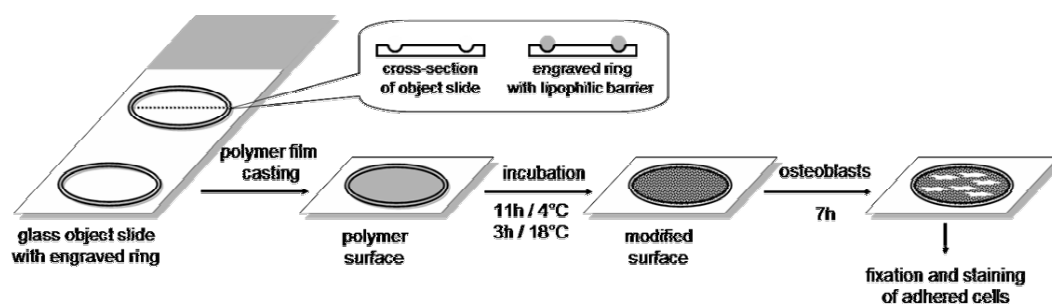


Fig. 3: Illustration of the experimental set-up.

2.5. Surface modification with RGD peptides

Different incubation protocols were used to modify the reactive copolymer surfaces. Details on these protocols are summarized in Table 1. In order to achieve a covalent anchoring of the RGD peptides to the reactive copolymers, the polymer films (1.77 cm^2) were incubated with 250 μL of a buffered solution of 2 mg/mL RGD peptide. Control surfaces were obtained by incubating polymer films with the non integrin-binding RAD peptides or the reaction buffer. During the incubation step with the bicarbonate reaction buffer, the amine-reactive *N*-hydroxysuccinimide ester of ST-NH-PEG₂PLA₂₀ was hydrolyzed, forming a negatively charged carboxylate residue. To obtain non-charged surfaces, other films were aminolyzed by incubation with ethanolamine (stop buffer). In a further control group, the effect of non-covalently attached RGD peptide was investigated. To this end, ST-NH-PEG₂PLA₂₀ surfaces were hydrolyzed by incubation with bicarbonate buffer before cyclo(-RGDfK-) was brought in contact with the polymer film.

Table 1: Description of diverse surface treatment protocols applied to prepare diblock copolymer surfaces for the cell adhesion studies.

Abbreviation	Incubation reagent	Incubation conditions
<i>ST-NH-PEG₂PLA₂₀ surfaces</i>		
RGD	2 mg/mL cyclo(-RGDfK-) in 0.15 M NaHCO ₃ , pH: 8,0	11h at 4°C + 3h at 18°C
RAD	2 mg/mL cyclo(-RADfK-) in 0.15 M NaHCO ₃ , pH: 8,0	11h at 4°C + 3h at 18°C
hydrolysis	0.15 M NaHCO ₃ , pH: 8,0	11h at 4°C + 3h at 18°C
stop	0.1 M ethanolamine in 0.15 M NaHCO ₃ , pH: 8,0	11h at 4°C + 3h at 18°C
hydrolysis RGD	1.) 0.15 M NaHCO ₃ , pH: 8,0 2.) 2 mg/mL cyclo(-RGDfK-) in 0.15 M NaHCO ₃ , pH: 8,0	1.) 11h at 4°C 2.) 3h at 18°C
<i>MP-NH-PEG₂PLA₄₀ surfaces</i>		
RGD	2 mg/mL cyclo(-RGDfE-)-spacerAA-C-OH in PBS, pH: 7,4	11h at 4°C + 3h at 18°C
RAD	2 mg/mL cyclo(-RADfE-)-spacerAA-C-OH in PBS, pH: 7,4	11h at 4°C + 3h at 18°C
buffer	PBS, pH: 7,4	11h at 4°C + 3h at 18°C

2.6. Cell adhesion study

In order to investigate cell adhesion on the modified polymer surfaces, 200 μ L of a cell suspension containing human osteoblasts at a concentration of 44,250 cells/mL, as determined with a hemacytometer, was seeded onto each marked area (5000 cells/cm², i.e., 8850 cells/marked area). Cells were allowed to attach for 7 hours [23,33]. The low seeding density of 5000 cells/cm² was chosen to avoid artifacts from cell aggregation. Non-attached cells were then removed by rinsing twice with PBS. The attached cells were fixed with 10 % formalin in PBS and cells were stained with an aqueous solution of safranin O (0.5%) (Sigma) before counting using light microscopy. A representative section of each seeded surface was counted and the cell count was extrapolated to the total surface area. All cell adhesion studies were performed under serum-free conditions.

With the objective to demonstrate that osteoblast adhesion to RGD-grafted surfaces was integrin-mediated, some cells were incubated with medium containing dissolved cyclo(-RGDfK-) peptide (0.2 mg/mL) to block the corresponding cell surface receptor, the $\alpha\beta3/\alpha\beta5$ integrin, prior to seeding on RGD-modified films [12]. The pretreated cells were also seeded onto TCPS (tissue culture polystyrene) in order to ensure that these cells were still able to undergo non-integrin mediated cell attachment.

2.7. *Study on cell shape*

The shape of the attached cells was evaluated under a light microscope (Leica DM IRB, Leica Microsystems Wetzlar, Wetzlar, Germany) and documented photographically (Panasonic System Camera, Japan; DYNAX, 600si Classic, Minolta, Ahrensburg, Germany) after staining with safranin O (0,5%).

To assess the shape of the attached cells by scanning electron microscopy (SEM), a further cell adhesion experiment was performed. For this study, 5,000 cells/cm² (8850 cells/film) were seeded on RGD- and RAD-modified ST-NH-PEG₂PLA₂₀ and MP-NH-PEG₂PLA₄₀ films. After 7 hours adhesion-time, the cells were rinsed with PBS and fixed with glutaraldehyde (2.5 % in PBS) for 15 min. Following repeated rinsing steps, cells were further fixed with an aqueous solution of OsO₄ (1 %) (Roth, Karlsruhe, Germany) for 30 min under ice-cooling. Excess OsO₄ was removed by washing with water. The object-slides were then frozen at -80°C and lyophilized (Christ Beta 2-16, Martin Christ Gefriertrocknungsanlagen; Osterode am Harz, Germany). For SEM, samples were mounted on aluminium stubs using conductive carbon tape and coated with gold - palladium (Polaron SC515, Fisons Surface Systems; Grinstead, UK). Photomicrographs were acquired at 10 kV on a DSM 950 (Carl Zeiss, Oberkochen, Germany).

2.8. *Statistical Analysis*

Cell numbers were determined (n = 4) and expressed as means \pm standard deviation (SD). Single factor analysis of variance (ANOVA) was used in conjunction with a multiple comparison test (Tukey test) to assess the statistical significance.

3. Results and Discussion

3.1. *Modification of the amine-reactive ST-NH-PEG₂PLA₂₀ films*

Since we intended to covalently bind the RGD peptides from low-concentrated aqueous solutions, reaction conditions had to favor aminolysis of the polymer's *N*-hydroxysuccinimide ester rather than hydrolysis. Therefore, the peptide sequences were dissolved in a sodium bicarbonate buffer at pH 8 to ensure the presence of a neutral ϵ -amino-group on the lysine side chain for coupling with the *N*-hydroxysuccinimide ester, while the nucleophilicity of the arginine side chain in the cyclic RGD peptide was nearly abolished due to protonation at pH 8 [11,29]. Typical reaction protocols of peptides or proteins with *N*-hydroxysuccinimide esters propose reaction times up to a few hours and a, at least initially, low reaction temperature to favor the formation of an amide bond. Therefore, the films were refrigerated (4°C) during the incubation step. Concurrently, an extended coupling time of 11 h was chosen to allow for passive diffusion of the RGD peptide to the reaction sites on the films (Fig. 3). From the plethora of characterized adhesion peptides, we chose a potent cyclic RGD peptide [cyclo(-RGDfK-)] (Fig. 2a) with $\alpha v\beta 3/\alpha v\beta 5$ integrin subtype selectivity to detect even low peptide grafting densities in cell adhesion experiments. The high affinity of this peptide to the αv subunit is associated with the insertion of D-phenylalanine (=f) in the cycle [14,28]. To confirm that the surface modification was successful, the number and shape of the attaching human osteoblasts, which are known to express the corresponding $\alpha v\beta 5/\alpha v\beta 3$ integrin [5,15], were examined.

3.2. *Cell adhesion study on modified ST-HN-PEG₂PLA₂₀ films*

The adhesion studies showed that osteoblast adhesion (Fig. 4) and spreading (Fig. 5a and 6) on cyclo(-RGDfK-)-modified ST-NH-PEG₂PLA₂₀ surfaces was significantly increased compared to the control surfaces 7 hours after seeding. 70% (68.9% \pm 8.8) of the seeded human osteoblasts had attached to RGD-modified ST-NH-PEG₂PLA₂₀ polymer films, while only 30% (31.8% \pm 5.0) adhered to films modified with the non integrin-binding cyclo(-RADfK-). Approximately 10% of the seeded cells attached to the polymer films incubated with reaction buffer (10.7% \pm 1.6) and the stop reagent ethanolamine (11.8% \pm 1.3). These results demonstrated that an effective covalent surface modification has been achieved during the incubation step. More specifically, on polymer films incubated with

buffer, which led to hydrolysis of the amine-reactive *N*-hydroxysuccinimide group and the formation of negatively charged surfaces, the cell adhesion was indistinguishable from the cell adhesion on non-charged surfaces, as generated by aminolysis with ethanolamine. Even on surfaces modified with the non integrin-binding cyclo(-RADfK-) peptide, which presents the positively charged arginine side chain and the negatively charged aspartate side chain in a similar configuration as in the cyclo(-RGDfK-) peptide, comparatively few cells were found attached. Hence, under serum-free conditions, the surface charge had no considerable influence on cell adhesion.

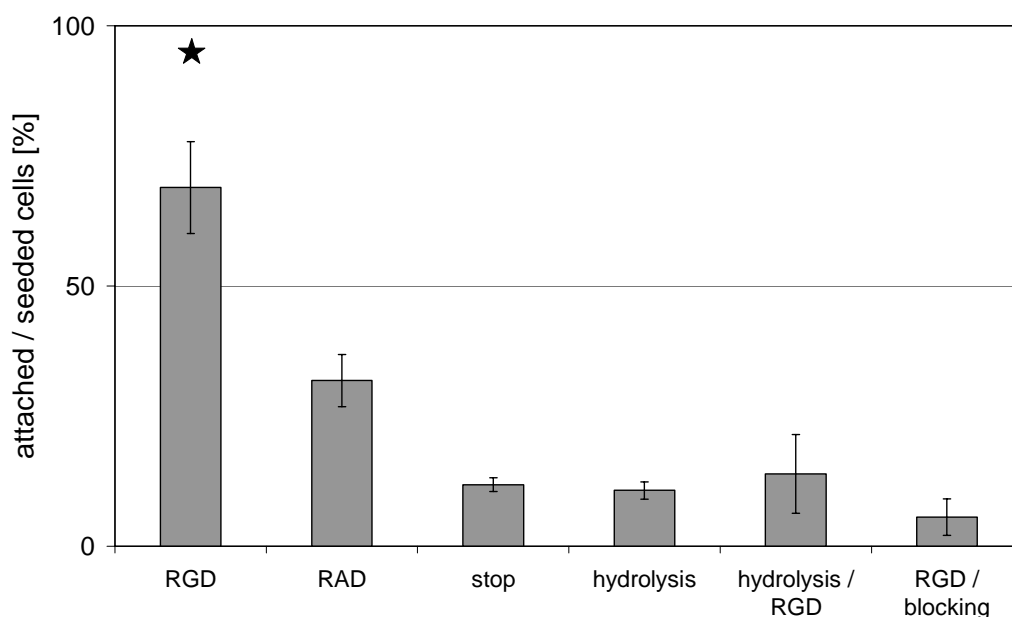


Fig. 4: Percentage of cell attachment normalized to the initial cell seeding density on modified ST-NH-PEG₂PLA₂₀ (9% PEG) surfaces 7 hours after cell seeding. Columns and error bars represent means \pm SD for $n = 4$. Statistical significance is indicated by a ★ ($p < 0.01$).

The specificity of the observed cell interaction with the RGD-modified surface was demonstrated in an integrin receptor blocking experiment. Therein, cells were incubated with dissolved cyclo(-RGDfK-) before they were seeded on RGD-grafted surfaces. Integrin blocking caused almost a complete loss of cell attachment to the RGD-modified surfaces ($5.6\% \pm 3.5$) (Fig. 4), demonstrating that the cell-biomaterial interactions are indeed integrin-specific. In order to test for the impact of any non-covalently attached, adsorbed cyclo(-RGDfK-) on cell adhesion and spreading on the polymer films, we treated ST-NH-PEG₂PLA₂₀ surfaces with buffer to hydrolyze the *N*-hydroxysuccinimide ester. Thereafter, these polymer films were incubated with the RGD peptide. In the cell adhesion test we found about 15% of the seeded cells attached to the film ($13.9\% \pm 7.5$), indicating a very low interaction with this control surface (Fig. 4).

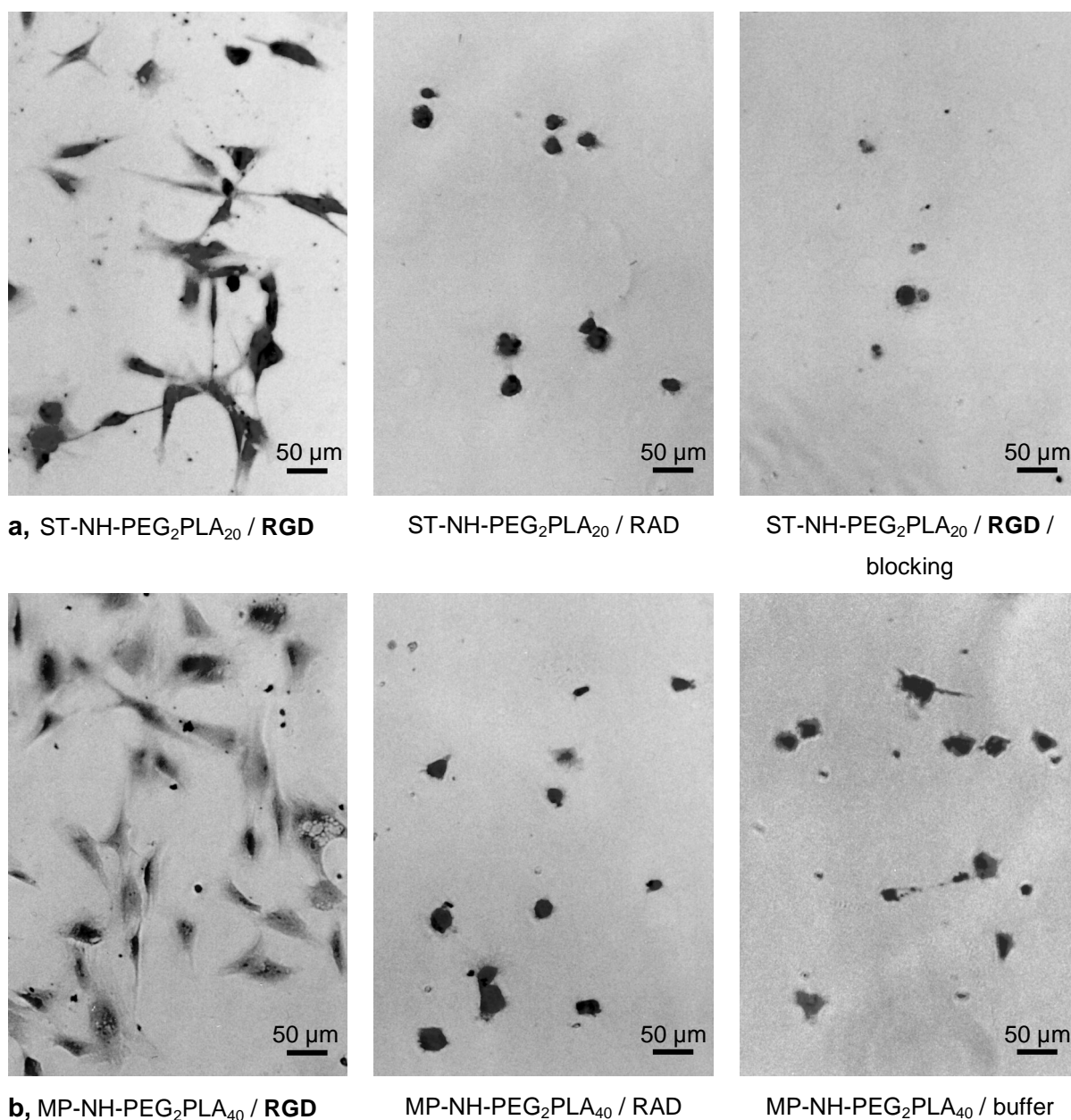


Fig. 5: Representative images depicting shape of human osteoblasts attached to peptide-modified polymer surfaces. a) Modified ST-NH-PEG₂PLA₂₀ surfaces. b) Modified MP-NH-PEG₂PLA₄₀ surfaces. Cells were stained with safranin O (0.5%) and appear in black. Scale bars represent 50 μ m.

In good accordance with the determined cell numbers in the cell adhesion study, we observed well-spread osteoblasts on the RGD-modified polymer surfaces, indicating a strong cell-biomaterial interaction (Fig. 5a and 6). Osteoblasts seeded on surfaces incubated with cyclo(-RADfK-) (Fig. 5a and 6), with the reaction buffer, with ethanolamine or with cyclo(-RGDfK-) after hydrolysis of the reactive *N*-hydroxysuccinimide ester (data not shown), however, remained rounded, indicating low cell-biomaterial interactions. Integrin blocking also resulted in round cells on cyclo(-RGDfK-) modified surfaces (Fig. 5), whereas

the blocked cells spread well when seeded on TCPS, which was used to control for any toxic effects of the dissolved peptide.

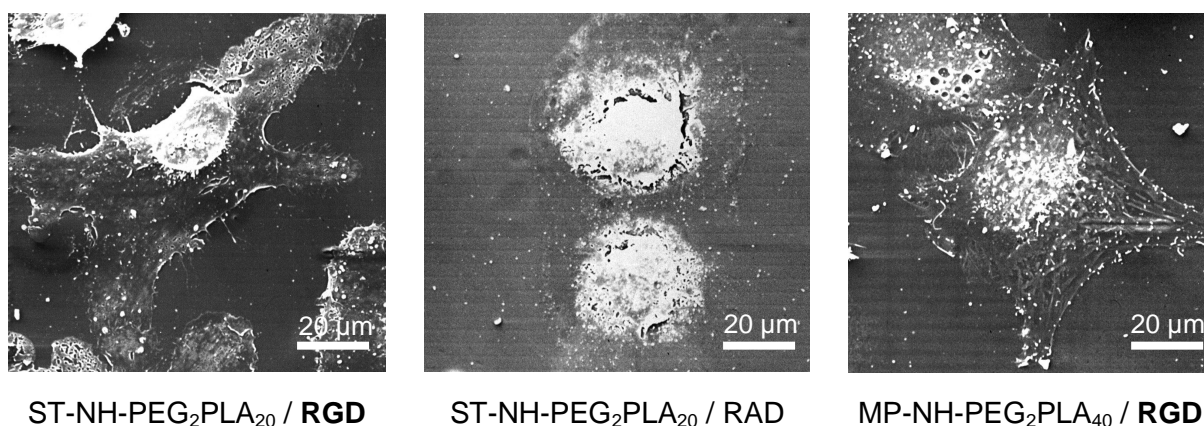


Fig. 6: Cell shape of human osteoblasts on RGD- and RAD-modified ST-NH-PEG₂PLA₂₀ polymer films and on RGD-modified modified MP-NH-PEG₂PLA₄₀ surfaces depicted by SEM. Scale bars represent 20 μm.

To summarize, the number of cells attached to ST-NH-PEG₂PLA₂₀ surfaces grafted with cyclo(-RGDfK-) was significantly increased compared to all control groups ($p < 0.01$). Although we currently have no instrumental means to identify this covalent attachment of the peptide, the adhesion study discussed above proves that a covalent surface modification was achieved and that human osteoblast adhesion is mediated by specific interactions between cells and the attached RGD peptides.

3.3. Modification of the thiol-reactive MP-HN-PEG₂PLA₄₀ films

To broaden the applicability of PEG-PLA based-reactive diblock copolymers to the attachment of other proteins and peptides via simple surface chemistry, a group of thiol-reactive copolymers (MP-NH-PEG-PLA) was recently developed [26]. Targeting the thiol groups of proteins allows for a more selective surface modification, as free thiol groups are less frequent compared to free amine groups. Additionally, the thiol-reactive maleic acid imides are stable in aqueous media and not prone to hydrolysis like amine-reactive *N*-hydroxysuccinimide esters. MP-NH-PEG₂PLA₄₀ and a cyclic RGD peptide carrying a free cysteine thiol group (Fig. 2b) were employed to test our surface modification strategy for a thiol-reactive diblock copolymer. We tested a copolymer composition (PEG₂PLA₄₀, 42kDa) with only 5% PEG that provides a lower surface density of reactive functionalities. However, this composition with a PLA block of 40 kDa offers a higher molecular weight, a glass transition temperature clearly above body temperature and therefore improved processing properties compared to the 22 kDa PEG₂PLA₂₀ copolymer [24,27].

3.4. Cell adhesion study on MP-NH-PEG₂PLA₄₀ films

As a result of the lower PEG content (5% PEG), a higher percentage of the seeded osteoblasts adhered to the buffer treated MP-NH-PEG₂PLA₄₀ films (Fig. 7), 55.0% \pm 7.3 compared to 10.7% \pm 1.6 cells on ST-NH-PEG₂PLA₂₀ films (9% PEG). This is in agreement with a previous study on rat marrow stromal cell adhesion to different MeO-PEG-PLAs [23,34]. However, after solid-state surface modification with RGD peptides, all (114% \pm 21.1; values exceeding 100% originate from the extrapolation of the counted areas to the total surface) seeded osteoblast adhered on the polymer film (Fig. 7). Moreover, they spread well on these surfaces (Fig. 5b and 6), indicating strong interactions between the cells and the tethered RGD peptides. Thus, both cell count and spreading demonstrate the efficacy of the chemical ligation. In contrast, no increase in cell count was found on RAD-modified films compared to the buffer treated surface (Fig. 7). Furthermore, cells on the control surfaces retained their round shape (Fig. 5). This means that despite the fact that unspecific cell adhesion was increased on the MP-NH-PEG₂PLA₄₀ compared to the ST-NH-PEG₂PLA₂₀ films, interactions between the control surfaces and the cells remained limited. Therefore, the widely spread cells on the RGD-modified MP-NH-PEG₂PLA₄₀ films indicate that a sufficient number of adhesion peptides are present even on this 42 kDa copolymer surface with only 5% PEG.

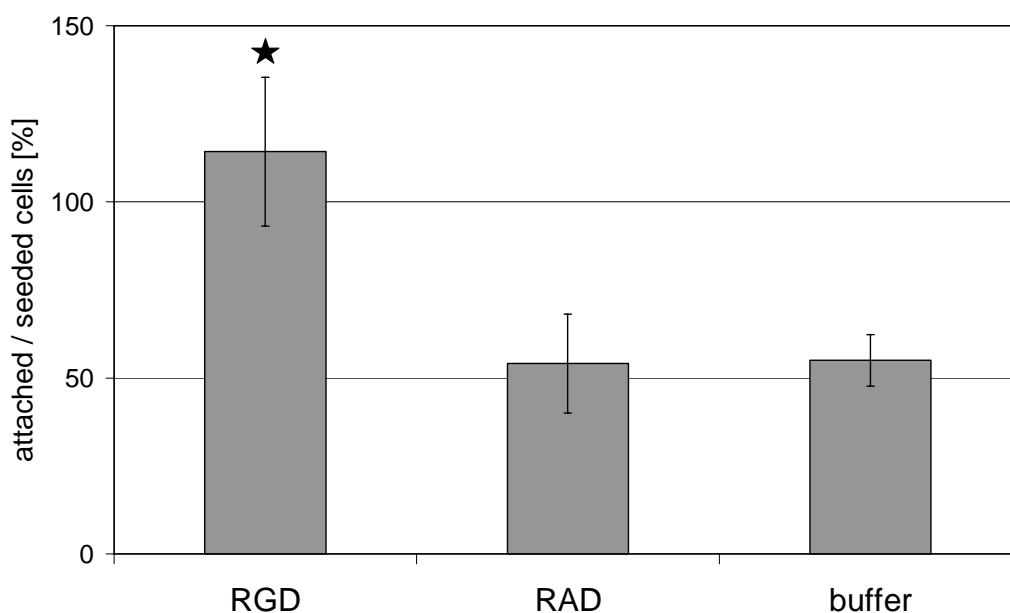


Fig. 7: Percentage of cell attachment normalized to the initial cell seeding density on modified MP-NH-PEG₂PLA₄₀ films (PEG content: 5%) 7 hours after cell seeding. Columns and error bars represent means \pm SD for $n = 3$. Statistical significance is indicated by a ★ ($p < 0.01$).

4. Conclusions

In conclusion, we showed the instant surface modification of preformed polymer films with high affinity adhesion peptides via two different linkers. The modification of low adhesive polymer films was performed by the simple incubation of amine- and thiol-reactive diblock copolymers, consisting of a reactive PEG and a PLA block. Although unspecific cell adhesion was shown to depend on the PEG content of the diblock copolymers, even MP-NH-PEG₂PLA₄₀ (5% PEG) displayed a sufficient density of reactive groups to provide for specific interactions with the $\alpha v\beta 5/\alpha v\beta 3$ integrin on human osteoblasts. As these reactive copolymers offer several modification options as well as variable mechanical properties and rates of biodegradation, these materials appear to be well suited to various customized applications in the field of tissue engineering and implant technology.

5. Acknowledgements

The authors thank the Bayerische Forschungstiftung (ForTePro) for their financial support. Special thanks are due to Allison Dennis, Department of Biomedical Engineering, Georgia Institute of Technology, Atlanta, GA, USA, for proof-reading.

6. References

- (1) LeBaron RG, Athanasiou KA. 'Extracellular matrix cell adhesion peptides: functional applications in orthopedic materials'. *Tissue Eng* (2000); **6**: 85-103.
- (2) Shakesheff KM, Cannizzaro SM, Langer R. 'Creating biomimetic micro-environments with synthetic polymer-peptide hybrid molecules'. *J Biomater Sci Polym Ed* (1998); **9**: 507-518.
- (3) Hu Y, Winn SR, Krajbich I, Hollinger JO. 'Porous polymer scaffolds surface-modified with arginine-glycine-aspartic acid-cysteine enhance bone cell attachment and differentiation in vitro'. *J Biomed Mater Res* (2003); **64A**: 583-590.
- (4) Schaffner P, Meyer J, Dard M, Wenz R, Nies B, Verrier S, Kessler H, Kantlehner M. 'Induced tissue integration of bone implants by coating with bone selective RGD-peptides in vitro and in vivo studies'. *J Mater Sci Mater Med* (1999); **10**: 837-839.
- (5) Gronthos S, Stewart K, Graves SE, Hay S, Simmons PJ. 'Integrin expression and function on human osteoblast-like cells'. *J Bone Miner Res* (1997); **12**: 1189-1197.
- (6) Ruoslahti E. 'RGD and other recognition sequences for integrins'. *Annu Rev Cell Dev Biol* (1996); **12**: 697-715.
- (7) Schaffner P, Dard MM. 'Structure and function of RGD peptides involved in bone biology'. *Cell Mol Life Sci* (2003); **60**: 119-132.
- (8) Aumailley M, Gurrath M, Muller G, Calvete J, Timpl R, Kessler H. 'Arg-Gly-Asp constrained within cyclic pentapeptides. Strong and selective inhibitors of cell adhesion to vitronectin and laminin fragment P1'. *FEBS Lett* (1991); **291**: 50-54.
- (9) Hersel U, Dahmen C, Kessler H. 'RGD modified polymers: biomaterials for stimulated cell adhesion and beyond'. *Biomaterials* (2003); **24**: 4385-4415.
- (10) Massia SP, Stark J. 'Immobilized RGD peptides on surface-grafted dextran promote biospecific cell attachment'. *J Biomed Mater Res* (2001); **56**: 390-399.
- (11) Hern DL, Hubbell JA. 'Incorporation of adhesion peptides into nonadhesive hydrogels useful for tissue resurfacing'. *J Biomed Mater Res* (1998); **39**: 266-276.
- (12) Shin H, Jo S, Mikos AG. 'Modulation of marrow stromal osteoblast adhesion on biomimetic oligo[poly(ethylene glycol) fumarate] hydrogels modified with Arg-Gly-Asp peptides and a poly(ethyleneglycol) spacer'. *J Biomed Mater Res* (2002); **61**: 169-179.
- (13) Cannizzaro SM, Padera RF, Langer R, Rogers RA, Black FE, Davies MC, Tendler SJ, Shakesheff KM. 'A novel biotinylated degradable polymer for cell-interactive applications'. *Biotechnol Bioeng* (1998); **58**: 529-535.
- (14) Kantlehner M, Schaffner P, Finsinger D, Meyer J, Jonczyk A, Diefenbach B, Nies B, Holzemann G, Goodman SL, Kessler H. 'Surface coating with cyclic RGD peptides

- stimulates osteoblast adhesion and proliferation as well as bone formation'. *ChemBioChem* (2000); **1**: 107-114.
- (15) Kantlehner M, Finsinger D, Meyer J, Schaffner P, Jonczyk A, Diefenbach B, Nies B, Kessler H. 'Selective RGD-mediated adhesion of osteoblasts at surfaces of implants'. *Angew Chem Int Ed Engl* (1999); **38**: 560-562.
- (16) Anselme K. 'Osteoblast adhesion on biomaterials'. *Biomaterials* (2000); **21**: 667-681.
- (17) Stile RA, Burghardt WR, Healy KE. 'Synthesis and characterization of injectable poly(N-isopropylacrylamide)-based hydrogels that support tissue formation in vitro'. *Macromolecules* (1999); **32**: 7370-7379.
- (18) Rowley JA, Madlambayan G, Mooney DJ. 'Alginate hydrogels as synthetic extracellular matrix materials'. *Biomaterials* (1999); **20**: 45-53.
- (19) Burdick JA, Anseth KS. 'Photoencapsulation of osteoblasts in injectable RGD-modified PEG hydrogels for bone tissue engineering'. *Biomaterials* (2002); **23**: 4315-4323.
- (20) Ishaug SL, Crane GM, Miller MJ, Yasko AW, Yaszemski MJ, Mikos AG. 'Bone formation by three-dimensional stromal osteoblast culture in biodegradable polymer scaffolds'. *J Biomed Mater Res* (1997); **36**: 17-28.
- (21) Schaefer D, Martin I, Shastri P, Padera RF, Langer R, Freed LE, Vunjak-Novakovic G. 'In vitro generation of osteochondral composites'. *Biomaterials* (2000); **21**: 2599-2606.
- (22) Gref R, Luck M, Quellec P, Marchand M, Dellacherie E, Harnisch S, Blunk T, Muller RH. 'Stealth' corona-core nanoparticles surface modified by polyethylene glycol (PEG): Influences of the corona (PEG chain length and surface density) and of the core composition on phagocytic uptake and plasma protein adsorption'. *Colloids Surf, B* (2000); **18**: 301-313.
- (23) Lieb E, Tessmar J, Hacker M, Fischbach C, Rose D, Blunk T, Mikos AG, Gopferich A, Schulz MB. 'Poly(D,L-lactic acid)-poly(ethylene glycol)-monomethyl ether diblock copolymers control adhesion and osteoblastic differentiation of marrow stromal cells'. *Tissue Eng* (2003); **9**: 71-84.
- (24) Lucke A, Tessmar J, Schnell E, Schmeer G, Gopferich A. 'Biodegradable poly(-lactic acid)-poly(ethylene glycol)-monomethyl ether diblock copolymers: structures and surface properties relevant to their use as biomaterials'. *Biomaterials* (2000); **21**: 2361-2370.
- (25) Tessmar JK, Mikos AG, Gopferich A. 'Amine-reactive biodegradable diblock copolymers'. *Biomacromolecules* (2002); **3**: 194-200.
- (26) Tessmar J, Mikos A, Gopferich A. 'The use of poly(ethylene glycol)-block-poly(lactic acid) derived copolymers for the rapid creation of biomimetic surfaces'. *Biomaterials* (2003); **24**: 4475-4486.
- (27) Hacker M, Tessmar J, Neubauer M, Blaimer A, Blunk T, Gopferich A, Schulz MB. 'Towards biomimetic scaffolds: Anhydrous scaffold fabrication from biodegradable amine-reactive diblock copolymers'. *Biomaterials* (2003); **24**: 4459-4473.

-
- (28) Haubner R, Gratiás R, Diefenbach B, Goodman SL, Jonczyk A, Kessler H. 'Structural and Functional Aspects of RGD-Containing Cyclic Pentapeptides as Highly Potent and Selective Integrin α V β 3 Antagonists'. *J Am Chem Soc* (1996); **118**: 7461-7472.
- (29) Besselink GAJ, Beugeling T, Bantjes A. 'N-Hydroxysuccinimide-Activated Glycine-Sepharose - Hydrolysis of Activated Groups and Coupling of Amino-Compounds.'. *App Biochem Biotech* (1993); **43**: 227-246.
- (30) Hersel, Ulrich. 'Monomeric and Multimeric RGD Peptides for Integrin mediated Cell Adhesion on Biomaterials and for Tumor Diagnostics'. *Ph.D. Thesis*. Technische Universität München, Institut für Organische Chemie und Biochemie. (2003)
- (31) Mayr-Wohlfart U, Kessler S, Puhl W, Gunther KP, Knochel W. 'BMP-4 of *Xenopus laevis* stimulates differentiation of human primary osteoblast-like cells'. *J Bone Joint Surg Br* (2001); **83**: 144-147.
- (32) Mörike M, Schulz M, Nerlich A, Koschnik M, Teller WM, Vetter U, Brenner RE. 'Expression of osteoblastic markers in cultured human bone and fracture callus cells'. *J Mol Med* (1995); **73**: 571-575.
- (33) Ishaug SL, Yaszemski MJ, Bizios R, Mikos AG. 'Osteoblast function on synthetic biodegradable polymers'. *J Biomed Mater Res* (1994); **28**: 1445-1453.
- (34) Gopferich A, Peter SJ, Lucke A, Lu L, Mikos AG. 'Modulation of marrow stromal cell function using poly(D,L-lactic acid)-block-poly(ethylene glycol)-monomethyl ether surfaces'. *J Biomed Mater Res* (1999); **46**: 390-398.

Chapter 3

Towards Biomimetic Scaffolds: Anhydrous Scaffold Fabrication from Biodegradable Amine-reactive Diblock Copolymers

Michael Hacker, Jörg Tessmar, Markus Neubauer, Andrea Blaimer,
Torsten Blunk, Achim Göpferich, Michaela B. Schulz

Department of Pharmaceutical Technology, University of Regensburg,
93040 Regensburg, Germany

Abstract

The development of biomimetic materials and their processing into three-dimensional cell carrying scaffolds is one promising tissue engineering strategy to improve cell adhesion, growth and differentiation on polymeric constructs developing mature and viable tissue. This study was concerned with the fabrication of scaffolds made from amine-reactive diblock copolymers, *N*-succinimidyl tartrate monoamine poly(ethylene glycol)-*block*-poly(D,L-lactic acid), which are able to suppress unspecific protein adsorption and to covalently bind proteins or peptides. An appropriate technique for their processing had to be both anhydrous, to avoid hydrolysis of the active ester, and suitable for the generation of interconnected porous structures. Attempts to fabricate scaffolds utilizing hard paraffin microparticles as hexane-extractable porogens failed. Consequently, a technique was developed involving lipid microparticles, which served as biocompatible porogens on which the scaffold forming polymer was precipitated in the porogen extraction media (*n*-hexane). Porogen melting during the extraction and polymer precipitation step led to an interconnected network of pores. Suitable lipid mixtures and their melting points, extraction conditions (temperature and time) and a low-toxic polymer solvent system were determined for their use in processing diblock copolymers of different molecular weights (22 and 42 kDa) into highly porous off-the-shelf cell carriers ready for easy surface modification towards biomimetic scaffolds. Insulin was employed to demonstrate the principle of instant protein coupling to a prefabricated scaffold.

1. Introduction

One major aim in tissue engineering is the development of transplantable tissue by seeding, proliferation and differentiation of isolated cells on biodegradable polymeric carriers [1]. Modifying the surface of such carriers in order to control the response of attached cells has proven to be a valuable tool for improving the development of mature and viable tissue [2,3]. For this purpose, adhesion proteins, their peptide motives [4-7] and growth factors [8-10] have been covalently bound to biomaterial surfaces. However, only few studies, primarily on hydrogels [11,12], transferred this concept beyond two-dimensions to three-dimensional applications, such as cell carrying scaffolds.

Control of surface composition and cell behavior through bound bioactive substances requires consideration of dynamic surface changes caused by the adsorption of serum proteins when the modified materials come into contact with body fluids. To this end, we have utilized diblock copolymers, consisting of a biodegradable lipophilic polymer block and a hydrophilic block to limit or suppress the non-specific adsorption process and concomitant disadvantageous side effects [13-15]. A biocompatible organic link, e.g. tartaric acid *N*-hydroxysuccinimide ester, which is capable of covalently binding biologically active molecules bearing free amine groups, was attached to the hydrophilic block in order to create a new class of non-adsorbing, amine-reactive polymers [16]. *N*-hydroxysuccinimide esters are among the most frequently used agents for protein crosslinking, labeling [17] and conjugation with PEG [18,19] under formation of stable amide linkages. Furthermore, they can be stored under moisture exclusive conditions for extended periods of time. Therefore, these amine-reactive diblock copolymers, carrying *N*-hydroxysuccinimide esters, are designed to be processed in their active state making amine-reactive off-the-shelf scaffolds available [16]. Finally, the surface of such pre-fabricated scaffolds can be modified just before use, by covalently binding proteins or peptides in an instantaneous manner, i.e. by simply incubating the polymeric construct with an aqueous solution containing the selected biomolecules. Such amine-reactive diblock copolymers, *N*-succinimidyl tartrate monoamine poly(ethylene glycol)-*block*-poly(D,L-lactic acid), with different block ratios, were recently synthesized in our group [16].

The study presented here aimed at the development of a technique for processing these polymers into scaffolds, which play a prominent role in tissue engineering since they provide a three-dimensional framework for cells to attach, proliferate and lay down extracellular matrix. This concept demands a highly porous and interconnected scaffold structure to ensure

sufficient space for tissue development and unimpaired diffusion of nutrients, oxygen and waste [20,21]. Processing amine-reactive polymers into scaffolds required consideration of two essential points: firstly, in order to preserve the active group from hydrolysis, aqueous media had to be avoided, and secondly, a sufficient surface density of reactive PEG-chains demands a low molecular weight PLA-block (20 to 40 kDa) [15]. Thus, we required an anhydrous, lab-scale scaffold fabrication technique, which would be suitable for processing low molecular weight polymers into highly porous scaffolds and would provide an interconnected pore structure.

Numerous methods for polymer processing into three-dimensional scaffolds have been described, according to the literature, such as polymer casting-salt leaching with or without subsequent compression molding [22-24], phase separation and gas foaming [25,26]. None of these methods, however, met all the demands listed above. Recently, two anhydrous processing techniques based on particulate leaching were published. Both involved hard paraffin microparticles prepared as pore forming devices [27,28]. One method started from a dispersion of such paraffin microparticles in a polymer solution and finally led to scaffolds with an interconnected pore structure by concomitant porogen extraction and polymer precipitation in warm *n*-hexane [29]. This hydrocarbon templating technique has been applied to a range of amorphous and semicrystalline high molecular weight polymers (> 70 kDa) with glass transition temperatures (T_g) exceeding 50 °C. This is well beyond the T_g of the polymers investigated in this study (31 – 43 °C). Moreover, this technique had been assumed to work only with polymers of more than 40 kDa [29]. Therefore, this study aimed at achieving the following three goals:

1. Employing the hydrocarbon templating technique to identify process parameters critical for the processing of low molecular weight polymers.
2. Developing an anhydrous polymer processing technique which is suitable for low molecular weight polymers and avoids non-physiological porogen materials.
3. Finally, proving the principle of the instant protein coupling to a preformed scaffold with insulin as model substance.

2. Materials and Methods

2.1. Materials

Both the biodegradable poly(D,L-lactic acid)-poly-(ethylene glycol)-monomethyl ether diblock copolymers (MeO-PEG_xPLA_y) as well as their amine-reactive derivatives ST-NH-PEG_xPLA_y (monoamine poly(ethylene glycol)-block-poly(D,L-lactic acid) activated with disuccinimidyl tartrate) were synthesized as previously described [14,16] (Fig. 1). *x* and *y* in PEG_xPLA_y represent the molecular weight of the PEG and the PLA block, respectively, in kDa. Table 1 gives a survey on molecular weight and polydispersity index (PI) of the investigated copolymers.

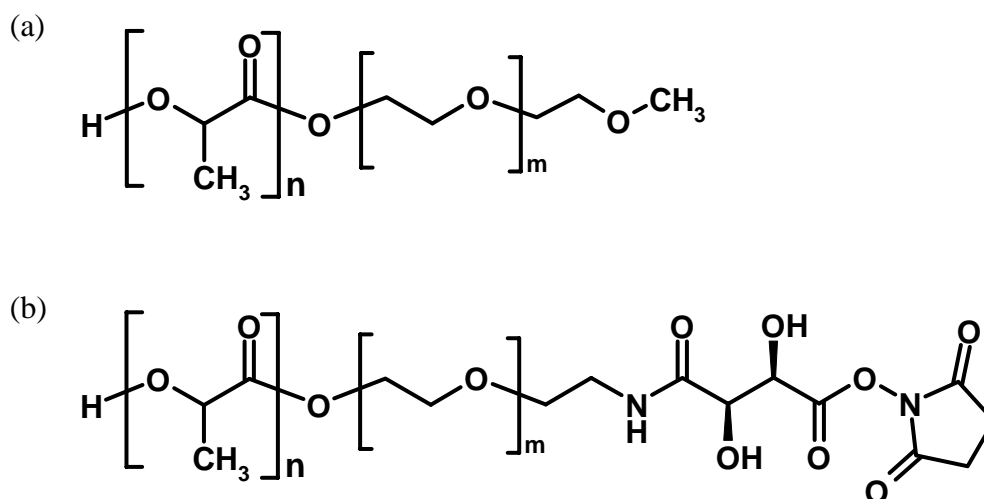


Fig. 1. Structures of the processed polymers. (a) poly(lactic acid)-block-poly(ethylene glycol)-monomethyl ether (MeO-PEG_xPLA_y); (b) poly(ethylene glycol)-block-poly(lactic acid)-monoamine activated with disuccinimidyl tartrate (ST-NH-PEG_xPLA_y). *m* and *n* represent the number of ethylene glycol and lactic acid units in the polymer. *x* and *y* represent the molecular weight (kDa) of the poly(ethylene glycol) and poly(lactic acid) chain.

Hard paraffin types with a melting temperature of 42 – 44 °C (P 42) and 46 – 48 °C (P 46) according to product specification were purchased from Merck (Darmstadt, Germany). Hard paraffin with a declared melting temperature of between 50 and 52 °C (P 50) was purchased from Fluka Chemicals (Buchs, Switzerland). All lipids (Dynasan® 114, Dynasan® 116, Softisan® 154 and Witepsol® H42) were kindly provided by SASOL Germany GmbH (Witten, Germany). Relevant properties of the bulk materials used for porogen microparticle preparation are summarized in Table 2.

Table 1: Physical properties of the processed polymers. Glass transition temperature as obtained with MDSC (2nd heating). Weight average molecular weight (M_w), number average molecular weight (M_n) and polydispersity indices ($PI = M_w/M_n$) of the polymers as determined from GPC.

Polymers	MDSC T _g [°C]	Molecular weight				
		Declared	GPC analysis			¹ H-NMR
			M _n	M _w	PI	M _n
MeO-PEG2PLA20	33.7	22 kDa	23,000	47,600	2.1	22,900
ST-NH-PEG2PLA20	31.1	22 kDa	22,800	39,200	1.7	---
MeO-PEG2PLA40	42.3	42 kDa	42,000	64,500	1.5	42,900
ST-NH-PEG2PLA40	38.1	42 kDa	43,200	65,200	1.5	---

Table 2: Physical properties and composition of materials used for porogen microparticle preparation.

Hard paraffin type	Density [g·cm ⁻³]	T _m [°C] of bulk material (specification)	T _m [°C] of side fractions (DSC)	T _m [°C] of side fractions (DSC)	
P 42	approx. 0.90	42 – 44	38.4	13.2	26.8
P 46		46 – 48	38.9	13.6	27.7
P 50		50 – 52	47.2	27.4	34.4

Lipid	composition			
Witepsol® H 42	0.97	41 – 43	35.8	1.6 % di- / 98.2 % tri-glycerides
Softisan® 154	0.95	53 – 58	54.2	3.5 % di- / 96.4 % tri-glycerides
Dynasan® 114	0.96	55 – 58	54.6	glyceryltrimyristat
Dynasan® 116		61 – 65	59.2	glyceryltripalmitat

Acetone, chloroform, ethyl methyl ketone (EMK), tetrahydrofuran (THF), which were used as polymer solvents, and *n*-hexane, utilized as a porogen extraction medium were purchased in analytical grade from Merck (Darmstadt, Germany). Solvents were dried over 4 Å molecular sieves (Carl Roth GmbH, Karlsruhe, Germany) prior to the processing of amine-reactive polymers.

2.2. GPC and ¹H-NMR analysis

The molecular weights of the diblock MeO-PEG-PLA copolymers were measured according to Lucke et al. [14]. The results indicated that both polymers were synthesized in the declared composition and molecular weight. With regard to the amine-reactive ST-NH-PEG-PLA copolymers, the composition and molecular weight of the H₂N-PEG-PLA precursor were confirmed with ¹H-NMR analysis during synthesis [16]. The declared number average molecular weights (Mn) of all diblock copolymers correlated well with the values for Mn obtained by GPC analysis. Furthermore, the polydispersity indices of the polymers indicated their appropriate molecular weight distribution.

2.3. DSC and MDSC analysis

The glass transition temperatures (T_g) of the polymers were measured utilizing modulated differential scanning calorimetry (MDSC). This method, which is characteristic for a heating rate associated with a sinusoidal temperature oscillation, was applied to detect the faint glass transition step with high resolution and to separate this thermal event from overlapping relaxation or melting phenomena typical for these diblock copolymers [14]. Generally, T_g of the diblock copolymers decreased with molecular weight. T_g of the reactive ST-NH-PEG_xPLA_y was slightly lower compared with the analog MeO-PEG_xPLA_y derivative in both cases.

Differential scanning calorimetry (DSC) was used to determine the melting points of different hard paraffin types and lipid bulk materials as well as the fabricated porogen microparticles. Paraffin residuals inside fabricated scaffolds were detected and quantified with DSC analysis, too. The detection of triglyceride residuals inside the scaffolds, however, was realized through MDSC.

For calorimetric analysis, all samples were precisely weighed in non-hermetic AutoDSC aluminum sample pans (TA Instruments, Alzenau, Germany). The sample pans were sealed using the sample encapsulating press (TA Instruments, Alzenau, Germany) and analyzed on a DSC 2920 equipped with a refrigerated cooling system and an autosampler (TA Instruments, Alzenau, Germany). An empty, sealed pan served as reference.

All measurements were carried out between -20 °C and 120 °C. Typically, samples were equilibrated at -20 °C for 15 min and heated to 120 °C at a heating rate of 2 °C/min (analysis of porogen materials (DSC) and determination of polymer's T_g (MDSC)) or 5 °C/min (determination of residual paraffin (DSC) and triglyceride (MDSC) content). After an

isothermal phase of 15 min, samples were cooled down to $-20\text{ }^{\circ}\text{C}$ at the same heating rate. Finally, after another isothermal phase of 15 min, samples were again heated to $120\text{ }^{\circ}\text{C}$ at the described heating rate. In case of MDSC measurements, a sinusoidal temperature modulation with a period of 60 s and a temperature amplitude of $1\text{ }^{\circ}\text{C}$ (determination of polymer's T_g) or $0.8\text{ }^{\circ}\text{C}$ (determination of residual lipids), was applied to both heating cycles.

The obtained thermograms were analyzed for melting temperature (onset point detection) and melting enthalpy (peak area) as well as glass transition temperature (obtained as half height of the transition step) with the *Universal Analysis for NT*[®] software provided with the DSC system.

2.4. Preparation of porogen microparticles

Microparticles were prepared using a melt dispersion technique. The hard paraffin types were processed by heating a mixture of 10 g hard paraffin with 12.5 ml of a 1.5% (m/v) aqueous solution of poly(vinyl alcohol) (PVA, 98% hydrolyzed, Aldrich Chemical Company, Milwaukee, USA) up to $65\text{ }^{\circ}\text{C}$. The mixture was emulsified by vortex mixing and subsequently casted into a larger volume (500 ml) of an ice-cooled ($5\text{ }^{\circ}\text{C}$) 0.1% (m/v) aqueous PVA solution stirred with a propeller stirrer. After 10 min the hardened particles were collected by filtration, intensively rinsed with water and vacuum dried at room temperature for 24 hours. Particles or aggregates larger than $710\text{ }\mu\text{m}$ were removed by sieving.

Lipid microparticles were fabricated as described above but without any polymeric surfactant. The size distribution of the prepared lipid microparticles was investigated using laser diffraction (Mastersizer 2000 Hydro 2000S, Malvern Instruments, Herrenberg, Germany) as follows: 100 mg lipid microparticles were suspended in $100\text{ }\mu\text{l}$ 3% (m/v) aqueous HPMC (Metolose 90 SH 100, Shin-Etsu Co. Ltd., Tokyo, Japan) solution using a vortex mixer. This suspension was diluted in the dispersion unit (water as dispersant) in accordance with the obscurity indicator on the instrument and stirred at $3000\text{ }\mu\text{m}$ under sonification (30% intensity) during the measurement. The volume based particle size distribution was calculated choosing the Fraunhofer approximation (Malvern Software V5.1).

2.5. Solubility of porogen microparticles

In order to quantify the solubility of the porogen microparticles in the polymer solvent under processing conditions, 100 mg particles were precisely weighed in glass vials. The vials were placed in a shaking water bath (frequency: 150 min^{-1}) at a temperature of $0\text{ }^{\circ}\text{C}$. 5 ml of cold

solvent mixture were added. After exactly 10 min of shaking the dispersion was filtered through a 0.2 μm solvent resistant regenerated nitrocellulose membrane filter (Spartan 30/A from Schleicher & Schuell, Dassel, Germany). The filtrate was collected in glass vials of known weight. Following solvent evaporation under a fume hood the vials were dried at 60 °C to constant weight. The amount of dissolved porogen material was measured as the weight increase of the vials.

This screening method was specifically adapted to the polymer processing conditions, concerning temperature and contact time (preparation of porogen particle dispersion and transfer into molds). To improve the resolution of this test, a low material to solvent ratio (100 mg per 5 ml) was chosen.

2.6. Scaffold fabrication

Describing the general procedure (Fig. 2), polymer was weighed in a glass vial and dissolved in the appropriate amount of solvent. Porogen microparticles were weighed into a separate vial. The amounts of polymer, porogen microparticles and solvent used per batch varied with respect to the polymer to porogen ratio and the concentration of the polymer solution, as described in the results section. After 1 h storage at $-20\text{ }^{\circ}\text{C}$ the porogen particles were transferred into the polymer solution and mixed for 5 min on ice. The resulting highly viscous dispersion was then transferred into a 5 ml polypropylene syringe and injected into cubic Teflon[®] molds (1 cm x 1 cm x 1cm with a cylindrical cavity of 0.8 cm in diameter. After a pre-extraction treatment step in *n*-hexane at 0 °C (Fig. 2 (*)), which was only applied when lipid microparticles served as porogens, the filled molds were submerged in warm *n*-hexane to precipitate the polymer and extract the porogen particles concurrently. This procedure was carried out in two separate *n*-hexane baths of different temperatures T_1 and T_2 for t_1 and t_2 with $t_1 + t_2 = 30$ min. Subsequently, the molds were transferred into an *n*-hexane bath of 0 °C for 5 min to solidify the generated structures. Finally, the porous cylindrical polymer constructs were removed from the molds and vacuum dried for 48 h. For further investigations the constructs were cut into 2 mm slices which were then addressed as scaffolds.

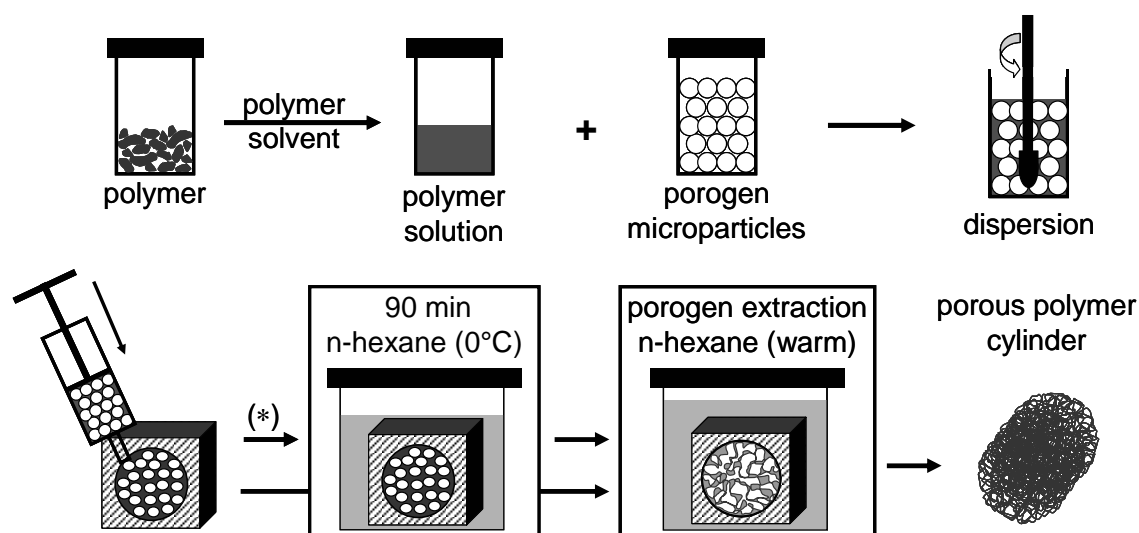


Fig. 2: Schematic illustration of the polymer processing procedure. (*) Pre-extraction treatment of molds in *n*-hexane at 0°C applied when lipids were used as porogen material.

2.7. Scaffold characterization

The overall structure of the fabricated porous constructs was visualized using a zoom stereo microscope (Wild M7A, Wild Heerbrugg Ltd., Heerbrugg, Switzerland). For examination of scaffold microstructure using scanning electron microscopy (SEM), samples were mounted on aluminum stubs with conductive carbon tape and coated with gold (Fig. 4) or gold–palladium (Fig. 9). All micrographs were obtained at 10 kV on a JEOL JSM-840 (Jeol Ltd., Tokyo, Japan) (Fig. 4) or a DSM 950 (Zeiss, Oberkochen, Germany) (Fig. 9).

Pore size distribution was determined by mercury intrusion porosimetry (AutoPore IV 9500, Micromeritics, Mönchengladbach, Germany). Scaffolds weighing approximately 25 mg were sealed in a penetrometer (3 bulb, 0.412 stem, powder; Micromeritics, Mönchengladbach, Germany) and subjected to analysis. The measurements were performed between 0.0007 and 100 MPa to determine pore-size distributions and porosities. A 30 s equilibration time was set for each intermediate data point. For data interpretation, a contact angle of 140° and a surface tension of 0.48 Nm⁻¹ were assumed. These measurements were kindly provided by Micromeritics.

2.8. *Attachment of human insulin to scaffold surfaces*

To evaluate the amine reactivity of the scaffold surface, human insulin served as model protein. In order to provide optimal conditions for the reaction of insulin's free amine groups and the activated esters of the polymer, the protein was dissolved (6 mg/ml) in a 0.1M NaHCO₃ buffer at pH = 8.0 with an urea content of 75 mg/ml. Scaffolds were incubated with 2 ml of this insulin solution for 2.5 hours at room temperature on a shaker in a micro test tube (Eppendorf, Hamburg, Germany). After rinsing with pure buffer and water, the scaffolds were freeze dried and prepared for GPC analysis: 50 mg of scaffold were dissolved in 400 μ l DMSO. DMSO is a solvent not only for the polymers and the insulin-polymer conjugates, but also for any free insulin that remained adsorbed to the scaffold even after rinsing. 1600 μ l of chloroform were then added to precipitate free insulin, thus separating adsorbed and covalently linked insulin. After filtration, 50 μ l of the solution were analyzed using GPC analysis equipped with a RF-551 fluorescence detector (Shimadzu, Duisburg, Germany). The resulting chromatograms were obtained at $\lambda_{\text{ex}} = 274$ nm and $\lambda_{\text{em}} = 308$ nm for the detection of insulin's amino acid tyrosine.

3. Results and Discussion

This study was concerned with processing low molecular weight amine-reactive ST-NH-PEG-PLA and the corresponding non-reactive MeO-PEG-PLA diblock copolymers (42 and 22 kDa (Table 1)) into highly porous and interconnected cell carriers. MeO-PEG_xPLA_y diblock copolymers were used to identify the decisive parameters for the processing of PEG-PLA diblock copolymers, which were then correlated to polymer's molecular weight and glass transition temperature (T_g) and finally adapted to the special properties of the amine-reactive derivatives.

A recently published hydrocarbon templating method [27,29] met our demands for anhydrous processing, for an interconnected pore structure, and for pore size control. This method involved preparation of a dispersion of paraffin microparticles in a polymer solution. This dispersion was transferred into a Teflon[®] mold and placed into warm *n*-hexane, a solvent for the porogen to achieve particulate leaching while being a poor solvent for the polymer. Thus, on contact with this solvent, the polymer precipitated on the extracted porogen particles leading to an interconnected scaffold architecture [27]. However, up to now only biodegradable polymers with a molecular weight of above 70 kDa had been processed and a limit of 40 kDa had been assumed by the authors. In order to develop a new processing method for low molecular weight diblock copolymers based on the hydrocarbon templating technique, it was necessary to investigate the limitations of this technique.

Three problems soon became obvious in preliminary investigations; firstly, the published extraction temperature of 45 - 50 °C over 20 min [29] or even 50 °C over 40 min [30] were incompatible with the low glass transition temperature (T_g) of the diblock copolymer investigated in this study and led a collapse of the constructs during processing. A survey of these polymers including their determined T_g and molecular weights, is given in Table 1. Secondly, lowering the extraction temperature made the commonly used high melting paraffin ($T_m = 53 - 57$ °C) [28] unsuitable as a porogen material due to insufficient extraction. Thirdly, lower melting hard paraffin was soluble in the published polymer solvent chloroform. Consequently, we varied each of the three parameters: the porogen material, the polymer solvent and the extraction conditions.

3.1. Scaffold fabrication using paraffin microparticles as porogens

3.1.1. Porogen material: Characterization of paraffin microparticles

Microparticles were prepared from three low melting hard paraffin types with declared melting points of 42 – 44 °C (P 42), 46 – 48 °C (P 46) and 50 – 52 °C (P 50), respectively. Although these paraffin types apparently offered a considerable range of melting points, the fabricated particles formed cohesive powders not allowing for the preparation of a homogeneous dispersion of these particles in a polymer solution, especially in case of the hard paraffin types P 42 and P 46. DSC analysis of bulk and processed hard paraffin clarified this behavior: instead of one endothermic melting peak, the thermograms revealed three peaks representing different hydrocarbon fractions (Table 2). Moreover, the predominant side fraction in each of the three investigated hard paraffin types melted at least 20 °C below the main hydrocarbon fraction. These low melting fractions were probably responsible for microparticle agglomeration. In consequence, only P 50 particles were suitable as porogen material for further experiments.

3.1.2. Polymer solvent

Methylene chloride or chloroform have been described as suitable polymer solvents [29]. Preliminary tests revealed that all three described hard paraffin types were soluble in these solvents to a considerable extent. Acetone, a non-solvent for the hard paraffin, would have been a suitable polymer solvent, but was excluded in early experiments due to its low boiling point, which disturbed the scaffold formation by forming gas bubbles during porogen extraction. To overcome these problems, we chose an azeotropic mixture of 65% (v/v) acetone and 35% (v/v) chloroform with a boiling point of 65°C as polymer solvent [31]. Since the azeotrope's boiling point was well above the ones of both single components, the addition of acetone did not limit the applicable extraction conditions.

Solubility tests of the porogen microparticles made of the three investigated hard paraffin types revealed that microparticle solubility increased with decreasing melting temperature (Fig. 3). The solubility of P 50 and P 46 microparticles was below 10 mg in 5 ml of the acetone - chloroform mixture. Less than 15 mg of P 42 were dissolved in 5 ml solvent mixture. Thus, the solubility of all three paraffin types was considered as being sufficiently low, however, due to the thermal characteristics described above, only P 50 was suitable as porogen material.

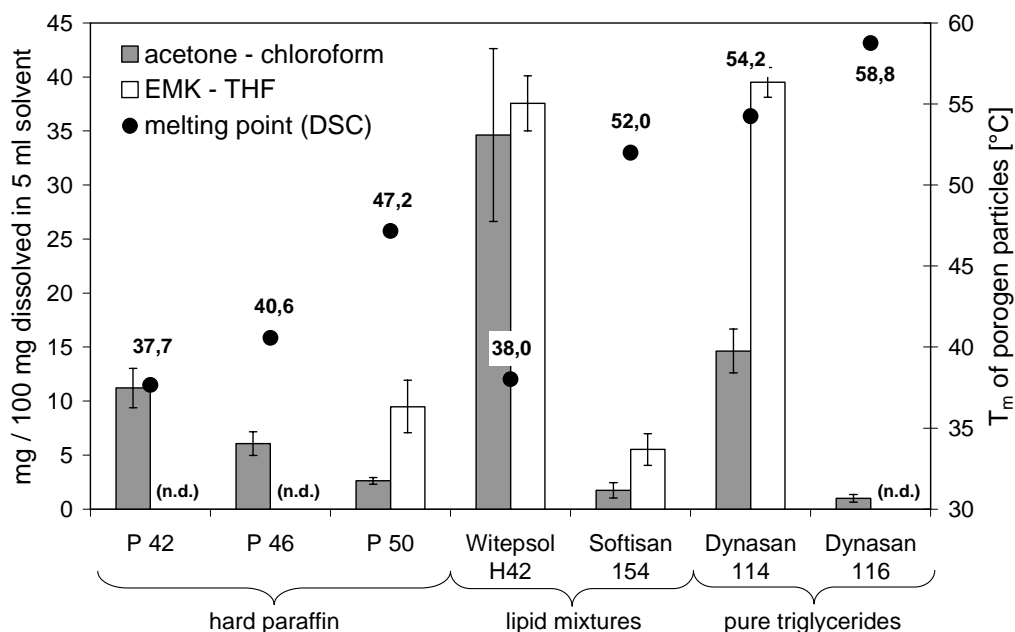


Fig. 3: Relative amount of dissolved porogen material in 5 ml of two different polymer solvent mixtures after 10 min (left axis). (n.d.): Value of porogen particle solubility in the EMK - THF mixture not determined. Columns and error bars represent means \pm SD for $n = 3$. Melting points of the porogen microparticles as obtained with DSC analysis (right axis).

Table 3: Determined processing conditions for the investigated polymers with different porogen materials.

Polymer	Porogen material	Polymer / porogen (w/w)	Conc. (polymer solution) (w/v)	Extraction conditions	
				step 1 (T_1 ; t_1)	step 2 (T_2 ; t_2)
Hard paraffin					
MeO-PEG ₂ PLA ₂₀	P 50	17.6 %	33 %	40°C ; 10 min	30°C ; 20 min
MeO-PEG ₂ PLA ₄₀	P 50	17.6 %	30 %	52°C ; 2 min	35°C ; 28 min
Witepsol : Softisan					
MeO-PEG ₂ PLA ₂₀	2 : 1	33 %	55.5 %	40°C ; 5 min	30°C ; 25 min
	1 : 1			45°C ; 5 min	33°C ; 25 min
MeO-PEG ₂ PLA ₄₀	1 : 1	25 %	42 %	45°C ; 10 min	35°C ; 20 min
ST-NH-PEG ₂ PLA ₂₀	1 : 1	33 %	55.5 %	40°C ; 5 min	33°C ; 25 min
ST-NH-PEG ₂ PLA ₄₀	1 : 1	33 %	55.5 %	40°C ; 10 min	35°C ; 20 min

3.1.3. *Extraction conditions: Influence of processing parameters on the scaffold microstructure*

Both MeO-PEG-PLA copolymers were processed with P 50 porogen microparticles (Table 3). Through choosing a fixed polymer to porogen ratio of 17.6 %, the amount of polymer solvent was the variable parameter, which was minimized to obtain a highly viscous, and therefore stable, dispersion of porogen particles in the polymer solution. Concentrations of the processed polymer solutions were 30 % (m/v) for MeO-PEG₂PLA₄₀ and 33 % (m/v) for MeO-PEG₂PLA₂₀ in the acetone – chloroform mixture.

By applying P 50 microparticles with a melting point clearly above the T_g of the copolymers, we investigated the influence of extraction conditions on pore structure. In order to avoid deformation of the polymer constructs, we set up a two-step extraction method applied for 30 min, involving two extraction temperatures: a high one, T_1 , near or exceeding the polymer's T_g for a certain time t_1 and a lower one, T_2 , clearly below T_g for a longer period $t_2 = 30 \text{ min} - t_1$. Three extraction schemes, one with $T_1 = 47 \text{ }^\circ\text{C}$ close to T_m of the porogen microparticles determined by DSC analysis, one with $T_1 = 52 \text{ }^\circ\text{C}$ at the upper limit of the declared melting range and the third with $T_1 = 42 \text{ }^\circ\text{C}$ at the T_g (42.3 $^\circ\text{C}$) of the polymer were applied for the processing of MeO-PEG₂PLA₄₀. Figure 4a shows the SEM pictures of scaffolds processed according to that scheme. These investigations revealed that an extraction temperature approaching the polymer's T_g led to stable constructs, but that they lacked the necessary interconnected microstructure (Fig. 4 a/1). A T_1 of 47 $^\circ\text{C}$ ($t_1 = 5 \text{ min}$) or 52 $^\circ\text{C}$ ($t_1 = 2$ or 5 min) followed by further extraction at $T_2 = 35 \text{ }^\circ\text{C}$ for $t_2 = 30 \text{ min} - t_1$, however, generated an interconnected pore structure (Fig. 4 a/2-4), indicating that an initial extraction temperature near the porogen's T_m is required for pore interconnectivity. Furthermore, the melting temperature determined by DSC proved to be representative as a benchmark for the determination of T_1 .

An increase of T_1 to 52 $^\circ\text{C}$ with $t_1 = 2 \text{ min}$ led to a very regular pore size formation (Fig. 4 a/3). These extraction conditions were therefore recommended in table 3 for the processing of MeO-PEG₂PLA₄₀. Nevertheless, exposure time to an extraction medium with a temperature well beyond the T_g had to be chosen with care. Extraction for $t_1 = 5 \text{ min}$ resulted in increasing pore sizes and a coarsening of the polymer structures (Fig. 4 a/4). A further increase in t_1 to up to more than 6 min caused scaffold deformation during processing. However, in the case of MeO-PEG₂PLA₄₀ the developed two step extraction technique allowed for the fabrication of scaffolds with the desired pore structure, despite the high melting point of the P 50 microparticles. In case of MeO-PEG₂PLA₂₀, T_1 was limited to

40 °C. Higher extraction temperatures resulted in the collapse of the polymer constructs. As expected from the investigation of MeO-PEG₂PLA₄₀, these conditions resulted in a honeycomb-like architecture of low interconnectivity, reflecting the size and shape of the porogen microparticles (Fig. 4 b). To sum up these results, extraction temperatures close to the melting point of the porogen during the first extraction step were a prerequisite for an interconnected pore structure. The process responsible for the formation of an interconnected structure appeared to be the melting of the porogen particles, which led to coalescing oil droplets on which the polymer precipitated.

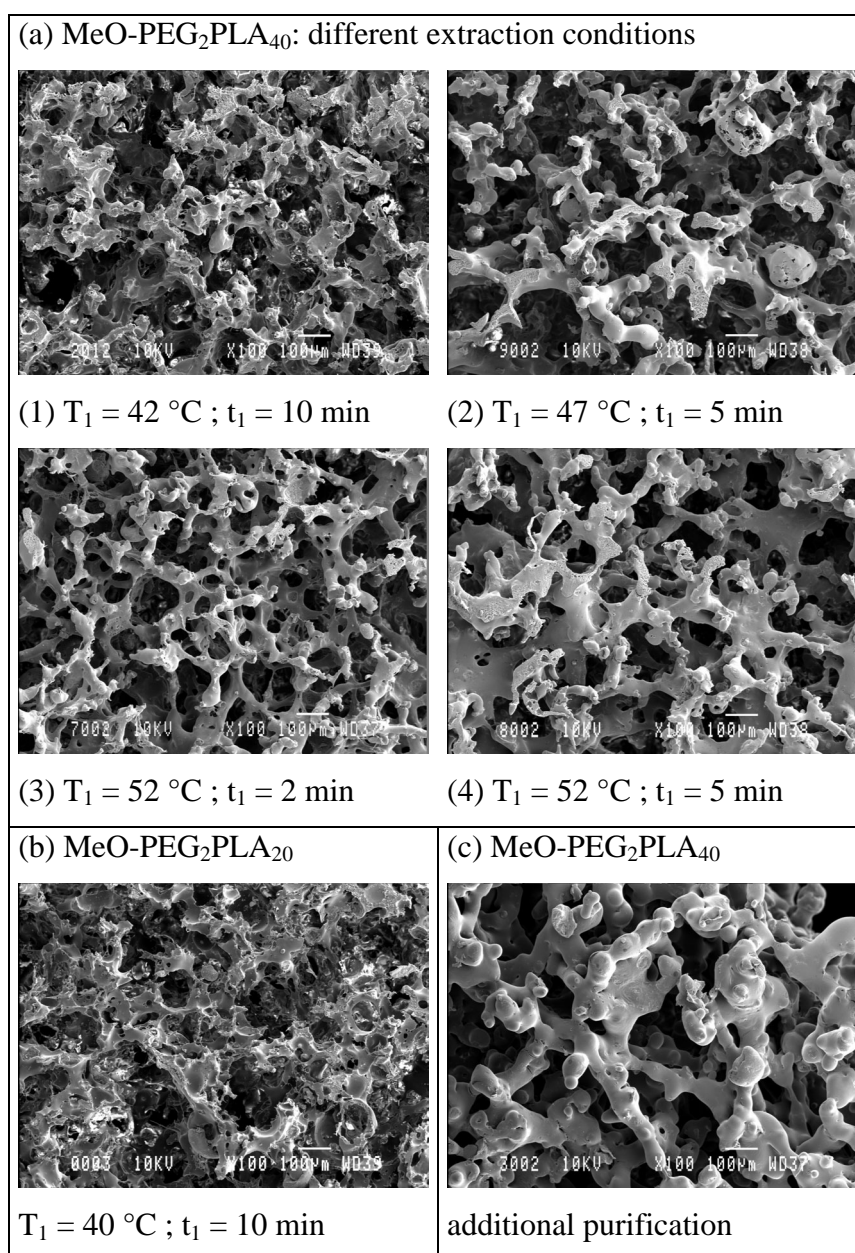


Fig. 4: SEM pictures (original magnification x100) of polymeric scaffolds prepared with P 50 microparticles as porogen: (a) The influence of extraction temperature (1-3) and extraction time (3+4) is shown for MeO-PEG₂PLA₄₀ scaffolds; (b) MeO-PEG₂PLA₂₀ scaffold; (c) MeO-PEG₂PLA₄₀ scaffold after 2h extraction in n-hexane (52°C).

3.1.4. Determination of residual paraffin

Complete paraffin extraction is crucial since this non-physiological material is non-biodegradable and is known to cause mineral oil granuloma (paraffinoma) [32,33] after parenteral application. To find out how complete the paraffin extraction had been, DSC analysis was employed to detect melting peaks of potential paraffin remnants inside fabricated scaffolds. To distinguish between paraffin melting and polymer relaxation, which both appeared as endothermic signals at about the same temperature during the first heating cycle, we analyzed the second heating cycle of every DSC run. In that cycle, relaxation phenomena were minimized due to controlled cooling after the first set of heating cycles. Since we aimed for quantification of porogen residuals, different mixtures of MeO-PEG₂PLA₄₀ and P 50 particles were prepared and analyzed in order to correlate the paraffin content with its melting enthalpy (the area under the melting peak). A linear correlation was found for the investigated area of 0.2 – 13.5 % paraffin (Fig. 5).

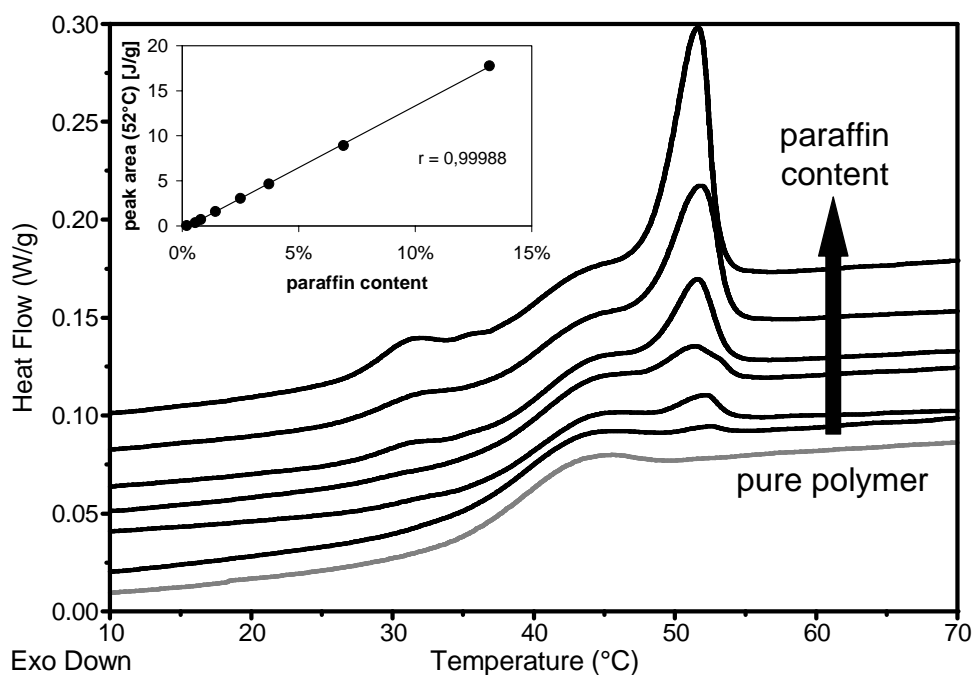


Fig. 5: DSC analysis of pure polymer and different MeO-PEG₂PLA₄₀ – P 50 microparticle mixtures (P 50 content: 0.2 – 4 %) used for calibration. Inserted figure shows the correlation between paraffin content of the mixtures and area under the melting peak.

In a typical thermogram of fabricated MeO-PEG₂PLA₄₀ scaffolds, the endothermic melting peaks (main + side fraction) of paraffin were detected surrounding the glass transition step of the diblock copolymer, indicating the presence of paraffin remnants (Fig. 6). As expected, these melting peaks were shifted towards lower temperatures relative to the pure particles. When no further purification steps were applied, paraffin remnants ranging from 2.5 % to 8 %

were found in the scaffolds. Even the application of thorough washing procedures such as 2h extraction in *n*-hexane at 52 °C, did not reduce the residual paraffin to below 1.8 – 2 %. These washing techniques, however, did cause strong alterations in the scaffold's microstructure (Fig. 4 c).

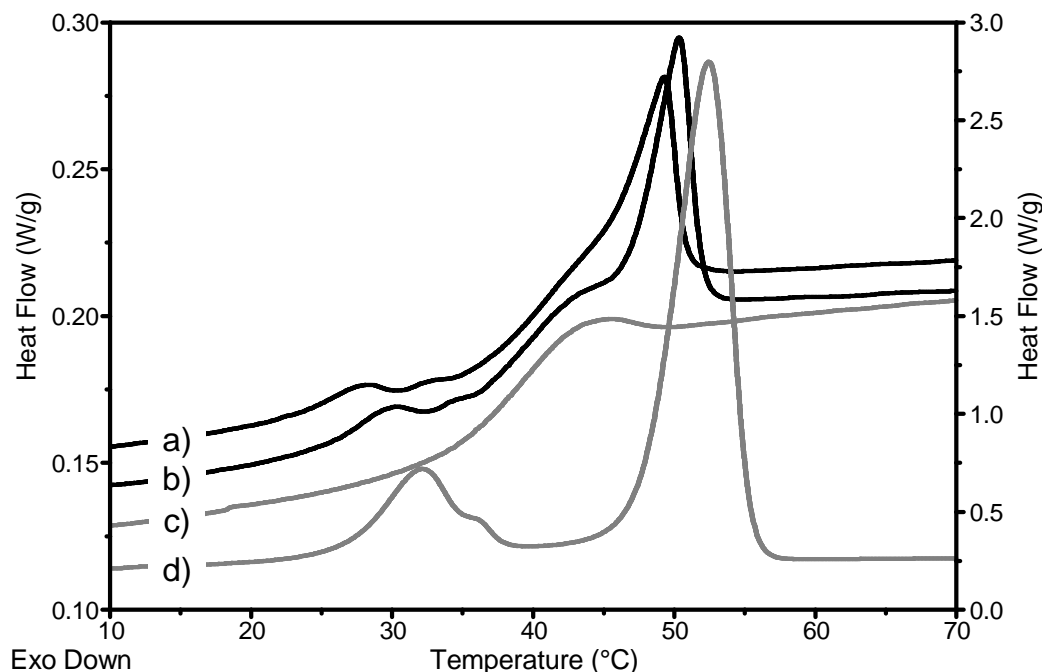


Fig.6: DSC thermograms obtained from (b) MeO-PEG₂PLA₄₀ scaffold after standard processing, (a) MeO-PEG₂PLA₄₀ scaffold after 2h extraction in *n*-hexane (52°C) and (c) pure MeO-PEG₂PLA₄₀ polymer (left axis). (d) Thermogram of P 50 microparticles (right axis).

To summarize the results concerning the suitability of hard paraffin as a porogen material for the processing of low molecular weight polymers, one can ascertain that besides the low biocompatibility of paraffin, it also lacked the flexibility in melting points necessary for the investigated polymers. Although we achieved well interconnected scaffolds with MeO-PEG₂PLA₄₀, considerable amounts of paraffin remained in the scaffolds even after extensive washing steps. Due to the large difference between the T_g of the polymer and the melting point of the porogen, we did not manage to obtain interconnected scaffolds with polymers of lower molecular weight, such as MeO-PEG₂PLA₂₀.

3.2. Scaffold fabrication using triglyceride mixtures as porogen material

The second aim of this study was the development of a new processing method in order to overcome the problems limiting the hydrocarbon templating technique. Paraffin was exchanged for physiologically tolerated triglycerides, which are known to serve as parenteral drug carriers in the form of solid lipid nanoparticles [34,35]. To further improve the physiological tolerance of scaffolds fabricated using this method, we also replaced the acetone – chloroform mixture used as polymer solvent with an ethyl methyl ketone (EMK) - tetrahydrofurane (THF) mixture (59:41) (v/v). In contrast to chloroform or methylene chloride, both solvents - EMK and THF - are classified as low toxic according to the ICH guideline Q3C [36].

3.2.1. Preparation and characterization of lipid microparticles

The first task was to identify triglycerides providing both a modest solubility in the polymer solvent and suitable melting properties. Particles from pure triglycerides (Dynasan[®]) and lipid mixtures (Witepsol[®], Softisan[®]) were prepared and analyzed with regard to their solubility in the polymer solvent mixtures and melting point according to DSC analysis. By blending different lipids, melting points were easily made variable within a certain range. As a measure for the solubility of the porogen microparticles in the polymer solvent, the screening method described in the paraffin section was applied. All lipid microparticles were obtained as a free flowing powder in contrast to the hard paraffin particles. No significant differences between bulk and particle melting points were observed with DSC analysis (data not shown).

Two general trends became obvious from these investigations. Firstly, following comparisons made within one class of lipids, such as the Dynasan[®] types or the mixed lipids, we found that the solubility generally increased with decreasing melting temperature, as was previously observed for the hard paraffin types (Fig. 3). The solubility of all particles tested in the EMK - THF mixture was slightly increased relative to the acetone - chloroform system. Secondly, pure triglycerides composed of only one type of fatty acid, therefore representing the better specified class of triglycerides, such as Dynasan[®] 114 and 116, appeared to have a higher degree of solubility than mixed triglycerides with a comparable melting point. More specifically, the solubility of Dynasan 114 particles was remarkably high, especially in the EMK - THF mixture, in spite of its relatively high melting temperature of above 50 °C. Dynasan 116 particles were only sparingly soluble in the tested solvent mixture, which was, however, irrelevant because its melting temperature was unacceptably high. Thus, Dynasan[®]

114 and 116 were classified as non-suitable porogen materials. Among the commercially available lipid mixtures which were tested alternatively, we chose Softisan[®] 154 and Witepsol[®] H 42, both of which had a triglyceride content of more than 95% and contained no monoglycerides or additional emulsifying agents (Table 2). Despite the high solubility of Witepsol[®] H 42, it was mixed with Softisan[®] 154 to prepare microparticles with a melting point of below 50°C. DSC analysis of microparticles prepared from such Witepsol[®] - Softisan[®] mixtures revealed a linear correlation between particle composition and melting point (Fig. 7). However, the solubility of these particles increased nonlinearly and only slowly with increasing Witepsol[®] content up to 50% (Fig. 7) under the applied conditions. The solubility of particles from a 1:1 mixture was below 15 mg in 5 ml of the EMK - THF solvent mixture. These particles were used for further experiments.

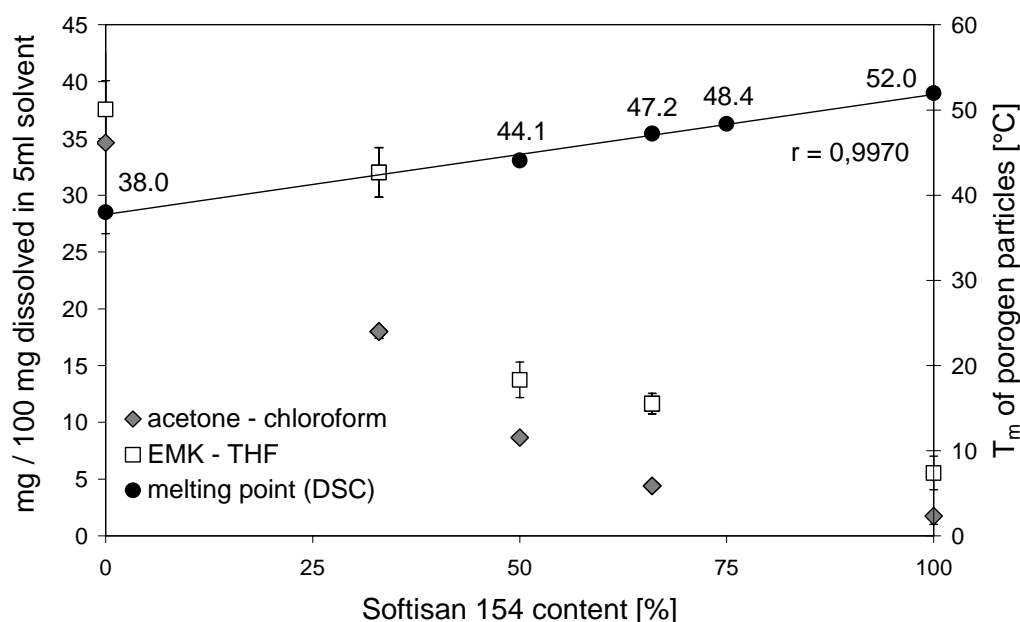


Figure 7: Determined solubility in two different solvent mixtures (left axis) and melting points (DSC) (right axis) of microparticles prepared from different mixtures of Witepsol[®] H42 and Softisan[®] 154. Symbols (◆ and □) and error bars represent means \pm SD for $n = 3$.

3.2.2. Determination of processing parameters and scaffold microstructure

The determined processing parameters are summarized in Table 3. Generally, the use of the described 1:1 triglyceride mixture (Witepsol[®]: Softisan[®]) as porogen material allowed for the desired reduction of extraction temperature approaching the glass transition temperatures of the investigated polymers.

Due to the increased density of the used lipids relative to paraffin (Table 2), sedimentation of molten porogen material in the polymer constructs was observed during scaffold processing

with the consequence of large cavity formation at the bottom of the constructs (Fig. 8 a). Two alterations of the processing method were necessary to suppress this phenomenon, both resulting in a viscosity increase of the dispersion of porogen microparticles in polymer solution. Firstly, the polymer to porogen ratio was increased from 17.6 % to 25 % in the case of MeO-PEG₂PLA₄₀ and to 33 % to process MeO-PEG₂PLA₂₀. Secondly, the filled molds were pre-treated in ice-cooled *n*-hexane (0 °C) for 90 minutes prior to porogen extraction (Fig. 2 (*)). Under these conditions the polymer solvent was partly extracted, causing the polymer concentration to further increase, while the porogen microparticles appeared to remain unchanged. Only the combination of these steps was successful in preventing lipid droplet sedimentation (Fig. 8 b).

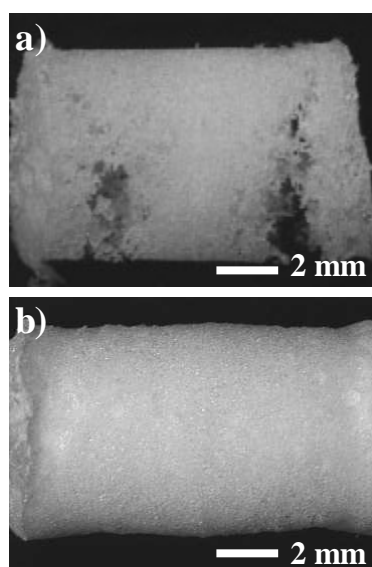


Fig. 8: Light micrographs (original magnification $\times 6$) of MeO-PEG₂PLA₄₀ scaffolds fabricated with particles from a 1:1 mixture (Witepsol : Softisan) as porogens: (a) no pre-extraction treatment; (b) 90 min in *n*-hexane (0 °C) before porogen extraction.

Processing of MeO-PEG₂PLA₄₀ with lipid microparticles was now possible at an extraction temperature $T_1 = 40$ °C close to the T_g (42.3 °C) of the polymer. Under these conditions, we obtained stable scaffolds providing an interconnected pore structure (Fig. 9 a/2). In accordance with the trend observed during polymer processing with paraffin microparticles scaffold permeability was compromised when the extraction temperature had been lowered to 35 °C (Fig. 9 a/3), which was nevertheless sufficient to completely extract the porogen. On the other hand, an increase of extraction temperature T_1 up to 45 °C, which could only be applied for a maximum of 10 min, led to an increase in pore interconnectivity (Fig. 9 a/1). This extraction temperature, optimized with regard to T_m (DSC) of the porogen microparticles (44.1 °C; Fig. 7), probably caused coalescence and growth of lipid droplets before their extraction, providing an explanation for the observed changes in scaffold structure.

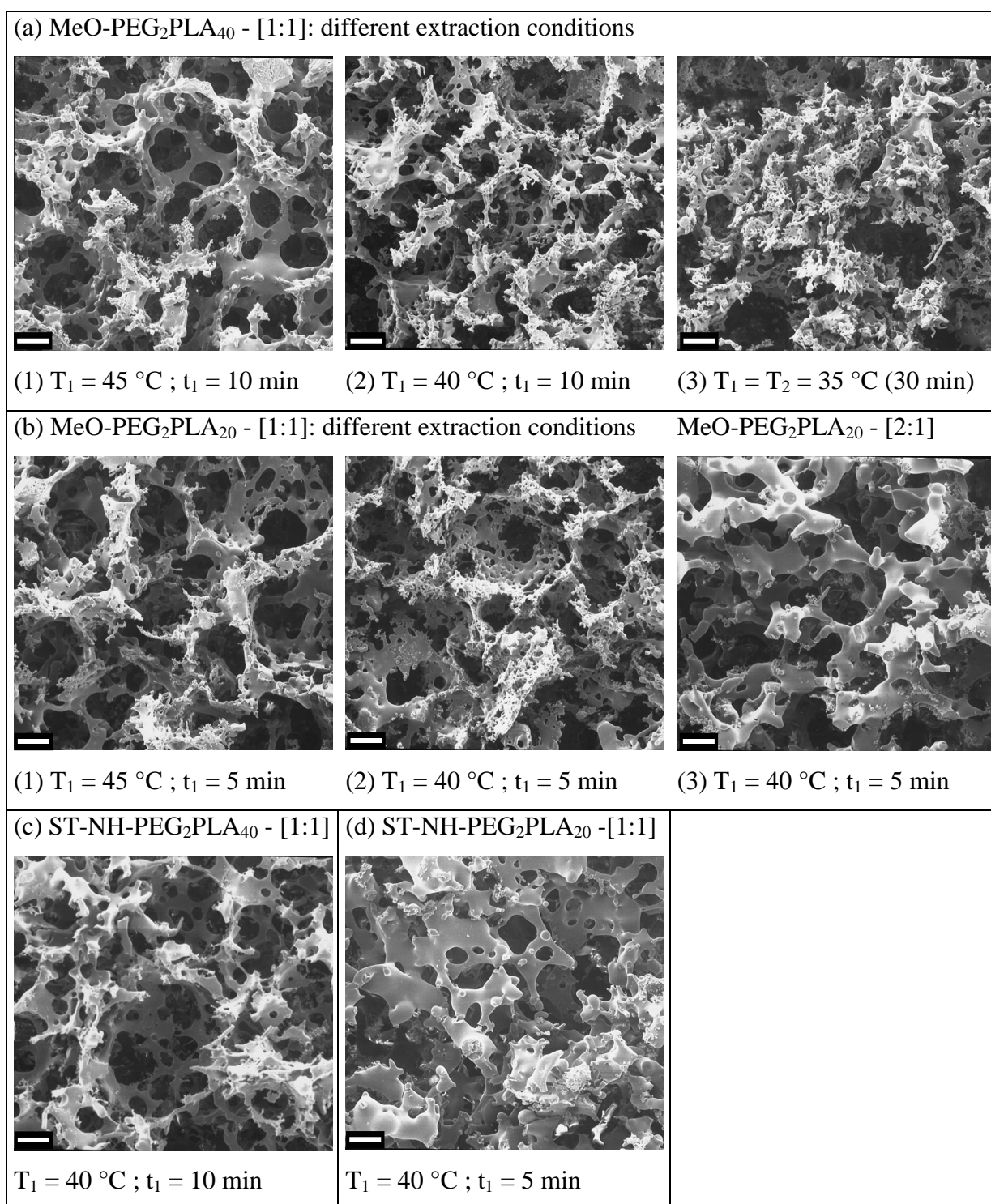


Fig. 9: SEM images (original magnification $\times 100$ – bars represent $100\text{ }\mu\text{m}$) of scaffolds prepared from different polymers with lipid microparticles as porogens: (a) MeO-PEG₂PLA₄₀ with the 1:1 mixture (Witepsol : Softisan) as porogen material; (b) MeO-PEG₂PLA₂₀ with 1:1 mixture and MeO-PEG₂PLA₂₀ with 2:1 mixture; (c) ST-NH-PEG₂PLA₄₀ with 1:1 mixture and (d) ST-NH-PEG₂PLA₂₀ / MeO-PEG₂PLA₂₀ (75:25) with particles from the 1:1 lipid mixture.

As a consequence of the favorable solubility properties of the 1:1 triglyceride mixture, MeO-PEG₂PLA₂₀ was also processed with these porogen microparticles. Consequently, an extraction temperature of $40\text{ }^\circ\text{C}$ or even $45\text{ }^\circ\text{C}$ was necessary to obtain an interconnected pore

structure. Combined with a reduction of t_1 to 5 min, these conditions were applicable without compromising the scaffold structure and interconnected pores were generated (Fig. 9 b/1,2). As observed with MeO-PEG₂PLA₄₀, an extraction temperature above the T_m (DSC) of the porogen material provided optimum pore microstructure.

Processing of MeO-PEG₂PLA₂₀ with different porogen materials further confirmed that even after pre-extraction incubation in *n*-hexane at 0 °C for 90 min, the velocity of porogen melting still had an effect on pore structure. After processing with the 1:1 mixture at 40 °C, the polymer precipitated in between the porogen particles forming wall like structures with some large interconnections and many small perforations (Fig. 9 b/2). On the other hand, condensed polymer structures were found after processing with the 2:1 mixture (Witepsol[®]: Softisan[®]) as porogen material (Fig. 9 b/3), most likely as a result of the accelerated porogen melting forming a continuous phase. Although a closer match of the porogen's melting point and the polymer's T_g was achieved with this 2:1 mixture, the scaffold structure was not much improved since irregular pores had been formed in the scaffold, possibly because of the relatively high degree of solubility of the porogen mixture in the polymer solvent (Fig. 7). Generally, it may be difficult to find triglyceride mixtures fulfilling both the requirement of an even lower melting point than the 1:1 mixture and a comparably low solubility in a polymer solvent. However, polymers with a lower T_g than those used in our study are not common as scaffold materials since they are prone to distortion processes due to a stability loss *in vitro* and *in vivo* at 37 °C. The particular structure of the diblock copolymers containing a hydrophilic swelling PEG chain used in this study may be the reason why scaffolds made from these polymers remained stable after loading with adhesive cells at 37 °C despite a low T_g of approximately 33 °C.

In summary, the MeO-PEG_xPLA_y copolymers of both molecular weights were successfully processed with particles prepared from lipid mixtures. The best results were obtained with the 1:1 mixture of Witepsol[®] H42 and Softisan[®] 154. Even though the DSC determined melting point of these microparticles was only 3 °C below the T_m (DSC) of the initially used P 50 microparticles (Fig. 10), the minimum extraction temperature creating an interconnected pore structure was decreased from 47 °C to 40 °C. Assuming that the formation of a continuous liquid porogen phase during extraction is required for pore interconnectivity, these findings could be explained by differences in these materials' melting behavior. Investigation of the different porogen microparticles revealed a broad melting signal of the triglyceride mixture and three narrow peaks of the hard paraffin (Fig. 10).

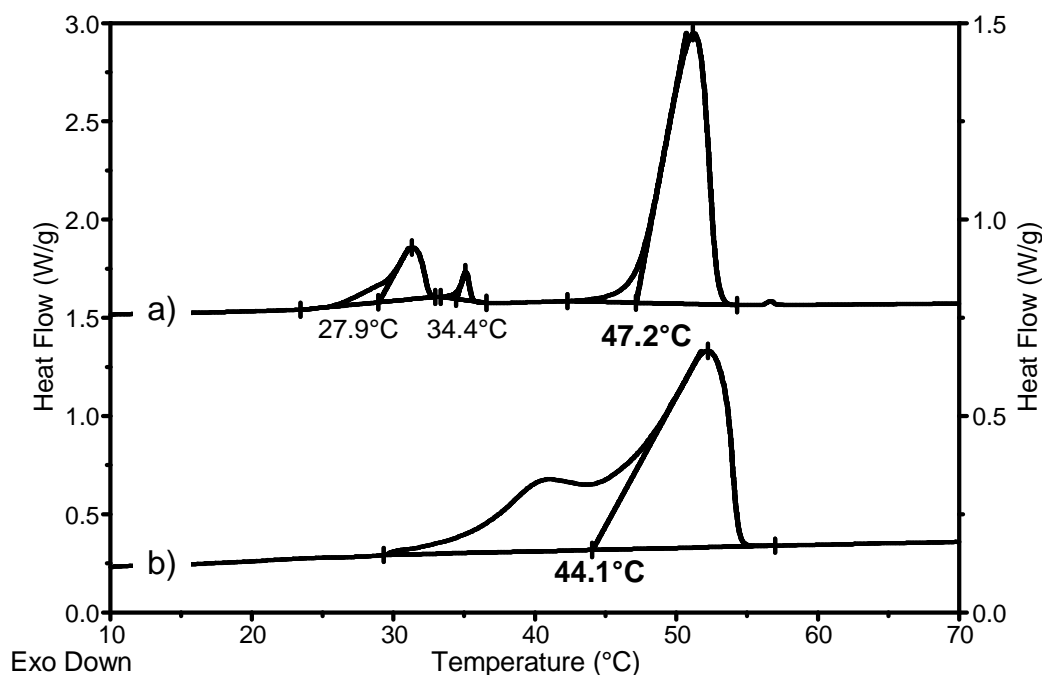


Fig. 10: Thermograms and melting points (bold: main fraction) of porogen microparticles prepared from (a) P 50 (left axis) and (b) the 1:1 mixture (Witepsol : Softisan) (right axis) as obtained from DSC analysis.

In the case of the triglyceride microparticles, a significant fraction of short chain triglycerides were already melted at 40 °C, consequently leading to pore interconnectivity (Fig. 9), while the narrow melting peak of the main fraction of P 50 microparticles explains why interconnected pore structures did not form below 47 °C (Fig. 4).

Although some additional changes were necessary to suppress sedimentation of the porogen particles in the mold, such as the increase of polymer content and pretreatment in cold *n*-hexane, which were expected to impede the scaffold structure, the desired highly porous and interconnected scaffold microstructure has been achieved. The polymers still remained moldable, possibly due to an extraction temperature T_1 close to or above the T_g , and were thus able to adapt to the variable form of the melting and coalescing lipid droplets.

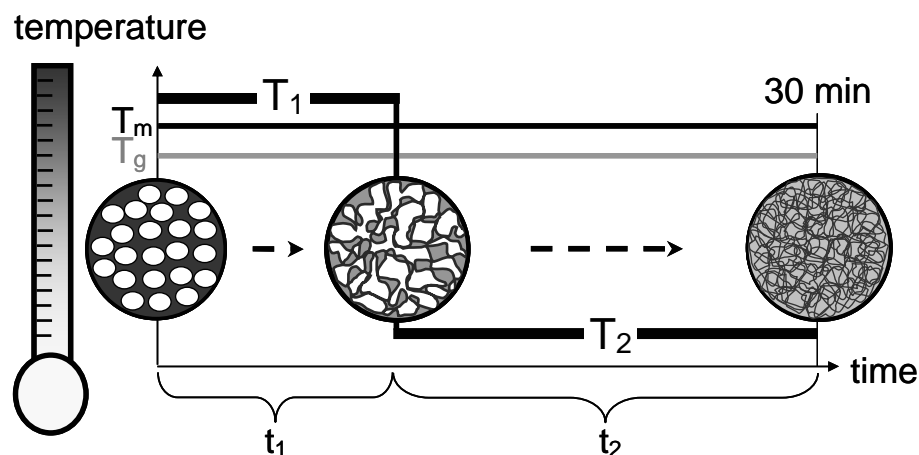


Fig. 11: Temperature course during the two-step extraction procedure. Schematic snapshots of the mold filling at three time points: 0, t_1 and 30 min.

We developed a general two step extraction procedure as shown in figure 11. Ideally, a lipid mixture with a melting point (T_m) close to the glass transition temperature (T_g), is used to prepare porogen microparticles. Extraction conditions should then be chosen in a way, such that extraction starts at T_1 above T_m for a short time t_1 (up to 10 min) and continues at T_2 below T_g for $t_2 = 30 \text{ min} - t_1$. Nevertheless, T_2 must be sufficiently high to allow for complete porogen extraction.

3.2.3. Determination of triglyceride residuals (MDSC)

To detect and quantify triglyceride residuals inside MeO-PEG₂PLA₄₀ scaffolds, MDSC analysis was applied for the following reason: due to the proximity of polymer's T_g to the porogen's T_m (Fig. 12), the endothermic signals of the glass transition step and porogen melting overlap. The amount of residual porogen material could only be calculated from the area under the melting peak appearing in the 2nd heating cycle if it was ensured that every deviation from a linear baseline after the transition step was a result of residual porogen melting and not of relaxation phenomena. In MDSC measurements, such phenomena appear in the total and the non-reversing heat flow, but are eliminated from the reversing heat flow. Consequently, the reversing heat flow of the 2nd heating cycle was analyzed.

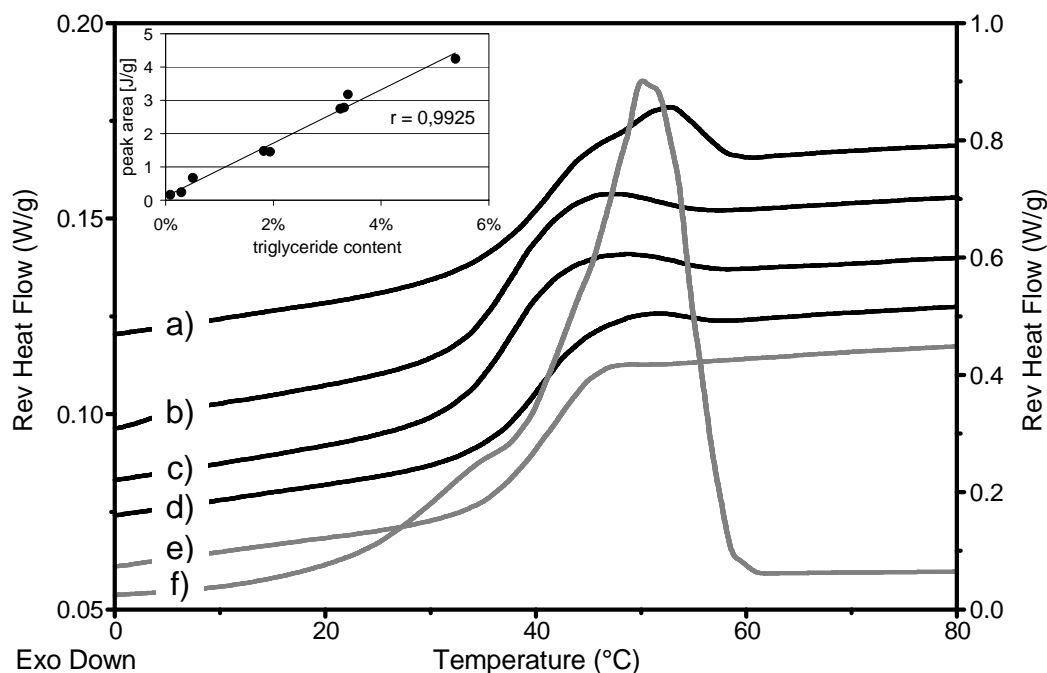


Fig. 12: MDSC thermograms obtained from MeO-PEG₂PLA₄₀ scaffolds (b: $T_1 = T_2 = 35\text{ }^\circ\text{C}$; $t = 30\text{ min}$) (c: $T_1 = 45\text{ }^\circ\text{C}$; $t_1 = 10\text{ min}$), MeO-PEG₂PLA₄₀ mixed with (a) 1.8 % and (d) 0.3 % of microparticles (1:1 mixture) as well as (e) pure MeO-PEG₂PLA₄₀ (left axis). (f) MDSC thermogram of lipid microparticles (1:1 mixture) (right axis). The inserted figure shows the correlation between lipid microparticle content and area under the melting peak.

For calibration, different mixtures of MeO-PEG₂PLA₄₀ and porogen microparticles prepared from the 1:1 lipid mixture (Witepsol[®]: Softisan[®]) were investigated in this way. A linear correlation between area under the melting peak and lipid microparticle content was found between 0.1 - 5.4 % (Fig. 12). In thermograms resulting from such calibration mixtures (Fig. 12 a, d) a concentration dependant melting peak was visible, overlapping the glass transition step of the pure polymer (Fig. 12 e). Hardly any melting peak caused by lipid residuals was found in the analysis of the MeO-PEG₂PLA₄₀ scaffolds, regardless of the extraction conditions (Fig. 12 b, c). Calculations revealed a residual lipid content of $0.7 \pm 0.1\%$. Interestingly, the initial extraction temperature T_1 had no effect on residual porogen content as long as T_2 was sufficient to dissolve the porogen microparticles in *n*-hexane.

Likewise, in MeO-PEG₂PLA₂₀ scaffolds, which were prepared with the same porogen microparticles, less than 1 % of residual porogen material was found (data not shown).

Thus, hardly any remnants of triglycerides, particularly less than found after polymer processing with paraffin microparticles, were detectable in the fabricated scaffolds. Moreover, in contrast to hard paraffin, the residual triglycerides finally undergo metabolism in a biological system. In combination with the low toxic EMK – THF mixture as polymer

solvent, we consider the developed method to be suitable for the fabrication of biocompatible scaffolds. In contrast to the paraffin system, triglyceride mixtures offer sufficient flexibility of melting points and solubility to meet the requirements of different low molecular polymers. Finally, the small-scale processing method presented here is expected to be adaptable to a broad range of established and newly developed polymers of various molecular weights.

3.2.4. *Processing of amine-reactive polymers and scaffold microstructure*

Since the best results in processing MeO-PEG-PLA diblock copolymers were obtained with the 1:1 mixture (Witepsol[®]: Softisan[®]), this porogen material was also used for the processing of the amine-reactive ST-NH-PEG-PLA derivatives (Table 3). Porogen microparticles were extracted at $T_1 = 40\text{ °C}$ for $t_1 = 10\text{ min}$ when ST-NH-PEG₂PLA₄₀ was processed and at $T_1 = 40\text{ °C}$ for $t_1 = 5\text{ min}$ to fabricate scaffolds from ST-NH-PEG₂PLA₂₀. These mild extraction conditions, shown to be sufficient in generating permeable pore structures inside MeO-PEG_xPLA_y scaffolds (Fig. 9 b, e), were chosen with regard to the lower T_g of both ST-NH-PEG_xPLA_y copolymers compared with their MeO-PEG_xPLA_y derivatives (Table 1). Furthermore, the polymer to porogen ratio was increased in order to suppress sedimentation and to ensure scaffold stability. Applying these modified conditions, scaffolds from pure ST-NH-PEG₂PLA₄₀ were successfully prepared. In the case of ST-NH-PEG₂PLA₂₀, however, a blend containing 25 % of MeO-PEG₂PLA₂₀ was necessary to obtain stable scaffolds.

Scanning electron microscopy showed a permeable pore microstructure inside ST-NH-PEG₂PLA₄₀ (Fig. 9 g) and ST-NH-PEG₂PLA₂₀ (Fig. 9 h) scaffolds. The pore structure of the ST-NH-PEG₂PLA₄₀ scaffolds in particular was comparable to the microstructures inside scaffolds prepared from MeO-PEG₂PLA₄₀ under the same extraction conditions.

3.2.5. *Pore size distribution and porosity*

Mercury intrusion porosimetry displayed a close correspondence between pore size distribution and porogen particle size in all investigated scaffolds. Scaffolds from MeO-PEG₂PLA₄₀ and ST-NH-PEG₂PLA₄₀ as well as MeO-PEG₂PLA₂₀ scaffolds showed a nearly identical pore size distribution, corresponding well with the size distribution (determined by laser diffraction) of the porogen microparticles used for their fabrication (Fig. 13). Additionally, a porosity of between 85 and 90 % was calculated for the investigated scaffolds.

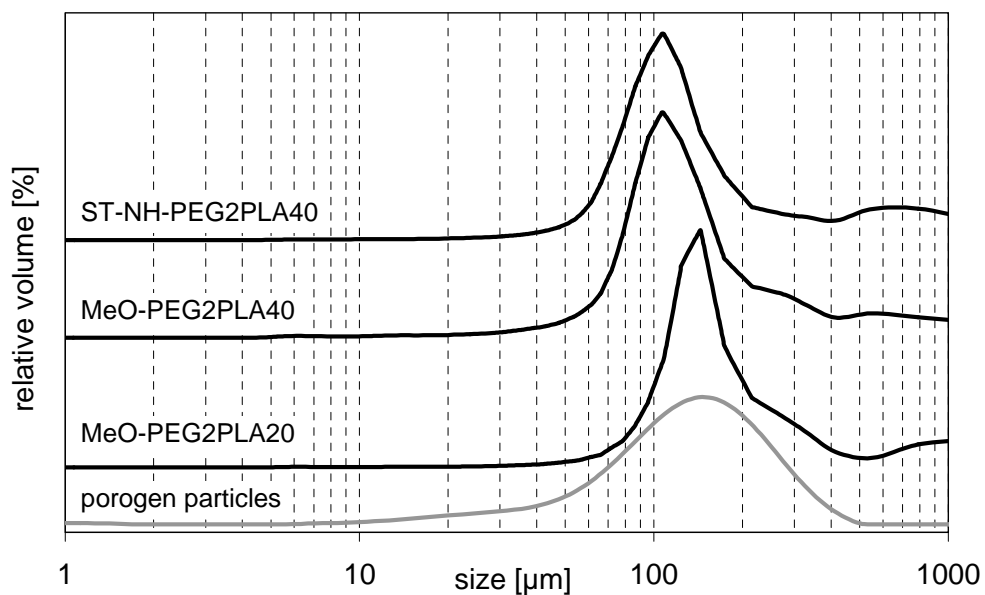


Fig. 13: Pore size distribution inside different scaffolds as obtained by mercury intrusion porosimetry. Porogen microparticle (1:1 mixture) size distribution as measured by laser diffraction.

3.3. Instant surface modification

Finally, our study aimed at proving the principle of instant protein attachment from an aqueous solution to the surface of a preformed scaffold with insulin as model protein. Therefore, scaffolds were submerged in a buffered (pH = 8) solution of insulin. After washing and freeze drying, GPC analysis was applied to detect covalently bound insulin. Adsorbed insulin was precipitated during sample preparation. In chromatograms of incubated ST-NH-PEG₂PLA₂₀ scaffolds, a strong fluorescence signal at the elution volume of the polymers (13 – 14 min) was detected (Fig. 14).

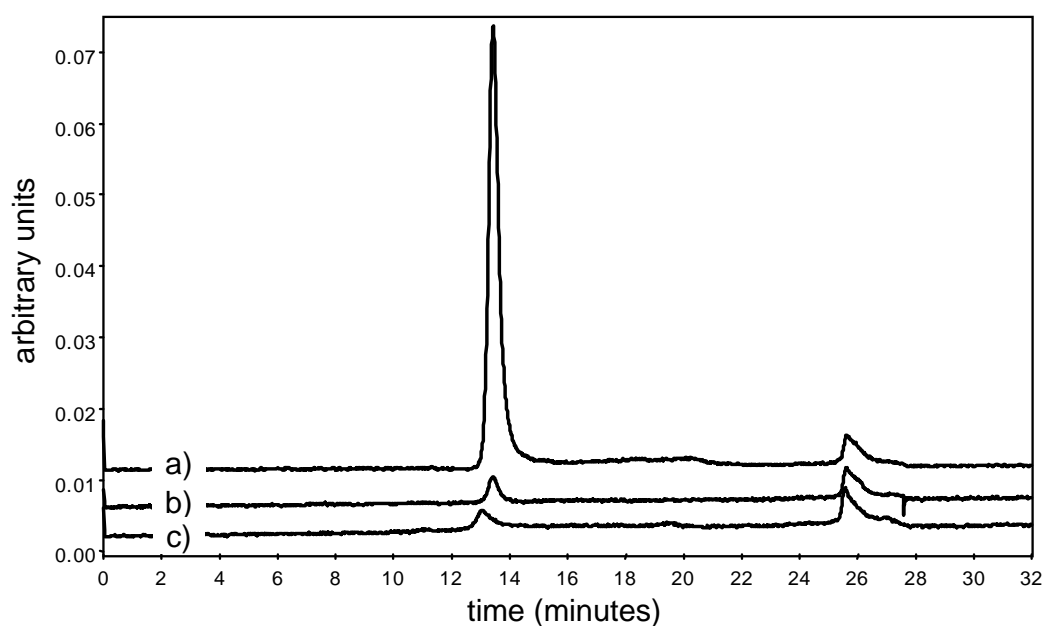


Fig. 14: Chromatograms of human insulin covalently attached to amine reactive scaffolds (fluorescence detection). (a) ST-NH-PEG₂PLA₂₀ + insulin; (b) ST-NH-PEG₂PLA₂₀ + buffer; (c) MeO-PEG₂PLA₂₀ + insulin.

Analysis of ST-NH-PEG₂PLA₄₀ scaffolds revealed similar results (data not shown) but signal intensity normalized to scaffold weight was lower. This decrease is most likely a result of the lower density of active groups on the scaffold surface when ST-NH-PEG₂PLA₄₀ with a molecular weight of 42 kDa is used instead of ST-NH-PEG₂PLA₂₀ (22 kDa). Thus, polymer reactivity was maintained during processing. Furthermore, the concept of instant protein binding from buffered solutions to a prefabricated scaffold was demonstrated.

Insulin was chosen as model substance because an insulin sensitive three-dimensional cartilage engineering model system has been developed [37], in which the biological activity of such surface modified scaffolds should be tested in future experiments.

4. Conclusions

We were able to process amine-reactive ST-NH-PEG-PLA diblock copolymers and their non-reactive MeO-PEG-PLA derivatives into stable and highly porous scaffolds using an anhydrous porogen leaching technique. ST-NH-PEG-PLA scaffolds were proven to be amine-reactive after scaffold fabrication. This enables us to fabricate scaffolds for future applications which can be easily conjugated with molecules containing free amine groups immediately preceding implantation or use in cell culture experiments.

We demonstrated the superiority of triglyceride mixtures relative to paraffin as porogen materials for scaffold fabrication especially with low molecular weight biodegradable polymers. Their physiological tolerance and applicability in fabricating free flowing microparticles of matching solubility and various melting points are outstanding characteristics of such triglyceride blends. We showed that initial porogen melting at extraction temperature was important in obtaining interconnected pore structures. However, working with low molecular weight polymers requires careful consideration of the extraction conditions. By combining high and low extraction temperatures with varying durations, as well as using porogen materials with melting points near the glass transition temperature of the polymer, the processing parameters were adapted to polymer properties.

5. Acknowledgements

The authors would like to thank Aventis Research & Technologies, Germany and the Bundesministerium für Bildung und Forschung (BMBF) who sponsored this work. Special thanks are due to Dr. D. Rose from the Working unit Material Investigation, University of Regensburg, Germany for SEM images of the scaffolds fabricated using hard paraffin microparticles. Thanks also go to SASOL Germany GmbH, Witten, Germany for providing Dynasan[®], Witepsol[®] and Softisan[®] and to Micromeritics, Mönchengladbach, Germany for mercury intrusion porosimetry.

6. References

- (1) Langer R, Vacanti JP. 'Tissue engineering'. *Science* (1993); **260**: 920-926.
- (2) Hubbell JA. 'Biomaterials in tissue engineering'. *Biotechnology (N Y)* (1995); **13**: 565-576.
- (3) Quirk RA, Chan WC, Davies MC, Tendler SJ, Shakesheff KM. 'Poly(L-lysine)-GRGDS as a biomimetic surface modifier for poly(lactic acid)'. *Biomaterials* (2001); **22**: 865-872.
- (4) Kantlehner M, Schaffner P, Finsinger D, Meyer J, Jonczyk A, Diefenbach B, Nies B, Holzemann G, Goodman SL, Kessler H. 'Surface Coating with Cyclic RGD Peptides Stimulates Osteoblast Adhesion and Proliferation as well as Bone Formation'. *Chembiochem* (2000); **1**: 107-114.
- (5) Shin MS, Kim SJ, Park SJ, Lee YH, Kim SI. 'Synthesis and characteristics of the interpenetrating polymer network hydrogel composed of chitosan and polyallylamine'. *J Appl Polym Sci* (2002); **86**: 498-503.
- (6) Massia SP, Stark J. 'Immobilized RGD peptides on surface-grafted dextran promote biospecific cell attachment'. *J Biomed Mater Res* (2001); **56**: 390-399.
- (7) Olbrich KC, Andersen TT, Blumenstock FA, Bizios R. 'Surfaces modified with covalently-immobilized adhesive peptides affect fibroblast population motility'. *Biomaterials* (1996); **17**: 759-764.
- (8) Zisch AH, Schenk U, Schense JC, Sakiyama-Elbert SE, Hubbell JA. 'Covalently conjugated VEGF-fibrin matrices for endothelialization'. *J Control Release* (2001); **72**: 101-113.
- (9) von-Recum H, Kikuchi A, Yamato M, Sakurai Y, Okano T, Kim SW. 'Growth factor and matrix molecules preserve cell function on thermally responsive culture surfaces'. *Tissue Eng* (1999); **5**: 251-265.
- (10) Sakiyama ES, Hubbell JA. 'Development of fibrin derivatives for controlled release of heparin-binding growth factors'. *J Control Release* (2000); **65**: 389-402.
- (11) Schense JC, Hubbell JA. 'Three-dimensional migration of neurites is mediated by adhesion site density and affinity'. *J Biol Chem* (2000); **275**: 6813-6818.
- (12) Rowley JA, Madlambayan G, Mooney DJ. 'Alginate hydrogels as synthetic extracellular matrix materials'. *Biomaterials* (1999); **20**: 45-53.
- (13) Gopferich A, Peter SJ, Lucke A, Lu L, Mikos AG. 'Modulation of marrow stromal cell function using poly(D,L-lactic acid)-block-poly(ethylene glycol)-monomethyl ether surfaces'. *J Biomed Mater Res* (1999); **46**: 390-398.

- (14) Lucke A, Tessmar J, Schnell E, Schmeer G, Gopferich A. 'Biodegradable poly(,-lactic acid)-poly(ethylene glycol)-monomethyl ether diblock copolymers: structures and surface properties relevant to their use as biomaterials'. *Biomaterials* (2000); **21**: 2361-2370.
- (15) Lieb E, Tessmar J, Hacker M, Fischbach C, Rose D, Blunk T, Mikos AG, Goeperich A, Schulz MB. 'Poly(D,L-lactic acid)-Poly(ethylene glycol)-Monomethyl Ether Diblock Copolymers Control Adhesion and Osteoblastic Differentiation of Marrow Stromal Cells'. *Tissue Eng* (2003); **9**: 71-84.
- (16) Tessmar JK, Mikos AG, Goeperich A. 'Amine-Reactive Biodegradable Diblock Copolymers'. *Biomacromolecules* (2002); **3**: 194-200.
- (17) Hermanson GT. *Bioconjugate techniques*. San Diego: Academic Press, 1996.
- (18) Greenwald RB. 'PEG drugs: an overview'. *J Control Release* (2001); **74**: 159-171.
- (19) Bailon P, Berthold W. 'Polyethylene glycol-conjugated pharmaceutical proteins'. *Pharm Sci Technol Today* (1998); **1**: 352-356.
- (20) Kellner K, Liebsch G, Klimant I, Wolfbeis OS, Blunk T, Schulz MB, Gopferich A. 'Determination of oxygen gradients in engineered tissue using a fluorescent sensor'. *Biotechnol Bioeng* (2002); **80**: 73-83.
- (21) Obradovic B, Carrier RL, Vunjak-Novakovic G, Freed LE. 'Gas exchange is essential for bioreactor cultivation of tissue engineered cartilage'. *Biotechnol Bioeng* (1999); **63**: 197-205.
- (22) Lu L, Mikos AG. 'The importance of New Processing Techniques in Tissue Engineering'. *MRS Bull* (1996); **21**: 28-32.
- (23) Goldstein AS, Zhu G, Morris GE, Meszlenyi RK, Mikos AG. 'Effect of osteoblastic culture conditions on the structure of poly(DL-lactic-co-glycolic acid) foam scaffolds'. *Tissue Eng* (1999); **5**: 421-434.
- (24) Widmer MS, Gupta PK, Lu L, Meszlenyi RK, Evans GR, Brandt K, Savel T, Gurlek A, Patrick-CW J, Mikos AG. 'Manufacture of porous biodegradable polymer conduits by an extrusion process for guided tissue regeneration'. *Biomaterials* (1998); **19**: 1945-1955.
- (25) Sheridan MH, Shea LD, Peters MC, Mooney DJ. 'Bioabsorbable polymer scaffolds for tissue engineering capable of sustained growth factor delivery'. *J Control Release* (2000); **64**: 91-102.
- (26) Harris LD, Kim BS, Mooney DJ. 'Open pore biodegradable matrices formed with gas foaming'. *J Biomed Mater Res* (1998); **42**: 396-402.
- (27) Shastri VP, Martin I, Langer R. 'Novel versatile process for the production of polymer foams'. *Mat Res Soc Proc* (1999); **550**: 149-153.
- (28) Ma PX, Choi JW. 'Biodegradable polymer scaffolds with well-defined interconnected spherical pore network'. *Tissue Eng* (2001); **7**: 23-33.

-
- (29) Shastri VP, Martin I, Langer R. 'Macroporous polymer foams by hydrocarbon templating'. *Proc Natl Acad Sci U S A* (2000); **97**: 1970-1975.
- (30) Martin I, Shastri VP, Padera RF, Yang J, Mackay AJ, Langer R, Vunjak-Novakovic G, Freed LE. 'Selective differentiation of mammalian bone marrow stromal cells cultured on three-dimensional polymer foams'. *J Biomed Mater Res* (2001); **55**: 229-235.
- (31) Hiaki T, Kurihara K, Kojima K. 'Vapor-Liquid Equilibria for Acetone + Chloroform + Methanol and Constituent Binary Systems at 101.3 kPa'. *J Chem Eng Data* (1994); **39**: 714-719.
- (32) Ho WS, Chan AC, Law BK. 'Management of paraffinoma of the breast: 10 years' experience'. *Br J Plast Surg* (2001); **54**: 232-234.
- (33) Munchow H. 'Paraffin-oil damage to tissue as in the example of calcified paraffinomas in mammae'. *Radiol Diagn (Berl)* (1966); **7**: 743-747.
- (34) Muller RH, Mader K, Gohla S. 'Solid lipid nanoparticles (SLN) for controlled drug delivery - a review of the state of the art'. *Eur J Pharm Biopharm* (2000); **50**: 161-177.
- (35) Mehnert W, Mader K. 'Solid lipid nanoparticles; Production, characterization and applications'. *Adv Drug Delivery Rev* (2001); **47**: 165-196.
- (36) International Conference on Harmonisation of technical requirements for registration of pharmaceuticals for human use. *ICH harmonized Tripartite Guideline (Q3C) Impurities: Residual solvents*. Draft 4 (1997). Available from <http://www.ich.org>
- (37) Kellner K, Schulz MB, Gopferich A, Blunk T. 'Insulin in tissue engineering of cartilage: A potential model system for growth factor application'. *J Drug Targeting* (2001); **9**: 439-448.

Chapter 4

Hansen Solubility Parameters as a Means to Replace Halogenated Solvents in Biomaterial Processing

Michael Hacker¹, Andrea Blaimer¹, Michaela B. Schulz^{1,2}, Achim Göpferich¹

¹ Department of Pharmaceutical Technology, University of Regensburg,
Universitaetsstrasse 31, 93040 Regensburg, Germany

² Department of Pharmaceutical Technology, University of Graz,
Schubertstrasse 6, 8010 Graz, Austria

Abstract

Hansen solubility parameters (HSPs) are accepted tools to describe the thermodynamic interactions between solvent molecules and polymers. In this study, these parameters were employed to systematically replace halogens and other toxic solvents used in an established scaffold fabrication technique with solvents with a low toxicity rating (ICH guideline Q3C) without any changes to the other processing parameters. To systematically search for solvent alternatives, the HSPs of the original solvent mixture were calculated and compared to the parameters of 26 class 3 solvents and binary mixtures thereof. The HSPs of a mixture containing methyl ethyl ketone 59% (v/v) and tetrahydrofurane 41% (v/v) were found to most closely fit the parameters calculated for the original acetone-chloroform-mixture. Using the alternative solvent mixture, poly(lactic-*co*-glycolic acid) and monomethyl ether-poly(ethylene glycol)-*co*-poly(lactic acid) could be processed into tissue engineering scaffolds without further changes to the procedure. Importantly, the solvent exchange only minimally affected the macro- and microstructure of the resulting scaffolds.

1. Introduction

Since 1970, when poly(glycolic acid) (PGA) was approved by the FDA for the use as a degradable suture material, the application of biodegradable polymers, especially poly(α -hydroxy acids), has proliferated throughout the biomaterial and medical sciences [1,2]. A plethora of drug release devices, orthopedic implants and fixation devices as well as cell carriers for tissue engineering applications have been fabricated from these materials [3-7]. Since lipophilic materials are not water-soluble, they must be processed either in their molten state or dissolved in organic solvents. In particular, the fabrication of microparticles and tissue engineering scaffolds from biodegradable polymers often employs halogenated solvents, such as methylene chloride and chloroform [8,9]. The elimination of these toxic solvents from such fabrication procedures, however, is necessary to avoid risks to human health and minimize any influence on the physicochemical properties of the product, such as microstructure, storage stability or the stability of encapsulated substances [10]. In tissue engineering applications, residual solvents may compromise cell development on the polymeric carriers. Due to their toxicity, regulatory authorities strictly limit halogenated solvent residuals. The International Conference on Harmonization (ICH), a project that brought together the regulatory authorities of Europe, Japan and the United States, published a guideline for residual solvents [11] that classifies the chemicals on the basis of their toxicity and gives exposure limits for each solvent. Halogenated solvents, such as methylene chloride and chloroform, are categorized as 'solvents to be limited' (class 2 solvents). Less toxic chemicals are labeled as class 3 solvents by this guideline (Table 1). Therefore, class 3 solvents should be used to replace halogenated solvents in biomaterial processing wherever possible.

This study particularly aimed at eliminating chloroform from a recently developed scaffold fabrication procedure [12]. This anhydrous porogen leaching technique allows for the processing of poly(lactic-co-glycolic acid) (PLGA) and diblock copolymers consisting of poly(ethylene glycol) (PEG) and poly(lactic acid) (PLA) into macroporous cell carriers (scaffolds) with an interconnected pore structure. In the first step of the process, an azeotropic mixture containing 65% (v/v) acetone and 35% (v/v) chloroform is used to dissolve the polymers. Solid lipid microparticles, the pore forming templates, are dispersed in the polymer solution and the dispersion is transferred into molds. Polymer precipitation and microparticle extraction are simultaneously initiated by submerging the molds in warm *n*-hexane [12]. To obtain macroporous, form-filling scaffolds, processes like solvent extraction, phase separation and porogen extraction have been carefully examined and related to each other during this

processing step. The process temperature and solvent composition are the key parameters in controlling these processes. With regard to the ICH guideline, we aimed at replacing chloroform by exclusively using class 3 solvents or mixtures thereof. However, the previously determined parameters for polymer processing should remain applicable. We hypothesized that by employing a solvent or a solvent mixture with solubility and miscibility properties comparable to the established acetone-chloroform-mixture, the substitution could successfully be accomplished. To avoid laborious empirical screenings, Hansen solubility parameters (HSPs) were used for a systematical search. We calculated the HSPs of the original acetone-chloroform-mixture and compared them to the parameters of 26 class 3 solvents and binary mixtures thereof. The solvent mixture, which most closely fit the acetone-chloroform-mixture, was used for PLGA and MeO-PEG-PLA processing without additional parameter changes. The macro- and microstructure of the resulting scaffolds was examined to determine the effect of the solvent exchange. Several class 3 solvents, which have similar HSPs to the acetone-chloroform-mixture, were also tested as polymer solvents.

2. Theory

The solubility parameter theory was originally established to describe the enthalpy of mixing of nonpolar, nonassociated solvents, but has been extended to apply to polar solvents and polymers. In coatings and paint technology, the solubility parameter is important for the selection of solvents and polymer plasticizers as well as to predict polymer and solvent compatibility with dyes, nonionic emulsifiers and pigments.

Hildebrand defined the total solubility parameter (δ) as the square root of the cohesive energy density (CED) [13], which is equal to the energy of vaporization (ΔE^v) per molar volume (V_m):

$$\delta = \sqrt{CED} = \sqrt{\frac{\Delta E^v}{V_m}} \quad (1)$$

The solubility parameter is a measure of all the intermolecular forces responsible for the material cohesion.

To predict interactions between two solvents or a solvent and a polymer, the difference between the solubility parameters of the molecules is determined. Similar solubility parameter values, resulting in a small difference, indicate strong interactions, meaning that two solvents are miscible or that the polymer will dissolve in the solvent.

With the objective of describing the quality of the interaction between two molecules more precisely, the total solubility parameter was decomposed into several terms representing different contributions to the free energy of mixing [14]. In the three-parameter (three-dimensional) Hansen approach, the interaction capacity of a compound arises from three partial solubility parameters that quantitatively describe the non-polar, dispersive interactions (δ_d), permanent dipole-dipole interactions (δ_p), and the hydrogen bonding forces (δ_h) [15-18].

The total solubility parameter is related to the partial ones by the following equation:

$$\delta_{total}^2 = \delta_d^2 + \delta_p^2 + \delta_h^2 \quad (2)$$

The values of the HSPs for many solvents were calculated from a large number of solubility data sets and are tabulated in literature [19]. In Table 1, the HSPs for the ICH class 3 solvents are listed based on published data [19]. Polymer solubility parameters can also be decomposed to a three-term set. Determination of this data, however, is a difficult and laborious undertaking. Nevertheless, the published total solubility parameter value of PLA is $9.8 - 10.2 \text{ cal}^{1/2} \text{ cm}^{-3/2}$ [20], which is equal to $20.1 - 20.9 \text{ MPa}^{1/2}$.

Hansen found that the complete miscibility of a polymer (subscript p) and a solvent (subscript s) is obtained when the difference in solubility parameters ($\Delta\delta$) is lower than the solubility radius R_p , which is characteristic for each polymer.

$$\Delta\delta = \sqrt{4(\delta_{ds} - \delta_{dp})^2 + (\delta_{ps} - \delta_{pp})^2 + (\delta_{hs} - \delta_{hp})^2} < R_p \quad (3)$$

So far, neither the solubility radius nor experimental HSPs have been determined for poly(α -hydroxy acids). The solubility radii described for other polymers range between 2 and 12 MPa^{1/2} [21-23].

Due to the incomplete data on biodegradable polymers, attempts to explain or predict the encapsulation efficacies and release data of proteins from biodegradable polymer microspheres in a thermodynamic approach that was exclusively based on HSPs proved to be insufficient [24,25]. The established scaffold fabrication technique [12], however, is even more complex in terms of the underlying thermodynamics. Different processes, namely solvent extraction, polymer precipitation and porogen material dissolution, have to be kinetically adapted to each other to fabricate interconnected pore structures [12]. Changes in the polymer or the extraction solvent will affect all three processes in different ways. Therefore, our intention was not to describe the entire fabrication procedure by means of HSPs, but rather to replace the halogenated polymer solvent mixture with a thermodynamically equivalent solvent or solvent mixture with a lower toxicity rating (class 3). Since the three-dimensional HSPs are quantities that exactly describe the thermodynamic properties of a solvent or a solvent mixture, they are the appropriate tools to accomplish this aim.

3. Materials and Methods

3.1. Materials

Poly(D,L-lactic-co-glycolic acid) (PLGA) (75:25), Resomer® RG756, was provided by Boehringer Ingelheim (Ingelheim, Germany). Poly(D,L-lactic acid)-*block*-poly(ethylene glycol)-monomethyl ether diblock copolymers (MeO-PEG₂PLA₄₀, MeO-240) (M_n = 42kDa) were synthesized in our laboratory [26]. The solid lipids that were used as porogen materials, namely Softisan® 154 and Witepsol® H42 were kindly provided by SASOL Germany GmbH (Witten, Germany). Acetone, chloroform, methyl ethyl ketone (MEK), tetrahydrofuran (THF) and ethyl acetate, which were used as polymer solvents, and *n*-hexane, *n*-pentane and *n*-heptane, which were utilized as porogen extraction media, were purchased in analytical grade from Merck (Darmstadt, Germany). The solubility parameters of these solvents are listed in Table 1.

Table 1: Hildebrand (δ_{total}) and three-dimensional Hansen solubility parameters of solvents listed in class 3 of the ICH guideline. The parameters of *n*-hexane and chloroform (ICH class 2) are included.

Solvent	Solubility Parameters [MPa ^{1/2}]				Solvent	Solubility Parameters [MPa ^{1/2}]			
	δ_d	δ_p	δ_h	δ_{total}		δ_d	δ_p	δ_h	δ_{total}
ICH class 3									
<u>Hydrocarbons</u>					<u>Ethers</u>				
<i>n</i> -Pentane	14.5	0.0	0.0	14.5	Ethyl ether	14.5	2.9	5.1	15.8
<i>n</i> -Heptane	15.3	0.0	0.0	15.3	Tetrahydrofuran	16.8	5.7	8.0	19.4
<u>Alcohols</u>					<u>Esters</u>				
1-Butanol	16.0	5.7	15.8	23.1	Butyl acetate	15.8	3.7	6.3	17.4
2-Butanol	15.8	5.7	14.5	22.1	Ethyl acetate	15.8	5.3	7.2	18.2
Ethanol	15.8	8.8	19.4	26.6	Ethyl formate	15.5	8.4	8.4	19.6
2-Methyl-1-propanol	15.1	5.7	16.0	22.7	Isobutyl acetate	15.1	3.7	6.3	16.8
1-Pentanol	16.0	4.5	13.9	21.7	Isopropyl acetate	14.3	8.4	5.7	17.6
1-Propanol	16.0	6.8	17.4	24.6	Methyl acetate	15.5	7.2	7.6	18.8
2-Propanol	15.8	6.1	16.4	23.5	Propyl acetate	14.1	8.1	7.8	18.0
<u>Ketones</u>					<u>Acids</u>				
Acetone	15.5	10.4	7.0	20.1	Acetic acid	14.5	8.0	13.5	21.3
Methyl ethyl ketone	16.0	9.0	5.1	19.0	Formic acid	14.3	11.9	16.6	25.0
Methyl isobutyl ketone	15.3	6.1	4.1	17.0	<u>Others</u>				
					Dimethylsulfoxide	18.4	16.4	10.2	26.6
ICH class 2									
<i>n</i> -Hexane	14.9	0.0	0.0	14.9	Chloroform	17.8	3.1	5.7	18.9

3.2. Hansen solubility parameter calculation of binary solvent mixtures

Based on the HSPs listed in Table 1, the three-dimensional HSPs of the established acetone-chloroform-mixture (65:35 (v/v)) were estimated according to the following equations (acetone: subscript a; chloroform: subscript c):

$$\delta_{dmix} = \Phi_a \delta_{da} + \Phi_c \delta_{dc} \quad \delta_{dmix}: \text{dispersive HSP of the mix,} \quad (4)$$

$$\delta_{pmix} = \Phi_a \delta_{pa} + \Phi_c \delta_{pc} \quad \delta_{pmix}: \text{polar HSP of the mix,} \quad (5)$$

$$\delta_{hmix} = \Phi_a \delta_{ha} + \Phi_c \delta_{hc} \quad \delta_{hmix}: \text{hydrogen bonding HSP of the mix,} \quad (6)$$

where Φ_a and Φ_c are the mole fractions for the two components of the mixture, namely acetone (a) and chloroform (c). Technically, the solubility parameter of a mixture of liquids is determined by calculating the volume-wise contributions of the solubility parameters of the individual components of the mixture.

3.3. Determination of the alternative solvent or solvent mixture

To systematically search for a thermodynamically equal, low-toxic solvent or solvent mixture, the following strategy was applied: Generally, every substance can be represented by a point in a three-dimensional coordinate system with its HSPs as coordinates (δ_d , δ_p , δ_h). By mixing two solvents, any HSP along a line in between the two points representing the mixture components can be attained (defined by equations (4)-(6)). From a pool of 26 ICH class 3 solvents, 325 binary solvent combinations are possible. Using an algorithm to plot the trajectory that is perpendicular to the line describing the solubility parameters for each of the 325 solvent mixtures and intersects the coordinates of the acetone-chloroform mixture (target), the coordinates (HSPs) that are closest to the target were determined for each mixture (Fig. 1). This operation determined the ‘best mix’ for each possible solvent combination.

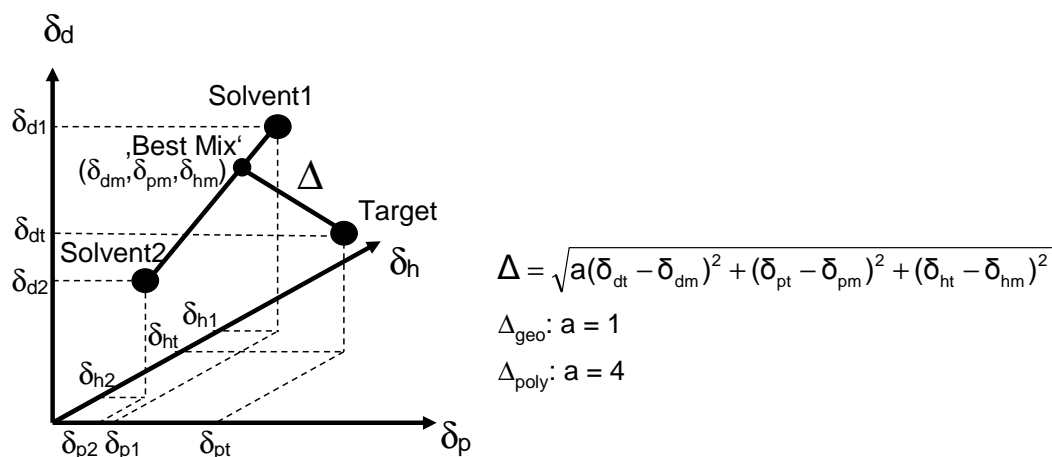


Fig. 1: Schematic illustration of the geometric algorithm used to determine alternative solvent mixtures thermodynamically comparable to the acetone-chloroform-mixture (target). For every binary solvent combination, the respective ‘best mix’ is determined by calculating the coordinates perpendicular to the target. Two values (Δ_{geo} and Δ_{poly}) expressing the distance between the best mix and the target parameter are calculated according to the depicted equations.

Concomitantly, the distance of the 325 ‘best mixes’ from the target was calculated. For each mix, we calculated the geometric distance Δ_{geo} and a further distance value Δ_{poly} , which was derived from the Hansen plot ($2\delta_d$, δ_p , δ_h) and calculated according to formula (3). Δ_{poly} emphasizes the significance of the dispersive solubility parameter, which Hansen identified for interactions involving polymers. Finally, the mixtures were ranked according to their geometric distance to the target point.

3.4. Scaffold fabrication procedure

To fabricate macroporous scaffolds from biodegradable polymers, we recently developed an anhydrous technique employing solid lipid microparticles as porogens [12] (Fig. 2). The solid lipid microparticles were prepared from either a 1:1 mixture of Softisan® 154 and Witepsol® H 42 (SH 1:1) or a 2:1 mixture (SH 2:1) using a melt dispersion technique. The resulting SH 1:1 microspheres with an average size distribution of $[d_{10}; d_{90}] = [68\mu\text{m}; 347\mu\text{m}]$ were used to process MeO-PEG₂PLA₄₀. SH 2:1 microparticles, average size distribution $[d_{10}; d_{90}] = [105\mu\text{m}; 319\mu\text{m}]$, served as the porogen material when PLGA was processed.

Briefly, the scaffold fabrication started with a polymer solution. PLGA was dissolved in the polymer solvent to obtain a final concentration of 308 mg/mL. In the case of MeO-PEG₂PLA₄₀, the concentration was 420 mg/mL. Under ice cooling, the polymer solution was mixed with the porogen particles. A polymer to porogen ratio of 1:4 (w/w) was chosen. The homogeneous dispersion was transferred into Teflon® molds (1.9 cm x 1.9 cm x 1.2 cm)

with a cylindrical cavity 0.8 cm in diameter. After a pre-extraction treatment step in *n*-hexane at 0°C (PLGA: 15 min, MeO-240: 90min), the molds were submerged in warm *n*-hexane to induce solvent extraction followed by the precipitation of the polymer and extraction of the lipid porogen. This procedure was carried out in two separate *n*-hexane baths with different temperatures T_1 (PLGA: 52°C, MeO-240: 40°C) and T_2 (PLGA: 40°C, MeO-240: 35°C) for $t_1 = 10\text{min}$ and $t_2 = 20\text{min}$. The resulting porous, cylindrical polymer constructs were allowed to cool in cold (0°C) *n*-hexane and were finally removed from the molds, vacuum dried for 48 h and cut into 2mm slices which were then described as scaffolds.

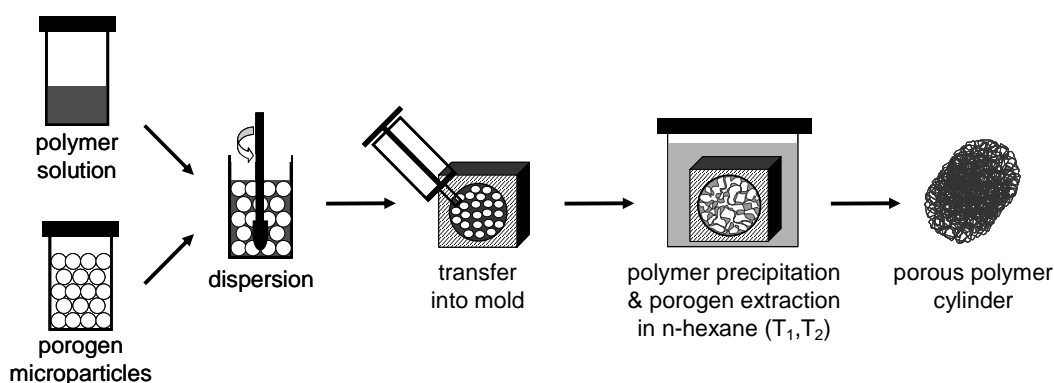


Fig. 2: Schematic illustration of the scaffold fabrication procedure. Molds are filled with a dispersion prepared from a polymer solution and triglyceride microparticles and submerged in warm *n*-hexane. In a two step extraction (T_1 , T_2), the porogen microparticles are extracted at two different temperatures, while the polymer is concomitantly precipitated forming macroporous polymer scaffolds.

3.5. Microscopic assessment of scaffold macro- and microstructure

The macrostructure of the porous polymer cylinders and scaffolds was examined using a zoom stereo microscope (Wild M7A, Wild Heerbrugg Ltd., Heerbrugg, Switzerland). The scaffold microstructure was visualized by scanning electron microscopy (SEM). For this procedure, samples were mounted on aluminum stubs with conductive carbon tape and coated with gold-palladium. All micrographs were obtained at 10 kV on a DSM 950 (Zeiss, Oberkochen, Germany).

3.6. Determination of solvent viscosity and polymer solution viscosity

The kinematic viscosity of the polymer solvents and solvent mixtures was determined at 25°C using a calibrated Ubbelohde capillary viscometer (size: 0c, Schott AG, Mainz, Germany) with a Lauda S5 detector (Lauda, Lauda-Königshofen, Germany), which was connected to a

Lauda PVS1 Processor Viscosity System with a PVS 2.28a analysis program (Lauda, Germany) ($n = 8$).

In order to determine the reduced viscosity of different polymer solutions ($c = 0.01 \text{ gcm}^{-3}$), we measured the kinematic viscosity of the polymer solutions at 25°C . All of the solutions were prepared in triplicate and each solution was measured 2-3 times. The relative viscosity was calculated from the average kinematic viscosity of each solution:

$$\eta_{rel} = \frac{\eta_{solution}}{\eta_{solvent}} . \quad (7)$$

The reduced viscosity was defined as:

$$\eta_{red} = \frac{(\eta_{rel} - 1)}{c} . \quad (8)$$

4. Results

4.1. Determination of low-toxic solvent alternatives

A total of 28 solvents are classified as ‘solvents with low toxic potential’ in class 3 of the ICH guideline ‘Impurities: Guideline for residual solvents’ [11]. Table 1 lists 26 class 3 solvents and the corresponding HSPs. Anisole and cumene, which also are class 3 solvents, were not considered in this study. Generally, the solvents listed in this class belong to several chemical substance classes ranging from non-polar hydrocarbons to alcohols and acids that show strong hydrogen bonding. This way, the class 3 solvents offer a broad spectrum of solubility parameters to choose from.

The solvents used in the original scaffold fabrication procedure are *n*-hexane, acetone and chloroform, with acetone and chloroform being used as a mixture to dissolve the polymer and *n*-hexane serving as extraction solvent. According to the ICH guideline, chloroform and *n*-hexane are classified as ‘solvents to be limited’ (class 2). The HSPs of these two solvents are listed in Table 2.

The main goal of this study was to find an alternative to the established acetone-chloroform-mixture (65:35 (v/v)) used as the polymer solvent. To define a measure for the thermodynamic interaction forces of this mixture, its HSPs were calculated according to equations (4)-(6). The parameters of the acetone-chloroform-mixture, representing the target coordinates for the systematic search, are listed in Table 2. An algorithm, described in the methods section, was used to compare the HSPs of 26 class 3 solvents and their binary mixtures with the target mixture in order to screen for a thermodynamically equal or at least similar solvent alternative. The ten best mixtures are listed in Table 2. All of them exhibited a geometric distance (Δ_{geo}) from the target below $1 \text{ MPa}^{1/2}$. A mixture of methyl ethyl ketone and tetrahydrofuran (59:41 (v/v)) fit best in terms of both Δ_{geo} and Δ_{poly} . In contrast to Δ_{geo} , which represents the spatial distance of the mixture HSPs to the target in a 3-D coordinate system (δ_{d} , δ_{p} , δ_{h}), Δ_{poly} is based on the Hansen plot ($2\delta_{\text{d}}$, δ_{p} , δ_{h}) that emphasizes the disperse interactions between polymer and solvent. Like four other mixtures, all indicated with a star (*) in Table 2, this mixture is free of nucleophilic solvents and therefore suitable for the processing of functional, electrophilic, reactive polymers [27].

Table 2: Solubility parameters (Hansen and Hildebrand) of the original solvent mixture and parameters calculated for the 10 best alternative class 3 solvent mixtures. Δ_{geo} and Δ_{poly} are measures for the distance of the calculated alternative mixtures to the target parameters. Solvent mixtures that are free of a nucleophilic component are indicated by a *.

Solvent Mixture	ratio (v/v)	Solubility Parameters [MPa ^{1/2}]				Distance		
		δ_d	δ_p	δ_h	δ_{total}	Δ_{geo}	Δ_{poly}	
<i>Target</i>								
Acetone : Chloroform	65 : 35	16.3	7.8	6.5	19.2	0.0	0.0	
<i>Alternatives</i>								
MEK : THF	59 : 41	16.3	7.6	6.3	19.1	0.3	0.1	*
MEK : 1-Pentanol	81 : 19	16.0	8.1	6.8	19.2	0.5	0.5	
Ethyl ether : DMSO	63 : 37	15.9	7.9	7.0	19.1	0.6	0.7	*
Methylacetat : MEK	46 : 54	15.8	8.2	6.3	18.7	0.7	1.3	*
2-Butanol : MEK	19 : 81	16.0	8.4	6.9	19.3	0.7	0.9	
1-Butanol : MEK	17 : 83	16.0	8.4	6.9	19.4	0.8	0.9	
Aceton : Butylacetat	57 : 43	15.6	7.5	6.7	18.6	0.8	2.0	*
Ethylacetat : MEK	43 : 57	15.9	7.4	6.0	18.6	0.8	1.1	*
MEK : 2-Propanol	84 : 16	16.0	8.5	6.9	19.4	0.9	1.1	
MEK : 2-Methyl-1-propanol	83 : 17	15.8	8.4	7.0	19.3	0.9	1.4	

Suitable alternatives for *n*-hexane, which was used in the fabrication process to induce phase separation and to extract the porogen material, can be found among the hydrocarbons listed in class 3 of the ICH guideline, namely *n*-pentane and *n*-heptane (Table 1). According to the solubility parameter theory, a 50:50 (v/v) mixture of both solvents would exactly meet the HSPs of *n*-hexane. From another point of view, the HSPs of all three hydrocarbons are considerably different from the other class 3 solvents since only disperse interactions contribute to the cohesive forces of a hydrocarbon. Therefore, any hydrocarbon that is a liquid under the applied extraction conditions should be suitable to induce polymer precipitation and to extract the porogen microparticles. Additionally, the number of organic solvents involved in the fabrication procedure should be kept to a minimum due to regulatory demands. Consequently, pure *n*-heptane was used to replace *n*-hexane, as the boiling point of *n*-pentane (36°C) is far below the extraction temperatures.

4.2. HSP-based illustration of solvents and solvent mixtures

(Two-dimensional solvent map)

Figure 3 illustrates the thermodynamic solvent characteristics in a two-dimensional map. In this plot, the partial solubility parameter for the disperse interactions, δ_d , and a partial solubility parameter δ_a , which combines the non-disperse interactions δ_p and δ_h (9), are used as coordinates for each solvent.

$$\delta_a = \sqrt{\delta_p^2 + \delta_h^2} \quad (9)$$

The introduction of the partial solubility parameter δ_a allows for a two-dimensional illustration, as it combines δ_p and δ_h . Furthermore, this particular reduction from using three to two dimensions to characterize the solvent does not affect δ_a , which is described as the dominant parameter in terms of polymer-solvent interactions [28].

The alcohols and acids are located in the upper left quadrant of this plot due to high values of δ_p and δ_h . Hydrocarbons can be found on the x-axis since only dispersive forces contribute to the cohesive forces in such solvents. The exceptional characteristics of DMSO, which is a solvent for many hydrophilic and lipophilic macromolecules, are well illustrated by its isolated position in the upper right quadrant of the plot ($\delta_d > 16$ and $\delta_a > 12.5$). Typical polymer solvents, such as chloroform (ICH class 2), however, show many dispersive interactions and few non-dispersive interactions, locating them in the lower right quadrant ($\delta_d > 16$ and $\delta_a < 12.5$). Tetrahydrofuran is the only class 3 solvent that appears in this quadrant.

The coordinates of the target, the acetone-chloroform-mixture (65:35 (v/v)), are located on a line between acetone and chloroform. MEK, THF and ethyl acetate can be identified as the three solvents exhibiting the closest distance to the target in this plot. Together with acetone, these solvents were additionally tested as polymer solvent alternatives.

4.3. *Polymer processing using alternative solvents*

In order to check for the effectiveness of the solvent search utilizing HSPs, PLGA scaffolds were processed with different solvents or solvent mixtures using the processing parameters developed for the acetone-chloroform-mixture (65:35 (v/v)). Additionally, *n*-heptane was employed as extraction solvent instead of *n*-hexane. The macro- and microstructure of the resulting macroporous polymer cylinders and scaffolds was analyzed by light microscopy and SEM. We investigated the following polymer solvents: MEK:THF (59:41 (v/v)), which was the result of the systematic solvent search, MEK, THF and ethyl acetate, three different pure solvents positioned closest to the target mixture in the two-dimensional solvent plot (Fig. 3), and pure acetone, which displays a larger distance to the target mixture, as the main component of the original solvent mixture.

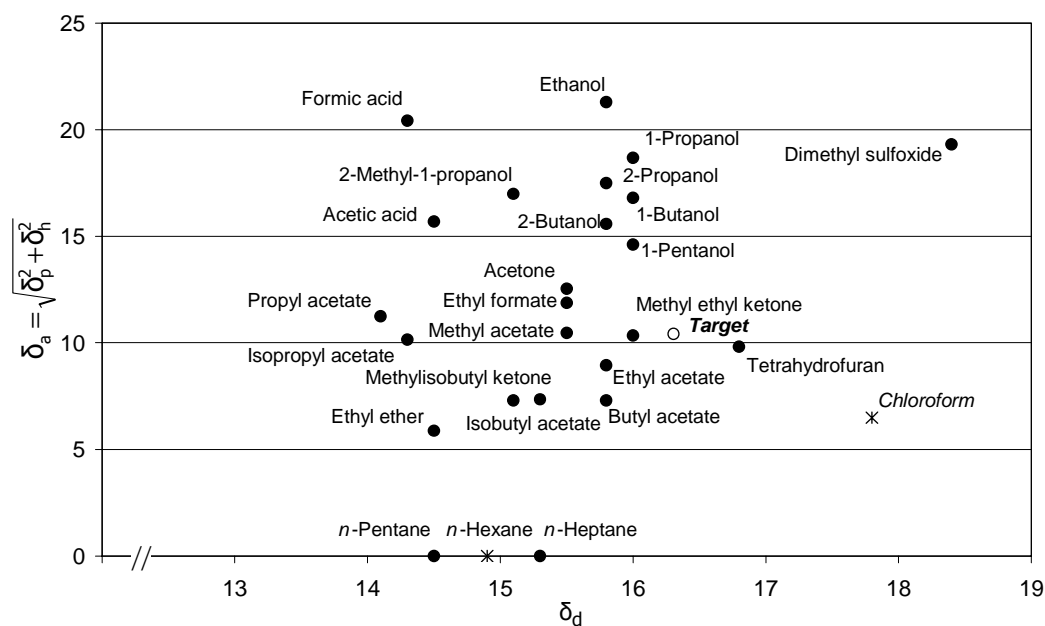


Fig. 3: Two-dimensional solvent map. 24 ICH class 3 solvents, *n*-hexane, chloroform, and the acetone-chloroform-mixture were illustrated in this coordinate plane using the dispersive solubility parameter (δ_d) and a partial parameter (δ_a), which combines the non-dispersive interactions, as coordinates.

PLGA scaffolds processed with the calculated best alternative polymer solvent mixture, MEK:THF (59:41 (v/v)), were nearly unaffected in their macroscopic and microscopic appearance. SEM revealed slightly thinner polymer bridges and smaller pore interconnections than with the target polymer solvent mixture (Fig. 4a,b; 5a,b). When either MEK or ethyl acetate was used as the polymer solvent alternative for the processing of PLGA, slight deformations of the polymer cylinders were observed. Additionally, the macrostructure of the resulting scaffolds appeared to be less regular (Fig. 4c,d). Nonetheless, SEM showed unaffected interconnected frameworks with these solvents. Acetone and THF, on the other hand, turned out to be unsuitable for the processing of the polymers under the established conditions.

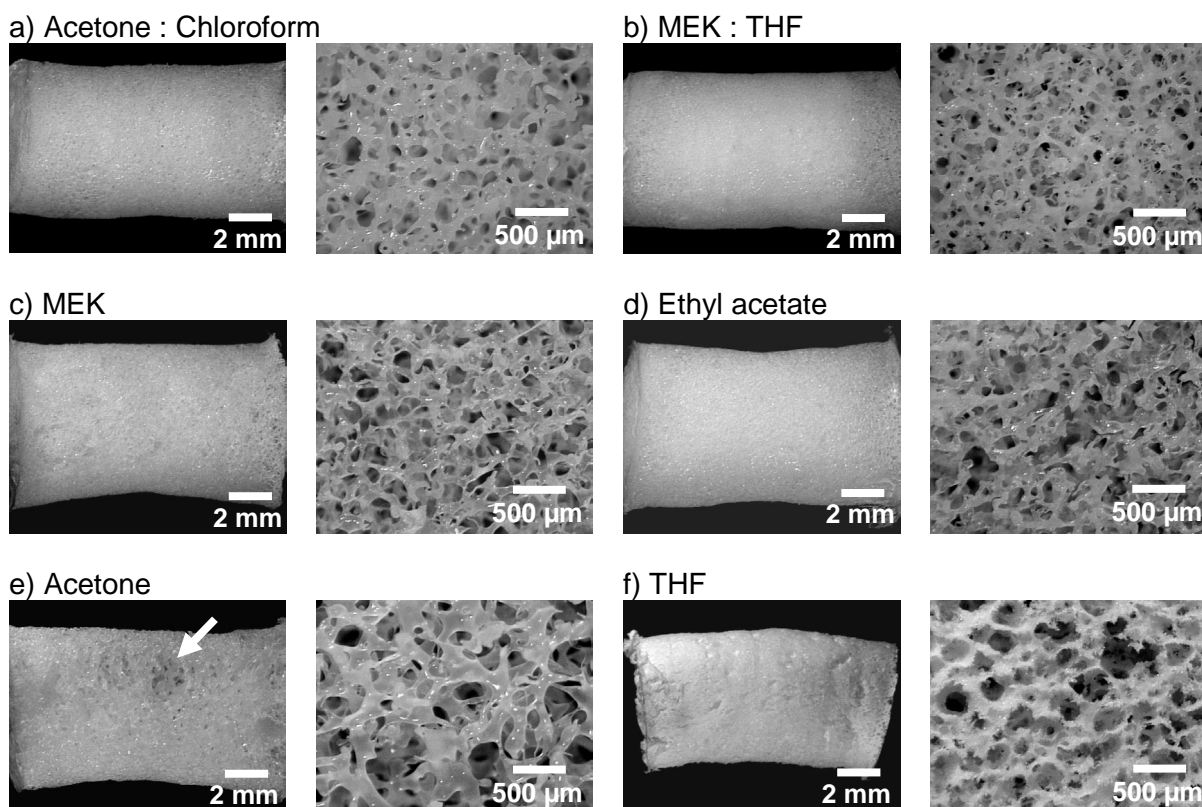


Fig. 4: Photographs depicting the macro- and microstructure of PLGA scaffolds fabricated according to the established protocol (a) and with alternative polymer solvents and *n*-heptane as extraction media (b-f). The arrow in (e) points to a mm-sized cavity (macro-cavity) on the surface of the polymeric cylinder.

When using acetone as an alternative polymer solvent, large cavities developed during polymer processing, which compromised the homogeneity of the generated polymer cylinders (Fig. 4e, 5e). In areas between these macrocavities (diameter > 1 mm), however, a macroporous framework was formed by condensed polymer bridges (Fig. 4e, 5e). Although the position of THF in the solvent plot is closer to the target mixture than that of ethyl acetate, the use of THF as the polymer solvent severely impaired scaffold macroporosity and pore interconnectivity (Fig. 4f, 5f). Furthermore, an incomplete extraction of the porogen materials was found in scaffolds fabricated with THF as the polymer solvent (data not shown).

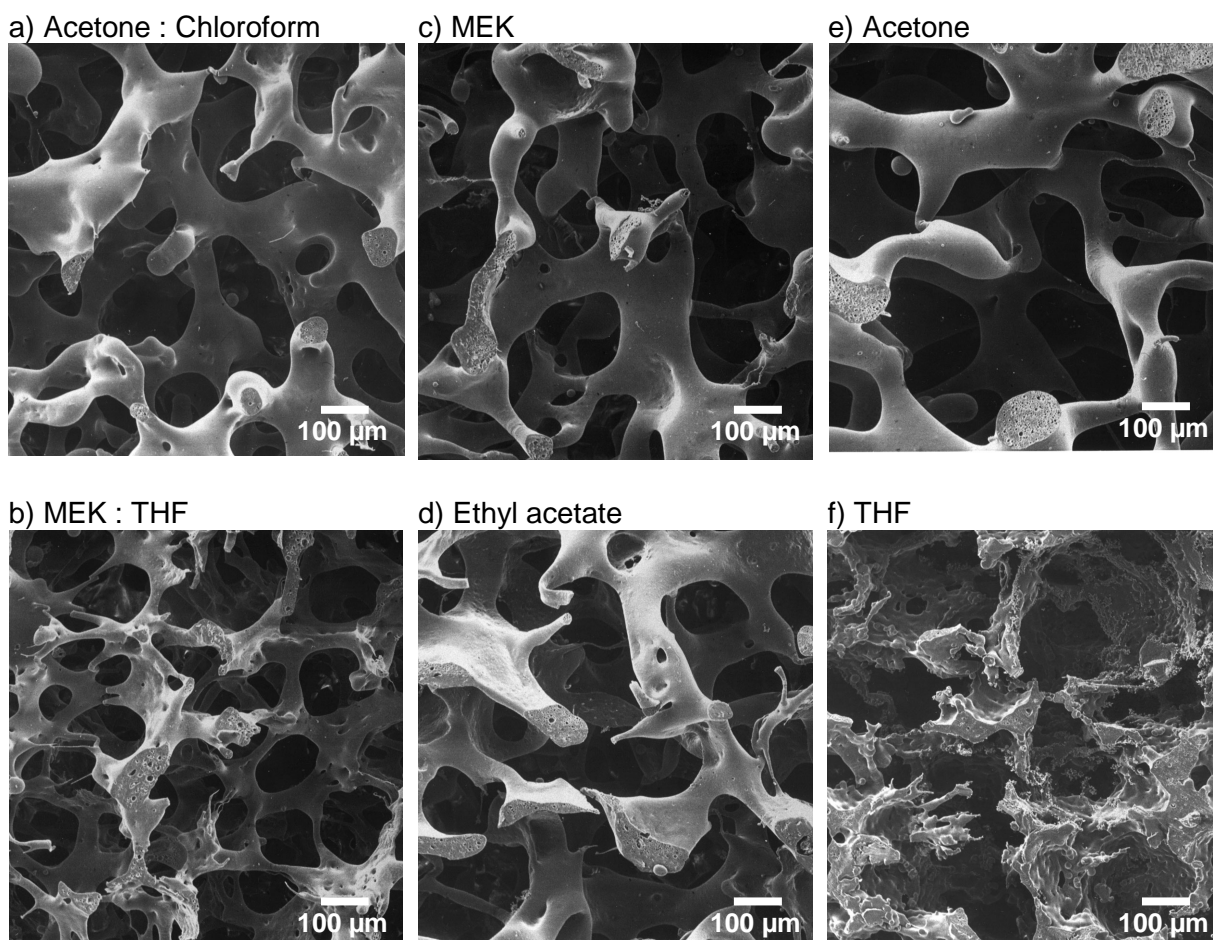


Fig. 5: PLGA scaffold microstructures as observed by SEM. Scaffolds were fabricated according to the established protocol (a) and with alternative polymer solvents and n-heptane as extraction media (b-f).

Macroscopic effects on MeO-PEG₂PLA₄₀ scaffolds processed with the MEK-THF-mixture (59:41 (v/v)), acetone and THF as polymer solvents were comparable to those observed for PLGA (Fig. 6). As found for the processing of PLGA, the best results were obtained by using the calculated thermodynamically similar solvent mixture (Fig. 6a,b). Processing with acetone as the solvent severely impaired the structural integrity of the resulting constructs as a result of extended phase separation. In the inner areas of the polymeric constructs, an almost complete phase separation was observed, which resulted in the formation of large polymer droplets instead of a continuous polymeric framework (Fig. 6c). MeO-PEG₂PLA₄₀ scaffolds fabricated with THF as the polymer solvent demonstrated a lack of macro- and microporosity (Fig. 6d)

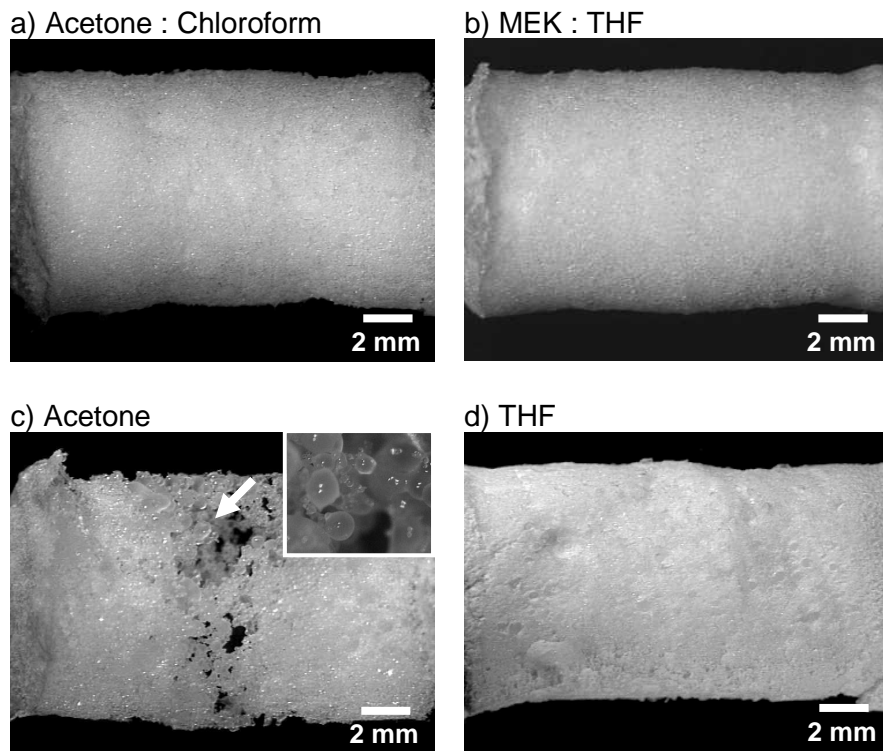


Fig. 6: Macrostructure of $\text{MeO-PEG}_2\text{PLA}_{40}$ scaffolds fabricated according to the established protocol (a) and by using polymer solvents and *n*-heptane as extraction media (b-d). The inserted figure (c) shows solid polymer droplets that were formed in the inner areas of the scaffold.

Table 3: Distance values and viscosity data for solvents and solvent mixtures tested in this study. Δ_{ex} represents the geometric distance of the solvent to the extraction media, *n*-heptane. Additionally, the kinematic viscosity (η) of the solvents and the reduced viscosity (η_{red}) of a PLGA solution (1% (m/v)) in the respective solvent is given.

Solvent	Δ_{geo}	Δ_{poly}	Δ_{ex}	δ_{d}	η [mm ² /s]	η_{red} [cm ³ /g]
Acetone:Chloroform (65:35)	0.0	0.0	10.3	16.3	0.3886	0.5321
MEK:THF (59:41)	0.3	0.1	10.0	16.3	0.4643	0.5384
Methyl ethyl ketone (MEK)	1.9	2.0	10.4	16.0	0.4545	---
Tetrahydrofurane (THF)	2.6	2.8	10.0	16.8	0.5077	---
Ethyl acetate	2.7	2.8	9.0	15.8	0.4699	---
Acetone	2.7	3.1	12.5	15.5	0.3714	---

5. Discussion

The interconnected porous microstructure of the scaffolds is generated during porogen extraction in warm *n*-hexane or *n*-heptane. Ideally, the porogen microparticle starts to melt shortly after the dispersion is brought into contact with the warm extraction medium. Subsequently, the molten triglycerides form a continuous phase that separates from the liquid polymer solution before the polymer solvent and the triglyceride phase are completely extracted by the extraction media. In other words, an interconnected porous network is only generated when the two liquid phases coexist for a sufficient amount of time before the polymer precipitates, forming condensed polymer sponges. Processing conditions that induce this phase separation were experimentally optimized for the acetone-chloroform-mixture (65:35 (v/v)). By using three-dimensional HSPs to theoretically determine a thermodynamically equivalent solvent mixture composed of ICH class 3 solvents, this solvent mixture was successfully replaced. Scaffolds exhibiting comparable macro- and microstructures were fabricated without any alteration of the other processing conditions. MEK, ethyl acetate, acetone and THF were also tested as polymer solvent alternatives due to their proximity to the target parameters (Fig. 3, Table 3). Scaffolds fabricated with MEK ($\Delta_{\text{geo}} = 1.9$; $\Delta_{\text{poly}} = 2.0$) or ethyl acetate ($\Delta_{\text{geo}} = 2.7$; $\Delta_{\text{poly}} = 2.8$) as the polymer solvent displayed only minor deformations and irregularities. Therefore, these solvents may be considered to be suitable solvent alternatives, requiring little adaptation of process parameters. THF ($\Delta_{\text{geo}} = 2.6$; $\Delta_{\text{poly}} = 2.8$), which is located closer to the target than ethyl acetate, however, turned out to be an unsuitable substitute. The observed macro- and microstructures indicated that the phase separation was insufficient, most likely because of the considerable solubility of the triglyceride porogen in THF (data not shown). The macrocavities that were observed when acetone ($\Delta_{\text{geo}}=2.7$; $\Delta_{\text{poly}}=3.1$) was tested as the polymer solvent, however, are indicative of an extended phase separation before polymer precipitation. Taken together, the HSPs proved to be a suitable means to systematically determine alternative solvents. The calculated distance alone, however, could not conclusively indicate whether a solvent is suitable for polymer processing or not (Table 3).

Recently, we investigated the solubility of the porogen triglyceride mixtures in the investigated solvents (data not shown). Attempting to correlate the determined solubility with the HSPs of the corresponding solvent revealed that the solubility exclusively correlates with the dispersive solubility parameter (δ_d). The onset of triglyceride solubility was determined at a solvent δ_d value of 16.5 and triglyceride solubility increased with increasing values of δ_d .

Liao et al. measured the dissolution rates of PLGA particles in different solvents [29]. High dissolution rates were found in chloroform ($\delta_d = 17.8$) and dichloromethane ($\delta_d = 18.2$). In solvents with lower and higher values of δ_d , significantly lower dissolution rates were measured. This data underlines the dominant influence of the solvent's dispersive solubility parameter on polymer and triglyceride solubility. With regard to δ_d , the solvents tested in this study are ranked as follows: δ_d (acetone) < δ_d (ethyl acetate) < δ_d (MEK) < δ_d (MEK:THF) = δ_d (acetone:chloroform) < 16.5 < δ_d (THF). This ranking correlates with the observed solvent effects on scaffold macro- and microstructure. THF ($\delta_d > 16.5$) was unsuitable for scaffold fabrication most likely due to mixing with the molten triglyceride phase. Conversely, acetone ($\delta_d = 15.5$) did not mix with the triglyceride phase, but due to its high Δ_{ex} (Table 3), the geometric distance to the parameters of the extraction media *n*-heptane, polymer solvent extraction was retarded, resulting in an extended demixing of polymer solution and triglyceride phase and subsequent formation of large cavities and polymer droplets (Fig. 4e, 5d). This effect was more pronounced when MeO-PEG₂PLA₄₀, a diblock copolymer of PEG and PLA, was processed. Generally, the processing of this diblock copolymer was more susceptible to parameter changes due to the polymer's lower molecular weight and glass transition temperature [12].

Based on these observations, the three-dimensional HSPs, and especially the partial parameter δ_d , proved as useful means to compare solvents in terms of their suitability for the established scaffold fabrication technique. Nevertheless, minor differences in microstructure between the scaffolds fabricated with the acetone-chloroform-mixture (65:35 (v/v)) and the thermodynamically similar MEK-THF-mixture (59:41 (v/v)) were observed. Since thinner polymer bridges and smaller pore interconnections resulted from processing with the MEK-THF-mixture, this structural difference likely resulted from polymer precipitation at an earlier time point in the phase separation. As two thermodynamically similar solvent mixtures are compared, the viscosity of the polymer solution is the remaining parameter that influences the time point of polymer precipitation. Consequently, we determined the kinematic viscosities of both solvent mixtures and the reduced viscosities of PLGA (1% (m/v)) solutions in both solvent mixtures (Table 3). According to the solubility parameter theory, we obtained comparable reduced viscosities for PLGA in both solvent mixtures. Substantial differences, however, were found for the kinematic viscosities of the pure solvent mixtures. In other words, a PLGA solution in the MEK-THF-mixture generally exhibits a higher viscosity than an equally concentrated solution in the acetone-chloroform-mixture. Together with data

gathered during another study (chapter 6), this viscosity difference was identified as the reason for the observed dissimilarity in scaffold microstructure.

In summary, solvents exhibiting HSPs similar to those of the acetone-chloroform-mixture proved to be suitable for polymer processing into macroporous, interconnected scaffolds if their dispersive solubility parameter value was smaller than 16.5. Additionally, the geometric difference between the HSPs of the solvent and extraction media should not exceed a value of 10.5 (Table 3).

6. Conclusion

This study described the replacement of two ICH class 2 solvents from an established scaffold fabrication procedure that makes use of two solvent dependant processes, namely solvent extraction and phase separation, to generate interconnected pore structures. The HSPs of the originally developed acetone-chloroform-mixture (65:35 (v/v)) were determined to systematically search for a thermodynamically comparable solvent mixture composed of class 3 solvents using a geometric algorithm. A MEK-THF-mixture (59:41 (v/v)) resulted from this search as suitable alternative. Scaffolds were fabricated using this mixture as the polymer solvent, with *n*-heptane replacing *n*-hexane as the extraction media without any alteration of other processing parameters. These results proved that three-dimensional HSPs are a useful means to compare and replace solvents with regard to their thermodynamic properties in biodegradable polymer processing. By illustrating the class 3 solvents in a two-dimensional solubility parameter map, ethyl acetate and MEK were identified as further polymer solvent alternatives. THF, which was also tested as solvent alternative, proved to not be suitable, identifying the dispersive solubility parameter (δ_d) as the key parameter. Generally, this solubility parameter based strategy holds great potential as a tool to replace halogenated solvents from other polymeric release device fabrication procedures.

7. References

- (1) Langer R, Folkman J. 'Polymers for the sustained release of proteins and other macromolecules'. *Nature* (1976); **263**: 797-800.
- (2) Brannon-Peppas L. 'Recent advances on the use of biodegradable microparticles and nanoparticles in controlled drug delivery'. *Int J Pharm* (1995); **116**: 1-9.
- (3) Langer R. 'Drug delivery and targeting'. *Nature* (1998); **392**: 5-10.
- (4) Langer R, Peppas NA. 'Advances in Biomaterials, Drug Delivery, and Bionanotechnology'. *AIChE J* (2003); **49**: 2990-3006.
- (5) Athanasiou KA, Agrawal CM, Barber FA, Burkhart SS. 'Orthopaedic applications for PLA-PGA biodegradable polymers'. *Arthroscopy* (1998); **14**: 726-737.
- (6) Freed LE, Vunjak NG, Biron RJ, Eagles DB, Lesnoy DC, Barlow SK, Langer R. 'Biodegradable polymer scaffolds for tissue engineering'. *Biotechnology (N Y)* (1994); **12**: 689-693.
- (7) Baldwin SP, Mark Saltzman W. 'Materials for protein delivery in tissue engineering'. *Adv Drug Delivery Rev* (1998); **33**: 71-86.
- (8) Jain RA. 'The manufacturing techniques of various drug loaded biodegradable poly(lactide-co-glycolide) (PLGA) devices'. *Biomaterials* (2000); **21**: 2475-2490.
- (9) Agrawal CM, Ray RB. 'Biodegradable polymeric scaffolds for musculoskeletal tissue engineering'. *J Biomed Mater Res* (2001); **55**: 141-150.
- (10) Witschi C, Doelker E. 'Residual solvents in pharmaceutical products: acceptable limits, influences on physicochemical properties, analytical methods and documented values'. *Eur J Pharm Biopharm* (1997); **43**: 215-242.
- (11) International Conference on Harmonisation of technical requirements for registration of pharmaceuticals for human use. *ICH harmonized Tripartite Guideline (Q3C) Impurities: Residual solvents*. Draft 4 (1997). Available from <http://www.ich.org>
- (12) Hacker M, Tessmar J, Neubauer M, Blaimer A, Blunk T, Gopferich A, Schulz MB. 'Towards biomimetic scaffolds: Anhydrous scaffold fabrication from biodegradable amine-reactive diblock copolymers'. *Biomaterials* (2003); **24**: 4459-4473.
- (13) Hildebrand JH, Scott RL. *The Solubility of Non-Electrolytes*. New York: Dover, 1964.
- (14) Barton AFM. 'Solubility parameters'. *Chem Rev* (1975); **75**: 731-754.
- (15) Hansen CM. 'The universality of the solubility parameter concept'. *Ind Eng Chem Prog Res Dev* (1969); **8**: 2-11.
- (16) Hansen CM. 'Three-dimensional solubility parameter-key to paint-component affinities: I. Solvents, plasticizers, polymers, and resins'. *J Paint Technol* (1967); **39**: 104-117.

-
- (17) Hansen CM. 'Three-dimensional solubility parameter-key to paint component affinities. II. Dyes, emulsifiers, mutual solubility and compatibility, and pigments'. *J Paint Technol* (1967); **39**: 505-510.
- (18) Hansen CM, Skaarup K. 'Three-dimensional solubility parameter-key to paint component affinities. III. Independent calculation of the parameter components'. *J Paint Technol* (1967); **39**: 511-514.
- (19) Grulke EA. 'Solubility Parameter Values'. In: Brandrup J, Immergut EH, Grulke EA, editors. *Polymer Handbook*. New York: John Wiley, 1999. p. VII/675-714.
- (20) Siemann U. 'The solubility parameter of poly(D,L-lactic acid)'. *Eur Polym J* (1992); **28**: 293-297.
- (21) Lindvig T, Michelsen ML, Kontogeorgis GM. 'A Flory-Huggins model based on the Hansen solubility parameters'. *Fluid Phase Equilib* (2002); **203**: 247-260.
- (22) Stoye D. 'Solvents'. In: *Ullmann's Encyclopedia of Industrial Chemistry, Vol. A 24*. Weinheim: VCH, 1993. p. 437-505.
- (23) Segarceanu O, Leca M. 'Improved method to calculate Hansen solubility parameters of a polymer'. *Prog Org Coat* (1997); **31**: 307-310.
- (24) Gander B, Wehrli E, Alder R, Merkle HP. 'Quality improvement of spray-dried, protein-loaded D,L-PLA microspheres by appropriate polymer solvent selection'. *J Microencapsul* (1995); **12**: 83-97.
- (25) Gander B, Johansen P, Nam-Tran H, Merkle HP. 'Thermodynamic approach to protein microencapsulation into poly(D,L-lactide) by spray drying'. *Int J Pharm* (1996); **129**: 51-61.
- (26) Lucke A, Tessmar J, Schnell E, Schmeer G, Gopferich A. 'Biodegradable poly(-lactic acid)-poly(ethylene glycol)-monomethyl ether diblock copolymers: structures and surface properties relevant to their use as biomaterials'. *Biomaterials* (2000); **21**: 2361-2370.
- (27) Tessmar JK, Mikos AG, Gopferich A. 'Amine-Reactive Biodegradable Diblock Copolymers'. *Biomacromolecules* (2002); **3**: 194-200.
- (28) Hansen, C. M. 'Three Dimensional Solubility Parameter and Solvent Diffusion Coefficient. Importance in Surface Coating Formulation.'. *Doctoral Dissertation*. Danish Technical Press, Copenhagen. (1967)
- (29) Liao CJ, Chen CF, Chen JH, Chiang SF, Lin YJ, Chang KY. 'Fabrication of porous biodegradable polymer scaffolds using a solvent merging/particulate leaching method'. *J Biomed Mater Res* (2002); **59**: 676-681.

Chapter 5

Solubility Parameters of Poly(lactic acid) and its Copolymers – Theoretical and Experimental Considerations

Michael Hacker¹, Andrea Blaimer¹, Michaela B. Schulz^{1,2}, Achim Göpferich¹

¹ Department of Pharmaceutical Technology, University of Regensburg,
Universitaetsstrasse 31, 93040 Regensburg, Germany

² Department of Pharmaceutical Technology, University of Graz,
Schubertstrasse 6, 8010 Graz, Austria

Abstract

The three-dimensional Hansen solubility parameters (HSPs) of a polymer provide detailed information on the thermodynamic properties of the molecule. Based on these parameters, molecular interactions with solvents, other polymers, plasticizers, dyes and therapeutic substances can be estimated. In this way, the HSPs are a means for the development and optimization of polymer processing and drug encapsulation techniques. This study utilizes both theoretical (group contribution method) and experimental (solubility measurements and the determination of viscosity numbers) methods to determine the HSPs of poly(D,L-lactic acid) (PLA) and copolymers with glycolic acid and poly(ethylene glycol). Different group contribution data sets were compared and discussed. The absolute HSP values calculated by this method appeared unrealistically high. On the basis of the solubility tests, a solvent map was introduced to distinguish between solvents and non-solvents for the polymers. Detailed information on the polymer-solvent interactions was obtained from the viscosity measurements.

1. Introduction

Lipophilic, biodegradable poly(α -hydroxy acids), such as poly(lactic acid) (PLA) or copolymers with poly(glycolic acid) (PLGA), are widely used in medical applications, ranging from sutures to orthopedic implants, cell carriers for tissue engineering, and depots for the long-term release of drugs, therapeutic proteins and genes [1-5]. Further attention has been drawn to block copolymers (MeO-PEG-PLA) synthesized from PLA and monomethyl ether-poly(ethylene glycol) (MeO-PEG), because they exhibit a reduced protein adsorption on their surfaces due to the hydrophilic PEG block [6,7]. Several biomedical devices, e.g. stealth nanoparticles and tissue engineering scaffolds have already been fabricated from MeO-PEG-PLA [8,9]. Due to their insolubility in water, organic solvents are required to process these biodegradable polymers and have to be removed after processing to avoid any risk to human health and to the stability of the encapsulated substances. However, finding suitable and minimally toxic organic solvents for polymer and drug processing can be the subject of long lasting empirical approaches that may culminate in a less than optimal result. In order to find a more systematic approach, we investigated the suitability of using solubility parameters to circumvent the problem (Chapter 4). The solubility parameters of solvents, polymers, and drugs are accepted tools to describe the thermodynamic properties of these molecules and estimate their interactions during biomaterial processing and/or drug encapsulation [10-13]. Solubility parameters can provide the means for a tailored solvent selection for pharmaceuticals [14] or a systematic replacement of halogenated and other toxic solvents from polymer processing techniques (Chapter 4).

Hildebrand defined the solubility parameter (δ) as the square root of the cohesive energy density (CED) of a non-polar, non-associated solvent [15]. The CED is the energy of vaporization (ΔE^v) per molar volume (V_m),

$$\delta = \sqrt{CED} = \sqrt{\frac{\Delta E^v}{V_m}}. \quad (1)$$

This theory has been extended to include polar solvents, polymers and drugs. Along with these developments, the Hildebrand solubility parameter was decomposed into several terms, representing different contributions to the cohesive energy [16]. According to Hansen, the cohesive energy arises from dispersive interactions, polar (permanent dipole-dipole) interactions and hydrogen bonding forces [17,18]. Consequently, the Hildebrand parameter was divided into three partial solubility parameters (δ_d : representing dispersive interaction

forces, δ_p : polar (permanent dipole-dipole) interactions and δ_h : hydrogen bonding and induced dipole interactions) that account for the different cohesive forces:

$$\delta^2 = \delta_d^2 + \delta_p^2 + \delta_h^2 \quad (2)$$

The three-dimensional Hansen solubility parameters (HSPs) give detailed information on the thermodynamic properties of a molecule and have already been determined for a variety of solvents [19].

It is common knowledge that poly(α -hydroxy acids) dissolve in a variety of solvents ranging from highly toxic ones, e.g. chloroform or toluene, to water-miscible solvents with low toxicity like *N*-methyl-2-pyrrolidone (NMP), which has been used as polymer solvent to develop injectable drug delivery systems [20,21]. However, only a few studies have focused on the determination of the related solubility parameters for these systems. Siemann calculated a total solubility parameter value of 9.8 – 10.2 cal^{1/2}cm^{-3/2} for PLA, which is equal to 20.1 – 20.9 MPa^{1/2}, by means of high precision density measurements and viscosity numbers [22]. Other studies have estimated the three-dimensional HSPs of PLA or PGA using a molecular group contribution method [10,23-25]. Interestingly, different HSP values resulted from these estimations, although they all based on the same method. This inconsistency and the lack of experimental data for the HSPs for these polymers likely account for the limited success of solubility parameter based thermodynamic approaches to model drug encapsulation [26].

This study reflects theoretical approaches and employs simple (in terms of instrumental equipment) methods to determine the three-dimensional HSPs of PLA, PLGA and PEG-PLA (MeO-PEG₂PLA₄₀). Polymer solubility parameters were calculated according to different group contribution methods and experimentally determined in solubility tests and from intrinsic viscosity data, according to a recently described method [27]. The theoretically and experimentally determined parameters are compared and discussed.

2. Materials and Methods

2.1. Materials

Poly(D,L-lactic acid) (PLA), Resomer® R206, $M_w = 126$ kDa (i.v. 0.6 dl/g) and poly(D,L-lactic-co-glycolic) (PLGA), synthesized from 75% lactic acid (LA) and 25% glycolic acid (GA), Resomer® RG756, $M_w = 90$ kDa (i.v. 0.6 dl/g) were kindly provided by Boehringer Ingelheim (Ingelheim, Germany). Monomethyl ether-poly(ethylene glycol)-block-poly(D,L-lactic acid) (PEG-PLA; MeO-PEG₂PLA₄₀; MeO-240), $M_n = 42$ kDa, which consists of a 2 kDa MeO-PEG block covalently bound to a 40 kDa PLA block, was synthesized and characterized as previously described [7]. The polymer structures are depicted in Figure 1.

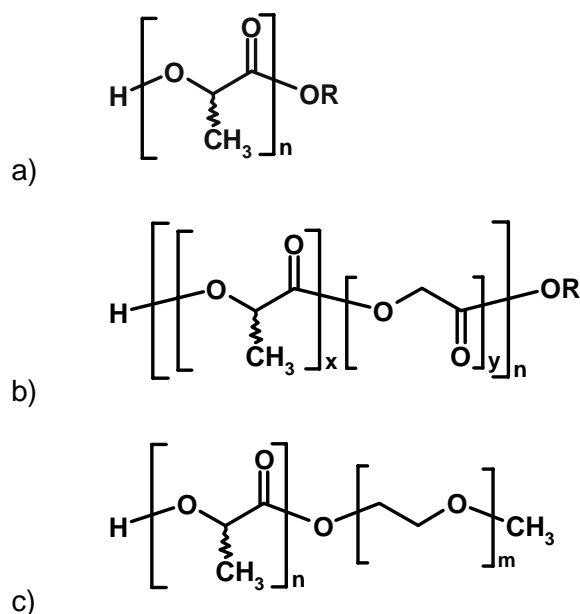


Fig. 1: Polymer structures. (a) Poly(D,L-lactic acid) (PLA); (b) Poly(D,L-lactic-co-glycolic acid) (PLGA); (c) Monomethyl ether-poly(ethylene glycol)-block-poly(D,L-lactic acid) (PEG-PLA; MeO-240). End-capped polymers were employed in this study (R: C₂H₅).

n-Hexane, diethyl ether, 1,4-dioxane, tetrahydrofuran (THF), acetone, methyl ethyl ketone (MEK), ethyl acetate, ethanol, 2-propanol, benzyl alcohol, and dimethyl sulfoxide, which were used as solvents in the solubility study, were purchased in analytical grade from Merck (Darmstadt, Germany). Acetonitrile (Baker, Deventer, The Netherlands) as well as chloroform, methylene chloride, and *N*-methyl-2-pyrrolidone (Carl Roth GmbH & Co, Karlsruhe, Germany) were purchased in HPLC grade. All solvents used for the viscosity measurements were purchased in analytical quality from Merck (Darmstadt, Germany), except acetone (Fluka, Taufkirchen, Germany).

The Hansen solubility parameters (HSPs) of the solvents are tabulated in the literature [19]. HSPs are additive components of the total Hildebrand value (δ) (Equation 2). Fractional parameters are mathematically derived from Hansen values and indicate the percent contribution that each Hansen parameter contributes to the Hildebrand value:

$$\delta_{df} = \frac{\delta_d}{\delta_d + \delta_p + \delta_h} \quad \delta_{pf} = \frac{\delta_p}{\delta_d + \delta_p + \delta_h} \quad \delta_{hf} = \frac{\delta_h}{\delta_d + \delta_p + \delta_h} \quad (3)$$

Thus, the sum of the three fractional HSP parameters is 1 or 100%.

2.2. Group contribution method

The Hansen solubility parameters (HSPs) for PLA, PGA, and PEG were estimated using group contribution methods according to Hoy and Hoftyzer and van Krevelen (HvK) [18,19,28]. These estimations are based on the repetitive structural unit of the polymers (Fig. 1). Details on these methods and the determination of the molar volume are described and discussed in the ‘results and discussion’ section.

2.3. Solubility tests

The solubility of the polymers in several solvents was tested using the following method: Stainless steel meshes of known weight (2 cm x 2 cm – mesh size: 0.5 mm) were coated with polymer by submerging the meshes in a concentrated solution (0.5 g/mL) of the polymer in acetone. After drying to constant weight, the loading with polymer was determined by measuring the weight increase of the meshes. To determine the polymer-solvent interactions, the polymer coated meshes were submerged in solvent (20 mL). After 1 min the meshes were removed from the solvent. Solvent droplets were removed from the meshes by intense shaking. The meshes were stored on Teflon®-coated paper and dried to constant weight under vacuum. The percent values, which are listed (Table 3), result from the amount of dissolved polymer normalized to the mass of polymer on the mesh. The values represent the average of 2 to 3 independent measurements.

2.4. Viscosity measurements

The kinematic viscosity of the solvents was determined at 25°C using a calibrated Ubbelohde capillary viscometer (size: 0c, Schott AG, Mainz, Germany) with a Lauda S5 detector (Lauda, Lauda-Königshofen, Germany), which was connected to a Lauda PVS1 Processor Viscosity System with a PVS 2.28a analysis program (Lauda, Germany) (n = 10).

In order to determine the intrinsic viscosity of the three polymers (PLA, PLGA, PEG-PLA) in different solvents, we measured the kinematic viscosity of polymer solutions ($c_1 = 0.01 \text{ gcm}^{-3}$ and $c_2 = 0.005 \text{ gcm}^{-3}$) at 25°C using the described measurement set-up. The polymer solutions were stirred in sealed glass flasks for at least 24 h before use. Prior to the measurement, the solutions were filtered through a 0.2 mm solvent resistant regenerated nitrocellulose membrane filter (Spartan 30/A from Schleicher & Schuell, Dassel, Germany). All solutions were prepared in triplicate and each solution was measured 2-3 times ($n \geq 6$). The relative viscosity was calculated from the average kinematic viscosity of each solution:

$$\eta_{rel} = \frac{\eta_{solution}}{\eta_{solvent}} . \quad (4)$$

The reduced viscosity resulted from:

$$\eta_{red} = \frac{(\eta_{rel} - 1)}{c} . \quad (5)$$

Finally, the intrinsic viscosity was calculated from the reduced viscosity at c_1 and c_2 :

$$[\eta] = \eta_{red}(c_1) - \frac{(\eta_{red}(c_1) - \eta_{red}(c_2))}{c_1 - c_2} . \quad (6)$$

2.5. Hansen solubility parameter determination of the investigated polymers

Following a method described in the literature [27], the measured solubility and viscosity data were used to determine the polymer HSPs. This approach is based on the quantification of interactions between the polymer and a solvent. These interactions are reflected in certain properties of the polymer solution, such as the intrinsic viscosity or the solubility of the polymer in the solvent. With increasing interactions between a polymer and a solvent, the solubility and the intrinsic viscosity of the polymer in that solvent increase. Therefore, a multiplication of each solvent solubility parameter with the unity-normalized intrinsic viscosity $[\eta]_i'$ or a unity-normalized solubility value of a polymer in that solvent allows for the creation of a weighted solubility parameter, reflecting the interaction between the polymer and the solvent. In this system, large values of this weighted parameter stand for high levels of interaction with the polymer.

The Hansen solubility parameters of a polymer are calculated from the weighted partial solubility parameters according to the following equations (shown here for the unity-normalized intrinsic viscosity):

$$\delta_{dp} = \frac{\sum \delta_{di} \cdot [\eta]'_i}{\sum [\eta]'_i} \quad \delta_{pp} = \frac{\sum \delta_{pi} \cdot [\eta]'_i}{\sum [\eta]'_i} \quad \delta_{hp} = \frac{\sum \delta_{hi} \cdot [\eta]'_i}{\sum [\eta]'_i} \quad (7)$$

Subscript index p designates the polymer and $[\eta]'_i$ is the normalized intrinsic viscosity of polymer in solvent i. Normalization of the intrinsic viscosity to unity was performed by dividing the intrinsic viscosity values by the maximum obtained intrinsic viscosity.

This parameter determination using weighted solubility parameters has also been described as the projection of the tested solvents in a 3-dimensional system with the coordinates δ_d ; δ_p ; δ_h . For each solvent, a weighted interaction sphere is defined by the unity-normalized interaction value (intrinsic viscosity or solubility). The sphere, including all individual polymer-solvent interaction spheres, has a center point at the HSP coordinates of the polymer and its radius represents the radius of interaction of the polymer.

To calculate this radius of interaction, the distance between the polymer HSPs (7) and the solvent coordinates were computed:

$$R_i = \sqrt{4(\delta_{di} - \delta_{dp})^2 + (\delta_{pi} - \delta_{pp})^2 + (\delta_{hi} - \delta_{hp})^2} \quad (8)$$

The highest value of R_i is considered the radius of interaction, R.

3. Results

3.1. Theoretical estimation of solubility parameters (Group contribution methods)

Group contribution methods have been extensively reviewed and data tables are provided for the estimated Hildebrand and Hansen solubility parameters of solvents, drugs and polymers [18,19,28-31]. The sets of group constants provided by Hoy and Hoftyzer together with van Krevelen seem to be the most widely used and comprehensive lists [28]. For polymers, the solubility parameters are generally estimated on the basis of the repetitive chemical units (Fig. 1). Thomasin et al. estimated a HSP triplet (δ_d ; δ_p ; δ_h) of 15.4; 8.5; 11.1 for PLA according to the Hoftyzer-van Krevelen (HvK) method (Table 1) [24].

Table 1: Solubility parameters as estimated for different polymers using the group contribution methods according to Hoftyzer-van Krevelen (HvK) or Hoy.

Polymer	Solubility Parameters [MPa ^{1/2}]				V _m [cm ³ /mol]	Method	Ref.
	δ_d	δ_p	δ_h	δ			
PLA	15.8	8.7	11.1	20.8	56.5 ^a	HvK	[24]
PLA	17.6	9.7	11.8	23.3	50.5	HvK / Fedors	[25]
PLA	16.0	8.8	11.2	21.4	55.7	HvK / general	this study
PLA	14.4	13.1	8.8	21.3	54.8	Hoy	this study
<i>PLA (average)^c</i>	<i>16.0</i>	<i>11.4</i>	<i>10.3</i>	<i>22.2</i>			
PGA	19.4	14.4	14.3	28.0	34.1	HvK / Fedors	[25]
PGA	16.8	12.4	13.3	24.7	39.4	HvK / general	this study
PGA	13.7	15.3	12.7	24.2	39.3	Hoy	this study
<i>PGA (average)^c</i>	<i>16.6</i>	<i>14.9</i>	<i>13.5</i>	<i>26.0</i>			
PLGA (75:25)	18.1	10.9	12.4	24.5	---	HvK / Fedors	this study
PLGA (75:25)	16.2	9.7	11.7	22.2	---	HvK / general	this study
PLGA (75:25)	14.2	13.6	9.8	22.0	---	Hoy	this study
<i>PLGA (75:25) (av.)^c</i>	<i>16.2</i>	<i>12.3</i>	<i>11.1</i>	<i>23.1</i>			
PEG	17.8	11.1	9.1	22.9	37.0	HvK / Fedors	[25]
PEG (crystalline)	17.2	10.7	9.0	22.2	37.3 ^b	HvK / general	this study
PEG	16.7	10.1	8.8	21.4	37.5	Hoy	this study
<i>PEG (average)^c</i>	<i>17.2</i>	<i>10.6</i>	<i>9.0</i>	<i>22.1</i>			

^a Value calculated from the partial solubility parameters and the group contributions

^b Molar volume was calculated according to the general method [34] applying the contributions for crystalline substances

^c Average values were calculated from the parameters estimated according to Hoy and HvK/Fedors

This method allows for the estimation of the three HSP terms, as follows (Table 2) [18,19,32]:

$$\begin{aligned}\delta_d &= \frac{\sum F_{di}}{V_m}, \\ \delta_p &= \frac{\sqrt{\sum F_{pi}^2}}{V_m}, \\ \delta_h &= \sqrt{\frac{\sum E_{hi}}{V_m}}.\end{aligned}\tag{8}$$

F_{di} , F_{pi} and E_{hi} refer to the specific functional group contributions: van der Waals dispersion forces (F_{di}), dipole-dipole interactions (F_{pi}), and hydrogen-bonding (E_{hi}). V_m represents the total molar volume.

Table 2: Component group contributions as proposed by Hoftyzer and van Krevelen. Contributions to the molar volume are adapted from a general method [35] and from Fedors [33,34].

Group	Component group contributions			Contribution to V_m		
	F_d [J ^{1/2} cm ^{3/2} /mol]	F_p [J ^{1/2} cm ^{3/2} /mol]	U_h [J/mol]	general amorphous	method crystalline	Fedors
-CH ₃	420	0	0	---	---	33.5
>CH ₂	270	0	0	16.37	14.68	16.1
>CH-	80	0	0	---	---	-1.0
>CH-CH ₃	---	---	---	32.72	29.35	---
-COO-	390	490	7000	23	21.5	18.0
-O-	100	400	3000	8.5	7.9	3.8

The values estimated by Thomasin et al. could not be reproduced using the listed group contributions (Table 2), as it was not clear how the molar volume (V_m) of the PLA unit was estimated. One possible data set to estimate V_m is provided by Fedors (Table 2) [19,32-34]. Nevertheless, this estimation leads to a molar volume of 50.5 cm³/mol, which is much lower than the value used by Thomasin et al. (Table 1). Consequently, relatively high values (17.6; 9.7; 11.8) resulted from this combination of HvK data with the Fedors V_m (HvK / Fedors) [25]. However, it is questionable whether a combination of the HvK data set and the Fedors data set is permissible or not. Consequently, we calculated the molar volume according to a general group contribution method presented in the literature [35]. This data set provides different values for crystalline or amorphous substances (Table 2). A molar volume of 55.7 cm³/mol was calculated for PLA from the values listed for amorphous substances. Intermediate HSP results (16.0; 8.8; 11.2), approaching those published by Thomasin et al., resulted from the calculation employing this molar volume in combination with the HvK data set (HvK /general). Additionally, we calculated the HSPs of PLA (14.4; 13.1; 8.8) on the

basis of an additional data set proposed by Hoy according to the listed values and equations in [32]. According to van Krevelen [32], the average values from between the two methods, HvK and Hoy, can be regarded as representative. Due to the considerable differences of both methods and the described ambiguity concerning the appropriate molar volume for the Hoftyzer-van Krevelen method, we kept both parameter triplets for later comparisons. The HSP values for poly(glycolic acid) (PGA) and poly(ethylene glycol) (PEG) were also determined according to both the Hoftyzer-van Krevelen and the Hoy methods. The molar volume of the polymer's repeating unit was estimated using both Fedors data and the general method (Table 1) for parameter estimation according to the HvK method. The HSPs of poly(lactic-*co*-glycolic acid) (PLGA) (75% lactic acid) were calculated from the HSP values estimated for PLA and PGA applying the following equations and listed in Table 1:

$$\begin{aligned}\delta_{d\ PLGA} &= 0.75 \cdot \delta_{d\ PLA} + 0.25 \cdot \delta_{d\ PGA} \\ \delta_{p\ PLGA} &= 0.75 \cdot \delta_{p\ PLA} + 0.25 \cdot \delta_{p\ PGA} \\ \delta_{h\ PLGA} &= 0.75 \cdot \delta_{h\ PLA} + 0.25 \cdot \delta_{h\ PGA}\end{aligned}\tag{9}$$

This way, the group contribution method can only be applied to determine the HSPs of random copolymers. For block copolymers such as MeO-PEG-PLA, however, this method is not suitable.

A high variability in the solubility parameter values was observed when they were estimated using different data sets (Table 1). The HvK method, in combination with the Fedors parameters to estimate V_m , led to the highest solubility parameter values (δ), while the lowest values resulted from the Hoy method. This inconsistency and the fact that neither the molecular weight nor the end group modification are taken into account, are the main concerns with group contribution methods. Since the absolute HSP values obtained from different data sets varied strongly, the fractional parameters (δ_{df} ; δ_{pf} ; δ_{hf}) that represent the relative values were computed and compared (Fig. 2). Differences were observed between the different polymers. Both group contribution methods, HvK and Hoy, resulted in a pronounced contribution of δ_p and δ_h to δ for PGA compared to PLA. This means that a solvent with a permanent dipole moment (δ_p) would interact stronger with PGA or PLGA than with PLA. In PEG the dispersive interactions are dominant.

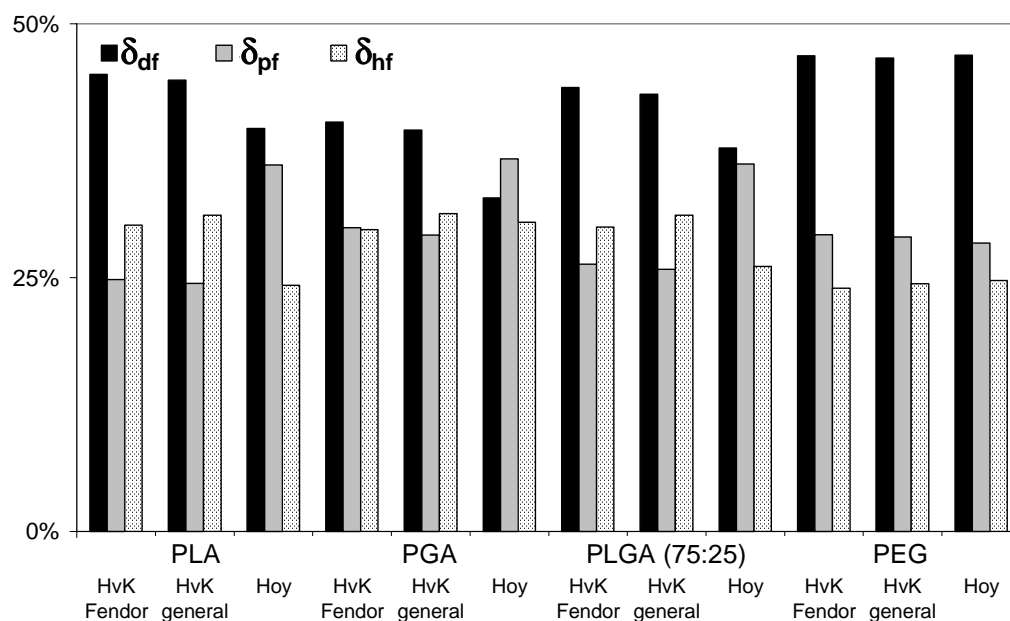


Fig. 2: Fractional parameters (percent contribution that each partial Hansen parameter contributes to the whole Hildebrand value) as determined for different polymers according to both group contribution methods (Hoftyzer-van Krevelen (HvK) and Hoy).

3.2. Experimental solubility parameter determination

The determination of Hansen solubility parameters of a polymer by classical methods includes testing the polymer solubility in different solvents with known solubility parameters or measuring polymer-solvent interactions by different methods, such as inverse phase gas chromatography [19]. Generally, solvents that interact with the polymer are represented by points in a three-dimensional space surrounded by a sphere with a radius defined by the quality and quantity of interaction. The coordinates of the center point of another sphere containing all these individual spheres derived from solvent-polymer interactions finally represent the Hansen solubility parameters of the polymer. The precise determination of the polymer-solvent interactions is essential, but accomplished with laborious testing when based on solubility experiments. Alternatively, inverse phase gas chromatography requires costly equipment and a column made from the investigated polymer. Capillary viscosimetry, however, is a widely established experimental method in polymer chemistry labs. A new method determines the quality and quantity of the polymer-solvent interactions by measuring the intrinsic viscosities, normalized to unity, of the polymer in several solvents [27]. The HSPs of the polymer are finally calculated from the parameters of the solvents used and the determined interaction values (7).

3.2.1. Map-Projection of the determined solubility data

The solvents used in these experiments were represented as points in a two-dimensional solvent map having as coordinates $(\delta_d; \delta_{p,h} = \sqrt{\delta_p^2 + \delta_h^2})$ (Fig. 3a).

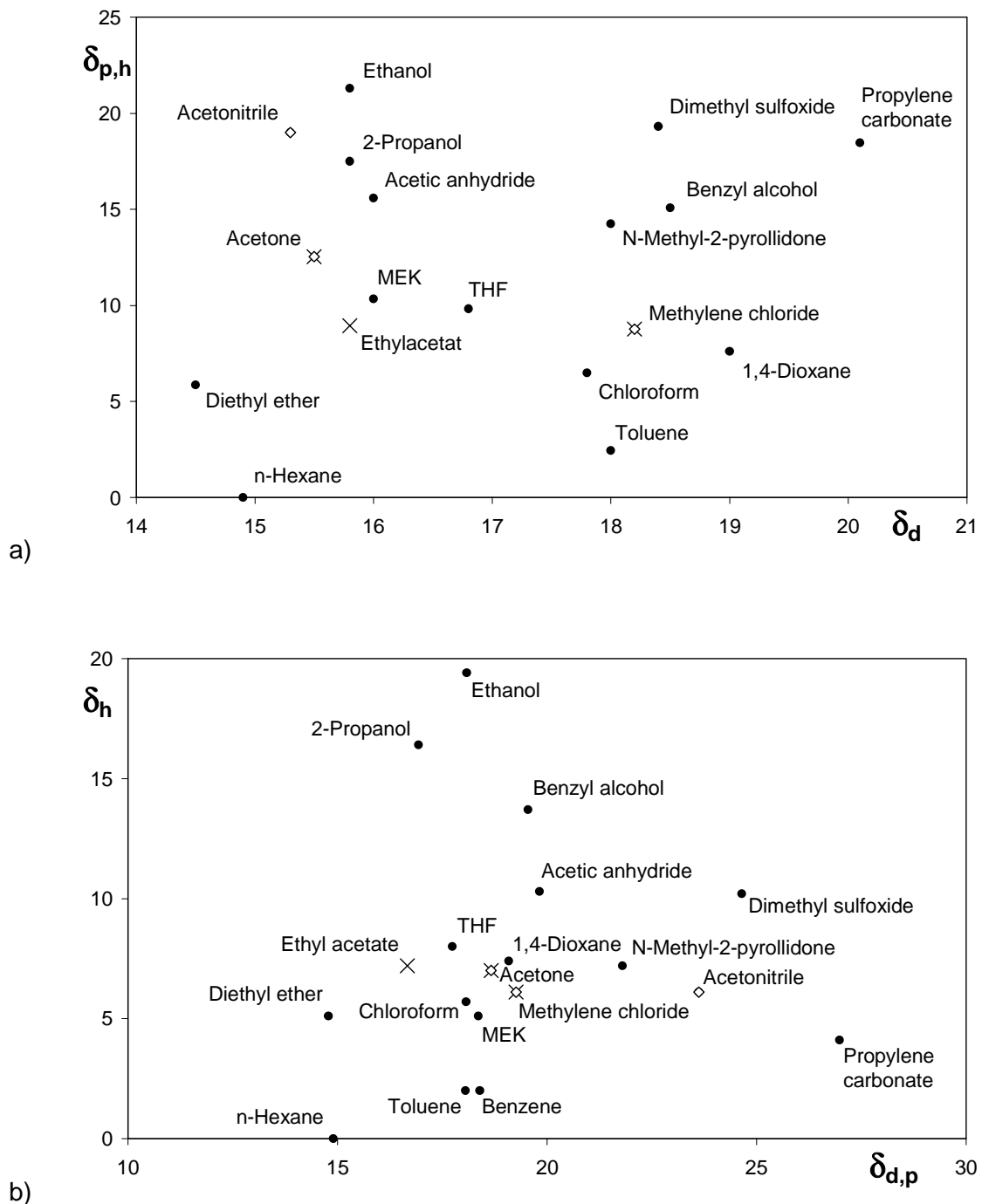


Fig. 3: Two-dimensional plot (solvent map) of the solvents used in this study. The plot is based on the Hansen solubility parameters of the solvents. The solvents are represented as points having as coordinates: a) $(\delta_d; \delta_{p,h} = \sqrt{\delta_p^2 + \delta_h^2})$ or b) $(\delta_{d,p} = \sqrt{\delta_d^2 + \delta_p^2}; \delta_h)$. Symbols indicate the three best solvents for PEG-PLA (x) and PLGA (\diamond) as determined in the solubility tests.

This illustration is frequently used because it separates the dispersive interactions from interactions resulting from permanent and induced dipoles and hydrogen bonding. To illustrate the observed and documented solubility data, however, this plot was unfavorable as acetone and methylene chloride, two excellent polymer solvents, were located in different quadrants. Furthermore, no rule of thumb for suitable polymer solvents could be defined on the basis of this plot. Many non-solvents, such as *n*-hexane, diethyl ether, 2-propanol and ethanol are characterized by a dispersive partial solubility parameter below 16. The same characteristic, however, applies for good polymer solvents, such as acetone, acetic anhydride and ethyl acetate. Based on the observation that the polar solubility parameter is a major factor for PLA and PGA solubility, we defined a new plot using a combined parameter $\delta_{d,p} = \sqrt{\delta_d^2 + \delta_p^2}$ and δ_h as axes (Fig. 3b). In the new plot one solubility center is located around acetone and methylene dichloride. Other polymer solvents are located near this triangle and at higher values of $\delta_{d,p}$. Furthermore, non-solvents are described by $\delta_{d,p} < 15.5$ and/or $\delta_h > 11$. This way, a suitable solvent plot was defined to discriminate between solvents and non-solvents for poly(lactic acid) and the investigated copolymers. Moreover, further evidence is provided that δ_p significantly contributes to the solubility of the polymers.

3.2.2. Solubility parameter calculation from solubility data

In our first attempt to determine the polymer solubility parameters, we set up a new solubility screening method. Following the described viscosity method, the dissolution rate of the polymers from a stainless steel mesh was determined in several solvents as a measure of polymer-solvent interactions. This experiment was performed with PLGA and PEG-PLA (Table 3). Solubility data for PLA was adapted from product information provided by Boehringer Ingelheim (Table 3). For each polymer, the HSPs were calculated from the solvent solubility parameters and the corresponding normalized dissolving capacities (Table 4). Realistic solubility parameter values resulted from this method for all three polymers, indicating that the highest solubility of the polymers was measured in methylene dichloride and thermodynamically similar solvents. The determined HSP values were lower compared to those obtained by the group contribution method. For PLA and PEG-PLA, similar relative contributions of the partial parameters were computed. The pronounced influence of δ_p on the cohesive properties of PLGA, which was discussed above, however, was not reflected by the determined partial HSPs.

Table 3: Solubility parameters of solvents employed in the solubility tests and viscosity measurements; Solubility of the polymers and the determined intrinsic viscosities $[\eta]$.

Solvent	HSPs [MPa ^{1/2}]			Solubility Tests			[η] [cm ³ /g]		
	δ_d	δ_p	δ_h	PEG-PLA	PLGA	PLA ^a	PEG-PLA	PLGA	PLA ^b
<u>Paraffinic Hydrocarbons</u>									
n-Hexane	14.9	0.0	0.0	3.5%	3.8%				
<u>Aromatic Hydrocarbons</u>									
Benzene	18.4	0.0	2.0						(63.0)
Toluene	18.0	1.4	2.0			>17%			(59.0)
<u>Halohydrocarbons</u>									
Methylene chloride	18.2	6.3	6.1	71.2%	23.0%	>40%			(98.0) ^c
Chloroform	17.8	3.1	5.7	52.7%	15.4%	>40%	41.77 ^c	94.80 ^c	89.75 ^c
<u>Ethers</u>									
Diethyl ether	14.5	2.9	5.1	3.7%	3.7%				
1,4-Dioxane	19.0	1.8	7.4	14.0%	6.2%	>30%			(69.0)
Tetrahydrofuran	16.8	5.7	8.0	52.5%	9.2%	>30%	28.66	61.29	62.08 (62.5)
<u>Ketones</u>									
Acetone	15.5	10.4	7.0	85.9%	23.3%	>40%	28.11	56.05	53.45
Methyl ethyl ketone	16.0	9.0	5.1	50.2%	14.6%		24.53	47.89	51.72
<u>Esters</u>									
Ethyl acetate	15.8	5.3	7.2	68.3%	13.9%		26.48	39.49	42.87 (66.0)
<u>Acids and Derivatives</u>									
Acetic anhydride	16.0	11.7	10.2	20.0%	9.0%				
Propylene carbonate	20.1	18.0	4.1			>30%			
<u>Alcohols</u>									
Ethanol	15.8	8.8	19.4	3.6%		<1%			
2-Propanol	15.8	6.1	16.4	0.1%	3.9%				
Benzyl alcohol	18.4	6.3	13.7	2.8%					
<u>N-Containing Solvents</u>									
Acetonitrile	15.3	18.0	6.1		24.8%	>30%			(31.0)
N-Methyl-2-pyrrolidone	18.0	12.3	7.2	13.9%	1.8%				
<u>S-Containing Solvents</u>									
Dimethyl sulfoxide	18.4	16.4	10.2			>30%			

^a Product information on Resomer® (Boehringer Ingelheim, Ingelheim, Germany): Solubility of PLA (high viscosity)

^b Values in brackets were adapted from the literature [22]

^c The maximum value of intrinsic viscosity to which the other values were normalized

3.2.3. Solubility parameter calculation from viscosity data

In a second attempt, the intrinsic viscosities of PLA, PLGA and PEG-PLA were determined in acetone, methyl ethyl ketone (MEK), ethyl acetate, tetrahydrofuran (THF) and chloroform. The weighted interaction capacities were computed by relating the measured intrinsic viscosities to the maximum intrinsic viscosity, which was determined for chloroform (Table 3). The HSPs that were calculated from the unity-normalized intrinsic viscosities and the corresponding solvent solubility parameters turned out to be nearly equal for the three investigated polymers (Table 4).

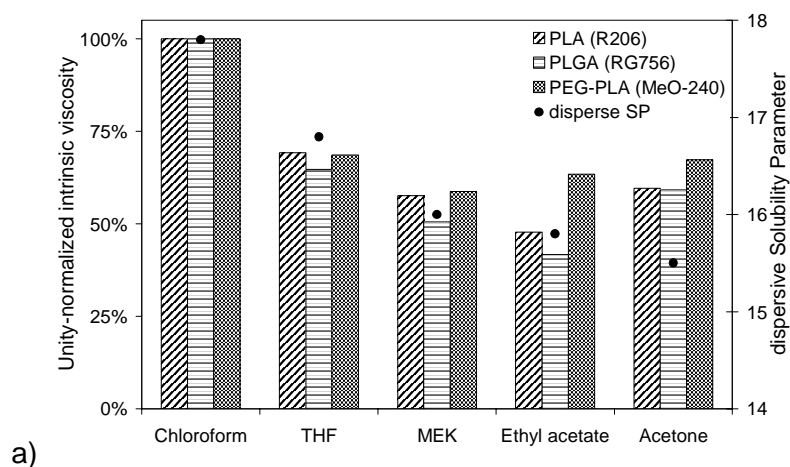
Table 4: Experimentally determined solubility parameter values for different biodegradable polymers.

Polymer	Solubility Parameters [$\text{MPa}^{1/2}$]				R [$\text{MPa}^{1/2}$]	Method
	δ_d	δ_p	δ_h	δ		
PLA	17.1	9.8	6.9	20.8		Solubility ^a
PLA (R 206)	16.6	6.3	6.5	18.9	4.7	Viscosity
PLA	17.6	4.7	5.6	19.0	14.1	Viscosity ^b
PLGA (RG 756)	15.7	7.5	8.8	19.4		Solubility
PLGA (RG 756)	16.6	6.2	6.5	18.9	4.8	Viscosity
PEG-PLA (MeO-240)	16.7	7.1	6.8	19.4		Solubility
PEG-PLA (MeO-240)	16.5	6.3	6.6	18.9	4.6	Viscosity

^a Values calculated from the solubility data listed in the product information on Resomer® (see Tab. 3)

^b Values calculated from intrinsic viscosity data published in the literature [22] (data reprinted in Tab. 3)

In good accordance with the solubility measurements, we measured almost equal polymer-solvent interactions in THF, MEK, ethyl acetate, and acetone, four solvents with entirely different HSPs, for all three polymers (Fig. 4a, Table 3).



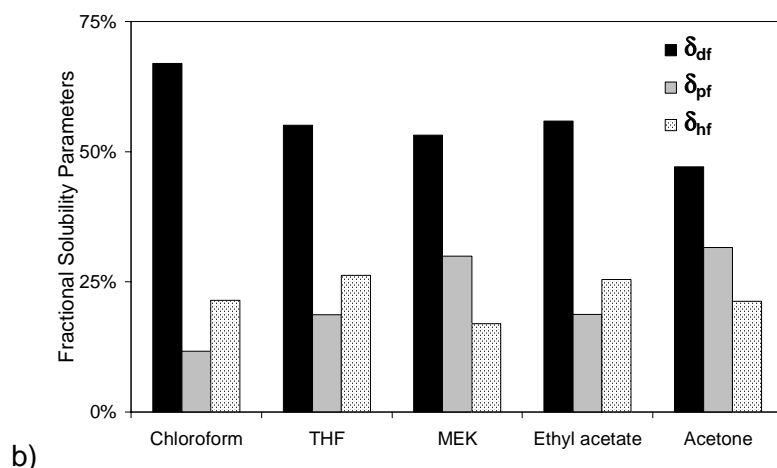


Fig. 4: a) Unity-normalized intrinsic viscosities determined for PLA, PLGA and PEG-PLA in different solvents (left axis). Disperse solubility parameter of the solvent (right axis). b) Fractional parameters of the solvents applied for the viscosity measurements.

Consequently, the polymer solubility parameters were computed as the center point of these solvents and chloroform (Fig. 5a). We might achieve a better discrimination between the different polymers by additionally testing solvents or solvent mixtures nearer to the determined parameters. Nevertheless, a closer insight in polymer-solvent interactions was enabled by comparing the unity-normalized intrinsic viscosities (Fig. 4a; Table 3). The interactions between the tested solvents and PLA and PLGA decreased with decreasing values of δ_d . Acetone, which offered the highest absolute and relative value of δ_p (Fig. 4b), was the exception to this correlation. As already discussed, δ_p contributes significantly to the thermodynamic interactions between PLA and PLGA and suitable solvents. In accordance to the values derived from the group contribution methods, this effect was more pronounced in the case of PLGA than with PLA. This result again indicates that the relation of the partial solubility parameters was predicted well by the applied group contribution methods (Table 1, Fig. 2). Like PLA and PLGA, PEG-PLA showed strong interactions with chloroform (Fig. 4a). In the other solvents, almost constant interactions were observed, most likely as an effect of the amphiphilic character of the diblock copolymer. To complete our studies, we calculated the HSPs for PLA on the basis of the viscosity data published by Siemann [22] (Table 3,4). The resulting parameters (17.6; 4.7; 5.6) were shifted towards a higher value for δ_d and lower values for δ_p and δ_h compared to the values obtained in our study (16.6; 6.3; 6.5) (Fig. 5b).

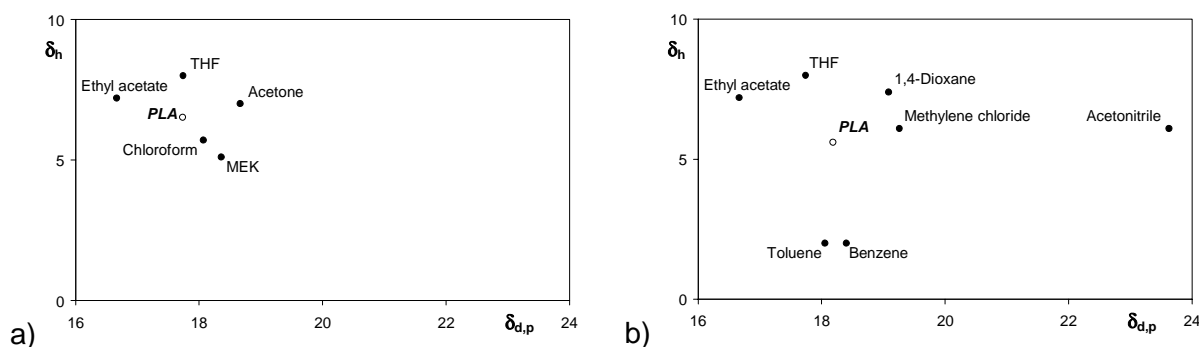


Fig. 5: Solvent map including PLA illustrating the viscosity measurements conducted in this study (a) or by Siemann [22] (solubility parameters of PLA were calculated as described in this study) (b).

This parameter alteration mainly resulted from the different solvents that were used by Siemann. Toluene, benzene and methylene dichloride are solvents that are described as having high δ_d and low δ_p and δ_h values compared to acetone, ethyl acetate and MEK (Table 3). Since Siemann's study examined a wider solvent range, including acetonitrile, which is characterized by a very high δ_p value, a large radius of interaction ($14.1 \text{ MPa}^{1/2}$) resulted from this data (Table 4). This high value, exceeding the typical range of interaction radii ($2\text{-}12 \text{ MPa}^{1/2}$) [27,36,37], nicely represents the broad range of solubility that was observed for these biodegradable polymers.

4. Discussion

The solubility parameter estimations, solubility test and viscosity measurements revealed that the solubility parameters of biodegradable poly(α -hydroxy acids) likely range near the values of methylene dichloride and chloroform. The highest intrinsic viscosity, as a measure for the interactions between solvent and polymer, was measured in chloroform for all of the tested polymers. The solubility tests showed that methylene dichloride was the best solvent for the polymers. Additional viscosity measurements might clarify whether methylene dichloride or chloroform shows higher interactions with the polymers. The average HSP values of both solvents are (δ_d ; δ_p ; δ_h = 18.0; 4.7; 5.9) resulting in a Hildebrand solubility parameter (δ) of 19.5, which is fairly close to the parameters calculated on the basis of the viscosity measurements (δ_d ; δ_p ; δ_h = 16.6; 6.3; 6.5 and δ = 18.9) (Table 4). The group contribution methods, however, led to much higher δ_p and δ_h values. Therefore, the experimentally determined parameters are considered more precise to those estimated by the group contribution methods.

In order to display the suitability of a solvent, it was important to not only focus on the HSP triplet, but also to consider a combined partial parameter $\delta_{d,p}$, resulting from δ_d and δ_p . Acetone, for example, proved to be a good solvent for the investigated polymers, although this solvent has a rather low δ_d , as is characteristic for most non-solvents (Table 3). However, acetone has a high δ_p . Therefore, the combination of δ_d and δ_p to a combined partial parameter $\delta_{d,p}$ versus δ_h seems to describe the solvent interactions with the polymers more precisely than the δ_d versus the $\delta_{p,h}$ plot. Figure 3b illustrates that the polymers were soluble in solvents with a $\delta_{d,p}$ exceeding 16 in combination with a δ_h smaller than 11. Only by introducing $\delta_{d,p}$ were we able to describe solubility trends for the investigated polymers.

Generally, no significant differences between the different biodegradable polymers investigated in this study were consistently evident across all of the methodologies. The viscosity measurements, however, enabled a closer insight into polymer-solvent interactions. Fig. 4a shows a decrease in the intrinsic viscosity of the solubilized polymers with decreasing solvent δ_d values. However, this trend did not apply to acetone, probably due to the high δ_p value of this solvent, highlighting the importance of the polar interactions. Moreover, with the different solvents, we always found a lower unity-normalized intrinsic viscosity for PLGA than for PLA (Fig. 4a). This did not hold true for acetone in accordance with the increased δ_p values calculated by the group contribution methods. Accordingly, the group contribution

methods can be regarded as useful tools to estimate the fractional solubility parameters for the investigated polymers. The fractional parameters highlight the ratio of the partial parameters and allow for an easier comparison of the different solvents and polymers. The absolute HSP values including those obtained by averaging the different methods, however, appeared too high with regard to δ_p and δ_h (Table 1). Compared to the experimentally determined values, the HSP computation performed according to the HvK method using the molar volumes approximated according to the general method (HvK/general) fit best (Table 1).

Among the tested methods, the viscosity measurements were found to be most suitable to investigate polymer-solvent interactions. As in many other methods, however, the resulting HSPs depend on the parameter range of the investigated solvents (Fig. 5). In a similar manner, the outstanding HSPs of propylene carbonate (20.1; 18.0; 4.1) influenced the HSPs of PLA calculated from the solubility data provided by Boehringer Ingelheim. Based on this data set, we determined a HSP triplet of (17.1; 9.8; 6.9) (Table 3); without propylene carbonate the values (16.7; 8.8; 7.2) would have been closer to those resulting from the viscosity study. Ideally, solvents near the borders of the solubility parameter maps should initially be included in any study attempting to determine a polymer's solubility parameters. Thereafter, solvents located close to the determined center point of solubility should be tested for a precise determination of the solubility parameter values.

5. Conclusion

Theoretical and experimental methods were applied to determine the Hansen solubility parameters of PLA (Resomer® R206), PLGA (Resomer® RG 756) and PEG-PLA (MeO-PEG₂PLA₄₀). HSPs computed according group contribution methods resulted in artificially high absolute values for δ_p and δ_h . The fractional parameters predicted by these methods, however, proved valuable. In solubility tests, the polymers demonstrated the best solubility in solvents offering a $\delta_{d,p}$ from 17 to 20 and a δ_h between 5 and 8. These parameters correlated well to the values calculated from the viscosity measurements. Although partial solubility parameter discrimination between the investigated polymers was not achieved, viscosity measurements provided detailed information on polymer-solvent interactions.

6. References

- (1) Gombotz WR, Pettit DK. 'Biodegradable polymers for protein and peptide drug delivery'. *Bioconjug Chem* (1995); **6**: 332-351.
- (2) Langer R, Peppas NA. 'Advances in Biomaterials, Drug Delivery, and Bionanotechnology'. *AIChE J* (2003); **49**: 2990-3006.
- (3) Panyam J, Labhasetwar V. 'Biodegradable nanoparticles for drug and gene delivery to cells and tissue'. *Adv Drug Delivery Rev* (2003); **55**: 329-347.
- (4) Jain RA. 'The manufacturing techniques of various drug loaded biodegradable poly(lactide-co-glycolide) (PLGA) devices'. *Biomaterials* (2000); **21**: 2475-2490.
- (5) Athanasiou KA, Agrawal CM, Barber FA, Burkhart SS. 'Orthopaedic applications for PLA-PGA biodegradable polymers'. *Arthroscopy* (1998); **14**: 726-737.
- (6) Gopferich A, Peter SJ, Lucke A, Lu L, Mikos AG. 'Modulation of marrow stromal cell function using poly(D,L-lactic acid)-block-poly(ethylene glycol)-monomethyl ether surfaces'. *J Biomed Mater Res* (1999); **46**: 390-398.
- (7) Lucke A, Tessmar J, Schnell E, Schmeer G, Gopferich A. 'Biodegradable poly(-lactic acid)-poly(ethylene glycol)-monomethyl ether diblock copolymers: structures and surface properties relevant to their use as biomaterials'. *Biomaterials* (2000); **21**: 2361-2370.
- (8) Gref R, Luck M, Quellec P, Marchand M, Dellacherie E, Harnisch S, Blunk T, Muller RH. 'Stealth' corona-core nanoparticles surface modified by polyethylene glycol (PEG): Influences of the corona (PEG chain length and surface density) and of the core composition on phagocytic uptake and plasma protein adsorption'. *Colloids Surf B* (2000); **18**: 301-313.
- (9) Hacker M, Tessmar J, Neubauer M, Blaimer A, Blunk T, Gopferich A, Schulz MB. 'Towards biomimetic scaffolds: Anhydrous scaffold fabrication from biodegradable amine-reactive diblock copolymers'. *Biomaterials* (2003); **24**: 4459-4473.
- (10) Thomasin C, Ho NT, Merkle HP, Gander B. 'Drug microencapsulation by PLA/PLGA coacervation in the light of thermodynamics. 1. Overview and theoretical considerations'. *J Pharm Sci* (1998); **87**: 259-268.
- (11) Forster A, Hempenstall J, Tucker I, Rades T. 'Selection of excipients for melt extrusion with two poorly water-soluble drugs by solubility parameter calculation and thermal analysis'. *Int J Pharm* (2001); **226**: 147-161.
- (12) Li J, Masso JJ, Guertin JA. 'Prediction of drug solubility in an acrylate adhesive based on the drug-polymer interaction parameter and drug solubility in acetonitrile'. *J Control Release* (2002); **83**: 211-221.
- (13) Hancock BC, York P, Rowe RC. 'The use of solubility parameters in pharmaceutical dosage form design'. *Int J Pharm* (1997); **148**: 1-21.

-
- (14) Kolar P, Shen JW, Tsuboi A, Ishikawa T. 'Solvent selection for pharmaceuticals'. *Fluid Phase Equilib* (2002); **194-197**: 771-782.
- (15) Hildebrand JH, Scott RL. *The Solubility of Non-Electrolytes*. New York: Dover, 1964.
- (16) Barton AFM. 'Solubility parameters'. *Chem Rev* (1975); **75**: 731-754.
- (17) Hansen, C. M. 'Three Dimensional Solubility Parameter and Solvent Diffusion Coefficient. Importance in Surface Coating Formulation.'. *Doctoral Dissertation*. Danish Technical Press, Copenhagen. (1967)
- (18) Barton AFM. *CRC Handbook of Solubility Parameters and Other Cohesion Parameters*. 1983.
- (19) Grulke EA. 'Solubility Parameter Values'. In: Brandrup J, Immergut EH, Grulke EA, editors. *Polymer Handbook*. New York: John Wiley, 1999. p. VII/675-714.
- (20) Shively ML, Coonts BA, Renner WD, Southard JL, Bennett AT. 'Physico-chemical characterization of a polymeric injectable implant delivery system'. *J Control Release* (1995); **33**: 237-243.
- (21) Packhaeuser CB, Schnieders J, Oster CG, Kissel T. 'In situ forming parenteral drug delivery systems: an overview'. *Eur J Pharm Biopharm* (2004); **58**: 445-455.
- (22) Siemann U. 'The solubility parameter of poly(D,L-lactic acid)'. *Eur Polym J* (1992); **28**: 293-297.
- (23) Gander B, Wehrli E, Alder R, Merkle HP. 'Quality improvement of spray-dried, protein-loaded D,L-PLA microspheres by appropriate polymer solvent selection'. *J Microencapsul* (1995); **12**: 83-97.
- (24) Thomasin C, Merkle HP, Gander B. 'Drug microencapsulation by PLA/PLGA coacervation in the light of thermodynamics. 2. Parameters determining microsphere formation'. *J Pharm Sci* (1998); **87**: 269-275.
- (25) Liu J, Xiao Y, Allen C. 'Polymer-Drug Compatibility: A Guide to the Development of Delivery Systems for the Anticancer Agent, Ellipticine'. *J Pharm Sci* (2004); **93**: 132-143.
- (26) Gander B, Johansen P, Nam-Tran H, Merkle HP. 'Thermodynamic approach to protein microencapsulation into poly(D,L-lactide) by spray drying'. *Int J Pharm* (1996); **129**: 51-61.
- (27) Segarceanu O, Leca M. 'Improved method to calculate Hansen solubility parameters of a polymer'. *Prog Org Coat* (1997); **31**: 307-310.
- (28) van Krevelen DW. *Properties of Polymers*. Amsterdam, The Netherlands: Elsevier, 1990.
- (29) Ahmad H, Yaseen M. 'Application of a chemical group contribution technique for calculating solubility parameters of polymers'. *Polym Eng Sci* (1979); **19**: 858-863.
-

- (30) Bustamante P, Escalera B, Martin A, Selles E. 'Predicting the solubility of sulfamethoxypyridazine in individual solvents I: calculating partial solubility parameters'. *J Pharm Sci* (1989); **78**: 567-573.
- (31) Breitzkreutz J. 'Prediction of intestinal drug absorption properties by three-dimensional solubility parameters'. *Pharm Res* (1998); **15**: 1370-1375.
- (32) van Krevelen DW. 'Chapter 7: Cohesive Properties and Solubility'. In: *Properties of Polymers*. Amsterdam, The Netherlands: Elsevier, 1990. p. 189-225.
- (33) Fedors RF. 'Method for estimating both the solubility parameters and molar volumes of liquids'. *Polym Eng Sci* (1974); **14**: 147-154.
- (34) Fedors RF. 'Method for estimating both the solubility parameters and molar volumes of liquids. Addendum'. *Polym Eng Sci* (1974); **14**: 472-
- (35) van Krevelen DW. 'Chapter 4: Volumetric Properties'. In: *Properties of Polymers*. Amsterdam, The Netherlands: Elsevier, 1990. p. 71-107.
- (36) Lindvig T, Michelsen ML, Kontogeorgis GM. 'A Flory-Huggins model based on the Hansen solubility parameters'. *Fluid Phase Equilib* (2002); **203**: 247-260.
- (37) Stoye D. 'Solvents'. In: *Ullmann's Encyclopedia of Industrial Chemistry, Vol. A 24*. Weinheim: VCH, 1993. p. 437-505.

Chapter 6

Solid Lipid Templating: A Versatile Lab-scale Fabrication Technique for Macroporous Tissue Engineering Scaffolds

Michael Hacker¹, Michael Ringhofer², Markus Neubauer¹, Thomas Vogel^{1,3},
Bernhard Appel¹, Torsten Blunk¹, Achim Göpferich¹, Michaela B. Schulz^{1,3}

¹ Department of Pharmaceutical Technology, University of Regensburg,
Universitätsstrasse 31, 93040 Regensburg, Germany

² Anton Paar GmbH, Anton Paar Strasse 20, 8054 Graz, Austria

³ Department of Pharmaceutical Technology, University of Graz,
Schubertstrasse 6, 8010 Graz, Austria

1. Introduction

The engineering of functional tissues from isolated mammalian cells and macroporous three-dimensional (3-D) biomaterial constructs holds great potential for applications in the medical and natural sciences [1-3]. A typical tissue engineering approach uses biocompatible, biodegradable, polymeric cell carriers (scaffolds) as an artificial extracellular matrix in combination with morphogenetic effectors (e.g. growth, differentiation and adhesion factors) and host cells that will respond to the signals of the effector substance [4]. In these attempts, the scaffolds play a pivotal role in cell seeding, proliferation, and new tissue formation in three dimensions [5]. Biodegradable poly(α -hydroxy acids), namely poly(D,L-lactic acid) (PLA) and copolymers (PLGA) with poly(glycolic acid) (PGA), are attractive and widely applied scaffolding materials with advantages over ceramics and metals because they degrade as the new tissues are formed [6,7]. In contrast to natural scaffolding materials, such as collagen, chitosan or chitin, these synthetic polymers can be supplied in reproducible quality and free of pathogenic or immunogenic organic residues. Depending on the mechanical properties of the tissue to be engineered and the extent of cell-material interaction desired, a suitable polymer has to be selected with regard to its degradation kinetic, composition and molecular weight. Consequently, materials with different characteristics, such as molecular weight, glass transition temperature and solubility, have to be processed into macroporous cell carriers with reproducible microstructure. Various techniques such as salt leaching [8,9], fibrous fabric processing [6], gas foaming [10], thermally induced phase separation [11] and several solid freeform fabrication techniques [12] have been developed to generate highly porous polymer scaffolds from biodegradable polymers. Despite the remarkable potential that some of these scaffolds have shown in attempts to engineer a variety of tissues, the “ideal” scaffold has not yet been developed [13,14]. The critical scaffold properties and demands on the fabrication procedure are the following: Architectural features, namely pore size and shape, pore wall morphology, porosity, surface area and pore interconnectivity, have to be controlled, as they have a direct impact on cell seeding, migration, growth, transport of oxygen, nutrients and wastes, and new tissue formation in three dimensions [15,16]. Therefore, control over architectural features, especially pore size and interconnectivity, during scaffold fabrication is essential. Fibrous fabrics, for instance, offer the ideal porosity and permeability. Their mechanical stability, however, is very low and only a few materials can be processed into such scaffolds. Salt leaching, on the other hand, is a technique that offers good control over the scaffold pore size and porosity. But even improved salt fusion

techniques result in scaffolds that lack sufficient pore interconnectivity [17,18]. The applicability of the processing method to a variety of polymers and polymer properties, which in large part predetermine the mechanical and degradation characteristics of a scaffold, is a further prerequisite for an ideal processing method. As some applications use experimental polymers that may contain hydrolysable functional groups [19] or require the encapsulation of growth factors during scaffold fabrication, an anhydrous fabrication technique is generally preferred. Moreover, lab-scale processing enables scaffold fabrication from small amounts of newly developed biodegradables and allows for the systematic testing of different architectural designs. Nevertheless, the fabrication should not be limited to a certain scaffold size. A recently published hydrocarbon templating technique met most of the described demands [20]. This technique was further improved with regard to biocompatibility and adaptability to low molecular weight block copolymers by our group [21]. The developed solid lipid templating technique uses solid lipid microparticles as porogens and non-halogenated polymer solvents to process biodegradable polymers into macroporous scaffolds, providing an interconnected pore structure. Pore interconnectivity is obtained by adjusting the porogen melting point and extraction conditions to the polymer's glass transition temperature. This way, a continuous molten lipid phase is formed during porogen extraction in warm *n*-hexane. Simultaneously, the polymer is precipitated at the phase boundary, leading to the formation of condensed polymer sponges [21].

In this study, we demonstrate the wide applicability of this technique. Processing conditions are described to fabricate tissue engineering scaffolds from several biodegradable polymers of different compositions and molecular weights. The pore size of the scaffolds was controlled by the size distribution of the porogen microparticles. During processing, the rheological behavior of the dispersion prepared from the polymer solution and porogen microparticles has major influence on micro- and microstructure of the resulting scaffolds. We observed that highly viscous dispersions resulted in low interconnectivity, while a low viscosity caused macroscopic deformation of the scaffold as well as coarsening of the microstructure. To address this process parameter, oscillating rheological measurements were performed. Since the viscosity of the dispersion also depends on the size of the particles of the solid phase, we controlled the viscosity by increasing the polymer concentration with increasing porogen particle size. The suitability of the fabricated scaffolds was tested using an established cartilage cell culture model [22].

2. Materials and Methods

2.1. Materials

Poly(D,L-lactic acid) (PLA), Resomer® R207, $M_w = 160$ kDa, $T_g = 54.8$ °C, poly(D,L-lactico-glycolic) (PLGA), Resomer® RG756, synthesized from 75% lactic acid (LA) and 25% glycolic acid (GA), $M_w = 90$ kDa, $T_g = 50.7$ °C, were kindly provided by Boehringer Ingelheim (Ingelheim, Germany). Monomethyl ether-poly(ethylene glycol)-block-poly(D,L-lactic acid) (MeO-PEG₂PLA₄₀; MeO-240), $M_n = 42$ kDa, $T_g = 43.0$ °C, which consist of a 2 kDa MeO-PEG block covalently bound to a 40 kDa PLA block, was synthesized and characterized as previously described [23].

The solid lipids that were used as porogen materials, namely Softisan® 154 and Witepsol® H42, were kindly provided by SASOL Germany GmbH (Witten, Germany). Methyl ethyl ketone (MEK), tetrahydrofuran (THF), ethyl acetate and *n*-hexane were purchased in analytical grade from Merck (Darmstadt, Germany).

2.2. Methods

2.2.1. Preparation of solid lipid microparticles

Microparticles were prepared using a melt dispersion technique. 10 g of the solid lipid mixture prepared from Softisan® 154 und Witepsol® H42 (SH), either SH 1:1 or SH 2:1, were weighed in a poly(propylene) tube. After the addition of 7.5 mL water, the tube was heated to 65 °C. In a normal batch, eight tubes were processed in parallel. The mixture was emulsified by turning the tube upside down 10 times and subsequently cast into a larger volume (600 mL) of stirred, cold (15 °C) water. After 10 min of constant stirring, the hardened particles were collected by filtration, rinsed with cold water and dried under laminar air flow for 3 days. Finally, the microparticles were separated into different size ranges by sifting with sieves (100µm, 300µm, 500µm, 710µm) (Retsch GmbH & Co. KG, Haan, Germany).

2.2.2. Particle size analysis

The size distribution of the prepared lipid microparticles was investigated using laser diffraction (Mastersizer 2000 Hydro 2000S, Malvern Instruments, Herrenberg, Germany) as follows: approximately 100 mg of lipid microparticles were directly added to the dispersion unit (Hydro 2000S), which was filled with an ethanol-water-mixture (68.2% (v/v), $\rho = 0.89 \text{ gcm}^{-3}$, refractive index: 1.36). The particles were dispersed by stirring at 3000 rpm for 5 min. The volume based particle size distribution was calculated using the Fraunhofer approximation (Malvern Software V5.1). Further values provided by the software included the average particle size ($d_{3,2}$) (surface weighted mean diameter) and specific surface area. The measurements were repeated in triplicate.

2.2.3. Scaffold fabrication procedure

To fabricate macroporous scaffolds from biodegradable polymers, we recently developed an anhydrous technique that uses solid lipid microparticles as porogens [21] (Fig. 1).

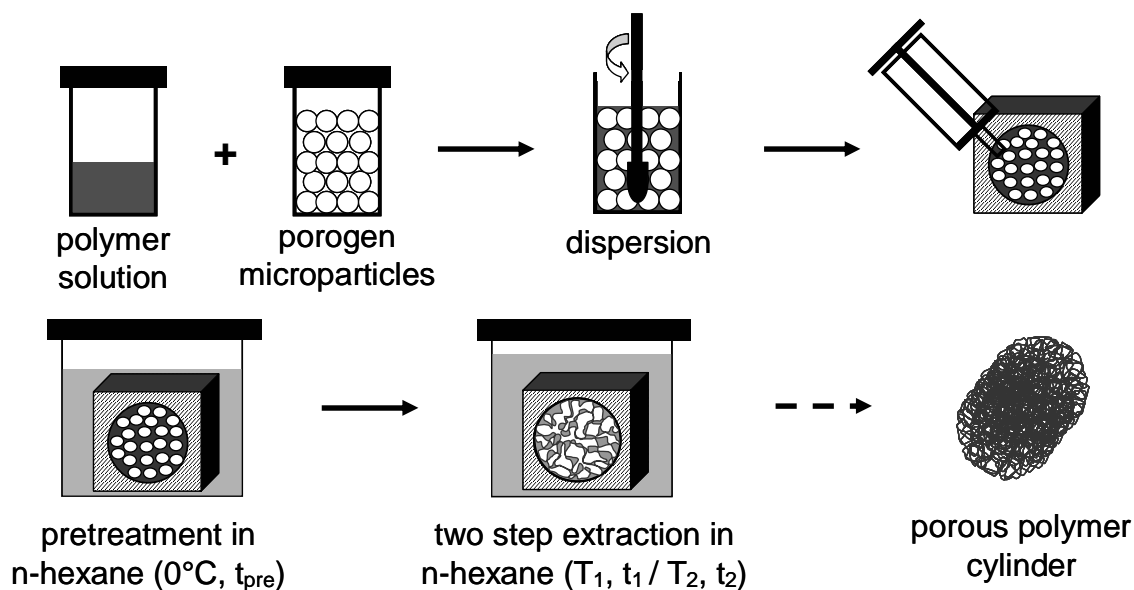


Fig. 1: Schematic illustration of the Solid Lipid Templating procedure. An organic solution of the polymer is mixed with the solid lipid microparticles. The resulting dispersion is transferred into molds, which were submerged in warm n-hexane for polymer precipitation and porogen extraction subsequent to a pretreatment in cold n-hexane.

Briefly, scaffold fabrication started with a polymer solution. Appropriate solvents and polymer concentrations are described in the results section. Under ice cooling, the polymer solution was mixed with the solid lipid microparticles. A polymer to porogen ratio of 1:4 (w/w) was used if not otherwise stated. The homogeneous dispersion was transferred into

Teflon® molds (1.9 cm x 1.9 cm x 1.2 cm) with a cylindrical cavity 0.8 cm in diameter. After a pre-extraction treatment step in *n*-hexane at 0°C (MeO-PEG₂PLA₄₀: 90min; other polymers: 15min), the molds were submerged in warm *n*-hexane to induce solvent extraction followed by the precipitation of the polymer and extraction of the lipid porogen. This procedure was carried out in two separate *n*-hexane baths of different temperatures T₁ and T₂ for t₁ and t₂ with t₁ + t₂ = 30 min. The resulting porous, cylindrical polymer constructs were allowed to cool in cold (0°C) *n*-hexane and were removed from the molds. After drying under vacuum for 48 h, the constructs were cut into 2 mm slices, which were then described as scaffolds. Table 1 gives a summary of the applied processing conditions.

Table 1: Porogen characteristics and processing parameters for the fabrication of scaffolds from different polymers. Porosity data of different PLGA (RG756) scaffolds was determined (mean ± standard deviation; n=3).

Polymer	Porogen material	Size range		Polymer content	Conc. (polymer solution)	Extraction conditions		Porosity
		d _{3,2}	d _{3,2}			step 1	step 2	
	Softisan 154: Witepsol H42	[µm]	[µm]	(w/w)	[mg/mL]	(T ₁ ; t ₁)	(T ₂ ; t ₂)	[%]
<i>Pore size / Rheology</i>								
PLGA (RG756)	2:1	100 - 300	200	20 %	330	52°C; 10'	40°C; 20'	---
PLGA (RG756)	2:1	300 - 500	360	20 %	350	52°C; 10'	40°C; 20'	---
PLGA (RG756)	2:1	500 - 710	590	20 %	365	52°C; 10'	40°C; 20'	---
MeO-240	1:1	100 - 300	180	25 %	435	45°C; 10'	35°C; 20'	---
<i>Porosity</i>								
PLGA (RG756)	2:1	100 - 300	200	20 %	330	52°C; 10'	40°C; 20'	90.4 ± 0.5
PLGA (RG756)	2:1	100 - 300	210	15 %	265	52°C; 10'	40°C; 20'	91.5 ± 0.4
PLGA (RG756)	2:1	100 - 300	210	10 %	185	52°C; 10'	40°C; 20'	94.1 ± 0.4
<i>Polymer type</i>								
MeO-240	1:1	100 - 300	200	20 %	400	45°C; 10'	35°C; 20'	---
MeO-240	1:1	300 - 500	400	20 %	410	45°C; 10'	35°C; 20'	---
PLA (R207)	2:1	100 - 300	180	20 %	230	52°C; 10'	40°C; 20'	---
PLA (R207)	2:1	300 - 500	255	20 %	250	52°C; 10'	40°C; 20'	---

2.2.4. Microscopic assessment of scaffold macro- and microstructure

The macrostructure of the porous polymer cylinders and scaffolds was examined using a zoom stereo microscope (Wild M7A, Wild Heerbrugg Ltd., Heerbrugg, Switzerland). The scaffold microstructure was visualized by scanning electron microscopy (SEM). For this procedure, samples were mounted on aluminum stubs with conductive carbon tape and coated with gold-palladium. All micrographs were obtained at 10 kV on a DSM 950 (Zeiss, Oberkochen, Germany).

2.2.5. *Oscillatory rheological measurements*

The dispersions of porogen particles in polymer solution prepared during scaffold fabrication were characterized using a Physica MCR 300 rheometer (Anton Paar GmbH, Graz, Austria) with a 2.5 cm sandblasted steel plate according to the following protocol: Under ice cooling, the polymer solution was mixed with the solid lipid microparticles for 3 min. The mixture was transferred to the rheometer using a polypropylenes syringe and equilibrated at 5°C. The measurement gap was set to 2 mm. After 60 sec, the first frequency sweep (100 – 0.1 Hz) was measured at a displacement of 0.01% and a temperature of 5°C. A second frequency sweep (100 – 0.1 Hz at 0.01% displacement) at 5°C followed another equilibration period of 3 min. The parameters recorded during the second frequency sweep were analyzed to determine the complex viscosity (η^*) of the dispersion. To compare different formulations, the values of the complex viscosity at 1Hz were interpolated.

2.2.6. *Determination of residual porogen material*

The detection of triglyceride residues inside the scaffolds was realized through modulated differential scanning calorimetry (MDSC). The samples were precisely weighed in non-hermetic AutoDSC aluminum sample pans (TA Instruments, Alzenau, Germany). The sample pans were sealed using the sample encapsulating press (TA Instruments, Alzenau, Germany) and analyzed on a DSC 2920 equipped with a refrigerated cooling system and an autosampler (TA Instruments, Alzenau, Germany). An empty, sealed pan served as reference.

All measurements were carried out between –20 °C and 120 °C. Typically, samples were equilibrated at –20 °C for 15 min and heated to 120 °C at a heating rate of 5 °C/min. After an isothermal phase of 15 min, samples were cooled to –20 °C at 5 °C/min. Finally, after another 15 min isothermal phase, samples were again heated to 120 °C at 5 °C/min. A sinusoidal temperature modulation with a period of 60 s and temperature amplitude of 0.8 °C was applied to both heating cycles.

The resulting thermograms (total heat flow of the second heating cycle) were analyzed for melting enthalpy (peak area) of the peak attributed to the melting lipid residuals located near the glass transition step of the polymer with the Universal Analysis for NT® software provided with the DSC system.

2.2.7. *Determination of scaffold porosity*

The porosity of the scaffolds was determined by measuring the dimensions and the mass of the porous polymer cylinders as obtained from fabrication (cylinder ends were cut away) [24].

The skeletal density of the cylinder (ρ) was calculated from the mass (m), the diameter (d) and the height (h) of the cylinder:

$$\rho = \frac{4 \cdot m}{\pi \cdot d^2 \cdot h} \quad (1)$$

The porosity (ε) was calculated from the density of the construct (ρ) and density (ρ_p) of the polymer ($\rho_p(\text{RG756}) = 1.26 \text{ gcm}^{-3}$):

$$\varepsilon = 1 - \frac{\rho}{\rho_p} \quad (2)$$

2.2.8. Chondrocyte cell culture

Primary chondrocytes were isolated from full-thickness bovine articular cartilage by digestion with type II collagenase (CellSystem, St. Katharinen, Germany) as previously described [25] and resuspended in culture medium (DMEM) containing 4.5 g/l glucose (Life Technologies GmbH, Karlsruhe, Germany), 584 mg/l glutamine, 10% FBS (Life Technologies GmbH, Karlsruhe, Germany), 50 U/mL penicillin, 50 $\mu\text{g/mL}$ streptomycin (Sigma-Aldrich Steinheim, Germany), 10 mM HEPES (Sigma-Aldrich Steinheim, Germany), 0.1 mM non-essential amino acids (Life Technologies GmbH, Karlsruhe, Germany), 0.4 mM proline (Sigma-Aldrich Steinheim, Germany), and 50 $\mu\text{g/mL}$ ascorbic acid (Sigma-Aldrich Steinheim, Germany). This medium was also used for cell seeding and cultivation.

The cells were seeded in spinner flasks, as described elsewhere [22]. In brief, a cell suspension containing 5×10^6 chondrocytes per scaffold was stirred at 80 rpm in a humidified (37 °C / 5% CO₂) incubator for two days to allow for cell attachment to the polymers. Cell-polymer constructs were transferred into 6-well plates (one construct and 6 mL culture medium per well) and cultured for three weeks on an orbital shaker at 50 rpm. Medium supplemented with different amounts of insulin (0 $\mu\text{g/mL}$, 0.05 $\mu\text{g/mL}$, 2.5 $\mu\text{g/mL}$) was completely exchanged three times per week.

At the end of the culture period, each cell-polymer construct was weighed (= wet weight) and cut in half. One part was prepared as histological sample by fixing in 2% glutaraldehyde in PBS for 30 min and then in 10% formalin. The samples were embedded in paraffin and cross-sectioned (5 μm thick). Deparaffinized sections were stained with hematoxylin and eosin (H&E) (C.I.: 45380, Sigma-Aldrich, Steinheim, Germany) for cells and safranin-O for glycosaminoglycans (GAG). The other half of the construct was used for biochemical analysis of the collagen content and GAG content [22].

3. Results

3.1. Control of pore size during scaffold fabrication

3.1.1. Porogen microparticle preparation

The solid lipid templating technique described here uses triglyceride microparticles prepared from a mixture of two solid lipids, Softisan[®] 154 und Witepsol[®] H42, as pore forming templates [21]. Despite the principle of melting the porogen particles during extraction and simultaneous polymer precipitation to generate interconnected pore networks, the pore forming particles are intended as a means to control the pore size distribution in the resulting scaffolds (Fig. 1). Solid lipid microparticles ranged in size from 50 μm to 1000 μm and were fractionated by sieving. The following size ranges were collected for scaffold fabrication: 100 - 300 μm , 300 - 500 μm and 500 - 710 μm . Figure 2 shows the particle size distribution within the three porogen classes, as determined by laser diffraction. The representative graphs depict narrow distributions characterized by D(0.5) values (the diameter below which 50% of the volume of particles are found) of about 210 μm (fraction: 100 - 300 μm), 365 μm (fraction: 300 - 500 μm) and 580 μm (fraction: 500 - 710 μm) that corresponded to the $d_{3,2}$ (surface weighted mean) values (Table 1).

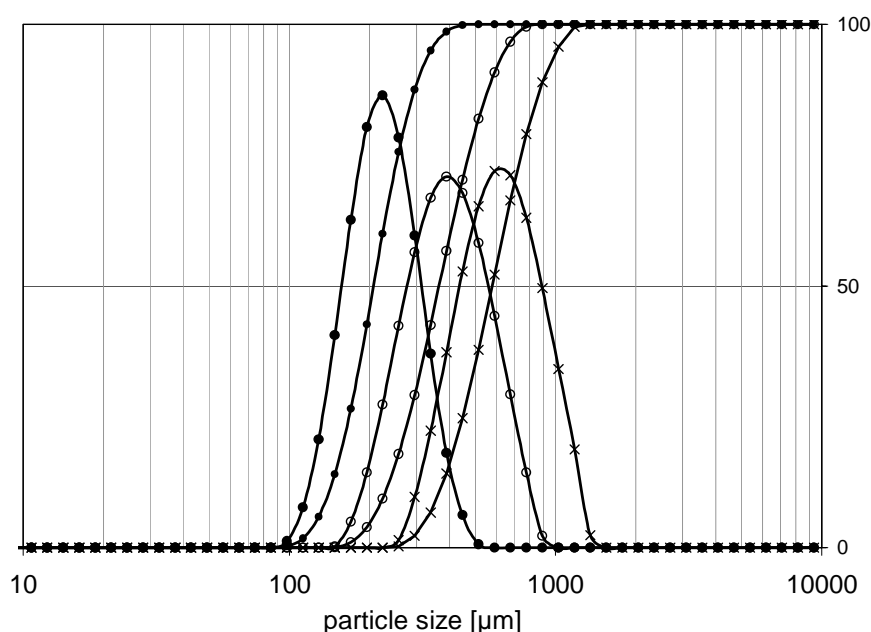


Fig. 2: Differential and cumulative porogen microparticle size distribution of different sieve fractions. ●: 100 - 300 μm , ○: 300 - 500 μm , ×: 500 - 710 μm . Particles were prepared from the 2:1 mixture of Softisan[®] 154 and Witepsol[®] H42.

3.1.2. Influence of polymer concentration on the scaffold structure

The solid lipid mixture consisting of two parts Softisan[®] 154 and one part Witepsol[®] H42 (SH 2:1), which melted at 47°C [21], was chosen as porogen material to process Resomer[®] RG756, a variety of PLGA with a glass transition temperature (T_g) of 50.7°C. This combination of polymer and porogen material with the porogen's melting point located a few degrees below the polymer's T_g was recently proposed as ideal [21].

The parameters that were used to process PLGA (Resomer[®] RG756) are listed in Table 1. Ethyl acetate, which has been identified as a low-toxic solvent suitable for the generation of well interconnected pore structures in a previous study (chapter 4), was used as solvent for all polymers, except PEG-PLA. If not otherwise stated, the polymer to porogen ratio was 20% (w/w). The extraction conditions depend on the melting point of the porogen microparticles and T_g of the polymer. The initial extraction step was carried out in *n*-hexane heated to 52°C for 10min and extraction continued at 40°C for 20 min. This way, the swift melting of the porogen particles during extraction generates pore interconnections.

During polymer processing, the rheological characteristics of the dispersion of porogen in the polymer solution have a major influence on the scaffold microstructure. In addition to the molecular weight and composition of the polymer and the type of polymer solvent, the concentration of the polymer solution influences the viscosity of the dispersion (Fig. 1).

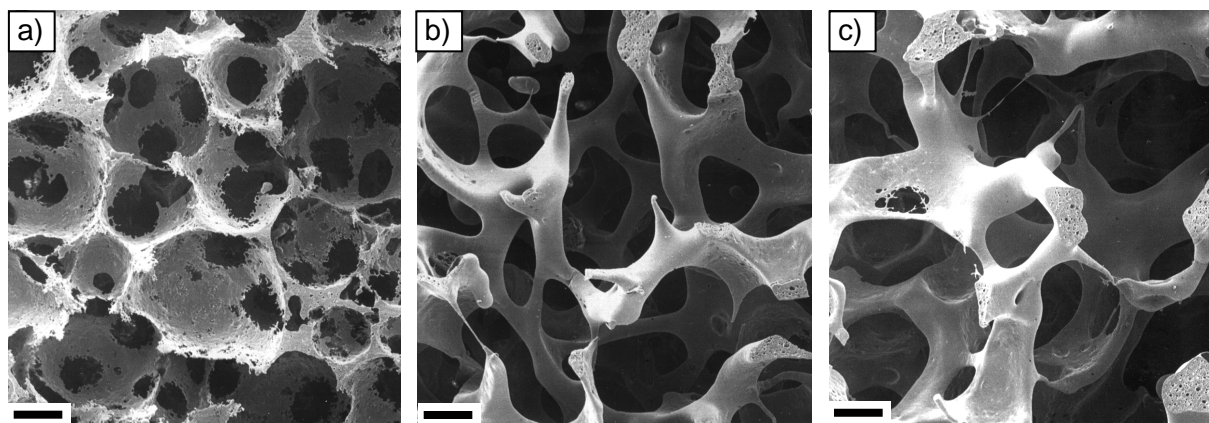


Fig. 3: Scanning electron micrographs of PLGA (RG756) scaffolds fabricated using different polymer concentrations. a) 380 mg/mL, b) 330 mg/mL, c) 300 mg/mL. Porogen particles were 100 - 300 μm in size. Scale bars represent 100 μm .

Figure 3 depicts the dependence of the scaffold microstructure on the concentration of the polymer solution used for processing. The scaffolds were prepared from PLGA (Resomer[®] RG756) using SH 2:1 microparticles (100 - 300 μm) as porogens and ethyl acetate as the polymer solvent. Polymer processing at the highest concentration (380 mg/mL) resulted in a

scaffold microstructure characterized by interconnected pores in the shape of the porogen microparticles (Fig. 3). Lower polymer concentrations (330 mg/mL and 300 mg/mL), in contrast, resulted in a highly permeable network of well condensed polymer sponges. The structure achieved with the lower concentrations closely resembles natural spongy bone [26]. An excessive decrease in polymer concentration (300 mg/mL), however, resulted in a dispersion with low viscosity that partly ran out of the mold (Fig. 4a). The deformation of the resulting polymer cylinder was described by the difference in length between the top and the bottom of the resulting scaffold cylinder (Fig. 4b). Hardly any deformation was observed for scaffolds prepared from the 380 mg/mL and 330 mg/mL polymer solutions. A significant scaffold deformation, however, was found when the polymer concentration was reduced to 300 mg/mL. Based on the data shown in Figures 3 and 4, a polymer concentration of 330 mg/mL is suitable to process PLGA (RG756) with SH 2:1 microparticles (100 - 300 μ m) into macroporous scaffolds with a spongy microstructure.

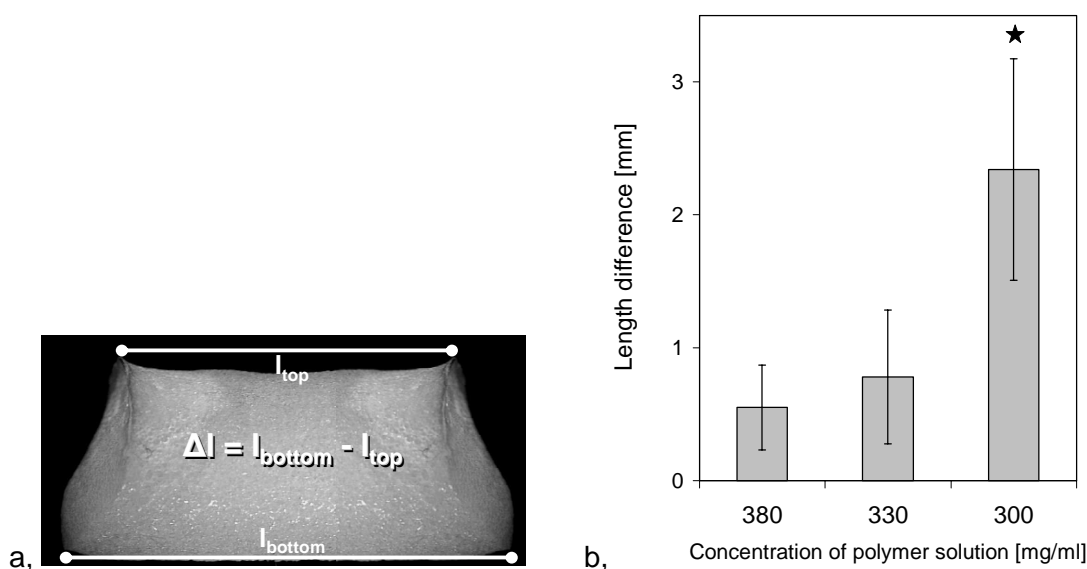


Fig. 4: a) Macroscopic view of a deformed scaffold as a result of low dispersion viscosity. To characterize the deformation the length difference (Δl) is calculated. b) Length difference measured on PLGA (RG756) scaffolds fabricated from differently concentrated polymer solutions. Columns represent average \pm standard deviation ($n=4$). Statistical significance ($p < 0.01$) is denoted by a ★.

3.1.3. Rheological characterization of the scaffolding dispersions

The experiments conducted to determine a suitable polymer concentration highlighted the pivotal role of dispersion viscosity for the scaffolding process. To evaluate whether the empirical approach could be rationalized by a rheological characterization of the scaffolding dispersion, we applied oscillation rheology. On a control stress rheometer equipped with a plate-plate geometry, frequency sweep measurements were performed. The complex viscosity (η^*) and the complex moduli, storage and loss modulus (G' and G''), were determined over a frequency range of 100 to 0.1 Hz. Figure 5 shows the frequency sweeps of the three dispersions with 300, 330 and 380 mg/mL PLGA.

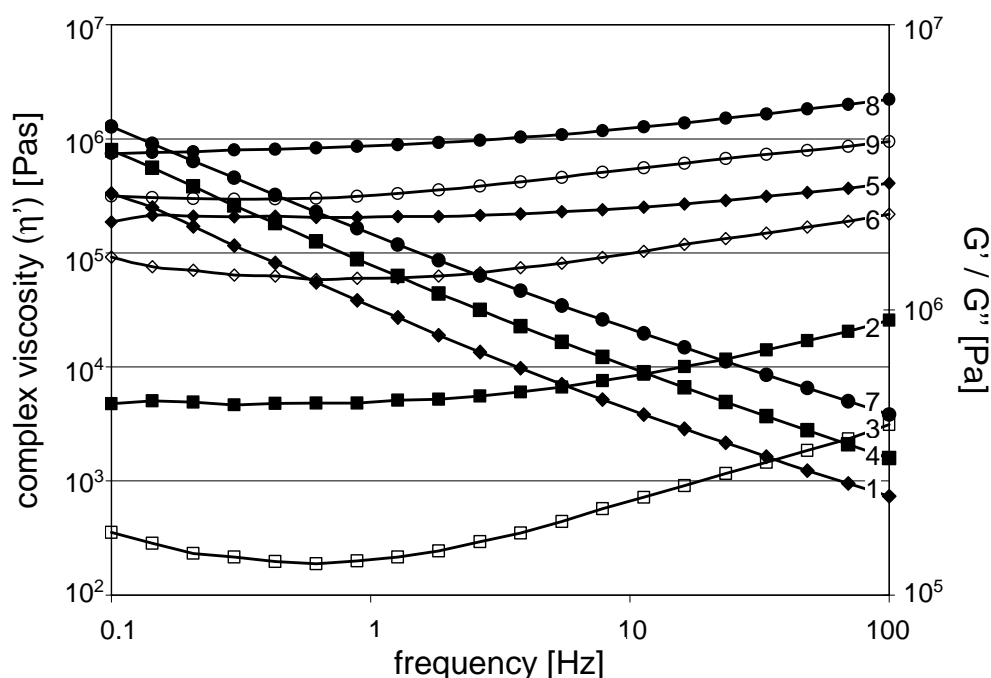


Fig. 5: Rheological measurements of dispersion prepared from differently concentrated RG756 solutions and SH 2:1 microparticles (100 – 300 μm). Frequency dependence of the dynamic moduli (G' , G'') and the complex viscosity (η^*) of the dispersions at 5°C. Rheograms 1, 2 and 3 (η^* , G' , G'') originate from a polymer concentration of 300 mg/mL; Rheograms 4, 5 and 6 (η^* , G' , G'') correspond to a concentration of 330 mg/mL; Rheograms 7, 8 and 9 correspond to 380 mg/mL.

All systems displayed storage and loss moduli that were frequency dependant. Typically, increasing the oscillatory frequency increased both the storage and loss modulus, whereas the dynamic viscosity decreased. In all three formulations, the storage modulus (G') exceeded the loss modulus (G'') and the systems may accordingly be described as gels. The logarithm of η^* at 1Hz was determined as a measure of the dispersion viscosity. The resulting complex viscosities are shown in Fig. 6.

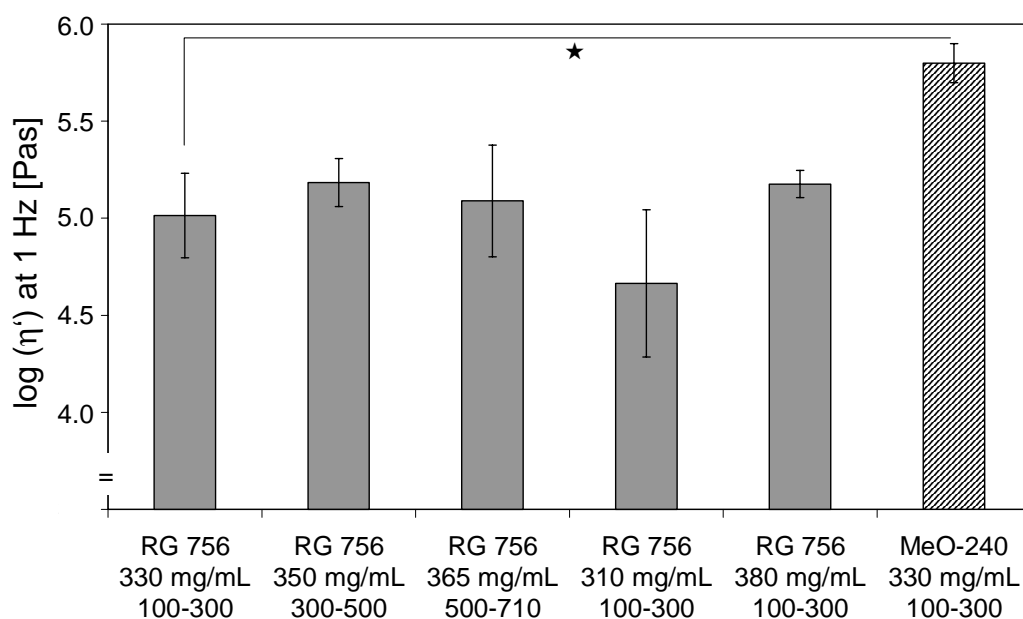


Fig. 6: Complex viscosity (η') at 1 Hz of dispersion prepared from different combination of polymer type, polymer concentration and porogen microparticle size. Statistical significance ($p < 0.05$) is denoted by a ★.

A value of 5.01 ± 0.22 was determined for the dispersion prepared from PLGA (RG756) in ethyl acetate (330 mg/mL) and SH 2:1 microparticles (100 - 300 μ m). For polymer processing using larger porogen particles, the polymer concentration was adapted to the surface area of the particles in order to match the complex viscosity to approximately 10^5 Pas at 1 Hz. Since an increase in average particle size results in a decrease in surface area, higher polymer concentrations were used in conjunction with larger particles (Table 1). The corresponding microstructures of the fabricated scaffolds are depicted in Figure 7.

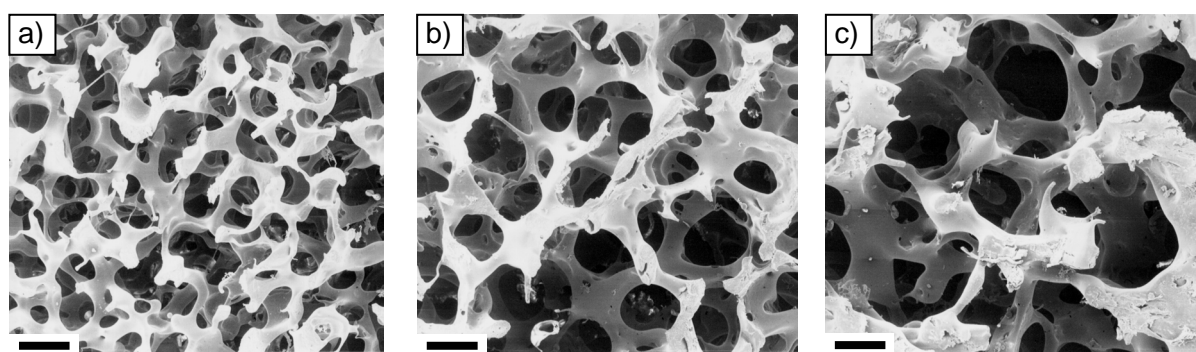


Fig. 7: Scanning electron micrographs of PLGA (RG756) scaffolds fabricated using porogen microparticles (SH 2:1) of different size ranges. a) 100 – 300 μ m, b) 300 – 500 μ m, c) 500 – 710 μ m. Scale bars represent 200 μ m.

By adjusting the dispersion viscosity to values between $10^{5.0}$ and $10^{5.2}$ Pas, highly interconnected scaffolds were generated from PLGA (RG756). The complex viscosity values of the dispersions prepared from the high- and the low-concentration PLGA solutions (380 mg/mL and 300 mg/mL) together with SH 2:1 microparticles (100 - 300 μ m) flank the viscosity range (Fig. 6) that was suitable range for scaffold fabrication from PLGA (RG756) dissolved in ethyl acetate. However, we found large standard deviations for dispersions with the low and intermediate PLGA concentration, 300 mg/mL and 330 mg/mL, respectively, as well as with large porogen particles. Hence a clear definition of a viscosity range distinguishing the optimal dispersion systems from non-optimal systems was not possible. Furthermore, a transfer of this viscosity range to considerably different polymer-solvent combinations was also not applicable. For the processing of MeO-PEG₂PLA₄₀ in a methyl ethyl ketone-tetrahydrofuran mixture, for example, a significantly higher viscosity proved to be optimal (Fig. 6). Correspondingly, optimal processing conditions for PLA (R207), a polymer with a higher molecular weight than PLGA (RG756), resulted in a dispersion characterized by a η' about one order of magnitude lower than that for PLGA (RG756) (data not shown).

The high variability in the viscosities of dispersions with low polymer content or high porogen particle size, however, seems to reflect the heterogeneity of their rheological behavior over the investigated frequency range. To describe this heterogeneity, we analyzed the relation between G' and G'' addressed by the loss factor ($\tan \delta = G''/G'$) (Fig. 5). We observed that the loss factor first decreased and then increased during the frequency sweep in the case of the low viscosity preparations correlating to G'' . The more highly concentrated dispersion, on the other hand, showed a more or less linear correlation between G'' and the oscillation frequency. The independent movement of porogen particles and polymer solution at low frequencies could provide an explanation for the heterogeneity observed for the less concentrated systems. Large non-linear frequency-dependent variations in G'' were found for dispersions with 300 mg/mL PLGA, while these variations were only weak with 330 mg/mL, indicating a mainly homogeneous system. Almost no variations were found with 380 mg/mL. Thus, a suitable dispersion system should behave homogeneously over the investigated frequency range. However, if the dispersion contained very low amounts of solvent such as the 380 mg/mL PLGA system, non-desired pore structures as shown in Figure 3a result. With polymer of higher molecular weight, such as the PLA (R207), lower polymer concentrations and viscosities result in homogeneous behavior, while a lower molecular weight polymer, MeO-PEG₂PLA₄₀, appears to need higher viscosities. As can be seen in Figure 7, the porogen

size distribution determined the pore size distribution in the resulting scaffolds, while comparable spongy microstructures could be generated.

3.1.4. Determination of lipid residuals in the scaffolds

As shown in Figure 8, the described extraction conditions (Table 1) are capable for a successful extraction of the porogen microparticles independent of the size distribution. Less than one percent (lipid per scaffold (w/w)) of residual porogen material was found by DSC analysis of the scaffolds.

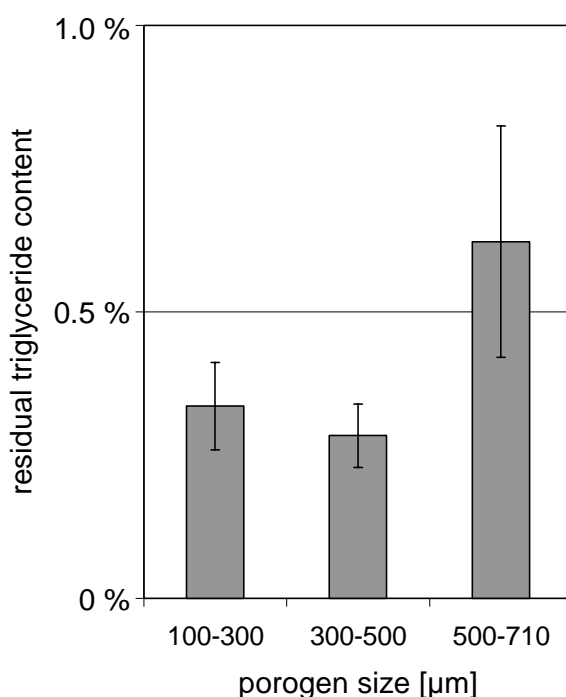


Fig. 8: Residual triglyceride content as determined by MDSC for PLGA (RG756) scaffolds fabricated using triglyceride microparticles of different size ranges.

3.2. Processing of different polymers

The processing parameters were determined and optimized for a variety of biodegradable polymers to demonstrate the versatility and adaptability of the solid lipid templating technique. First, MeO-PEG₂PLA₄₀, as a representative for low molecular weight polymer with glass transition temperatures slightly above body temperature, was processed into macroporous scaffolds with an interconnected pore structure. The scaffolds were fabricated from 20% (w/w) MeO-PEG₂PLA₄₀ dissolved in a methyl ethyl ketone-tetrahydrofurane-mixture (59:41 (v/v)) (400 mg/mL) and 80% (w/w) lipid microparticles with a low melting point (SH1:1, $T_m = 44^\circ\text{C}$) adapted to the low glass transition temperature of the polymer [21].

Following a 90 min (t_{pre}) pretreatment in cold *n*-hexane to stabilize the dispersion, the extraction conditions were adapted to the melting point of the porogen microparticles and the glass transition temperature of the polymer (step 1: 45°C for 10'; step 2: 35°C for 20') (Table 1 and Fig. 9a). The pore size of the scaffolds corresponded to the porogen particle size (100 - 300 μ m or 300 - 500 μ m) (Fig. 9a,b). The processing conditions are listed in Table 1.

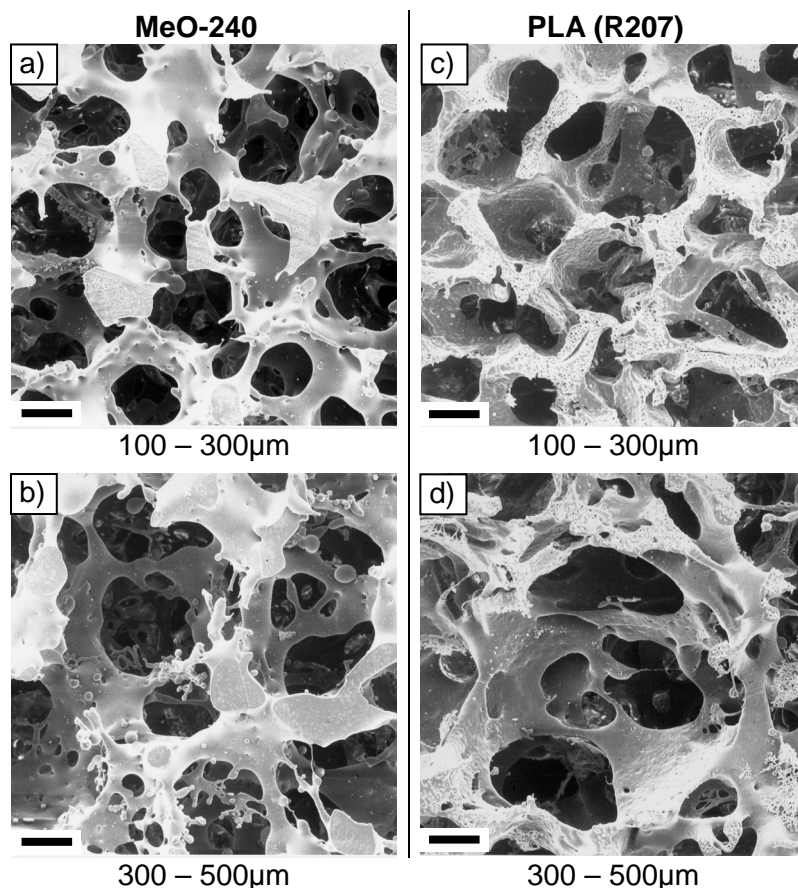


Fig. 9: Scanning electron micrographs of scaffolds fabricated from several polymers using porogen particles of different composition and sizes. a) MeO-PEG₂PLA₄₀ / SH 1:1 (100 - 300 μ m), a) MeO-PEG₂PLA₄₀ / SH 1:1 (300 - 500 μ m), c) PLA (R207) / SH 2:1 (100 - 300 μ m), d) PLA (R207) / SH 2:1 (300 - 500 μ m). Scale bars represent 100 μ m.

As a representative for high molecular weight biodegradables, PLA (R207) was processed. A sufficient dispersion viscosity was achieved with comparably low polymer concentrations (Table 1). Lipid microparticles with a melting point of 49°C (SH 2:1) were used as porogen material and extracted under the corresponding conditions (step 1: 52°C for 10'; step 2: 40°C for 20'). Control experiments (data not shown) revealed that the microstructure was not improved by using solid lipid microparticles with a higher melting point in combination with higher extraction temperatures. Control over the pore size was again achieved by varying the size of the porogen particles and adapting the amount of polymer solvent (Table 1 and Fig. 9c,d).

3.3. *Control of scaffold porosity*

The use of different size porogens had no effect on the bulk porosity of PLGA (RG756) scaffolds (data not shown). A significant increase in porosity was achieved by reducing the polymer content during processing (Table 1). PLGA (RG756) scaffolds fabricated from 20% (w/w) polymer and 80% (w/w) solid lipid microparticles displayed a porosity of $90.4\% \pm 0.5$. An increase in porogen content to 85% resulted in a porosity of $91.5\% \pm 0.4$. A (high) porosity of $94.1\% \pm 0.4$ was found for scaffolds fabricated with 90% pore forming microparticles (Table 1). The suitable processing conditions are also listed in Table 1. The increase of the porogen concentration necessitated a relative increase in the amount of polymer solvent to homogeneously disperse the porogen microparticles, resulting in decreasing concentrations of the polymer solutions.

3.4. *Scaffold testing: Engineering of cartilaginous tissue*

An established, insulin-dependent three-dimensional culture system to engineer cartilage from bovine chondrocytes [22] was transferred from fiber meshes to PLGA (RG756) scaffolds fabricated by solid lipid templating to test the applicability of the scaffolds. The scaffolds that were used in this experiment were fabricated with a polymer content of 17.5% using a porogen size of 100 - 300 μm .

Generally, the resulting tissue quality was comparable to that typically obtained with fiber meshes. An insulin dependent tissue development and extracellular matrix production was indicated by increasing wet weights along with the dose of exogenously administered insulin (Table 2). After 3 weeks, the wet weight of scaffolds receiving no exogenous insulin was $88.3 \text{ mg} \pm 18.9$. The dry weight of an empty scaffold after fabrication was 10 mg. Scaffolds receiving exogenous insulin had a significantly higher weight. A 2.5-fold increase in the wet weight was found from 88 mg for controls to 211 mg for 2.5 $\mu\text{g/mL}$ insulin. In all constructs, the cells deposited collagen and glycosaminoglycan (GAG), two major extracellular matrix (ECM) components of cartilaginous tissue. The ECM production was stimulated by exogenous insulin in a dose-dependent manner. The collagen fraction (amount of collagen per wet weight) was increased by insulin supplementation. No difference in the amount of collagen was identified between the two insulin concentrations (Table 2). The glycosaminoglycan (GAG) fraction also increased with the dose of supplemented insulin. The constructs of the insulin (2.5 $\mu\text{g/mL}$) group showed an approximately 2-fold higher GAG fraction than constructs receiving no insulin (Table 2).

Table 2: Construct characteristics of chondrocytes cultured on PLGA scaffolds for 21 days with and without supplementation of insulin. Data represents the mean \pm standard deviation of four independent measurements.

	control	insulin [$\mu\text{g}/\text{mL}$]	
		0.05	2.5
wet weight (ww) [mg]	88.3 \pm 18.9	143.5 \pm 8.9	211.4 \pm 19.8
collagen [mg]	1.9 \pm 0.3	3.8 \pm 0.4	5.6 \pm 0.5
collagen / ww [%]	2.2 \pm 0.0	2.7 \pm 0.0	2.7 \pm 0.0
GAG [mg]	2.1 \pm 0.5	5.3 \pm 0.8	9.0 \pm 1.0
GAG / ww [%]	2.4 \pm 0.2	3.7 \pm 0.4	4.3 \pm 0.1

The different amounts of GAG were also reflected in histological sections of the cell-polymer constructs, stained red with safranin-O for GAG. The extracellular matrix (ECM) of control constructs receiving no insulin stained unevenly for GAG (Fig. 10a). Even with the low insulin concentration (0.5 $\mu\text{g}/\text{mL}$), the staining was evenly distributed (Fig. 10b). The ECM in constructs receiving 2.5 $\mu\text{g}/\text{mL}$, showed strong positive staining for GAG up to the edge of the tissue (Fig. 10 c).

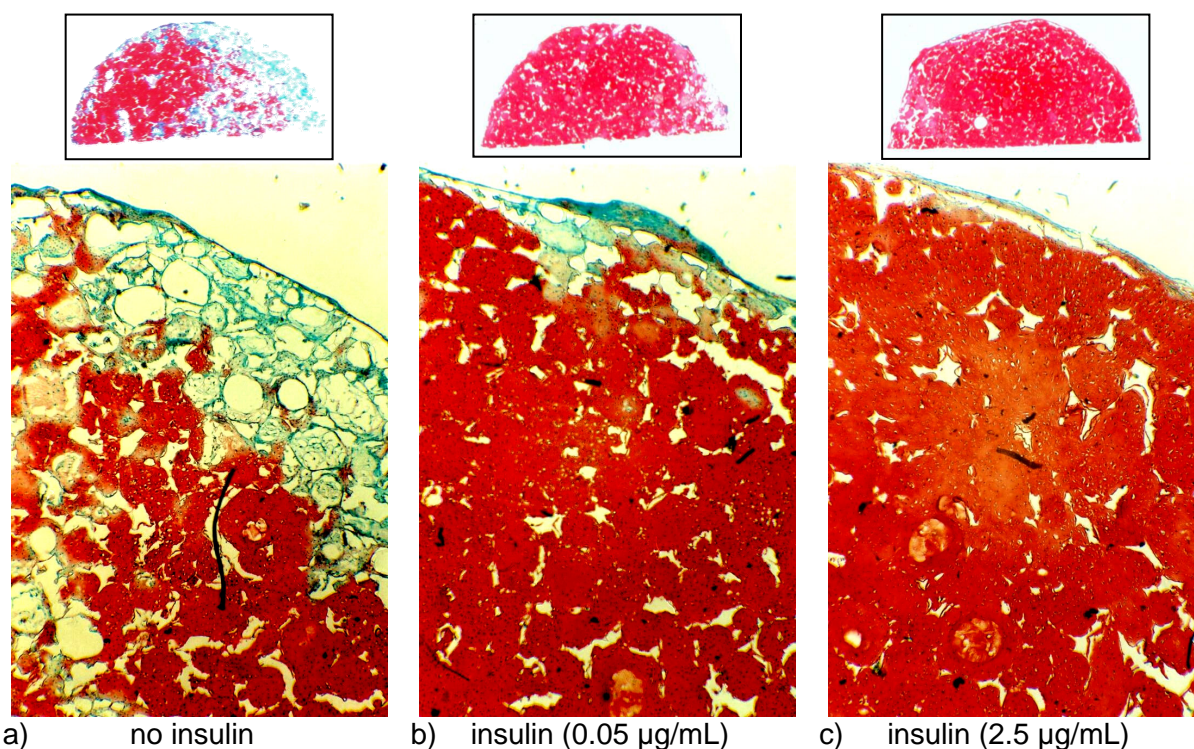


Fig. 10: Histological cross sections of three week constructs (bovine chondrocytes on PLGA (RG756) scaffolds) cultured with (0.05 $\mu\text{g}/\text{mL}$ and 2.5 $\mu\text{g}/\text{mL}$) and without the supplementation of insulin. GAG in extracellular matrix was stained red with safranin-O.

4. Discussion

Macroporous biodegradable cell carriers (scaffolds) are a major component of many tissue engineering techniques, because they provide the three-dimensional matrix for cell seeding, migration, growth, and the new tissue formation [16]. Living tissue constructs, engineered *in vitro* or *in vivo*, hold great promise to advance basic research on tissue development and function, drug development and testing as well as transplantation and reconstructive medicine. To match the wide variety of applications and tissue types, scaffold properties have to be variable and easily adaptable in terms of mechanical stability, degradation kinetics and architectural features, such as pore size and shape. Since mechanical properties and degradation kinetics are predetermined by the scaffolding material, an appropriate fabrication technique must be capable of processing a wide range of polymers [27]. Additionally, the control of key architectural properties, such as high porosity and pore interconnectivity that result in a high scaffold permeability, has to be guaranteed by the scaffold fabrication technique.

In the present study, we present the fabrication of macroporous scaffolds with high inter-pore connectivity from different biodegradable polymers using the recently developed solid lipid templating technique [21]. Solid lipid templating combines the principles of phase separation and porogen leaching to generate spongy scaffolds. Starting with a polymer solution and solid lipid microparticles, a dispersion is prepared and subsequently transferred into molds, which are finally submerged in warm *n*-hexane to precipitate the polymer and extract the porogens (Fig. 1). Mechanistically, the interconnected porous microstructure of the scaffolds is generated during this extraction step. Ideally, the solid lipid microparticles start to melt shortly after the dispersion is brought into contact with the warm extraction medium. Subsequently, the molten triglycerides form a continuous phase that separates from the liquid polymer solution before the polymer solvent and the triglyceride phase are completely extracted by the extraction media.

Various biodegradable polymers that differ in molecular weight, glass transition temperature, composition and hydrophilicity were processed into scaffolds with a microstructure similar to that of spongy bone [26] by adapting the processing parameters to three different polymers (Table 1 and Fig. 9). Ideally, porogen materials with melting points a few degrees below the glass transition temperature of the polymers were chosen. Ethyl acetate was used to dissolve all of the polymers except MeO-PEG₂PLA₄₀, which was dissolved in a MEK-THF-mixture. The concentration of the polymer solution had to be adapted to the type and molecular weight

of the polymer and the amount and average particle size of the solid lipid microspheres. The dispersion prepared from the porogen particles and the polymer solution optimally contains a sufficient amount of solvent to prolong the phase separation period until the final polymer precipitation in order to create highly interconnected frameworks (Fig. 3). At the same time, the dispersion has to be viscous enough to not flow out of the mold, which limits the amount of solvent (Fig. 4). Oscillatory rheological measurements were conducted to characterize the suitable viscosity range (Fig. 5). A complex viscosity of 10^5 Pas at 1 Hz was appropriate for the processing of PLGA (RG756). Different viscosity values were found to be optimal when polymers that differ in composition and/or molecular weight were processed. A higher dispersion viscosity than that described for PLGA (RG756) was required for the processing of a low molecular weight polymer. For the processing of high molecular weight polymers, however, a lower dispersion viscosity is suggested. Suitable viscosities for all of the investigated polymers were in the range from 10^4 to 10^6 Pas, as determined at an oscillation frequency of 1 Hz. A fine tuning of the scaffold properties based on the viscosity of the scaffolding dispersion, however, seems to be unsuitable. More detailed data may be provided by frequency sweeps and the analysis frequency dependent loss factor. Non-linear changes in the loss factor may indicate a non-homogeneous dispersion system, while a strictly linear correlation seems to be a sign for dispersion with an excessively high polymer content resulting in honeycomb-like scaffold pore structures.

With the objective of controlling the pore size of the scaffolds by varying the size of the porogen microparticles, different sieve fractions were processed. The concentration of the polymer solution that was mixed with the microparticles was adapted to the surface area of the particles, so as to keep the dispersion viscosity constant and the rheological behavior unchanged (Fig. 6). This adaptation enabled the fabrication of spongy scaffolds with pore sizes ranging from 100 μm to more than 700 μm (Fig. 7 and 9). Control over this architectural property offers the possibility for systematic pore size testing and optimization focused on the individual application. For special applications, this technique allows one to fill a mold with dispersions containing different porogen size fractions to fabricate scaffolds with a pore size gradient [28]. In addition to the pore size, the scaffold porosity is another architectural property, which could be influenced by changing the polymer to porogen ratio. Porosities higher than 90% are achievable with this protocol.

PLGA (RG756) scaffolds fabricated by solid lipid templating were tested using an established insulin-dependant cartilage cell culture system [22]. Bovine chondrocytes could be homogeneously seeded on the highly permeable polymeric scaffolds. After 3 weeks of *in vitro*

culture, considerable amounts of extracellular matrix were synthesized by the chondrocytes. Histological staining with safranin-O confirmed the presence of glycosaminoglycans (GAG), a cartilage-specific extracellular matrix component, in the scaffolds, albeit unevenly distributed. The supplementation of exogenous insulin dose-dependently increased the wet weight of the constructs as well as collagen and GAG production. Histological cross-sections of the constructs showed a strong and homogenous staining for GAG throughout the entire scaffold. Thus, the scaffolds proved to be sufficiently permeable to cells, nutrients and wastes and allowed for cartilage tissue development throughout the whole scaffold. In fact, the results were comparable to those obtained on fiber meshes, which represent the “gold-standard” for porosity and permeability. No sign of dedifferentiation was observed, but rather the chondrocytes reacted strongly to the exogenous insulin stimuli, resulting in an improved tissue development. In summary, the generated microstructure proved to be suitable for cartilage tissue engineering and will be used for the cultivation of other tissue types in future experiments.

As shown in this study, solid lipid templating is a technique that can be adapted to a variety of different polymers, offers easy control of architectural properties, such as pore size and porosity, and generates spongy frameworks characterized by high pore interconnectivity. In addition, this technique avoids aqueous media so that experimental polymers bearing hydrolysable functional groups or water-soluble polymers can be incorporated into the scaffolding. Further advantages of this technique include: First, bioactive proteins, such as growth factors, can be directly encapsulated as solids during scaffold fabrication and will be released when the scaffold is brought into contact with body fluids or cell culture medium. Second, there is no requirement for sophisticated equipment, unlike the textile technology, solid free-form fabrication or three-dimensional printing. Third, the porogen extraction is completed after 30 min, while conventional porogen leaching techniques require extraction times from hours up to days. Fourth, the scaffold can be directly fabricated into a specific anatomical shape with a mold. Fifth, the process can be easily expanded or automated for large-scale production.

5. Conclusion

In conclusion, the solid lipid templating technique is capable of producing tailored cell carriers for a variety of tissue engineering and biomedical applications. Processing conditions can be adapted to a variety of polymers offering different physical, mechanical and degradation properties. Architectural properties, such as pore size and porosity can be easily controlled and pore interconnectivity can be guaranteed.

6. References

- (1) Langer R, Vacanti JP. 'Tissue engineering'. *Science* (1993); **260**: 920-926.
- (2) Cima LG, Vacanti JP, Vacanti C, Ingber D, Mooney D, Langer R. 'Tissue engineering by cell transplantation using degradable polymer substrates'. *J Biomed Eng* (1991); **113**: 143-151.
- (3) Mooney DJ, Mikos AG. 'Growing new organs'. *Sci Am* (1999); **280**: 60-65.
- (4) Tabata Y. 'The importance of drug delivery systems in tissue engineering'. *Pharm Sci Technol Today* (2000); **3**: 80-89.
- (5) Liu X, Ma PX. 'Polymeric scaffolds for bone tissue engineering'. *Ann Biomed Eng* (2004); **32**: 477-486.
- (6) Freed LE, Vunjak NG, Biron RJ, Eagles DB, Lesnoy DC, Barlow SK, Langer R. 'Biodegradable polymer scaffolds for tissue engineering'. *Biotechnology (N Y)* (1994); **12**: 689-693.
- (7) Agrawal CM, Ray RB. 'Biodegradable polymeric scaffolds for musculoskeletal tissue engineering'. *J Biomed Mater Res* (2001); **55**: 141-150.
- (8) Mikos AG, Thorsen AJ, Czerwonka LA, Bao Y, Langer R, Winslow DN, Vacanti JP. 'Preparation and characterization of poly(-lactic acid) foams'. *Polymer* (1994); **35**: 1068-1077.
- (9) Mikos AG, Sarakinos G, Leite SM, Vacanti JP, Langer R. 'Laminated three-dimensional biodegradable foams for use in tissue engineering'. *Biomaterials* (1993); **14**: 323-330.
- (10) Mooney DJ, Baldwin DF, Suh NP, Vacanti JP, Langer R. 'Novel approach to fabricate porous sponges of poly(-lactic-co-glycolic acid) without the use of organic solvents'. *Biomaterials* (1996); **17**: 1417-1422.
- (11) Nam YS, Park TG. 'Biodegradable polymeric microcellular foams by modified thermally induced phase separation method'. *Biomaterials* (1999); **20**: 1783-1790.
- (12) Leong KF, Cheah CM, Chua CK. 'Solid freeform fabrication of three-dimensional scaffolds for engineering replacement tissues and organs'. *Biomaterials* (2003); **24**: 2363-2378.
- (13) Ma PX, Choi JW. 'Biodegradable polymer scaffolds with well-defined interconnected spherical pore network'. *Tissue Eng* (2001); **7**: 23-33.
- (14) Sachlos E, Czernuszka JT. 'Making tissue engineering scaffolds work. Review on the application of solid freeform fabrication technology to the production of tissue engineering scaffolds'. *Eur Cell Mater* (2003); **5**: 29-40.
- (15) Hutmacher DW. 'Scaffolds in tissue engineering bone and cartilage'. *Biomaterials* (2000); **21**: 2529-2543.

-
- (16) Hutmacher DW. 'Scaffold design and fabrication technologies for engineering tissues - State of the art and future perspectives'. *J Biomater Sci , Polym Ed* (2001); **12**: 107-124.
- (17) Murphy WL, Dennis RG, Kileny JL, Mooney DJ. 'Salt Fusion: An Approach to Improve Pore Interconnectivity within Tissue Engineering Scaffolds'. *Tissue Eng* (2002); **8**: 43-52.
- (18) Holy CE, Fialkov JA, Davies JE, Shoichet MS. 'Use of a biomimetic strategy to engineer bone'. *J Biomed Mater Res* (2003); **65A**: 447-453.
- (19) Tessmar JK, Mikos AG, Goepferich A. 'Amine-Reactive Biodegradable Diblock Copolymers'. *Biomacromolecules* (2002); **3**: 194-200.
- (20) Shastri VP, Martin I, Langer R. 'Macroporous polymer foams by hydrocarbon templating'. *Proc Natl Acad Sci U S A* (2000); **97**: 1970-1975.
- (21) Hacker M, Tessmar J, Neubauer M, Blaimer A, Blunk T, Gopferich A, Schulz MB. 'Towards biomimetic scaffolds: Anhydrous scaffold fabrication from biodegradable amine-reactive diblock copolymers'. *Biomaterials* (2003); **24**: 4459-4473.
- (22) Kellner K, Schulz MB, Gopferich A, Blunk T. 'Insulin in tissue engineering of cartilage: A potential model system for growth factor application'. *J Drug Targeting* (2001); **9**: 439-448.
- (23) Lucke A, Tessmar J, Schnell E, Schmeer G, Gopferich A. 'Biodegradable poly(,-lactic acid)-poly(ethylene glycol)-monomethyl ether diblock copolymers: structures and surface properties relevant to their use as biomaterials'. *Biomaterials* (2000); **21**: 2361-2370.
- (24) Ma PX, Zhang R. 'Synthetic nano-scale fibrous extracellular matrix'. *J Biomed Mater Res* (1999); **46**: 60-72.
- (25) Freed LE, Marquis JC, Nohria A, Emmanuel J, Mikos AG, Langer R. 'Neocartilage formation in vitro and in vivo using cells cultured on synthetic biodegradable polymers'. *J Biomed Mater Res* (1993); **27**: 11-23.
- (26) Nazarian A, Muller R. 'Time-lapsed microstructural imaging of bone failure behavior'. *J Biomech* (2004); **37**: 55-65.
- (27) Wu L, Ding J. 'In vitro degradation of three-dimensional porous poly(,-lactide-co-glycolide) scaffolds for tissue engineering'. *Biomaterials* (2004); **25**: 5821-5830.
- (28) Sherwood JK, Riley SL, Palazzolo R, Brown SC, Monkhouse DC, Coates M, Griffith LG, Landeen LK, Ratcliffe A. 'A three-dimensional osteochondral composite scaffold for articular cartilage repair'. *Biomaterials* (2002); **23**: 4739-4751.

Chapter 7

Synthesis and Characterization of Injectable, Thermogelling Poly(*N*-isopropylacrylamide)-grafted Gelatin (PNiPAAm-gelatin)

Michael Hacker¹, Thomas Vogel², Markus Neubauer¹, Bernhard Appel¹, Miriam Breunig¹,
Torsten Blunk¹, Achim Göpferich¹, Michaela B. Schulz^{1,2}

¹ Department of Pharmaceutical Technology, University of Regensburg,
Universitaetsstrasse 31, 93040 Regensburg, Germany

² Department of Pharmaceutical Technology, University of Graz,
Schubertstrasse 6, 8010 Graz, Austria

1. Introduction

In living tissues, cells are embedded in a three-dimensional hydrated, insoluble network of proteins and glycosaminoglycans, the extracellular matrix (ECM). The ECM proteins interact with cells via integrins, which are heterodimeric receptors in the cell membrane, and regulate their development, migration, proliferation and metabolic function. In recent years, a variety of hydrogel materials have been explored for use as ECM substitutes. Both natural and synthetic hydrogel forming materials have been studied as a means of cell transplantation to reconstruct tissue defects. Natural materials, such as fibrin and especially collagen, are of interest since they are ECM proteins and susceptible to cell-triggered proteolysis by matrix metalloproteases, which enables cell invasion and migration and subsequent remodeling of the gel matrix. Furthermore, the highly ordered nanostructure of collagen plays an important role in various biological events in the body during development and regeneration processes. Consequently, these materials have been employed as cell carriers in numerous studies that were focused on the regeneration of various tissues, ranging from vascular grafts to bone [1-5]. However, natural materials have some inherent limitations in clinical use, primarily because of handling issues, the difficulty in engineering desired properties, the importance (necessity) of pathogen removal and immunogenicity. Alternatively, synthetic materials based on acrylamides, poly(vinyl alcohol) and poly(ethylene glycol) have been extensively studied as hydrogel cell carriers for tissue engineering applications [6,7]. In particular, injectable, *in situ* gel forming systems based on synthetic polymers offer several advantages beyond the ease of mass production and assurance of pathogen removal: a moldable material can fill the shape of any defect, may easily incorporate cells and therapeutic agents or signaling molecules (e.g. growth factors) and only requires a minimally invasive surgical procedure for placement. Different mechanisms, such as chemical or ionic crosslinking, solvent exchange, or gelation in response to temperature or pH change, may be involved in the *in situ* gel formation [8]. Particularly, thermally gelling hydrogels that employ the principles of (lower critical) phase separation are promising injectable ECM substitutes. Such hydrogel systems gel exclusively in response to a temperature increase above the lower critical solution temperature (LCST), the temperature at which phase separation starts and results in the formation of a gel. Poly(*N*-isopropylacrylamide) (PNiPAAm) exhibits an LCST of approximately 32°C but the hydrogels formed by unmodified PNiPAAm collapse substantially as the temperature is increased above the LCST. Copolymers containing small amounts of acrylic acid, poly(ethylene glycol), or hyaluronic acid, however, demonstrated

reversible gelation around body temperature without significant syneresis [9] [10]. This study aimed at the synthesis of a thermoreversibly gelling ECM substitute based on a PNiPAAm composite. Since PNiPAAm has to be crosslinked or copolymerized with hydrophilic macromolecules to obtain stable hydrogels, we intended to develop a PNiPAAm-gelatin conjugate. Gelatin, which is derived from collagen, was selected because it shows many collagen-like characteristics, but exhibits no antigenicity [11]. Like collagen, gelatin interacts with cells and is a substrate for matrix metalloproteinases. Gelatin is known to form gels below room temperature and liquefies upon heating. Crosslinked gelatin is widely used as a biological glue in surgical operations and a material for tissue engineering scaffolds [12,13]. By copolymerization with PNiPAAm, we aimed at developing a hydrogel that is a sol at room temperature and below is injectable and gels exclusively upon heating. These properties allow for easy preparation of homogenous cell suspensions and drug carriers in the liquid state of the hydrogel system that will gel upon injection into the body. Moreover, solutions of growth factors in the liquid form of the hydrogel could be stored at low temperatures, ready for use. In this study, we synthesized PNiPAAm-gelatin-conjugates from three different type A gelatins and characterized the educts and products by size exclusion chromatography and oscillating rheology. The LCSTs of the conjugates was determined by turbidity titration and differential scanning calorimetry. Bone marrow stromal cells and primary chondrocytes were encapsulated in the gel and cultivated to access cell viability in the matrix.

2. Materials and Methods

2.1. Materials

Type A gelatin with bloom values of 140 (G140, IEP = 8.5) and 300 (G300, IEP = 9.0) was provided by DGF Stoess AG (Ebersberg, Germany). G220, a type A gelatin with a bloom value of 220, was provided by Rousselot (Paris, France).

N-acryloylsuccinimide, *N*-isopropylacrylamide (NiPAAm) and poly(*N*-isopropylacrylamide) (PNiPAAm), were purchased from Sigma-Aldrich (Deisenhofen, Germany). Ammonium persulfate (APS) and *N,N,N',N'*-tetramethylethylenediamine (TEMED) were obtained from Serva (Serva Electrophoresis GmbH, Heidelberg, Germany).

2.2. Methods

2.2.1. Synthesis of the PNiPAAm-gelatin conjugates

500 mg of gelatin were dissolved in 50 mL phosphate buffer, pH 7.4, at 27°C and 10 mg of *N*-acryloylsuccinimide were added. The solution was stirred in the absence of light for three days at 27°C to introduce acryloyl groups into the gelatin via acrylation of amine groups at the peptide chain termini or lysine side chains. Following dilution with distilled water to 600 mL, the solution was concentrated to 100 mL by ultrafiltration using a Vivaflow® 50 crossflow unit with a 50 cm² 30,000 Da nominal molecular weight cutoff (nMWCO) polyethersulfone membrane (Vivascience AG, Hannover, Germany). The diluting and concentrating process was repeated three times to remove unreacted acrylic acid. After the final concentrating step, the solution volume was raised to 250 mL with phosphate buffer and 1.25 g (G140) or 1.5 g (G220, G300) of *N*-isopropylacrylamide were added. Polymerization was performed at 27°C under nitrogen atmosphere by the addition of 0.2 mL of 10% aqueous APS solution and 0.2 mL of TEMED to the reaction mixture. After a 4 h reaction time under UV irradiation, the solution was diluted with distilled water to 600 mL. The diluted solution was concentrated to 100 mL by using a Vivaflow® 50 crossflow unit (nMWCO: 30 kDa). The diluting and concentrating process was repeated three times to remove unreacted monomer and low molecular weight substances. After the final concentrating process, the PNiPAAm-gelatin

conjugates were obtained by lyophilization (Christ Beta 2-16, Martin Christ Gefriertrocknungsanlagen GmbH, Osterode am Harz, Germany) with a yield of about 75%.

2.2.2. *Investigation of the PNiPAAm-gelatin conjugates using gel-filtration chromatography (GFC)*

PNiPAAm-gelatin conjugates and the gelatins were investigated by GFC using a HPLC system with a LC-10AT pump, SIL-10AD_{VP} autosampler, SPD-10AV UV-detector, and SCL-10A_{VP} controller (all from Shimadzu, Duisburg, Germany). Typically, 50 μ L of each sample (20 mg/mL) were analyzed on a TSK-Gel G 4000SWX column with a TSK guardcolumn SW XL (Tosoh Bioscience, Phenomenex, Aschaffenburg, Germany). The mobile phase, which was also used as sample solvent, was a 0.05 M phosphate buffer, pH 6.8, supplemented with 0.5% sodium dodecylsulfate (SDS) and 0.1 M Na₂SO₄. The chromatograms were recorded at a flow rate of 0.5 mL/min by UV detection at 210 nm. For data acquisition and analysis, the ClassVP 5.03 HPLC software (Shimadzu) was used.

2.2.3. *Size exclusion chromatography (SEC)*

To determine the molecular weight distribution of the PNiPAAm chains in the conjugates, the samples were digested with 3 mL of a papainase solution (4.5 U/mL in PBE buffer) (CellSystem, St. Katharinen, Germany) for two days at room temperature. After freeze drying, 3 mL of HPLC-grade chloroform (Carl Roth GmbH, Karlsruhe, Germany) were added and the samples were shaken for 6 h. After centrifugation (Beckmann GS-15 R Centrifuge, Beckmann Instruments Inc., Fullerton, CA, USA) at 1500 rpm for 10 min, the supernatant was filtered through a solvent-resistant regenerated nitrocellulose membrane filter with a 0.2 μ m pore diameter (Spartan 30/A, Schleicher & Schuell, Dassel, Germany). To determine the weight and number average molecular weight of the PNiPAAm chains, a 50 μ L volume of the filtrate was analyzed by gel-permeation chromatography. The samples were separated by passage through a Phenogel 1000 \AA column (5 μ m, 300 x 7.8 mm, Phenomenex, Torrance, CA, USA) and a pre-column (Phenogel 5 μ m, 50 x 7.8 mm) using a Shimadzu 10A_{VP} HPLC system with RID 10 refractive index detector and an SPD 10AV_{VP} UV-detector. The columns were maintained at 35°C, using a CTO-10AC_{VP} column oven. The mobile phase was HPLC-grade chloroform (Roth) at a flow rate of 0.9 mL/min. Chromatograms were recorded using RI detection. The molecular weights were calculated from the elution volume of poly(styrene) standards with narrow molecular weight distribution (Phenomenex) using the Class VP GFC software package included with Class VP 5.03 software (Shimadzu).

2.2.4. $^1\text{H-NMR}$ spectroscopy

For recording ^1H nuclear magnetic resonance ($^1\text{H-NMR}$) spectra, 30 mg of the conjugate, gelatin, or PNiPAAm were dissolved in 1 mL of D_2O (Deutero, Kastellaun, Germany). Spectra were taken at 300.13 MHz on a Bruker Advance 300 spectrometer (Rheinstetten, Germany) equipped with a dual sample head and an autosampler.

2.2.5. Determination of the lower critical solution temperature (LCST)

To determine the lower critical solution temperature (LCST), which is the temperature at which the conjugates start to phase separate, we used both a spectrometric method and differential scanning calorimetry (DSC). Spectropic measurements were taken on a 941 Spectrophotometer (Bio-Tek Kontron Instruments, Neufahrn, Germany). The transmittance of visible light ($\lambda = 500$ nm; path length = 1cm) through the conjugate or PNiPAAm solutions (5% (w/v)) was recorded as the hydrogel temperature was varied from 25 to 35°C at 0.1 - 0.25°C/min. The initial break point of the curve on the plot of transmittance versus temperature indicates the LCST [14]. In addition, the LCST of the hydrogels was determined by differential scanning calorimetry on a DSC 2920 equipped with a refrigerated cooling system and an autosampler (TA Instruments, Alzenau, Germany). 15 μl hydrogel (5% (w/v) in PBS) were sealed in hermetic sample pans. A sealed pan containing 15 μl PBS served as reference. Sample and reference, were cooled to 0°C, kept isothermal for 10 min and then heated to 45°C at 2°C/min. The LCST was determined as the onset point of the endothermic signal upon heating using the *Thermal Solutions for NT* software provided with the system. All samples were repeated in triplicate.

2.2.6. Rheometry studies

The samples were dissolved in phosphate-buffered saline (PBS) (Gibco, USA) at a concentration of 5% (m/v) and the dynamic viscoelastic properties of the aqueous solutions were examined by using a rheometer (Rheolyst AR1000, TA Instruments, New Castle, DE, USA) with a 6 cm steel cone (1 degree). The dynamic moduli, G' (storage modulus) and G'' (loss modulus), were measured during the course of heating, cooling and heating. To this end, the samples were equilibrated at 5°C for 10 min, heated from 5 to 40°C, cooled down from 40 to 5°C, and finally heated up again to 40°C. The heating and cooling rate during these experiments was 1°C/min. The measurements were performed at the observing frequency of 1 Hz and a displacement of 4×10^{-3} rad. In addition, G' and G'' were also observed over the frequency range of 0.02 to 100 Hz at 5 and 40°C.

2.2.7. Viability testing

Rat mesenchymal stromal cells (rMSCs) were harvested, selected and expanded as described in the literature [15]. After the first subculture, the rMSCs were encapsulated in 300 μ L PNiPAAm-gelatin hydrogels in 12-well plates (Corning Costar, Bodenheim, Germany) by mixing equal volumes of an rMSC dispersion in medium (2×10^6 cells/mL) and a conjugate solution (10% CG140 (m/v)) ($n = 4$). After gelation in a humidified incubator (37°C , 5% CO_2), 1 mL of medium containing 10% serum was added. Samples were harvested on day 3. In brief, after washing the gels with PBS, 0.25% trypsin/EDTA was added to digest the matrix. The cells were collected by centrifugation at 200 g at 4°C for 5 min. After washing the pellet with PBS, cells were again centrifuged and resuspended in PBS. Samples were analyzed with a FACSCalibur flow cytometer (Becton Dickinson, Heidelberg, Germany) before and subsequent to the addition of propidium iodide (1 $\mu\text{g/mL}$). Propidium iodide fluorescence was measured on the FL3 emission channel through a 670 nm longpass filter, following excitation with an argon ion laser source at 488 nm. For each sample, 2×10^4 cells were collected. To determine the number of dead cells in the samples, two parameter dot plots of cell size (forward scatter) versus propidium iodide (FL3) were used. The dot plots were divided into four quadrants. Dead cells were assessed by counting the events in the upper right quadrant. Prior to the addition of propidium iodide, less than 0.1% of cells appeared in this region.

2.2.8. Chondrocyte cell culture

Primary chondrocytes were isolated from full-thickness bovine articular cartilage by digestion with type II collagenase [16]. Cells were then resuspended in DMEM (Dulbecco's Modified Eagle's Medium; Life Technologies GmbH, Karlsruhe, Germany) supplemented with 0.4 mM proline (Sigma-Aldrich, Steinheim, Germany), 10 mM HEPES buffer (Sigma-Aldrich, Steinheim, Germany), 0.1 mM non-essential amino acids (Life Technologies GmbH, Karlsruhe, Germany), 50 U/mL penicillin, 50 $\mu\text{g/mL}$ streptomycin (Sigma-Aldrich, Steinheim, Germany), 50 $\mu\text{g/mL}$ ascorbic acid (Sigma-Aldrich, Steinheim, Germany), and 10% FBS. The same medium was also used for cell cultivation. Chondrocyte-loaded hydrogels were prepared by mixing a cell suspension (5×10^6 chondrocytes per mL) with an equal volume of CG140 (10% (w/v)) in DMEM. 600 μl of chondrocyte-loaded hydrogel (1.5×10^6 cells) were filled into a glass ring (diameter: 8 mm), which was centered in a well in a 6 well plate. To gel the hydrogels, the plates were placed in a humidified incubator (37°C , 5% CO_2). After gelation, the glass rings were carefully removed and 6 mL of culture medium

containing either 0 or 2.5 $\mu\text{g/mL}$ insulin were added. Finally, the well plates were placed on an orbital shaker (Stuart Scientific, Surrey, United Kingdom) at 50 rpm and cultured for 14 days. The culture medium, containing either 0 or 2.5 $\mu\text{g/mL}$ insulin, was changed every two to three days.

Samples were prepared for histological analysis by incubation in 2% glutaraldehyde in PBS for 30 min and subsequent storage in 10% formalin. After careful rinsing, the formalin-fixed samples were embedded in Tissue Tek (Sakura Finetek, Torrance, CA, USA) and sectioned (10 μm) using a Microtome Cryostat (Microm, Walldorf, Germany). The sections were stained with hematoxylin and eosin (H&E) for cells and safranin-O for glycosaminoglycans (GAG) [17].

3. Results

3.1. Synthesis of PNiPAAm-gelatin conjugates

PNiPAAm-gelatin conjugates were synthesized from three different type A gelatins with a bloom value of 140, 220 and 300. Synthesis started with the acrylation of gelatin in aqueous solution at pH 7.4. *N*-Acryloylsuccinimide reacted with free amine groups on both the chain terminus and the lysine residues of the peptide (Fig. 1).

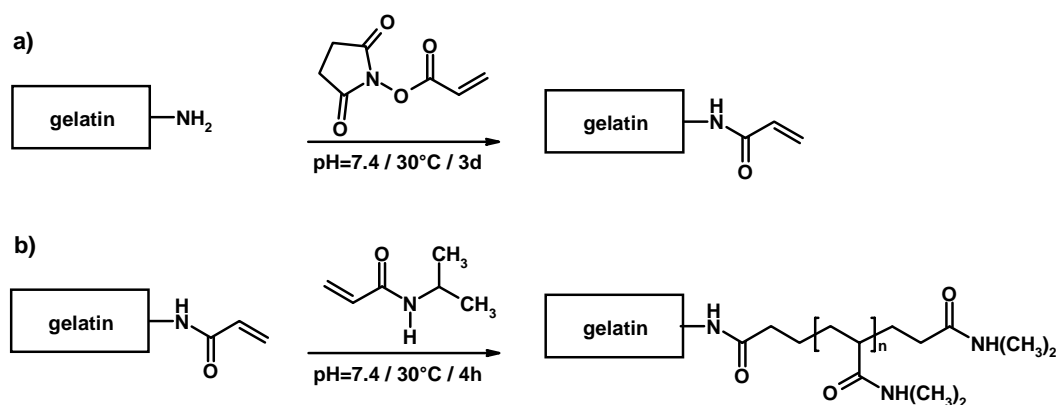


Fig. 1: Synthesis of PNiPAAm-gelatin. a) Acrylation of gelatin by reaction with *N*-acryloylsuccinimide. b) Polymerization of NiPAAm. Please note that more than one amine group is derivatized per gelatin molecule.

This way, several electron-poor double bonds were introduced per gelatin molecule. *N*-isopropylacrylamide was polymerized on the olefins, forming poly(*N*-isopropylacrylamide) chains linked to the gelatin backbone. All PNiPAAm-gelatin conjugates (CG140, CG220 and CG300) were soluble in water, PBS and cell culture medium and gave viscous solutions at

ambient temperatures. Figure 2a-c shows representative gel-filtration chromatograms of the gelatin types used in this study. All of the gelatins exhibited a wide molecular weight distribution. Gelatin G140 and G 300, which were provided by the same supplier, consist of mainly the same factions of high molecular weight peptide fragments. The different bulk properties, expressed by the bloom value, result from a significant fraction of low molecular weight peptide chains that is present in G140. G220, which is characterized by an intermediate bloom values, correspondingly exhibits a peak molecular weight located between the low molecular weight fraction of G140 and the high molecular weight fractions of G300. A representative chromatogram of the conjugate CG140 is shown in Figure 2d. A considerable increase in molecular weight was exhibited, while no considerable fractions of unreacted gelatin were visible. Between the different conjugates (CG140, CG220 and CG300), no differences were observed by GFC (data not shown).

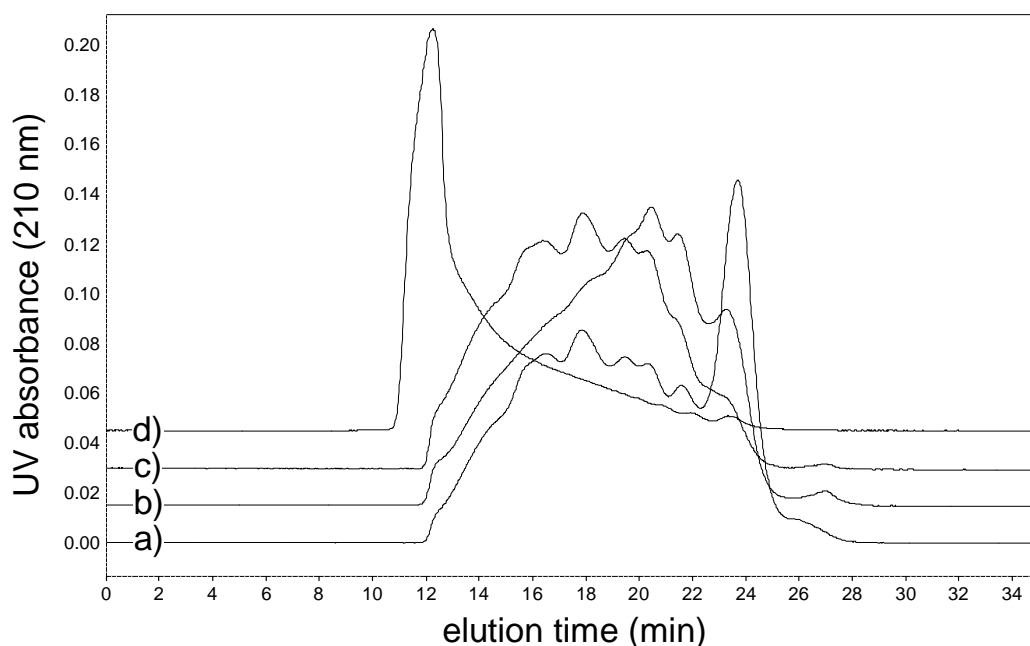


Fig. 2: Molecular weight distribution of: a) gelatin G140, b) gelatin G220, c) gelatin G300 and d) PNiPAAm-gelatin CG140 as obtained by gel filtration chromatography (GFC).

Since the conjugate molecular weights seemed to reach or even exceed the exclusion limit of the column, the conjugates were digested to investigate the size distribution of the synthesized PNiPAAm chains for any differences between the conjugates. To this end, the PNiPAAm chains were extracted from the lyophilized, papainase-digested conjugates in chloroform. The filtered chloroform fractions were analyzed using size exclusion chromatography (SEC). As displayed by the chromatograms (Fig. 3), again no backbone size dependent differences were observed. Chromatograms 3a and 3c show the chloroform-soluble fractions of digested

gelatin G140 and G300, respectively. The two peaks (onset at 12 and 13 min) represent amino acids that were extracted by chloroform. The digestion enzyme papainase faintly appears (8.5 - 11 min) in the chromatograms. In chromatograms of the digested conjugates (Fig. 3b,d), however, a peak at 7.5 min indicates the presence of high molecular weight polymers, the PNiPAAm chains. Molecular weight analysis (calibrated with polystyrene standards) of these peaks resulted in $M_w = 5.6 \times 10^4$ Da, $M_n = 4.9 \times 10^4$ Da (PI = 1.15) for CG300 and $M_w = 4.7 \times 10^4$ Da, $M_n = 4.1 \times 10^4$ Da (PI = 1.15) for CG140. Commercially available PNiPAAm was also exposed to papainase, lyophilized, extracted with chloroform and analyzed. This experiment confirmed that PNiPAAm was not affected by the digestion procedure (data not shown).

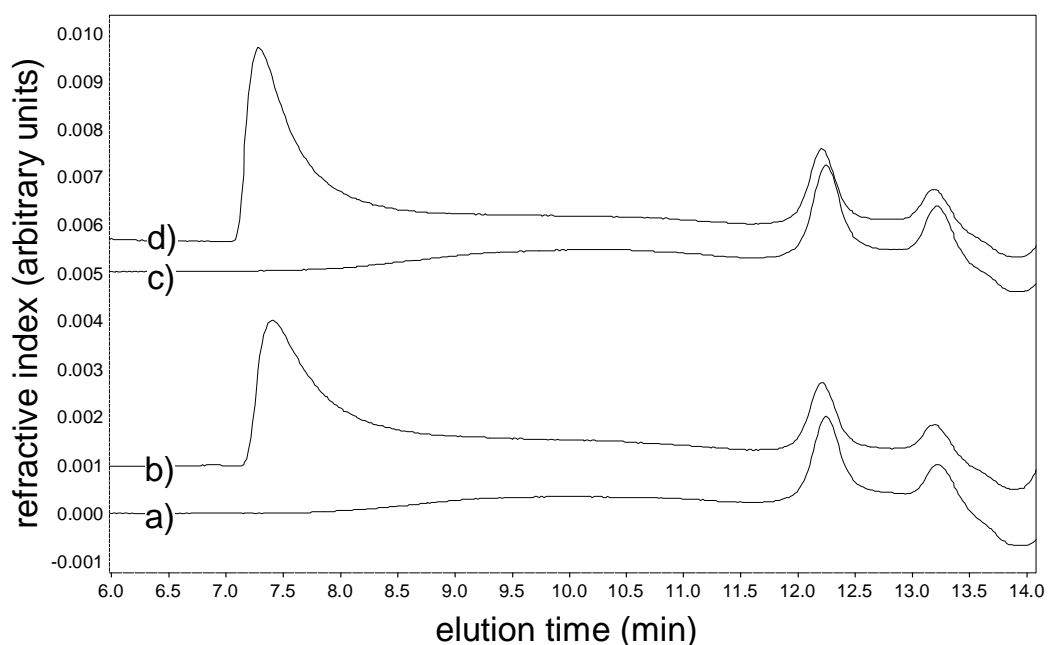


Fig. 3: Evaluation of the molecular weight distribution of the grafted PNiPAAm chains: Chromatograms obtained from the following papainase-digested samples by SEC: a) gelatin G140, b) PNiPAAm-gelatin CG140, c) gelatin G300 and d) PNiPAAm-gelatin CG300.

$^1\text{H-NMR}$ spectra of G140, CG140 and PNiPAAm, all dissolved in D_2O are shown in Figure 4. The CG140 spectrum contained the characteristic peaks of PNiPAAm and the peaks attributed to G140. The peak at 4.7 ppm resulted from residual water in the conjugate and/or in D_2O . The four characteristic peaks that can be found in the spectra of CG140 and PNiPAAm represent the $-\text{CH}_3$ groups (1.2 ppm) in NiPAAm, the $-\text{CH}_2$ (1.6 ppm) and $-\text{CH}$ (2.0 ppm) groups in the PNiPAAm backbone, and the isopropyl $-\text{CH}$ group (3.8 ppm) in NiPAAm. These NMR data are consistent with both the chemical structure of the macromolecules and other published reports [18,19].

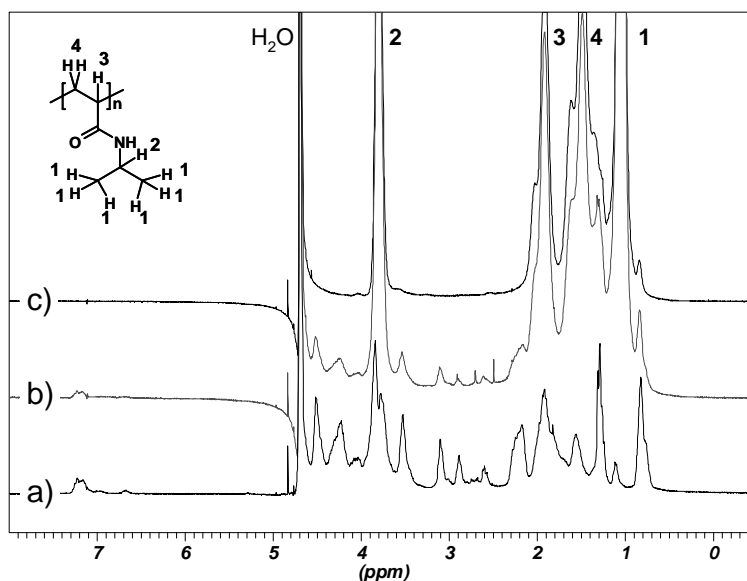


Fig. 4: ^1H -NMR spectra of a) gelatin G140, b) PNiPAAm-gelatin CG140, c) PNiPAAm in D_2O .

3.2. Gelation of the conjugates on heating

At room temperature, aqueous solutions of the conjugates (typically: 5% (m/v) in PBS) were colorless, transparent and liquid. When heated to 37°C , the conjugate solutions turned into stiff, white-colored opaque hydrogels without any volume change and loss of water (Fig. 5). PNiPAAm solutions, however, exhibited a considerable amount of collapse and released a large fraction of water. The photographs depicted in Figure 5 were taken 6 h after gelation in an incubator.

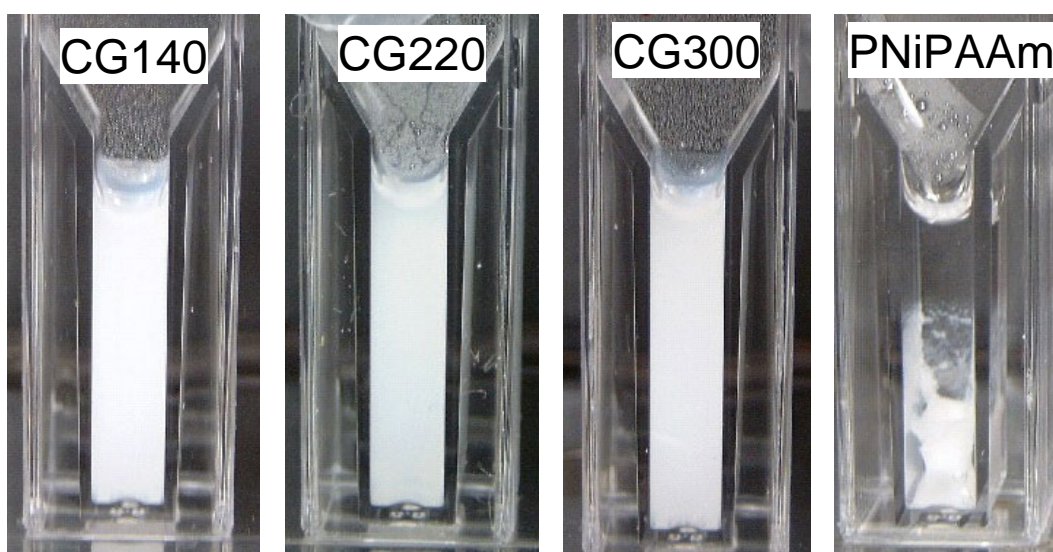


Fig. 5: Photographic images of thermogelled PNiPAAm-gelatin conjugates and PNiPAAm (concentration: 5% (m/v)) obtained 6h after gelation at 37°C .

The lower critical solution temperatures (LCSTs) of the thermoreversible gelling conjugate solutions (5% (m/v) in PBS) were determined by both a spectroscopic method and differential scanning calorimetry (DSC) [14]. By measuring the effect of temperature on the transmittance of visible light ($\lambda=500$ nm) through the conjugates, LCSTs of around 31°C were determined for the conjugates and PNiPAAm (Table 1). For all substances, a sharp phase transition was recorded, spanning approximately 0.6°C. The LCSTs determined are in agreement with the LCST published for PNiPAAm [14,20]. Similar values resulted from the LSCT determination using DSC. Repeated heating and cooling cycles had no effect on the phase transition temperature of the conjugates, indicating the thermoreversible properties of the hydrogels. Compared to the photospectrometric method, the calorimetric method can be automated and might be advantageous for routine measurements.

Table 1 Lower critical solution temperature (LCST) of the synthesized gelatin-PNiPAAm conjugates and PNiPAAm, as determined by photospectrometry and differential scanning calorimetry (DSC).

Hydrogel	LCST [°C]	
	Photospectrometry	DSC
CG140	30.8 ± 0.2	30.2 ± 1.2
CG220	31.1 ± 0.2	30.2 ± 0.5
CG300	31.2 ± 0.0	29.8 ± 1.9
PNiPAAm	30.9 ± 0.3	28.1 ± 2.8

3.3. Rheological behavior of PNiPAAm-gelatin conjugates

Figure 6 shows the frequency dependence of the dynamic moduli, storage (G') and loss (G'') modulus, observed on the PNiPAAm-gelatin conjugate solution (5% (w/v) in PBS) at characteristic temperatures. At a low temperature (5°C) and a mid-temperature (20°C) (data not shown) the loss modulus G'' was larger than the storage modulus G' and both dynamic moduli increased with the oscillating frequency in the frequency range from 0.02 to 80 Hz. Typically, this rheological behavior is attributed to a sol. At higher frequencies, a shear-induced destruction of the system was observed. In contrast, at a temperature (40°C) above the LCST the dynamic moduli showed much larger values than those at temperatures below the LCST and remained constant over a wide range of oscillatory frequencies, indicating a gelled, rigid system. Correspondingly, G' significantly exceeded G'' .

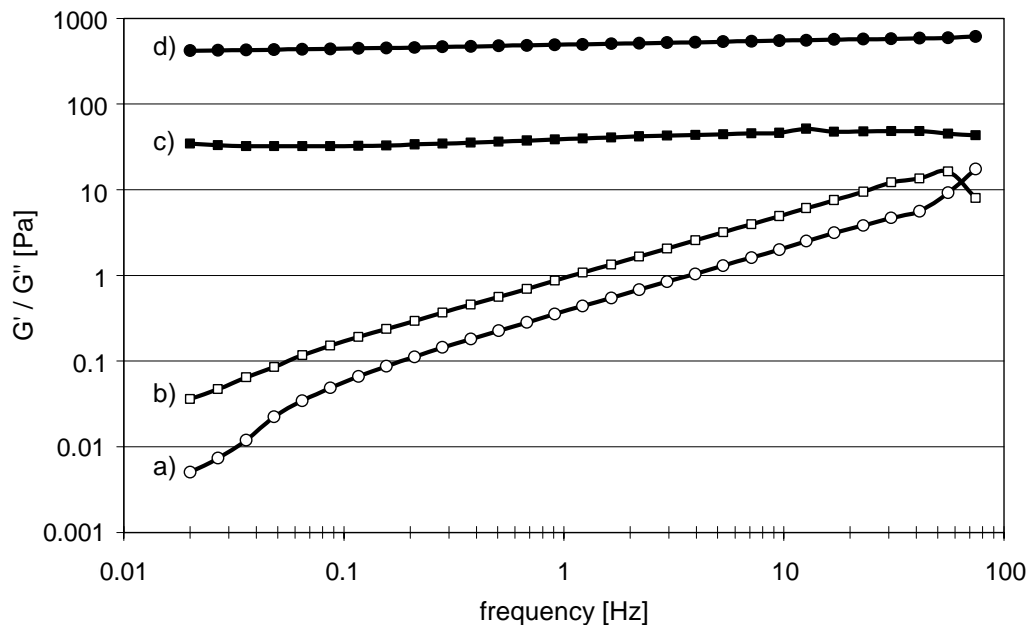


Fig. 6: Frequency dependence of the dynamic moduli (G' and G'') of the PNiPAAm-gelatin conjugate CG 140 (5% (w/v) in PBS): a) Storage modulus (G') at 5°C, b) loss modulus (G'') at 5°C, c) loss modulus (G'') at 40°C and d) storage modulus (G') at 40°C.

Representative plots of the dynamic moduli as well as the phase angle (δ) as a function of temperature are shown for CG140 (5% (w/v) in PBS) in Figure 7.

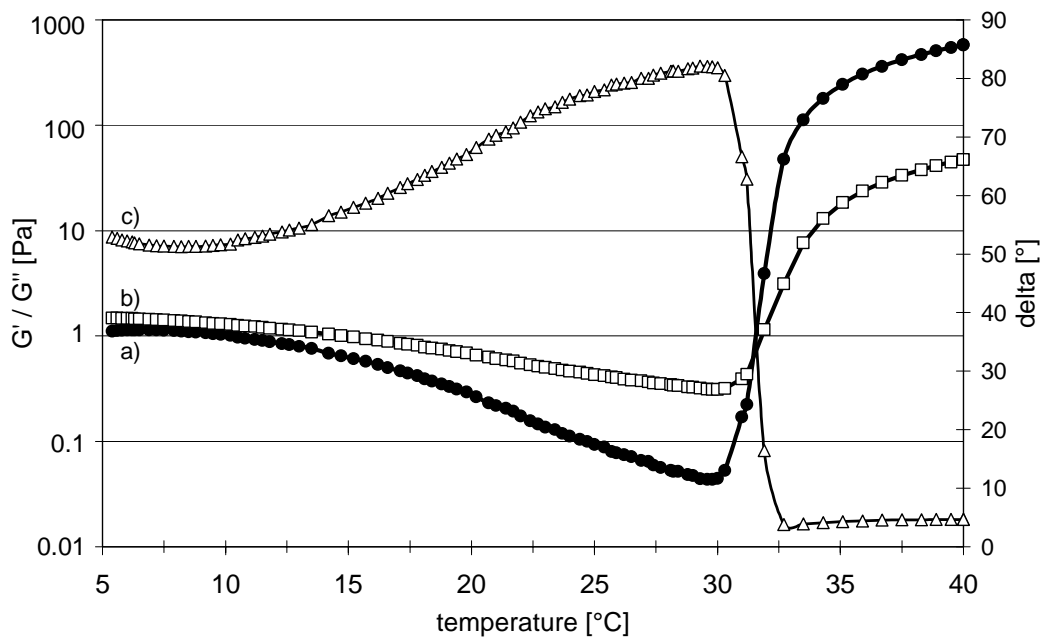


Fig. 7: Temperature dependence of the dynamic moduli (G' , G'') and phase angle of the PNiPAAm-gelatin conjugate CG 140 (5% (w/v) in PBS): a) Storage modulus (G'), b) loss modulus (G'') and c) phase angle.

Upon heating from 5°C to 30°C, both the storage and the loss modulus only decreased about one order of magnitude. Additionally, the loss modulus (G'') was higher than the storage modulus (G') along this temperature range, indicating that even at low temperatures the conjugate solution did not form a gel. Correspondingly, a phase angle of 45° was measured at 5°C, which increased to 80° upon heating. This rheological behavior of the conjugate is indicative for an almost complete quenching of the rheological properties of gelatin by the PNiPAAm chains. A solution of the gelatin G140 (5% (w/v) in PBS), however, did form a gel at 5°C, which was characterized by a phase angle of 1° at 5°C and a G' exceeding G'' by about two orders of magnitude. This gelatin gel liquefied at 27°C, which was accompanied by the characteristic cross-over of the moduli and an increase of the phase angle (data not shown). When the temperature of the conjugate (CG140) solution was further increased, a gel was formed, as indicated by an increase of the dynamic moduli and the typical cross-over of G' and G'' at a temperature near the determined LCST. Correspondingly, the phase angle dropped below 10°. During the temperature increase from 30°C to 40°C, the storage modulus (G') increased by four orders of magnitude.

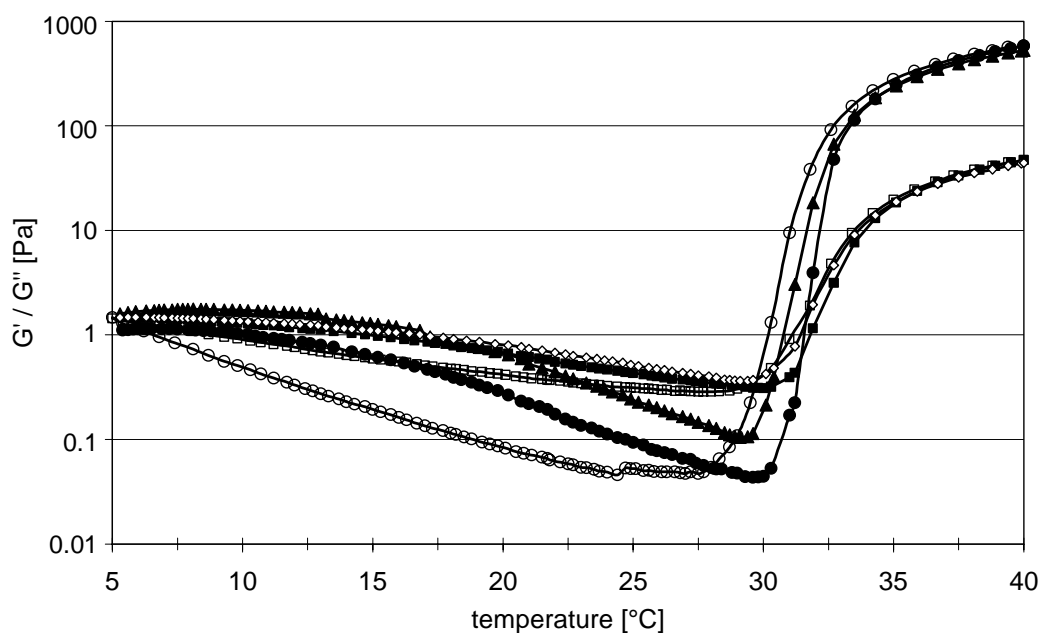


Fig. 8: Thermoreversible rheological behavior the PNiPAAm-gelatin conjugate CG 140 (5% (w/v) in PBS): G' (\bullet) and G'' (\blacksquare) on the first heating cycle (5-40°C), G' (\circ) and G'' (\square) on cooling (40-5°C) and G' (\blacktriangle) and G'' (\diamond) on the second heating cycle (5-40°C).

With the objective of demonstrating the reversibility of the phase transition and thermogelation, the dynamic moduli were recorded during a heating, a cooling and another heating cycle (Fig. 8). During the three cycles, the curves were almost identical; note that G' and G'' reached exactly the same values after the first and the second gelation and no syneresis was observed. Again, conjugate gelation was only observed at temperatures above 30°C and not on cooling.

3.4. *Viability test*

Rat marrow stromal cells (rMSCs) were encapsulated in the hydrogels and cultivated for 3 days. After 3 days, the cells were isolated from the hydrogels. Dead cells were stained with propidium iodide and counted by a flow cytometer. $11.7\% \pm 1.4$ of the counted cells were fluorescent, indicating that around 90% of the encapsulated rMSC were viable after 3 days of culture and the isolation procedure.

3.5. *Chondrocyte cell culture*

3.5.1. *Chondrocyte cell culture*

To test the applicability of the developed conjugates in tissue engineering, bovine chondrocytes were encapsulated in the thermogelling matrices. After 14 days of cultivation, viable extracellular matrix-producing chondrocytes were found encapsulated in CG140 hydrogels (Fig. 9). Without the supplementation of insulin, only a few of the chondrocytes in the inner areas of the hydrogel produced a GAG (glycosaminoglycan)-rich extracellular matrix, stained red with safranin-O (Fig. 9a). Insulin supplementation (2.5 $\mu\text{g}/\text{mL}$) over 14 days, however, induced a considerably increased production of GAG. As can be seen from the photomicrographs, the GAG production originates from the encapsulated cells (Fig. 9b). As a result of the low cell density, which has to be increased in future experiments, the chondrocytes lay isolated and not in lacunae, which are typical for mature cartilaginous tissue.

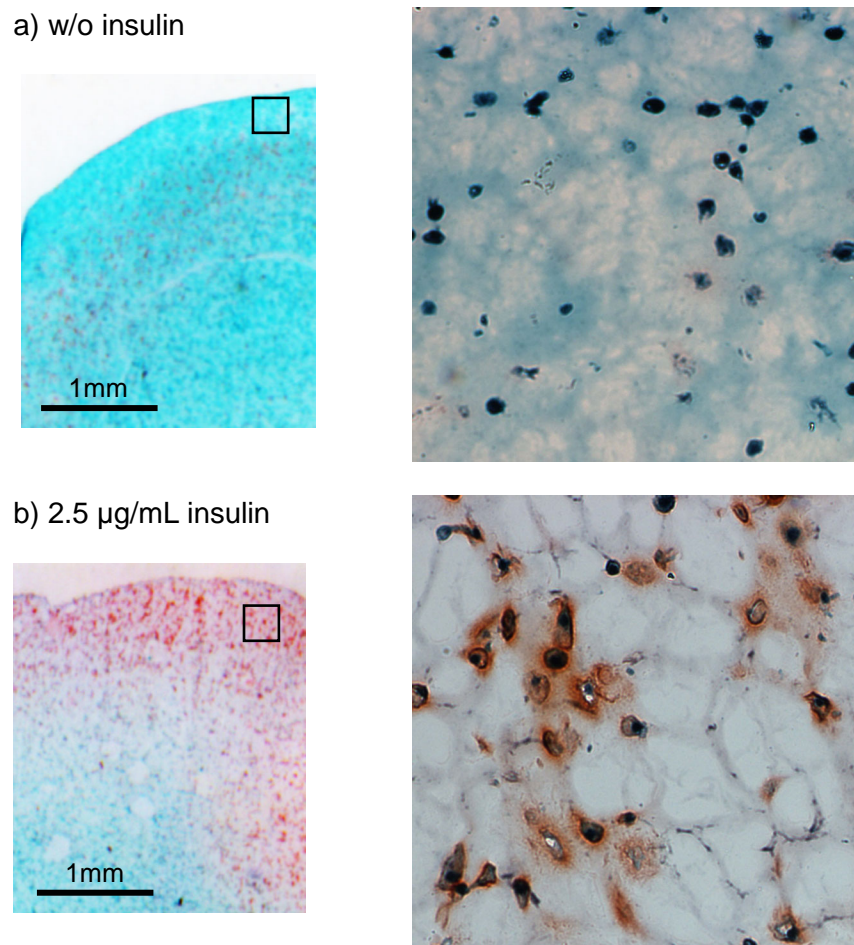


Fig. 9: Safranin-O/fast green-stained histological cross-sections of two week constructs, bovine chondrocytes encapsulated in thermogelled CG 140 (5% (w/v) in medium), grown in culture medium with 10% FBS: a) without supplementation of insulin, b) supplementation of 2.5 $\mu\text{g}/\text{mL}$ insulin. GAG-rich extracellular matrix appears red, other extracellular matrix components are stained green. The large image (original magnification $\times 100$) represents the marked section in the small image ($\times 4$).

4. Discussion

With the objective of developing an injectable extracellular matrix (ECM) substitute, we synthesized a conjugate of gelatin, a protein derived from the natural extracellular matrix protein collagen, and poly(N-isopropylacrylamide) (PNiPAAm), a polymer offering unique thermoresponsive phase transition characteristics with a LCST slightly below body temperature. Hoffman and co-workers first applied PNiPAAm-based polymers to injectable drug delivery systems and other functional matrices for biomedical applications [6,21-23]. By copolymerization with other polymers, several thermogelling biomaterials for cell encapsulation were developed [9,10]. Gelatin, the other component of the conjugate, is known as a cell adhesive matrix but is soluble in water at physiological temperature. Therefore, various insolubilization techniques, mainly crosslinking procedures, have been applied to make use of gelatin as an ECM substitute in tissue engineering devices [24-26]. Evidently, these techniques are often not suitable to *in vivo* gelation due to the toxicity of the available crosslinking agents. Ideally, the grafting of PNiPAAm chains to a gelatin backbone would change the rheological properties of gelatin in such a way that gelation of conjugate solutions occurs on heating and not on cooling, which would be typical for gelatin hydrogels. Additionally, the gelatin backbone would support the formation of a stable, non-shrinking hydrogel, as linear PNiPAAm hydrogels alone collapse at body temperature [20]. Two other research groups have recently synthesized similar conjugates [10,27,28]. Matsuda and co-workers synthesized PNiPAAm-gelatin conjugates from a multiply derivatized dithiocarbamylated low molecular weight gelatin (9.5×10^4 Da) by iniferter-based photopolymerization. They successfully employed their conjugates as a matrix for cartilage tissue engineering [29,30]. Cell viability inside these conjugates strongly depended on the concentration of PNiPAAm-gelatin and the molecular weight of the PNiPAAm graft chain. Acceptable viability was only found for a gel prepared at low concentration (5%) of the conjugate with high molecular weight PNiPAAm graft chains (1.3×10^5 Da) [29]. Yoshioka et al. synthesized the conjugate from acrylated gelatin by a thermally induced polymerization of NiPAAm that is similar to our approach. The resulting conjugate demonstrated gelation upon either heating or cooling. Unfortunately, no information was provided on the molecular weight of the gelatin used and the synthesized conjugate [27].

Based on the synthesis described by Yoshioka et al., we synthesized PNiPAAm-gelatin conjugates from high molecular weight type A gelatins (Fig. 2). The investigated gelatin types showed a broad molecular weight distribution, characteristic for gelatin, with an onset

retention time of 12 min, corresponding to a molecular weight (M_w) of more than 4×10^5 Da. While no details are provided in the literature concerning the pH, we kept the pH at 7.4 during acrylation and polymerization by using phosphate buffer as the reaction medium. The synthesis led to high molecular weight conjugates of about 10^6 Da or more. For a more detailed analysis of the conjugates, the molecular weight of the grafted PNiPAAm chains was investigated after conjugate digestion with papainase. This procedure allows for the characterization of the PNiPAAm chains that had been formed at the gelatin backbone under the conditions of conjugate preparation. To our knowledge, no other author has performed this characterization step in connection to these conjugates. Molecular weights of approx. 5×10^4 Da were determined for PNiPAAm, similar to those obtained by Ibusuki et al. [29,31]. The theoretical gelatin content of the conjugates was 28.6% (CG140) and 25% (CG220, CG300). This gelatin content seems to be sufficient for e.g. cartilage tissue engineering, since a successful product with a similar gelatin content was described in the literature [30,31].

The PNiPAAm-gelatin conjugates exhibited a LCST of around 31°C (Table 1) and formed form-filling, stiff hydrogels at physiological temperature without any loss of water (Fig. 5). Figure 5 also depicts the collapse of a hydrogel formed by linear PNiPAAm chains of similar molecular weight as the grafted chains. Similar phenomena were observed for crosslinked PNiPAAm-gelatin conjugates or mixtures of gelatin and PNiPAAm (data not shown). In contrast to PNiPAAm, complete precipitation was not obtained for the developed high molecular weight PNiPAAm-gelatin conjugates, suggesting that, although PNiPAAm chains collapsed at temperatures above LCST, gelatin molecules appeared to hinder intramolecular aggregation, thus avoiding the complete precipitation in the diluted state at the investigated concentration (5% (w/v)).

The rheological characterization of the synthesized conjugates revealed that the gelatin is ideally masked by the grafted PNiPAAm chains. Using oscillating rheological measurements, the real and imaginary parts, G' and G'' , as well as the phase angle of the complex shear modulus are examined. The observed G' and G'' represent the elasticity term and the viscosity term of the material at the oscillatory frequency. A solution of CG140 (5% (w/v) in PBS) was a viscoelastic fluid ($G' < G''$ and $\delta > 45^\circ$) at temperatures below the LCST (Fig. 6 and 7). At temperatures above the LCST, it behaved as viscoelastic solid ($G' > G''$ and $\delta < 45^\circ$). In other words, the PNiPAAm-gelatin conjugate perfectly fulfills the demands on an injectable cell and/or drug carrier. At low temperatures, conjugate solutions formed a viscous liquid that can be easily mixed with cells in suspensions or dissolved drugs. The moldable liquids can be injected and quickly form a rigid gel at body temperature without any loss of

water. The perfect reversibility of this phase transition behavior was shown for the synthesized conjugates by rheological measurements and DSC. In no other study we did find this exact reversibility of gelation, highlighting the purity of the product.

Since the developed conjugates offered the desired gelation characteristics, cell encapsulation experiments were conducted to assess the cytocompatibility of the conjugates and the gelation procedure. A viability of around 90% was found for rat mesenchymal stromal cells (rMSCs) after encapsulation in the synthesized conjugates for 3 days. As described in the literature, any cytotoxic effect of the matrix would have become visible within the first 3 days [28].

In order to finally test the applicability of the developed conjugates as cell carriers for tissue engineering applications, we encapsulated bovine chondrocytes and cultured them under conditions that have been shown to support cartilage formation on polymeric fiber meshes [32]. To stimulate extracellular matrix formation and to check for the biochemical activity of the cells, insulin was supplemented to some cultures. Generally, no cytotoxic effects were observed over the cultivation time of 14 days. Moreover, exogenous insulin stimulated GAG formation, indicating that the encapsulated chondrocytes maintained differentiation and biological function. Obviously, a much higher cell density is required to engineer coherent tissues. Nevertheless, the PNiPAAm-gelatin conjugates demonstrated great potential for their use as injectable ECM substitutes for tissue engineering applications.

Generally, a variety of applications for injectable extracellular matrix substitutes can be imagined in the field of tissue engineering. These hydrogels may serve as cell carriers for the engineering of several soft tissues, such as skin or adipose tissue, or even cartilage and bone tissue. In combination with suitable growth factors, injectable ECM substitutes can be designed as biomimetic matrices that promote and guide nerve regeneration or neovascularization of large defects. Furthermore, the micrometer-scale pore network of polymeric cell carriers (scaffolds) can be filled with the injectable, artificial ECM. This way, the nanofibrous structure of the gel-forming conjugate molecules mimics the natural nanoscale interactions between cells and extracellular matrix proteins, while the scaffold provides additional mechanical strength.

5. Conclusion

In this study, PNiPAAm-gelatin conjugates were synthesized from several type A gelatins in a two-step reaction. The resulting high molecular weight conjugates underwent thermoreversible gelation upon heating above their LCST, which was determined by photospectrometry and DSC. Oscillating rheological measurements were employed to investigate this phase separation and gelling behavior. Finally, high cell viability in the hydrogels was demonstrated for mesenchymal stromal cells. Chondrocytes that were encapsulated in the conjugates could be stimulated for GAG production over 14 days. Altogether, the developed conjugates are promising ECM substitutes for many tissue engineering applications.

6. Acknowledgements

The authors like to thank Joerg Tessmar and Antonios G. Mikos (Department of Bioengineering, Rice University, Houston, Texas, USA) for placing the oscillating rheometer at our disposal.

7. References

- (1) Ye Q, Zund G, Benedikt P, Jockenhoewel S, Hoerstrup SP, Sakyama S, Hubbell JA, Turina M. 'Fibrin gel as a three dimensional matrix in cardiovascular tissue engineering'. *Eur J Cardiothorac Surg* (2000); **17**: 587-591.
- (2) Tabata Y, Miyao M, Ozeki M, Ikada Y. 'Controlled release of vascular endothelial growth factor by use of collagen hydrogels'. *J Biomater Sci , Polym Ed* (2000); **11**: 915-930.
- (3) Cummings CL, Gawlitta D, Nerem RM, Stegemann JP. 'Properties of engineered vascular constructs made from collagen, fibrin, and collagen-fibrin mixtures'. *Biomaterials* (2004); **25**: 3699-3706.
- (4) Geiger M, Li RH, Friess W. 'Collagen sponges for bone regeneration with rhBMP-2'. *Adv Drug Delivery Rev* (2003); **55**: 1613-1629.
- (5) Friess W. 'Collagen in drug delivery and tissue engineering'. *Adv Drug Delivery Rev* (2003); **55**: 1529-1530.
- (6) Hoffman AS. 'Hydrogels for biomedical applications'. *Adv Drug Delivery Rev* (2002); **54**: 3-12.
- (7) Temenoff JS, Mikos AG. 'Injectable biodegradable materials for orthopedic tissue engineering'. *Biomaterials* (2000); **21**: 2405-2412.
- (8) Gutowska A, Jeong B, Jasionowski M. 'Injectable gels for tissue engineering'. *Anat Rec* (2001); **263**: 342-349.
- (9) Stile RA, Burghardt WR, Healy KE. 'Synthesis and characterization of injectable poly(N-isopropylacrylamide)-based hydrogels that support tissue formation in vitro'. *Macromolecules* (1999); **32**: 7370-7379.
- (10) Ohya S, Nakayama Y, Matsuda T. 'Thermoresponsive artificial extracellular matrix for tissue engineering: Hyaluronic acid bioconjugated with poly(N-isopropylacrylamide) grafts'. *Biomacromolecules* (2001); **2**: 856-863.
- (11) Sela M, Arnon R. 'Studies on the chemical basis of the antigenicity of proteins. I. Antigenicity of polypeptide gelatins'. *Biochem J* (1960); **75**: 91-103.
- (12) Guilmet D, Bachet J, Goudot B, Laurian C, Gigou F, Bical O, Barbagelatta M. 'Use of biological glue in acute aortic dissection. Preliminary clinical results with a new surgical technique'. *J Thorac Cardiovasc Surg* (1979); **77**: 516-521.
- (13) Kang HW, Tabata Y, Ikada Y. 'Fabrication of porous gelatin scaffolds for tissue engineering'. *Biomaterials* (1999); **20**: 1339-1344.
- (14) Schild HG, Tirrell DA. 'Microcalorimetric detection of lower critical solution temperatures in aqueous polymer solutions'. *J Phys Chem* (1990); **94**: 4352-4356.

- (15) Lieb E, Tessmar J, Hacker M, Fischbach C, Rose D, Blunk T, Mikos AG, Goepferich A, Schulz MB. 'Poly(D,L-lactic acid)-Poly(ethylene glycol)-Monomethyl Ether Diblock Copolymers Control Adhesion and Osteoblastic Differentiation of Marrow Stromal Cells'. *Tissue Eng* (2003); **9**: 71-84.
- (16) Freed LE, Marquis JC, Nohria A, Emmanuel J, Mikos AG, Langer R. 'Neocartilage formation in vitro and in vivo using cells cultured on synthetic biodegradable polymers'. *J Biomed Mater Res* (1993); **27**: 11-23.
- (17) Lillie RD, Fullmer HM. *Histopathologic techniques and practical histochemistry*. New York: McGraw Hill, 1976.
- (18) Rodin VV, Izmailova VN. 'NMR method in the study of the interfacial adsorption layer of gelatin'. *Colloids Surf A* (1996); **106**: 95-102.
- (19) Wang LQ, Tu K, Li Y, Zhang J, Jiang L, Zhang Z. 'Synthesis and characterization of temperature responsive graft copolymers of dextran with poly(N-isopropylacrylamide)'. *Reactive and Functional Polymers* (2002); **53**: 19-27.
- (20) Chen G, Hoffman AS. 'Graft copolymers that exhibit temperature-induced phase transitions over a wide range of pH'. *Nature* (1995); **373**: 49-52.
- (21) Dong Lc, Hoffman AS. 'Synthesis and application of thermally reversible heterogels for drug delivery'. *J Control Release* (1990); **13**: 21-31.
- (22) Miura M, Cole CA, Monji N, Hoffman AS. 'Temperature-dependent absorption/desorption behavior of lower critical solution temperature (LCST) polymers on various substrates'. *J Biomater Sci, Polym Ed* (1994); **5**: 555-568.
- (23) Chen G, Hoffman AS. 'Preparation and properties of thermoreversible, phase-separating enzyme-oligo(N-isopropylacrylamide) conjugates'. *Bioconjug Chem* (1993); **4**: 509-514.
- (24) Sung HW, Huang DM, Chang WH, Huang RN, Hsu JC. 'Evaluation of gelatin hydrogel crosslinked with various crosslinking agents as bioadhesives: in vitro study'. *J Biomed Mater Res* (1999); **46**: 520-530.
- (25) Choi YS, Hong SR, Lee YM, Song KW, Park MH, Nam YS. 'Studies on gelatin-containing artificial skin: II. Preparation and characterization of cross-linked gelatin-hyaluronate sponge'. *J Biomed Mater Res* (1999); **48**: 631-639.
- (26) Ito A, Mase A, Takizawa Y, Shinkai M, Honda H, Hata KI, Ueda M, Kobayashi T. 'Transglutaminase-mediated gelatin matrices incorporating cell adhesion factors as a biomaterial for tissue engineering'. *J Biosci Bioeng* (2003); **95**: 196-199.
- (27) Yoshioka H, Mori Y, Tsukikawa S, Kubota S. 'Thermoreversible gelation on cooling and on heating of an aqueous gelatin-poly(N-isopropylacrylamide) conjugate'. *Polym Adv Technol* (1998); **9**: 155-158.
- (28) Ohya S, Nakayama Y, Matsuda T. 'Material design for an artificial extracellular matrix: cell entrapment in poly (N-isopropylacrylamide) (PNIPAM)-grafted gelatin hydrogel'. *Artif Organs* (2001); **4**: 308-314.

- (29) Ibusuki S, Fujii Y, Iwamoto Y, Matsuda T. 'Tissue-engineered cartilage using an injectable and in situ gelable thermoresponsive gelatin: fabrication and in vitro performance'. *Tissue Eng* (2003); **9**: 371-384.
- (30) Ibusuki S, Iwamoto Y, Matsuda T. 'System-Engineered Cartilage Using Poly(N-isopropylacrylamide)-Grafted Gelatin as in Situ-Formable Scaffold: In Vivo Performance'. *Tissue Eng* (2003); **9**: 1133-1142.
- (31) Morikawa N, Matsuda T. 'Thermoresponsive artificial extracellular matrix: N-isopropylacrylamide-graft-copolymerized gelatin'. *J Biomater Sci , Polym Ed* (2002); **13**: 167-183.
- (32) Kellner K, Schulz MB, Gopferich A, Blunk T. 'Insulin in tissue engineering of cartilage: A potential model system for growth factor application'. *J Drug Targeting* (2001); **9**: 439-448.

Chapter 8

Summary
and
Conclusions

1. Summary

Cell carriers (scaffolds) play a pivotal role in attempts to engineer living tissues from isolated cells for tissue reconstruction and basic research. In these attempts, cell carriers serve as an artificial extracellular matrix that accommodates mammalian cells and guides their growth, differentiation and tissue development in three dimensions [1]. Generally, an appropriate cell carrier is designed to mimic the cell's natural environment. Thus, the scaffolding material and architecture differ according to the tissue type [2]. The appropriate scaffolds for musculoskeletal tissue, bone and cartilage are preferably made from ceramics, metals or lipophilic polymers to obtain sufficient mechanical stability. Conversely, hydrophilic, gel-forming polymers are widely used as extracellular matrix substitutes for cell encapsulation and the engineering of soft tissue [3]. For the design of functional, biomimetic cell carriers, both material concepts are of interest and addressed in this thesis.

This work focused primarily on the fabrication of functional, macroporous cell carriers from biodegradable polymers. Several important design criteria and characteristics have been identified for such scaffolds during the last decade. Ideally, the scaffolds should: (i) be three-dimensional and highly porous with an interconnected pore network for cell growth and flow transport of nutrients and metabolic waste; (ii) be biocompatible and resorbable with controllable degradation and resorption rates to match cell/tissue growth in vitro and/or in vivo; (iii) have a suitable surface chemistry for cell attachment, proliferation, and differentiation and (iv) have mechanical properties to match those of the tissues at the site of implantation [4].

The design of a functional scaffold starts with the selection of the appropriate scaffolding material. In light of the enormous number of biodegradable polymers that have been developed and characterized so far, it might be relatively simple to find an ideal material in terms of mechanical properties and degradation kinetics. The surface chemistry of these polymers, however, is far from optimal. The major concern is that the interaction of these lipophilic polymers with the surrounding biological environment may lead to the non-selective adsorption of proteins. This process in turn triggers a number of non-specific cellular responses and may lead to uncontrollable tissue development and growth [5]. To overcome these limitations, biodegradable polymers were recently developed that contain a hydrophilic polymer block to suppress the adsorption of proteins and a linker molecule activated for reaction with biologically active molecules, such as adhesion peptides or growth factors [6].

These biodegradable, activated diblock copolymers are promising materials for the fabrication of cell carriers with a biomimetic surface design. Furthermore, polymer degradability and mechanical properties can be varied and adapted to different types of tissue by altering the copolymer ratio and crystallinity of the lipophilic block. Using two different bifunctional linkers, namely disuccinimidyl tartrate and *N*-succinimidyl 3-maleinimido propionate, which were covalently attached to monoamine poly(ethylene glycol)-*block*-poly(D,L-lactic acid) (H₂N-PEG-PLA), amine-reactive (ST-NH-PEG-PLA) and thiol-reactive diblock copolymers (MP-NH-PEG-PLA) were recently synthesized and their functionality was demonstrated using fluorescent dyes and model proteins containing free amine or thiol groups [6,7].

The first objective towards the fabrication of functional cell carriers was to affect cell adhesion to these reactive diblock copolymers by covalently attaching adhesion-mediating peptides (**Chapter 2**). To this end, films of both amine-reactive (ST-NH-PEG₂PLA₂₀) and thiol-reactive derivatives (MP-NH-PEG₂PLA₄₀) were modified with cyclic $\alpha\beta3/\alpha\beta5$ integrin subtype specific RGD peptides simply by incubation of the films with buffered solutions of the peptides. A non-binding RAD peptide analogue served as a control. Human osteoblasts, known to express these integrins, were used to determine cell-polymer interactions. The adhesion experiments revealed that less than 20% of the seeded cells adhered to the unmodified ST-NH-PEG₂PLA₂₀ surfaces (PEG-content: 9 %) and about 50 % of seeded cells were found on buffer treated MP-NH-PEG₂PLA₄₀ films (PEG-content: 5%). The adhered cells exhibited a round shape indicating only a low level of cell-biomaterial interaction. This correlation between the PEG-content of the PEG-PLA diblock copolymers and the amount and shape of adhered cells was consistent with the data known for marrow stromal cells on non-reactive MeO-PEG-PLA surfaces [8,9]. On all RGD-modified polymer films, however, the adhesion of human osteoblasts was significantly increased (up to 100% adhesion) compared to the RAD-modified or unmodified surfaces. In addition, cells were widely spread on the RGD-modified films, indicating strong cell-surface interactions, whereas cells on the RAD-modified films retained their round morphology. Several control groups proved the covalent attachment of the peptides. This study was able to demonstrate the envisioned surface modification concept and show the biological efficacy of the instant surface modification procedure.

To process these diblock copolymers into tissue engineering scaffolds, a suitable fabrication technique was developed (**Chapter 3**). This technique had to account for the physicochemical properties of the polymers as well as the general demands on scaffold microstructure, namely high porosity, control of pore size and high interconnectivity. Furthermore, the absence of

water during polymer processing was a key prerequisite to prevent hydrolysis of the amine-reactive *N*-hydroxysuccinimide ester. To this end, an anhydrous technique was developed, which utilizes solid lipid microparticles dispersed in the polymer solution as pore forming devices. Simultaneous polymer precipitation and porogen extraction in warm *n*-hexane generated macroporous scaffolds. The adjustment of the porogen particle's melting point to the polymer's glass transition temperature was shown to be a key step in generating the interconnected pore networks. Scaffolds from amine-reactive polymers were successfully fabricated and, as a model protein, insulin was covalently attached to the scaffold surface in a simple incubation procedure. The success of this experiment indicated the preservation of the polymer's amine-reactivity during processing. Recently, the covalent attachment of bFGF was also demonstrated on such scaffolds. In preliminary experiments, bFGF modified scaffolds promoted vascular ingrowth after subcutaneous implantation in nude mice. To confirm these findings, bFGF loaded scaffolds are currently being investigated in two different in vivo models.

For processing, the polymers were dissolved in an acetone-chloroform-mixture (65:35 (v/v)) and the triglyceride microparticles were extracted in *n*-hexane. According to the ICH guidelines on residual solvents, chloroform and *n*-hexane are classified as class 2 solvents and their use should be limited. A thermodynamically equivalent polymer solvent mixture of less toxic solvents (ICH class 3) was systematically determined using Hansen Solubility Parameters (HSPs) to eliminate chloroform from the fabrication technique without changing other processing parameters (**Chapter 4**). The HSPs of a mixture containing methyl ethyl ketone 59% (v/v) and tetrahydrofuran 41% (v/v) were found to best fit the parameters calculated for the acetone-chloroform-mixture. Using this alternative solvent mixture and *n*-heptane as an alternative extraction medium, PLGA and MeO-PEG₂PLA₄₀ were processed into tissue engineering scaffolds without parameter changes. Moreover, the solvent exchange had only negligible effects on the macro- and microstructure of the resulting scaffolds.

A follow-up study focused on determining the solubility parameters of PLA, PLGA and MEO-PEG-PLA (**Chapter 5**). Theoretical and experimental methods, namely group contribution methods, solubility and viscosity measurements, were employed to determine the solubility parameters of the polymers. A two-dimensional solvent map was introduced that allows for discrimination between solvents and non-solvents for the polymers. Viscosity measurements provided further information on the partial polymer-solvent interactions.

In addition to the surface chemistry (**Chapter 2 and 3**) and biocompatibility (**Chapter 4**), the architectural and mechanical properties of a cell carrier greatly influence cell proliferation,

differentiation and tissue development. Control over these properties during polymer processing is mandatory for scaffold adaptation to different applications and types of tissue. Processing parameters that allow for the processing of various biodegradable polymers of different compositions and molecular weights (22 - 160 kDa) were determined for the solid lipid templating technique (SLT). Pore interconnectivity, as one important architectural feature, was controlled by the extraction temperature and the porogen's melting point. The pore size of the scaffolds was controlled by the size distribution of the porogen microparticles. During processing, the rheological behavior of the dispersion prepared from the polymer solution and porogen microparticles, which has major influence on micro- and macrostructure of the resulting scaffolds, was characterized by oscillating rheological measurements. The suitability of the fabricated scaffolds was tested using an established cartilage cell culture model [10] (**Chapter 6**).

To overcome limitations in the nutrient and oxygen supply inside tissue engineered cell-polymer constructs, strategies to promote the ingrowth of blood vessels are under intensive investigation [11,12]. Our strategy to promote angiogenesis within cell-polymer-constructs started with the development of a hydrogel matrix, which is injectable inside cell seeded scaffolds and consists of a combination of cell-adhesive and non-adhesive domains to support the migration of endothelial cells and smooth muscle cells (**Chapter 7**). In detail, poly(*N*-isopropylacrylamide) (PNiPAAM) chains were covalently attached to gelatin type A as a cell-adhesive core protein to obtain an injectable, thermoreversibly gelling hydrogel. The synthesis of these conjugates involved the acrylation of gelatin in the first step and the polymerization of NiPAAM in the second step. Different types of gelatin type A were tested and conjugates were synthesized with varying gelatin contents. The conjugates, containing gelatin types with bloom values ranging from 140 to 300, underwent gelation slightly below body temperature (approx. 31°C). Oscillating rheological measurements were employed to investigate this phase separation and gelling behavior, and revealed the characteristic cross-over of G' (storage modulus) and G'' (loss modulus) during gelation. Finally, high cell viability in the hydrogels was demonstrated for mesenchymal stromal cells. Chondrocytes that were encapsulated in the conjugates could be stimulated for glycosaminoglycan production over 14 days. Altogether, the developed conjugates represent injectable and cytocompatible ECM substitutes.

2. Conclusions

In conclusion, a biocompatible, anhydrous scaffold fabrication technique was developed that allows for the fabrication of functional cell carriers: (i) The process allows for the fabrication of spongy scaffolds from amine-reactive diblock copolymers polymers that have been shown to bind adhesion peptides in a simple incubation procedure and enhance osteoblast adhesion in their RGD-modified form. This way, surface-reactive cell carriers were fabricated that can be easily modified to mimic a biological environment and specifically guide cell adhesion and/or development. The reactive polymers are designed to bind peptides and proteins within a short reaction time even after the prolonged storage of prefabricated scaffolds. A preliminary study with bFGF-modified scaffolds that were subcutaneously implanted in nude mice showed that the ingrowth of blood vessels was enhanced by the attached peptide. To strengthen these findings, bFGF-modified scaffolds are currently being investigated in two different animal models, including a rat cranial defect. (ii) Solid lipid templating (SLT) has proved to be a widely adaptable technique to fabricate well-structured scaffolds with different pore sizes and pore structures from various polymers in a controlled manner. Therefore, polymer development may profit from this technique, as it can be adapted to fabricate scaffolds from small amounts of newly developed materials in the absence of water. Thus, new polymers can be easily screened in three-dimensional cell culture experiments. Generally, the solid lipid templating technique seems to be advantageous over state-of-the-art polymer casting-particulate leaching techniques for several reasons: Firstly, in SLT, the porogen particles are extracted concomitantly to polymer precipitation, which promotes pore interconnectivity. Secondly, the porogen extraction is finished after 30 min, while salt leaching techniques require extraction times lasting from hours to days. Thirdly, the absence of water during polymer processing allows for the processing of hydrolysable polymers and the direct incorporation of water-soluble compounds, such as growth factors or hydrophilic polymers. (iii) As a result of the permeable, highly interconnected microstructure, rat mesenchymal stromal cells (rMSCs) and bovine chondrocytes could be homogeneously seeded on poly(lactic-*co*-glycolic acid) scaffolds. rMSC-seeded constructs have already been successfully induced towards adipose and bone tissue.

Finally, an injectable hydrogel-forming conjugate from gelatin and PNiPAAm was synthesized to address the need for neovascularization in tissue engineered scaffolds. On the basis of the thermogelling conjugates, an injectable system will be developed that also incorporates release devices, e.g. calcium-alginate microparticles, loaded with angiogenic growth factors, such as VEGF, PDGF or bFGF. The fabrication of these release systems was established during this work and is currently being optimized [13]. Additionally, the angiogenic potential of the developed matrices is being investigated in the rat aortic model [14].

3. References

- (1) Yang S, Leong KF, Du Z, Chua CK. 'The design of scaffolds for use in tissue engineering. Part I. Traditional factors'. *Tissue Eng* (2001); **7**: 679-689.
- (2) Karp JM, Dalton PD, Shoichet MS. 'Scaffolds for tissue engineering'. *MRS Bull* (2003); **28**: 301-306.
- (3) Hoffman AS. 'Hydrogels for biomedical applications'. *Adv Drug Delivery Rev* (2002); **54**: 3-12.
- (4) Hutmacher DW. 'Scaffolds in tissue engineering bone and cartilage'. *Biomaterials* (2000); **21**: 2529-2543.
- (5) Lu L, Kam L, Hasenbein M, Nyalakonda K, Bizios R, Gopferich A, Young JF, Mikos AG. 'Retinal pigment epithelial cell function on substrates with chemically micropatterned surfaces'. *Biomaterials* (1999); **20**: 2351-2361.
- (6) Tessmar JK, Mikos AG, Gopferich A. 'Amine-Reactive Biodegradable Diblock Copolymers'. *Biomacromolecules* (2002); **3**: 194-200.
- (7) Tessmar J, Mikos A, Gopferich A. 'The use of poly(ethylene glycol)-block-poly(lactic acid) derived copolymers for the rapid creation of biomimetic surfaces'. *Biomaterials* (2003); **24**: 4475-4486.
- (8) Gopferich A, Peter SJ, Lucke A, Lu L, Mikos AG. 'Modulation of marrow stromal cell function using poly(D,L-lactic acid)-block-poly(ethylene glycol)-monomethyl ether surfaces'. *J Biomed Mater Res* (1999); **46**: 390-398.
- (9) Lieb E, Tessmar J, Hacker M, Fischbach C, Rose D, Blunk T, Mikos AG, Gopferich A, Schulz MB. 'Poly(D,L-lactic acid)-Poly(ethylene glycol)-Monomethyl Ether Diblock Copolymers Control Adhesion and Osteoblastic Differentiation of Marrow Stromal Cells'. *Tissue Eng* (2003); **9**: 71-84.
- (10) Kellner K, Schulz MB, Gopferich A, Blunk T. 'Insulin in tissue engineering of cartilage: A potential model system for growth factor application'. *J Drug Targeting* (2001); **9**: 439-448.
- (11) Ennett AB, Mooney DJ. 'Tissue engineering strategies for in vivo neovascularisation'. *Expert Opin Biol Ther* (2002); **2**: 805-818.
- (12) Nomi M, Atala A, Coppi PD, Soker S. 'Principals of neovascularization for tissue engineering'. *Mol Aspects Med* (2002); **23**: 463-483.
- (13) Pignitter, Marc. 'Entwicklung eines Freisetzungssystems für angiogenetische Wachstumsfaktoren auf Grundlage von Alginatmikropartikeln'. *Diplomarbeit*. Karl-Franzens-Universität Graz. (2004)
- (14) Nicosia RF, Villaschi S, Smith M. 'Isolation and characterization of vasoformative endothelial cells from the rat aorta'. *In Vitro Cell Dev Biol Anim* (1994); **30A**: 394-399.

Appendix

1. Abbreviations

λ_{em}	emission wavelength
λ_{ex}	excitation wavelength
ΔE^v	energy of vaporization
$^1\text{H-NMR}$	proton nuclear magnetic resonance
AAc	acrylic acid
aFGF	acid fibroblast growth factor
ANOVA	analysis of variance
APS	ammonium persulfate
bFGF	basic fibroblast growth factor
BMBF	Bundesministerium für Bildung und Forschung
BMP(s)	bone morphogenetic protein(s)
CAD	computer-aided design
CED	cohesive energy density
CO ₂	carbon dioxide
cyclo(-RADfE-)	cyclo(-Arg-Ala-Asp-D-Phe-Glu-)
cyclo(-RADfK-)	cyclo(-Arg-Ala-Asp-D-Phe-Lys-)
cyclo(-RGDfE-)	cyclo(-Arg-Gly-Asp-D-Phe-Glu-)
cyclo(-RGDfK-)	cyclo(-Arg-Gly-Asp-D-Phe-Lys-)
Da	Dalton
DMEM	Dulbecco's modified eagle's medium
DSC	differential scanning calorimetry
ECM	extracellular matrix
EGF	Epidermal Growth Factor
E_{hi}	hydrogen bonding
EMK	ethyl methyl ketone
FBS	fetal bovine serum
FDA	Food and drug administration
F_{di}	group contribution for dispersive forces
F_{pi}	group contribution for polar forces (permanent dipoles)
GA	glycolic acid
GAG	glycosaminoglycan
GFC	gel filtration chromatography
GPC	gel permeation chromatography
H ₂ N-PEG-PLA	monoamine-poly(ethylene glycol)- <i>block</i> -poly(D,L-lactic acid)
HEPES	4-(2-hydroxyethyl)-1-piperazineethanesulfonic acid
HPLC	high performance liquid chromatography
HPMC	hydroxypropyl methylcellulose
HSP(s)	Hansen solubility parameter(s)

HvK	Hoflyzer - van Krevelen
ICH	International Conference on Harmonization
IEP	isoelectric point
kDa	kilo Dalton
kV	kilo volt
LA	lactic acid
LCST	lower critical solution temperature
MDSC	modulated differential scanning calorimetry
MeO-PEG	monomethyl ether-poly(ethylene glycol)
MeO-PEG-PLA	monomethyl ether-poly(ethylene glycol)- <i>block</i> -poly(D,L-lactic acid)
MeO-PEG _x PLA _y	see above
Mn	number average molecular weight
MPa	megapascal
MP-NH-PEG ₂ PLA ₄₀	MP-NH-PEG-PLA (42 kDa)
MP-NH-PEG-PLA	3-maleimido propylamido-poly(ethylene glycol)- <i>block</i> -poly(D,L-lactic acid)
MW	molecular weight
Mw	weight average molecular weight
N ₂ H-PEG ₂ PLA ₂₀	monoamine-poly(ethylene glycol)- <i>block</i> -poly(D,L-lactic acid) (22 kDa)
NGF	nerve growth factor
NiPAAm	<i>N</i> -isopropylacrylamide
NMP	<i>N</i> -methyl-2-pyrrolidone
NMWCO	nominal molecular weight cutoff
OPF	oligo(poly(ethylene glycol)-fumarate)
OPTN	Organ Procurement and Transplantation Network
OsO ₄	osmium tetroxide
P 42	paraffin microparticles (T _m ≈ 42°C)
P 46	paraffin microparticles (T _m ≈ 46°C)
P 50	paraffin microparticles (T _m ≈ 50°C)
PBS	phosphate buffered saline
PDGF	platelet-derived growth factor
PEG	poly(ethylene glycol)
PEG ₂ PLA ₂₀	poly(ethylene glycol)- <i>block</i> -poly(D,L-lactic acid) (22 kDa)
PEG-PLA	poly(ethylene glycol)- <i>block</i> -poly(D,L-lactic acid)
PEO	poly(ethylene oxide)
PEO-PPO-PEO	poly(ethylene oxide)-poly(propylene oxide)-poly(ethylene oxide)
PGA	poly(glycolic acid)
PI	polydispersity index
PLA	poly(D,L-lactic acid)
PLGA	poly(D,L-lactic- <i>co</i> -glycolic acid)
PLLA	poly(L-lactic acid)
PNiPAAm	poly(<i>N</i> -isopropylacrylamide)

poly(PF-co-EG)	poly(propylene fumarate- <i>co</i> -ethylene glycol)
PPF	poly(propylene fumarate)
PPO	poly(propylene oxide)
PVA	poly(vinyl alcohol)
RAD	tripeptide: Arg-Ala-Asp
RGD	tripeptide: Arg-Gly-Asp
RI	refractive index
RID	refractive index detector
rMSCs	rat mesenchymal stromal cells
rpm	rotations per minute
SD	standard deviation
SDS	sodium dodecylsulfate
SEC	size exclusion chromatography
SEM	scanning electron microscopy
SH	mixture of Softisan® 154 and Witepsol® H42
SLT	Solid Lipid Templating
spacerAA	spacer amino acid
ST-NH-PEG ₂ PLA ₂₀	Succinimidyl tartrate-amido-poly(ethylene glycol)- <i>block</i> -poly(D,L-lactic acid) (22 kDa)
TCPS	tissue culture polystyrene
TEMED	<i>N,N,N',N'</i> -tetramethylethylenediamine
T _g	glass transition temperature
TGF-β1	transforming growth factor β1
THF	tetrahydrofurane
TIPS	thermally induced phase separation
T _m	melting temperature (point)
UV	ultraviolet light or irradiation
V/v	volume per volume
VEGF	vascular endothelial growth factor
V _m	molar volume
δ	Hildebrand (total) solubility parameter
δ _d , δ _p , δ _h	partial solubility parameters (dispersive, polar and hydrogen-binding forces)

2. Hansen Solubility Parameters of common solvents (25°C)

Solvent	CAS Number	Molar volume (cm ³ /mol)	Solubility Parameters (MPa ^{1/2})			
			δ_d	δ_p	δ_h	δ
PARAFFINIC HYDROCARBONS						
n-Butane	106-97-8	101.4	14.1	0.0	0.0	14.1
n-Pentane	109-66-0	116.2	14.5	0.0	0.0	14.5
Pentane (iso)	78-78-4	117.4	13.7	0.0	0.0	13.7
n-Hexane	110-54-3	147.4	14.9	0.0	0.0	14.9
n-Heptane	142-82-5	147.4	15.3	0.0	0.0	15.3
n-Octane	111-65-9	163.5	15.6	0.0	0.0	15.6
Cyclohexane	110-82-7	108.7	16.8	0.0	0.2	16.8
Methylcyclohexane	108-87-2	128.3	16.0	0.0	1.0	16.0
AROMATIC HYDROCARBONS						
Benzene	71-43-2	89.4	18.4	0.0 ^a	2.0	18.6
Toluene	108-88-3	106.8	18.0	1.4	2.0	18.2
Naphthalenen ^b	91-20-3	111.5	19.0	2.0	5.9	20.0
Styrene	1-42-5	115.6	18.6	1.0	4.1	19.0
o-Xylene	95-47-6	121.2	17.8	1.0	3.1	18.0
HALOHYDROCARBONS						
Methylene dichloride	75-09-2	63.9	18.2	6.3	6.1	20.3
Chloroform	67-66-3	80.7	17.8	3.1	5.7	19.0
Dichlorodifluoromethane	75-71-8	92.3	12.3	2.0	0.0	12.5
Trichlorofluoromethane	75-69-4	92.8	15.3	2.0	0.0	15.5
Bromotrifluoromethane	75-63-8	97.0	9.6	2.5	0.0	10.0
Carbon tetrachloride	56-23-5	97.1	17.8	0.0	0.6	17.8
Chlorobenzene	108-90-7	102.1	19.0	4.3	2.0	19.6
Perfluoro-n-heptane	335-57-9	227.3	12.1	0.0	0.0	12.5
ETHERS						
Furan	110-00-9	72.5	17.8	1.8	5.3	18.6
Epichlorohydrin	106-89-8	79.9	19.0	10.2	3.7	21.9
Tetrahydrofuran	109-99-9	81.7	16.8	5.7	8.0	19.4
1,4-Dioxane	123-91-1	85.7	19.0	1.8	7.4	20.5
Diethyl ether	60-29-7	104.8	14.5	2.9	5.1	15.8
KETONES						
Acetone	67-64-1	74.0	15.5	10.4	7.0	20.1
Methyl ethyl ketone (2-butanone)	78-93-3	90.1	16.0	9.0	5.1	19.0
Cyclohexanone	108-94-1	104.0	17.8	6.3	5.1	19.6
Diethyl ketone (3-pentanone)	96-22-0	106.4	15.8	7.6	4.7	18.2
Acetophenone	98-86-2	117.4	19.6 ^a	8.6	3.7	21.7
Methyl iso-butyl ketone (2-hexanone)	591-78-6	125.8	15.3	6.1	4.1	17.0
ALDEHYDES						
Acetaldehyde	75-07-0	57.1	14.7	8.0	11.3	20.3
2-Furfuraldehyde (Furfural)	98-01-1	83.2	18.6	14.9	5.1	24.3
Butyraldehyde	123-72-8	88.5	14.7	5.3	7.0	17.2
Benzaldehyde	100-52-7	101.5	19.4	7.4	5.3	21.5

Solvent (cont.)	CAS Number	Molar volume (cm ³ /mol)	Solubility Parameters (MPa ^{1/2})			
			δ_d	δ_p	δ_h	δ
ESTERS						
Methyl acetate	79-20-9	79.7	15.5	7.2	7.6	18.8
Ethyl formate	109-94-4	80.2	15.5	8.4	8.4	19.6
Propylene carbonate (1,2-propanediol cyclic carbonate)	108-32-7	85.0	20.1	18.0	4.1	27.2
Ethyl acetate	141-78-6	98.5	15.8 ^a	5.3	7.2 ^a	18.2
Diethyl carbonate	105-58-8	121.0	16.6	3.1	6.1	18.0
Diethyl sulfate	64-67-5	131.5	15.8	14.7	7.2	22.7
2-Ethoxyethyl acetate (Cellusolve acetate)	111-15-9	136.2	16.0	4.7	10.6	19.6
Dimethyl phthalate	131-11-3	163.0	18.6 ^a	10.8 ^a	4.9	22.1
Diethyl phthalate	84-66-2	198.0	17.6	9.6	4.5	20.5
Di-n-butyl phthalate	84-74-2	266.0	17.8 ^a	8.6	4.1	20.3
n-Butyl benzyl phthalate	85-68-7	306.0	19.0	11.3	3.1	22.3
Iso-propyl palmitate ^c	2239-78-3	330.0	14.3	3.9	3.7	15.3
Di-n-butyl sebacate	109-43-3	339.0	14.5	3.9	3.7	15.5
Methyl oleate ^d	112-62-9	340.0	14.5	3.9	3.7	15.5
Diocetyl phthalate (bis(2-ethylhexyl) phthalate)	117-81-7	377.0	16.6	7.0	3.1	18.2
NITROGEN-CONTAINING COMPOUNDS						
Acetonitrile	75-05-8	52.6	15.3	18.0	6.1	24.6
Acrylonitrile	107-13-1	67.1	16.5	17.4	6.8	24.8
Propionitrile	107-12-0	70.9	15.3	14.3	5.5	21.7
Butyronitrile	109-74-0	87.0	15.3	12.5	5.1	20.5
Nitromethane	75-52-5	54.3	15.8	18.8	5.1	25.0
Nitroethane	79-24-3	71.5	16.0	15.5	4.5	22.7
Ethanolamine (2-aminoethanol)	141-43-5	60.2	17.2	15.5	21.3	31.5
Ethylene diamine	107-15-3	67.3	16.6	8.8	17.0	25.4
2-Pyrrolidone (2-pyrrolidinone)	616-45-5	76.4	19.4	17.4	11.3	28.4
Pyridine	110-86-1	80.9	19.0	8.8	5.9	21.7
Morpholine	110-91-8	87.1	18.8	4.9	9.2	21.5
Aniline	62-53-3	91.5	19.4	5.1	10.2	22.5
N-Methyl-2-pyrrolidone	872-50-4	96.5	18.0	12.3	7.2	22.9
Diethylamine	109-87-7	103.2	14.9	2.3	6.1	16.4
Formamide	75-12-7	39.8	17.2	26.2	19.0	36.6
Dimethylformamide	68-12-2	77.0	17.4	13.7	11.3	24.8
N,N-Dimethylacetamide	127-19-5	92.5	16.8	11.5	10.2	22.7
SULFUR-CONTAINING COMPOUNDS						
Carbon disulfide	75-15-0	60.0	20.5	0.0	0.6	20.5
Dimethyl sulfoxide (methyl sulfoxide)	67-68-5	71.3	18.4	16.4	10.2	26.6
Ethanthiol ^c (ethyl mercaptan)	75-08-1	74.3	15.8	6.5	7.2	18.4
Dimethyl sulfone ^b (methyl sulfone)	67-71-0	75.0	19.0	19.4	12.3	29.9
ACID HALIDES AND ANHYDRIDES						
Acetyl chloride	75-36-5	71.0	15.8	10.6	3.9	19.4
Succinic anhydride ^b	108-30-5	66.8	18.6	19.2	16.6	31.5
Acetic anhydride	108-24-7	94.5	16.0 ^a	11.7 ^a	10.2 ^a	22.3

Solvent (cont.)	CAS Number	Molar volume (cm ³ /mol)	Solubility Parameters (MPa ^{1/2})			
			δ_d	δ_p	δ_h	δ
ALCOHOLS						
Methanol	67-56-1	40.7	15.1	12.3	22.3	29.7
Ethanol	64-17-5	58.5	15.8	8.8	19.4	26.6
Allyl alcohol (2-propen-1-ol)	107-18-6	68.4	16.2	10.8	16.8	25.8
1-Propanol	71-23-8	75.2	16.0	6.8	17.4	24.6
2-Propanol	67-63-0	76.8	15.8	6.1	16.4	23.5
Furfuryl alcohol	98-00-0	86.5	17.4	7.6	15.1	24.3
1-Butanol (butyl alcohol)	71-36-3	91.5	16.0	5.7	15.8	23.1
Benzyl alcohol	100-51-6	103.6	18.4	6.3	13.7	23.7
Cyclohexanol	108-93-0	106.0	17.4	4.1	13.5	22.5
1-Pentanol	71-41-0	109.0	16.0	4.5	13.9	21.7
Ethyl lactate	687-47-8	115.0	16.0	7.6	12.5	21.7
Ethylene glycol monomethyl ether (2-methoxyethanol)	109-86-4	79.1	16.2	9.2	16.4	24.8
Diethylene glycol monomethyl ether (2-(2-methoxyethoxy)ethanol)	111-77-3	118.0	16.2	9.2	12.3	22.3
Ethylene glycol mono-n-butyl ether (2-butoxyethanol) Butyl Cellusolve	111-76-2	131.6	16.0	5.1	12.3	22.3
1-Octanol (capryl alcohol)	111-87-5	157.7	17.0	3.3	11.9	20.9
Triethylene glycol mono-oleyl ether		418.5	13.3	3.1	8.4	16.0
ACIDS						
Formic acid	64-18-6	37.8	14.3	11.9	16.6	25.0
Acetic acid	64-19-7	57.1	14.5	8.0	13.5	21.3
Benzoic acid ^b	65-85-0	100.0	18.2	7.0	9.8	21.9
n-Octanoic acid ^c	124-07-2	159.0	15.1	3.3	8.2	17.6
Oleic acid	112-80-1	320.0	14.3	3.1	5.5	15.8
Stearic acid ^b	57-11-4	326.0	16.4	3.3	5.5	17.6
PHENOLS						
Phenol	108-95-2	87.5	18.0	5.9	14.9	24.1
1,3-Benzenediol ^b (resorcinol)	108-46-3	87.5	18.0	8.4	21.1	28.8
m-Cresol	108-39-4	104.7	18.0	5.1	12.9	22.7
Methyl salicylate	119-36-8	129.0	16.0	8.0	12.3	21.7
WATER						
Water ^c	7732-18-5	18.0	15.5 ^a	16.0 ^a	42.4 ^a	47.9
POLYHYDRIC ALCOHOLS						
Ethylene glycol	107-21-1	55.8	17.0	11.0	26.0	32.9
Glycerol	56-81-5	73.8	17.4	12.1	29.3	36.2
Propylene glycol (1,2-propanediol)	57-55-6	73.6	16.8	9.4	23.3	30.3

^a Altered from previously published value

^b Solid, treated as supercooled liquid

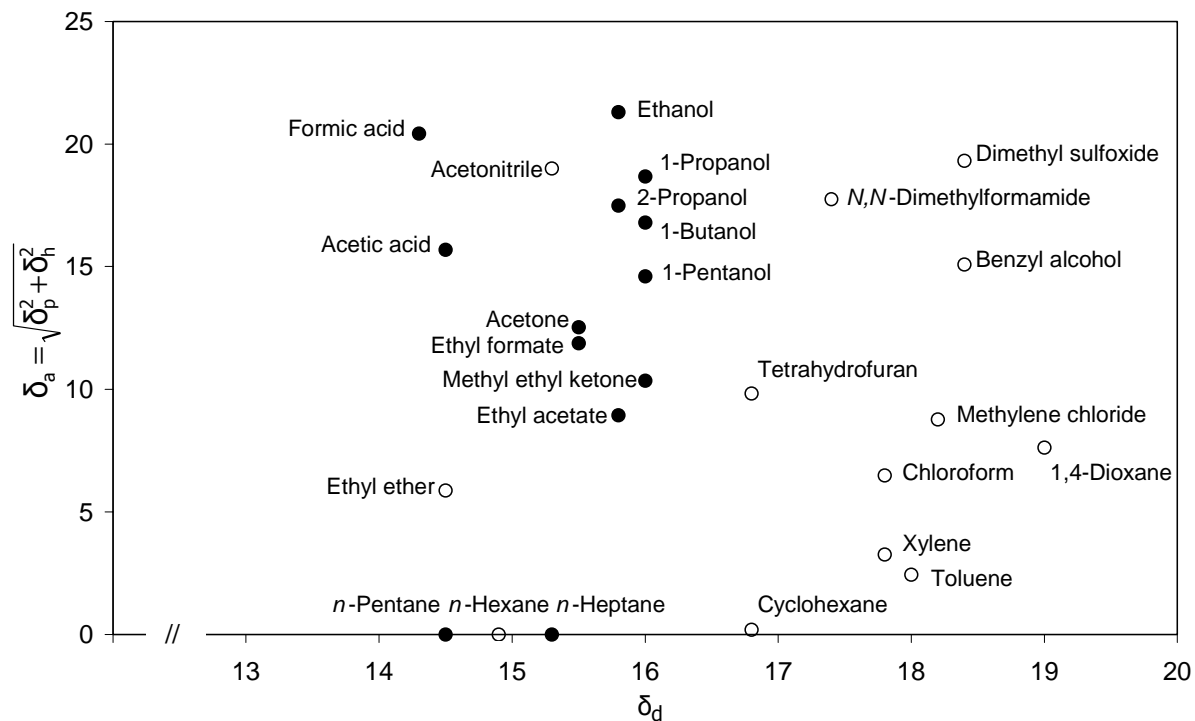
^c Values uncertain

^d Impure commercial product of this nominal formula

Data adapted from:

Grulke EA. 'Solubility Parameter Values'. In: Brandrup J, Immergut EH, Grulke EA, editors. *Polymer Handbook*. New York: John Wiley, 1999. p. VII/675-714.

3. Solubility Parameter Map



Solvent-Map: Two-dimensional illustration of several solvents based on their Hansen Solubility Parameters. Filled symbols: ICH class 3 solvents; Open symbols: ICH class 2 solvents. X-axis: dispersive solubility parameter (δ_d); Y-axis: partial solubility parameter (δ_a) that combines all non-dispersive interaction forces.

4. Program Listing

Listing of the algorithm used for the calculation of Hansen Solubility Parameters of binary solvent mixtures (GFA Basic 4.1 for Windows):

```

REM 3D Hansen-Löslichkeitsparameterberechnung von LM-Mischungen von Michael Hacker 2000/2001
DIM lm$(50), lpd(50), lpp(50), lph(50), lpg(50),
t!pd(50,50),t!pp(50,50),t!ph(50,50),el!pd(50,50),el!pp(50,50),el!ph(50,50),et!3(50,50),tsumme(50,50),esumme(50,50),psumme(50,50),tdist(50,50),e
dist(50,50)
cn|=1,lm$(cn)="Aceton", lpd(cn)=15.5, lpp(cn)=10.4 , lph(cn)=7, lpg(cn)=20.1
cn|=2,lm$(cn)="Ameisensäure", lpd(cn)=14.3, lpp(cn)=11.9, lph(cn)=16.6, lpg(cn)=25
cn|=3,lm$(cn)="1-Butanol", lpd(cn)=16.0, lpp(cn)=5.7, lph(cn)=15.8, lpg(cn)=23.1
cn|=4,lm$(cn)="2-Butanol", lpd(cn)=15.8, lpp(cn)=5.7, lph(cn)=14.5, lpg(cn)=22.1
cn|=5,lm$(cn)="Butylacetat", lpd(cn)=15.8, lpp(cn)=3.7, lph(cn)=6.3, lpg(cn)=17.4
cn|=6,lm$(cn)="Dimethylsulfoxide", lpd(cn)=18.4, lpp(cn)=16.4, lph(cn)=10.2, lpg(cn)=26.6
cn|=7,lm$(cn)="Essigsäure", lpd(cn)=14.5, lpp(cn)=8, lph(cn)=13.5, lpg(cn)=21.3
cn|=8,lm$(cn)="Ethanol", lpd(cn)=15.8, lpp(cn)=8.8, lph(cn)=19.4, lpg(cn)=26.6
cn|=9,lm$(cn)="Ethylacetat", lpd(cn)=15.8, lpp(cn)=5.3, lph(cn)=7.2, lpg(cn)=18.2
cn|=10,lm$(cn)="Ethylether", lpd(cn)=14.5, lpp(cn)=2.9 , lph(cn)=5.1, lpg(cn)=15.8
cn|=11,lm$(cn)="Ethylformat", lpd(cn)=15.5, lpp(cn)=8.4, lph(cn)=8.4, lpg(cn)=19.6
cn|=12,lm$(cn)="Heptan", lpd(cn)=15.3, lpp(cn)=0 , lph(cn)=0, lpg(cn)=15.3
cn|=13,lm$(cn)="Isobutylacetat", lpd(cn)=15.1, lpp(cn)=3.7, lph(cn)=6.3, lpg(cn)=16.8
cn|=14,lm$(cn)="Isopropylacetat", lpd(cn)=14.3, lpp(cn)=8.4 , lph(cn)=5.7, lpg(cn)=17.6
cn|=15,lm$(cn)="Methylacetat", lpd(cn)=15.5, lpp(cn)=7.2, lph(cn)=7.6, lpg(cn)=18.8
cn|=16,lm$(cn)="Methylethylketon", lpd(cn)=16, lpp(cn)=9.0, lph(cn)=5.1, lpg(cn)=19
cn|=17,lm$(cn)="Methylisobutylketon", lpd(cn)=15.3, lpp(cn)=6.1, lph(cn)=4.1, lpg(cn)=17
cn|=18,lm$(cn)="2-Methyl-1-propanol", lpd(cn)=15.1, lpp(cn)=5.7, lph(cn)=16, lpg(cn)=22.7
cn|=19,lm$(cn)="Pentan", lpd(cn)=14.5, lpp(cn)=0, lph(cn)=0, lpg(cn)=14.5
cn|=20,lm$(cn)="1-Pentanol", lpd(cn)=16, lpp(cn)=4.5, lph(cn)=13.9, lpg(cn)=21.7
cn|=21,lm$(cn)="1-Propanol", lpd(cn)=16, lpp(cn)=6.8, lph(cn)=17.4, lpg(cn)=24.6
cn|=22,lm$(cn)="2-Propanol", lpd(cn)=15.8, lpp(cn)=6.1, lph(cn)=16.4, lpg(cn)=23.5
cn|=23,lm$(cn)="Propylacetat", lpd(cn)=14.1, lpp(cn)=8.1, lph(cn)=7.8, lpg(cn)=18.0
cn|=24,lm$(cn)="Tetrahydrofuran", lpd(cn)=16.8, lpp(cn)=5.7, lph(cn)=8, lpg(cn)=19.4
cn|=25,lm$(cn)="Chloroform", lpd(cn)=17.8, lpp(cn)=3.1, lph(cn)=5.7, lpg(cn)=19
cn|=26,lm$(cn)="Aceton", lpd(cn)=15.5, lpp(cn)=10.4 , lph(cn)=7, lpg(cn)=20.1
cn|=27,lm$(cn)="Acetonitril", lpd(cn)=15.3, lpp(cn)=18, lph(cn)=6.1, lpg(cn)=24.6
cn|=28,lm$(cn)="Ameisensäure", lpd(cn)=14.3, lpp(cn)=11.9, lph(cn)=16.6, lpg(cn)=25
cn|=29,lm$(cn)="Benzylalkohol", lpd(cn)=18.4, lpp(cn)=6.3, lph(cn)=13.7, lpg(cn)=23.7
cn|=30,lm$(cn)="1-Butanol", lpd(cn)=16.0, lpp(cn)=5.7, lph(cn)=15.8, lpg(cn)=23.1
cn|=31,lm$(cn)="Chloroform", lpd(cn)=17.8, lpp(cn)=3.1, lph(cn)=5.7, lpg(cn)=19
cn|=32,lm$(cn)="Dichlormethan", lpd(cn)=18.2, lpp(cn)=6.3, lph(cn)=6.1, lpg(cn)=20.3
cn|=33,lm$(cn)="Diethylether", lpd(cn)=14.5, lpp(cn)=2.9 , lph(cn)=5.1, lpg(cn)=15.8
cn|=34,lm$(cn)="Dimethylformamid", lpd(cn)=17.4, lpp(cn)=13.7, lph(cn)=11.3, lpg(cn)=24.8
cn|=35,lm$(cn)="Dimethylsulfoxid", lpd(cn)=18.4, lpp(cn)=16.4, lph(cn)=10.2, lpg(cn)=26.6
cn|=36,lm$(cn)="1,4-Dioxan", lpd(cn)=19, lpp(cn)=1.8, lph(cn)=7.4, lpg(cn)=20.5
cn|=37,lm$(cn)="Essigsäure", lpd(cn)=14.5, lpp(cn)=8, lph(cn)=13.5, lpg(cn)=21.3
cn|=38,lm$(cn)="Ethanol", lpd(cn)=15.8, lpp(cn)=8.8, lph(cn)=19.4, lpg(cn)=26.6
cn|=39,lm$(cn)="Ethylacetat", lpd(cn)=15.8, lpp(cn)=5.3, lph(cn)=7.2, lpg(cn)=18.2
cn|=40,lm$(cn)="Ethylformat", lpd(cn)=15.5, lpp(cn)=8.4, lph(cn)=8.4, lpg(cn)=19.6
cn|=41,lm$(cn)="n-Hexan", lpd(cn)=14.9, lpp(cn)=0, lph(cn)=0, lpg(cn)=14.9
cn|=42,lm$(cn)="Methanol", lpd(cn)=15.1, lpp(cn)=12.3, lph(cn)=22.3, lpg(cn)=29.7
cn|=43,lm$(cn)="Methylethylketon", lpd(cn)=16, lpp(cn)=9.0, lph(cn)=5.1, lpg(cn)=19
cn|=44,lm$(cn)="Methylsalicylat", lpd(cn)=16, lpp(cn)=8, lph(cn)=12.3, lpg(cn)=21.7
cn|=45,lm$(cn)="1-Pentanol", lpd(cn)=16, lpp(cn)=4.5, lph(cn)=13.9, lpg(cn)=21.7
cn|=46,lm$(cn)="2-Propanol", lpd(cn)=15.8, lpp(cn)=6.1, lph(cn)=16.4, lpg(cn)=23.5
cn|=47,lm$(cn)="Propylacetat", lpd(cn)=14.1, lpp(cn)=8.1, lph(cn)=7.8, lpg(cn)=18.0
cn|=48,lm$(cn)="Tetrahydrofuran", lpd(cn)=16.8, lpp(cn)=5.7, lph(cn)=8, lpg(cn)=19.4
cn|=49,lm$(cn)="Toluol", lpd(cn)=18, lpp(cn)=1.4, lph(cn)=2, lpg(cn)=18.2
cn|=50,lm$(cn)="Wasser", lpd(cn)=15.5, lpp(cn)=16.0, lph(cn)=42.4, lpg(cn)=47.9
dstyle 1%=WS_BORDER|WS_TABSTOP|ES_CENTER

```

```

DLGBASE UNIT
DIALOG #1,1,1,345,140,"3D Hansen-Löslichkeitsparameter-Berechnung von LM-Mischungen V3.2 (by Lerxst 2001)"
LTEXT "Gewünschte Löslichkeitsparameter : ",1002,10,11,140,10
LTEXT "disp.",1006,151,22,20,10
LTEXT "pol.",1007,184,22,20,10
LTEXT "hyd.",1008,213,22,20,10
EDITTEXT "",1003,150,10,20,10,dstyle1%
EDITTEXT "",1004,180,10,20,10,dstyle1%
EDITTEXT "",1005,210,10,20,10,dstyle1%
LTEXT "Lösungsmittelauswahl : ",1009,10,40,140,10
LTEXT "ICH Klasse 3",1010,160,40,100,10
LTEXT "Laborausstattung",1011,160,50,100,10
CHECKBOX "",1012,150,39,10,10,BS_AUTORADIOBUTTON
CHECKBOX "",1013,150,49,10,10,BS_AUTORADIOBUTTON
LTEXT "Abstandseingabe (maximal bzw. exakt) : ",1014,10,71,160,10
EDITTEXT "",1015,170,70,40,10,dstyle1%
PUSHBUTTON "LM-Mischung berechnen",1016,10,90,100,14,WS_TABSTOP
LTEXT "WEITERE MODULE :",1017,260,10,80,12
PUSHBUTTON "Abstand eines Lösungsmittels",1018,260,25,120,14,WS_TABSTOP
PUSHBUTTON "Abstand einer best. Mischung",1019,260,45,120,14,WS_TABSTOP
PUSHBUTTON "Mischung mit def. Abstand",1020,260,68,120,14,WS_TABSTOP
PUSHBUTTON "Schließen",1001,10,110,60,14,WS_TABSTOP
PUSHBUTTON "Pur",1025,80,110,30,14,WS_TABSTOP
LTEXT "Best .:",1021,130,92,25,10
LTEXT "",1022,160,90,220,12,SS_CENTER|WS_BORDER
LTEXT "",1023,160,110,220,12,SS_CENTER|WS_BORDER
PUSHBUTTON "Auswahl anzeigen",1024,10,50,90,12
CHECKBOX "Polymernäherung",1040,10,24,100,10,BS_AUTOCHECKBOX
ENDDIALOG
DLG FILL 1,RGB(192,192,192)
SHOWDIALOG #1
~SendMessage(DLGITEM(1,1012), BM_SETCHECK, TRUE, 0)
REPEAT
GETEVENT
IF MENU(11)=WM_COMMAND
SELECT MENU(12)
CASE 1001
ende!=TRUE
CASE 1012
Imwahl|=0
CASE 1013
Imwahl|=1
CASE 1016
GOSUB GetParameter
distmax=VAL(_WIN$(DLGITEM(1,1015)))
GOSUB Berechnung_equal
GOSUB Ergebnis_equal
CASE 1018
GOSUB LMdist
CASE 1019
GOSUB Mixdist
CASE 1020
GOSUB GetParameter
dist=VAL(_WIN$(DLGITEM(1,1015)))
IF dist <>0
GOSUB Abstand_misch
ELSE
_WIN$(DLGITEM(1,1022))="Bitte geben Sie einen Abstand > 0 ein !"
_WIN$(DLGITEM(1,1023))=""
ENDIF
CASE 1024
GOSUB LMAnzeige
CASE 1025
GOSUB GetParameter
GOSUB PURTest
CASE 1040

```

```

IF polyn|=0
  polyn|=1
ELSE
  polyn|=0
ENDIF
ENDSELECT
ENDIF
UNTIL ende!
CLOSEDIALOG #1

> PROCEDURE GetParameter
wlpd=VAL(_WIN$(DLGITEM(1,1003)))
wlpp=VAL(_WIN$(DLGITEM(1,1004)))
wlph=VAL(_WIN$(DLGITEM(1,1005)))
RETURN
> PROCEDURE LMAnzeige
OPENW #1,2,300,690,300,0
TITLEW #1,"Lösungsmittelauswahl"
zeij=0
FOR Imp|=1+(lmwahl|*25) TO 24+(lmwahl|*1)+(lmwahl|*25) STEP 2
  INC zeij
  TEXT 10,zeij*20,Imp|-(lmwahl|*25)
  TEXT 40,zeij*20,lm$(Imp|)
  TEXT 200,zeij*20,lpd(Imp|)
  TEXT 240,zeij*20,lpp(Imp|)
  TEXT 280,zeij*20,lph(Imp|)
  IF Imp|<>50
    TEXT 370,zeij*20,(Imp|+1)-(lmwahl|*25)
    TEXT 400,zeij*20,lm$(Imp|+1)
    TEXT 550,zeij*20,lpd(Imp|+1)
    TEXT 590,zeij*20,lpp(Imp|+1)
    TEXT 630,zeij*20,lph(Imp|+1)
  ENDIF
NEXT Imp|
COLOR 249
PRINT " Zum Fortsetzen bitte Taste drücken"
KEYGET pause
CLOSEW #1
RETURN

> PROCEDURE LMdist
LOCAL subende!,res$
DLGBASE UNIT
DIALOG #2,350,1,160,290,"Abstandsberechnung"
zeij=0
FOR Imp|=1+(lmwahl|*25) TO 24+(lmwahl|*1)+(lmwahl|*25) STEP 2
  INC zeij
  CHECKBOX lm$(Imp|),(2000+Imp|),5,((zeij-1)*20),90,20,BS_AUTORADIOBUTTON
  IF Imp|<>50
    CHECKBOX lm$(Imp|+1),(2000+Imp|+1),95,((zeij-1)*20),90,20,BS_AUTORADIOBUTTON
  ENDIF
NEXT Imp|
PUSHBUTTON "Distanz berechnen",2051,5,260,80,14,WS_TABSTOP
PUSHBUTTON "Schließen",2052,95,260,60,14,WS_TABSTOP
ENDDIALOG
SHOWDIALOG #2
DLG FILL 2,RGB(192,192,192)
REPEAT
GETEVENT
IF MENU(11)=WM_COMMAND
  IF 2000<MENU(12) AND MENU(12)<2051 THEN slm|=MENU(12)-2000
  SELECT MENU(12)
  CASE 2051
    GOSUB GetParameter
    tsumme=SQR((polyn|*3+1)*(wlpd-lpd(slm|))^2+(wlpp-lpp(slm|))^2+(wlph-lph(slm|))^2)
    res$="Abstand zu "+lm$(slm|)+" : "+STR$(ROUND(tsumme,1))+ " (" +STR$(ROUND((tsumme)^2,1))+")"

```

```

    _WIN$(DLGITEM(1,1022))=""
    _WIN$(DLGITEM(1,1023))=res$
CASE 2052
  subende!=TRUE
CASE 1040
  IF polyn|=0
    polyn|=1
  ELSE
    polyn|=0
  ENDF
ENDSELECT
ENDIF
UNTIL subende!
CLOSEDIALOG #2
RETURN
> PROCEDURE Berechnung_equal
t1|=0,t2|=0
FOR t1|=1+(l|wahl|*25) TO 24+(l|wahl|*1)+(l|wahl|*25)
  FOR t2|=t1| TO 24+(l|wahl|*1)+(l|wahl|*25)
    IF t1|<>t2|
      FOR t3=0 TO 1 STEP 0.01
        t|pd(t1|,t2|)=t3*|pd(t1|)+(1-t3)*|pd(t2|)
        t|pp(t1|,t2|)=t3*|pp(t1|)+(1-t3)*|pp(t2|)
        t|ph(t1|,t2|)=t3*|ph(t1|)+(1-t3)*|ph(t2|)
        tsumme(t1|,t2|)=SQR((polyn|*3+1)*(w|pd-t|pd(t1|,t2|))^2+(w|pp-t|pp(t1|,t2|))^2+(w|ph-t|ph(t1|,t2|))^2)
        IF t3=0 THEN
          et3(t1|,t2|)=ROUND(t3,2)
          esumme(t1|,t2|)=tsumme(t1|,t2|)
        ENDF
        IF tsumme(t1|,t2|)<esumme(t1|,t2|)
          et3(t1|,t2|)=ROUND(t3,2)
          esumme(t1|,t2|)=tsumme(t1|,t2|)
        ENDF
      NEXT t3
    ENDF
  NEXT t2|
NEXT t1|
RETURN

> PROCEDURE Ergebnis_equal
OPENW #2,2,300,690,400,0
TITLEW #2,"Lösungsmittelaustausch"
LOCAL dcount|,res1$,res2$
dcount|=0
t1|=0,t2|=0
COLOR 0
IF l|wahl|=0 THEN
  best=esumme(1,2)
ELSE IF l|wahl|=1
  best=esumme(26,27)
ENDIF
FOR t1|=1+(l|wahl|*25) TO 24+(l|wahl|*1)+(l|wahl|*25)
  FOR t2|=t1| TO 24+(l|wahl|*1)+(l|wahl|*25)
    IF t1|<>t2| THEN
      elpd(t1|,t2|)=ROUND(et3(t1|,t2|)*|pd(t1|)+(1-et3(t1|,t2|))*|pd(t2|),1)
      elpp(t1|,t2|)=ROUND(et3(t1|,t2|)*|pp(t1|)+(1-et3(t1|,t2|))*|pp(t2|),1)
      elph(t1|,t2|)=ROUND(et3(t1|,t2|)*|ph(t1|)+(1-et3(t1|,t2|))*|ph(t2|),1)
      IF esumme(t1|,t2|)<best THEN
        best=esumme(t1|,t2|)
        best1|=t1|
        best2|=t2|
      ENDF
    IF esumme(t1|,t2|)<=distmax AND ROUND(et3(t1|,t2|),2)>0 AND ROUND(et3(t1|,t2|),2)<>1 THEN
      INC dcount|
      PRINT " Mix: ";l|m$(t1|);" und ";l|m$(t2|);" - ratio: ";et3(t1|,t2|);" / ";ROUND(1-et3(t1|,t2|),2);" - value: ";elpd(t1|,t2|);" ";elpp(t1|,t2|);"
      ";elph(t1|,t2|);" dist.: ";ROUND(esumme(t1|,t2|),1)

```

```

IF INT(dcount/20)=dcount/20
PRINT
PRINT "Bitte Taste für weitere Ergebnisse drücken"
REPEAT
UNTIL INKEY$<>""
CLS
dcount|=0
ENDIF
ENDIF
ENDIF
NEXT t2|
NEXT t1|
res1$=lm$(best1|)+ " und "+lm$(best2|)+ " - "+STR$(et3(best1|,best2|))+ " zu "+STR$(ROUND(1-et3(best1|,best2|),2))
res2$="Parameter: "+STR$(ROUND(elpd(best1|,best2|),1))+ " "+STR$(ROUND(elpp(best1|,best2|),1))+ "
"+STR$(ROUND(elph(best1|,best2|),1))+ " Abstand: "+STR$(ROUND(esumme(best1|,best2|),1))
_WIN$(DLGITEM(1,1022))=res1$
_WIN$(DLGITEM(1,1023))=res2$
PRINT
COLOR 249
PRINT " Ergebnisausgabe beendet - Bitte Taste drücken"
KEYGET pause
CLOSEW #2
RETURN
> PROCEDURE Abstand_misch
OPENW #3,2,300,690,400,0
TITLEW #3,"Lösungsmittel in definiertem Abstand"
LOCAL dcount|,res1$,res2$
dcount|=0
best=dist*1000
bdist=dist*1000
brdist=dist*1000
t1|=0,t2|=0
FOR t1|=1+(lmwahl|*25) TO 24+(lmwahl|*1)+(lmwahl|*25)
FOR t2|=t1| TO 24+(lmwahl|*1)+(lmwahl|*25)
IF t1|<>t2|
tdist(t1|,t2|)=dist
FOR t3=0 TO 1 STEP 0.01
t|pd(t1|,t2|)=t3*|pd(t1|)+(1-t3)*|pd(t2|)
t|pp(t1|,t2|)=t3*|pp(t1|)+(1-t3)*|pp(t2|)
t|ph(t1|,t2|)=t3*|ph(t1|)+(1-t3)*|ph(t2|)
tsumme(t1|,t2|)=SQR((polyn|*3+1)*(w|pd-t|pd(t1|,t2|))^2+(w|pp-t|pp(t1|,t2|))^2+(w|ph-t|ph(t1|,t2|))^2)
IF t3=0
et3(t1|,t2|)=ROUND(t3,2)
esumme(t1|,t2|)=tsumme(t1|,t2|)
ENDIF
IF ABS(tsumme(t1|,t2|)-dist)<tdist(t1|,t2|)
tdist(t1|,t2|)=ABS(tsumme(t1|,t2|)-dist)
edist(t1|,t2|)=tsumme(t1|,t2|)
et3(t1|,t2|)=ROUND(t3,2)
esumme(t1|,t2|)=tsumme(t1|,t2|)
ENDIF
IF ABS(tsumme(t1|,t2|)-brdist)
brdist=ABS(tsumme(t1|,t2|)-brdist)
bdist=tsumme(t1|,t2|)
ENDIF
NEXT t3
ENDIF
NEXT t2|
NEXT t1|
cabs=dist*1000
FOR t1|=1+(lmwahl|*25) TO 24+(lmwahl|*1)+(lmwahl|*25)
FOR t2|=t1| TO 24+(lmwahl|*1)+(lmwahl|*25)
IF t1|<>t2| THEN
elpd(t1|,t2|)=ROUND(et3(t1|,t2|)*|pd(t1|)+(1-et3(t1|,t2|))*|pd(t2|),1)
elpp(t1|,t2|)=ROUND(et3(t1|,t2|)*|pp(t1|)+(1-et3(t1|,t2|))*|pp(t2|),1)
elph(t1|,t2|)=ROUND(et3(t1|,t2|)*|ph(t1|)+(1-et3(t1|,t2|))*|ph(t2|),1)

```

```

ENDIF
IF ABS(esumme(t1|,t2|)-dist)<cabs THEN
  cabs=ABS(esumme(t1|,t2|)-dist)
  cabst1|=t1|
  cabst2|=t2|
ENDIF
IF ROUND(esumme(t1|,t2|))=dist THEN
  INC dcount|
  PRINT " Mix: ";lm$(t1|);" und ";lm$(t2|);" - ratio: ";et3(t1|,t2|);" / ";ROUND(1-et3(t1|,t2|),2);" - value: ";elpd(t1|,t2|);" ";elpp(t1|,t2|);"
  ";elph(t1|,t2|);" dist.: ";ROUND(esumme(t1|,t2|),1)
  IF INT(dcount|/20)=dcount|/20
    PRINT
    PRINT " Bitte Taste für weitere Ergebnisse drücken"
    REPEAT
      UNTIL INKEY$<>""
    CLS
    dcount|=0
  ENDIF
ENDIF
NEXT t2|
NEXT t1|
IF cabst1|<>1 OR cabst2|<>1 AND cabst1|<>26 OR cabst2|<>26 AND ROUND(dist)=ROUND(esumme(cabst1|,cabst2|))
  res1$=lm$(cabst1|)+ " und "+lm$(cabst2|)+ " - "+STR$(et3(cabst1|,cabst2|))+ " zu "+STR$(ROUND(1-et3(cabst1|,cabst2|),2))
  res2$="Parameter: "+STR$(ROUND(elpd(cabst1|,cabst2|),1))+ " "+STR$(ROUND(elpp(cabst1|,cabst2|),1))+ "
"+STR$(ROUND(elph(cabst1|,cabst2|),1))+ " Abstand: "+STR$(ROUND(esumme(cabst1|,cabst2|),1))
  _WIN$(DLGITEM(1,1022))=res1$
  _WIN$(DLGITEM(1,1023))=res2$
ELSE
  res1$=""
  res2$=""
  _WIN$(DLGITEM(1,1022))=res1$
  _WIN$(DLGITEM(1,1023))=res2$
  COLOR 249
  PRINT
  PRINT " Nächster erreichbarer Abstand: ";ROUND(bdist,1)
ENDIF
COLOR 249
PRINT
PRINT " Ergebnisausgabe beendet - Bitte Taste drücken"
KEYGET pause
CLOSEW #3
RETURN
> PROCEDURE PURTest
best=100000
t1|=0
FOR t1|=1+(lmwahl|*25) TO 24+(lmwahl|*1)+(lmwahl|*25)
  tsumme=SQR((polyn|*3+1)*(wlpd-lpd(t1|))^2+(wlpp-lpp(t1|))^2+(wlph-lph(t1|))^2)
  IF tsumme<best
    best=tsumme
    et1|=t1|
    esumme=tsumme
  ENDIF
NEXT t1|
res1$=lm$(et1|)
res2$="Parameter: "+STR$(lpd(et1|))+ " "+STR$(lpp(et1|))+ " "+STR$(lph(et1|))+ " Abstand: "+STR$(ROUND(esumme,1))+ "
"+STR$(ROUND((esumme)^2,1))+ "
  _WIN$(DLGITEM(1,1022))=res1$
  _WIN$(DLGITEM(1,1023))=res2$
RETURN
> PROCEDURE Mixdist
LOCAL subende!,res1$,res2$,zeij,mlpd,mlpp,mlph
DLGBASE UNIT
DIALOG #3,350,1,160,310,"Abstandsberechnung einer definierten Mischung"
zeij=0
GROUPBOX "Lösungsmittel 1: ",3000,2,1,89,260,BS_GROUPBOX|WS_GROUP
FOR lmp|=1+(lmwahl|*25) TO 24+(lmwahl|*1)+(lmwahl|*25)

```

```

INC zeij
RADIOBUTTON lm$(Imp),(3000+Imp),3,zeij*10,87,10,BS_AUTORADIOBUTTON
NEXT Imp|
zeij=0
GROUPBOX "Lösungsmittel 2:",3060,94,1,89,260,BS_GROUPBOX|WS_GROUP
FOR Imp|=1+(lmwahl|*25) TO 24+(lmwahl|*1)+(lmwahl|*25)
  INC zeij
  RADIOBUTTON lm$(Imp),(3060+Imp),95,zeij*10,87,10,BS_AUTORADIOBUTTON
NEXT Imp|
PUSHBUTTON "Distanz berechnen",3051,5,280,80,14,WS_TABSTOP
PUSHBUTTON "Schließen",3052,95,280,60,14,WS_TABSTOP
LTEXT "Anteil von Lösungsmittel 1 in % : ",3200,7,266,130,10
EDITTEXT "",3201,135,265,15,10,WS_BORDER|WS_TABSTOP|SS_CENTER
ENDDIALOG
SHOWDIALOG #3
DLG FILL 3,RGB(192,192,192)
REPEAT
  GETEVENT
  IF MENU(11)=WM_COMMAND
    IF 3000<MENU(12) AND MENU(12)<3051 THEN slm1|=MENU(12)-3000
    IF 3060<MENU(12) AND MENU(12)<3111 THEN slm2|=MENU(12)-3060
    SELECT MENU(12)
    CASE 3051
      GOSUB GetParameter
      alm1=VAL(_WIN$(DLGITEM(3,3201)))/100
      tsumme=SQR((polyn|*3+1)*(wlpd-(alm1*lpd(slm1|)+(1-alm1)*lpd(slm2|)))^2+(wlpp-(alm1*lpp(slm1|)+(1-alm1)*lpp(slm2|)))^2+(wlph-
(alm1*lph(slm1|)+(1-alm1)*lph(slm2|)))^2)
      mlpd=ROUND(alm1*lpd(slm1|)+(1-alm1)*lpd(slm2|),1)
      mlpp=ROUND(alm1*lpp(slm1|)+(1-alm1)*lpp(slm2|),1)
      mlph=ROUND(alm1*lph(slm1|)+(1-alm1)*lph(slm2|),1)
      res1$=lm$(slm1|)+" / "+lm$(slm2|)+" "+STR$(alm1)+" zu "+STR$(1-alm1)
      res2$="Parameter: "+STR$(mlpd)+" "+STR$(mlpp)+" "+STR$(mlph)+" Abstand: "+STR$(ROUND(tsumme,1))+"
("+STR$(ROUND((tsumme)^2,1))+"")
      _WIN$(DLGITEM(1,1022))=res1$
      _WIN$(DLGITEM(1,1023))=res2$
    CASE 3052
      subende!=TRUE
    CASE 1040
      IF polyn|=0
        polyn|=1
      ELSE
        polyn|=0
      ENDIF
    ENDSELECT
  ENDIF
UNTIL subende!
CLOSEDIALOG #3
RETURN

```

5. Curriculum Vitae

Name: Michael Christian Hacker
Date of birth: May 27, 1974
Place of birth: Erlangen, Germany
Nationality: German
Marital Status: single

Education:

09/80 - 07/84 Elementary School: Michael-Poeschke-Schule, Erlangen
09/84 - 06/93 Grammar School: Ohm-Gymnasium, Erlangen
07/93 university-entrance diploma (Abitur)

Civilian service:

10/93 - 12/94 Civilian Service at the Bayerisches Rotes Kreuz,
Kreisverband Erlangen-Hoechstadt,
Department: Social Services in Erlangen

Professional Training:

11/94 - 10/98 Studies of Pharmacy: Friedrich-Alexander-University, Erlangen
11/98 - 04/99 Pharmaceutical Traineeship: Heumann Pharma, Feucht
(Department: Quality control)
05/99 - 10/99 Pharmaceutical Traineeship: Sebaldus-Apotheke, Erlangen
22.12.1999 Acquisition of the license to practice as pharmacist

02/2000 Pharmacist: Föhren-Apotheke, Erlangen
03/2000 – today PhD program at the Department of Pharmaceutical Technology
of the University of Regensburg, Prof. Achim Göpferich

6. List of Publications

PUBLICATIONS

1. TISSUE ENGINEERING **9**
(2003) P. 71 – 84
Lieb E., Tessmar J., Hacker M., Fischbach C., Rose D., Blunk T., Mikos A., Göpferich A., Schulz M.B.:
"Poly(D,L-lactic acid)-poly(ethylene glycol)-monomethyl ether Diblock Copolymers Control Adhesion and Osteoblastic Differentiation of Marrow Stromal Cells"
2. BIOMATERIALS **24**
(2003)
P. 4459–4473
(CHAPTER 3)
Hacker M., Tessmar J., Neubauer M., Blaimer A., Blunk T., Göpferich A., Schulz M.B.:
"Towards biomimetic scaffolds: Anhydrous scaffold fabrication from biodegradable amine-reactive diblock copolymers"
3. TISSUE ENGINEERING
10 (2004) P. 215
Fischbach C., Seufert J., Staiger H., Hacker M., Neubauer M., Göpferich A., and Blunk T.:
"Three-Dimensional in Vitro Model for Adipogenesis: Comparison of Culture Conditions"
4. BIOMATERIALS
(ACCEPTED)
(CHAPTER 2)
*Hacker M. *, Lieb E. *, Tessmar J., Kunz-Schughart L.A., Fiedler J., Dahmen C., Hersel U., Kessler H., Schulz M.B., Göpferich A.:*
"Mediating Specific Cell Adhesion to Low-adhesive Diblock Copolymers by Instant Modification with Cyclic RGD Peptides"
(*equally contributing authors)
5. TISSUE ENGINEERING
(ACCEPTED)
E. Lieb, S. Milz, T. Vogel, M. Hacker, M. Dauner, M.B. Schulz.:
"Effects of TGF- β 1 on Bone-Like Tissue Formation in Three-Dimensional Cell Culture. Part I: Culture Conditions and Tissue Formation"
6. EXPERIMENTAL CELL
RESEARCH
(ACCEPTED)
C. Fischbach, T. Spruß, B. Weiser, M. Neubauer, C. Becker, M. Hacker, A. Göpferich, T. Blunk:
"Generation of mature fat pads in vitro and in vivo utilizing 3-D long-term culture of 3T3-L1 preadipocytes"
7. EUROPEAN JOURNAL OF
PHARMACEUTICS AND
BIOPHARMACEUTICS
(TO BE SUBMITTED)
(CHAPTER 4)
M. Hacker, A. Blaimer, M.B. Schulz, A. Göpferich:
"Hansen Solubility Parameters as a Means to Replace Halogenated Solvents in Biomaterial Processing"

8. TISSUE ENGINEERING
(TO BE SUBMITTED)
(CHAPTER 6) *M. Hacker, M. Ringhofer, M. Neubauer, T. Vogel, B. Appel, T. Blunk, A. Göpferich, M.B. Schulz.*
"Solid Lipid Templating: A Versatile Lab-scale Fabrication Technique for Macroporous Tissue Engineering Scaffolds"
9. EUROPEAN JOURNAL OF
PHARMACEUTICS AND
BIOPHARMACEUTICS
(TO BE SUBMITTED)
(CHAPTER 7) *M. Hacker, T. Vogel, M. Neubauer, B. Appel, M. Breunig, T. Blunk, A. Göpferich, M.B. Schulz.*
"Synthesis and Characterization of Injectable, Thermogelling poly(*N*-isopropylacrylamide)-grafted Gelatin (PNiPAAm-gelatin)"

KONFERENZ ABSTRACTS

- 2.2.2001 CRS German Chapter Annual Meeting in Saarbrücken, Germany: *M. Hacker, J. Tessmar, M. Neubauer, A. Blaimer, T. Blunk, M.B. Schulz, A. Göpferich*: "Water-free manufacture of Me.PEG-PLA scaffolds for tissue engineering applications" (Poster)
- 10.10. - 13.10.2001 DPhG Jahrestagung in Halle: *Hacker M., Schulz M.B., Göpferich A.*: "Using Hansen Solubility Parameters to calculate less toxic alternatives for halogenated solvents in polymer processing" (Talk)
- 10.10. - 13.10.2001 DPhG Jahrestagung in Halle: *Hacker M., Teßmar J., Lieb E., Neubauer M., Blunk T., Göpferich A., Schulz M.B.*: "Development of a Fabrication Method for Scaffolds used in Tissue Engineering"
- 7.11. - 10.11.2001 1st Biennial Meeting of the European Tissue Engineering Society ETES 2001: *M. Hacker, J. Tessmar, M. Neubauer, T. Blunk, M.B. Schulz, A. Göpferich*: "Towards the Manufacture of Biomimetic Scaffolds" (Poster)
- 7.11. - 10.11.2001 1st Biennial Meeting of the European Tissue Engineering Society ETES 2001: *J. Teßmar, K. Kellner, M. Neubauer, M. Hacker, M.B. Schulz, T. Blunk, A. Göpferich*: "PEGylation of Insulin - towards the synthesis of biomimetic polymers"

- 7.11. – 10.11.2001 1st Biennial Meeting of the European Tissue Engineering Society ETES 2001: *M. Neubauer, C. Fischbach, E. Lieb, M. Hacker, J. Tessmar, M.B. Schulz, A. Göpferich, T. Blunk*: “Adipogenesis of Rat Marrow Stromal Cells in Two- and Three-Dimensional Cell Culture”
- 26.11. – 30.11.2001 MRS 2001 Fall Meeting in Boston, MA, USA: *M. Hacker, J. Tessmar, M. Neubauer, E. Lieb, T. Blunk, A. Göpferich, M.B. Schulz*: “Anhydrous scaffold fabrication from sensitive biodegradable polymers” (**Talk**)
- 11.1. – 13.1.2002 Keystone Symposia 2002 "Molecular Control of Adipogenesis and Obesity" in Keystone, CA, USA: *M. Neubauer, C. Fischbach, E. Lieb, M. Hacker, J. Tessmar, M.B. Schulz, A. Göpferich, T. Blunk*: “Exposure to Basic Fibroblast Growth Factor Enhances Adipogenesis of Rat Marrow Stromal Cells in vitro”
- 20.7. – 25.7.2002 29th International Symposium on Controlled Release of bioactive materials in Seoul, Korea: *M. Neubauer, J. Tessmar, M. Hacker, C. Fischbach, M.B. Schulz, T. Blunk, A. Goepferich*: “Towards Engineered Adipose Tissue Using Bone Marrow Stromal Cells and Basic Fibroblast Growth Factor”
- 31.5. – 2.6.2002 5th Annual Meeting of the GZG / ETCS in Regensburg, Germany: *M. Hacker, J. Tessmar, M. Neubauer, T. Blunk, A. Goepferich, M.B. Schulz*: “Macroporous biodegradable scaffolds for controlled surface modification” (**Poster**)
- 31.5. – 2.6.2002 5th Annual Meeting of the GZG / ETCS in Regensburg, Germany: *S. Drotleff, J. Tessmar; K. Kellner, M. Hacker; M. Neubauer, M.B. Schulz, T. Blunk, A. Goepferich*: “Biomimetic Polymers for Tissue Engineering – Characterisation of Polymers and of Proteins for their Surface Modification”
- 31.5. – 2.6.2002 5th Annual Meeting of the GZG / ETCS in Regensburg, Germany: *Lieb E., Milz S., Hacker M., Dauner M., Göpferich A., Schulz M.B.*: “3-D cell culture on poly(L-lactic-co-glycolic acid) fiber meshes for the evaluation of TGF- β 1 effects in bone tissue engineering”

- 31.5. – 2.6.2002 5th Annual Meeting of the GZG / ETCS in Regensburg, Germany: *M. Neubauer, C. Fischbach, E. Lieb, M. Hacker, J. Tessmar, P. Bauer-Kreisel, M.B. Schulz, A. Gopferich, T. Blunk*: “Adipogenesis of Rat Marrow Stromal Cells in Two- and Three-Dimensional Cell Culture”
- 9.10. – 12.10.2002 DPhG Jahrestagung in Berlin, Germany: *M. Hacker, E. Lieb, J. Tessmar, U. Hersel, C. Dahmen, H. Kessler, A. Göpferich, M.B. Schulz* :
“Controlling cell – biomaterial interactions: Instant modification of 'stealth' surfaces with RGD-peptides”
(Poster)
- 9.10. – 12.10.2002 DPhG Jahrestagung in Berlin, Germany: *Lieb E., Milz S., Hacker M., Dauner M., Göpferich A., Schulz M.B.*:
”3-D cell culture for the evaluation of growth factor effects on bone formation with TGF- β 1 as model protein”
- 8.12. – 10.12.2002 5th Annual Meeting of the Tissue Engineering Society in Kobe, Japan: *M. Hacker, M. Neubauer, H.-J. Untch, J. Tessmar, E. Lieb, T. Blunk, A. Goepferich, M. B. Schulz*:
“Solid lipid templating: Macroporous scaffold fabrication from biodegradable polymers” **(Talk)**
- 8.12. – 10.12.2002 5th Annual Meeting of the Tissue Engineering Society in Kobe, Japan: *Lieb E., Milz S. Hacker M., Dauner M., Göpferich A., Schulz M.B.*:
”In Vitro Effects of TGF- β 1 on Rat Marrow Stromal Cells for Bone Tissue Engineering”
- 27.3. – 29.3.2003 Joint Annual Meeting of the German and Swiss Connective Tissue Society in Ulm, Germany:
Lieb E., Hacker M., Tessmar J., Fiedler J., Hersel U., Dahmen C., Kessler H., Göpferich A., Schulz M.B. :
“Towards controlled cell adhesion to biodegradable polymers”
- 7.10. – 11.10.2003 DPhG Jahrestagung in Würzburg, Germany:
Hacker M., Vogel T., Neubauer M., Drotleff S., Teßmar J., Blunk T., Göpferich A., Schulz M.B.: “Solid lipid templating: Anhydrous scaffold fabrication for tissue engineering” **(Talk)**

- 4.3. – 10.3.2004 Keystone Symposia in Banff, Canada:
Neubauer M., Fischbach C., Bauer-Kreisel P., Lieb E., Hacker M., Schulz MB., Goepferich A., Blunk T.:
"Adipogenesis of Mesenchymal Stem Cells in Three-Dimensional Cell Culture"
- 17.5. – 21.5.2004 7th World Biomaterials Congress in Sydney, Australia:
M. Hacker, E. Lieb, J. Tessmar, J. Fiedler, C. Dahmen, U. Hersel, H. Kessler, M.B. Schulz, A. Göpferich:
"Mediating Specific Cell Adhesion to Low-adhesive Diblock Copolymers by Instant Modification with RGD-peptides"
(Poster)
- 17.6. – 19.6.2004 International Conference "Strategies in Tissue Engineering" in Würzburg, Germany:
Neubauer M., Hacker M., Bauer-Kreisel P., Fischbach C., Schulz M.B., Goepferich A., Blunk T.:
"Adipogenesis of Mesenchymal Stem Cells in Three-dimensional Cell Culture"
- 17.6. – 19.6.2004 International Conference "Strategies in Tissue Engineering" in Würzburg, Germany:
Pongratz M., Hacker M., Wolinski H., Kohlwein S.D., Göpferich A., Schulz M.B.:
"In-vitro Evaluation of the Angiogenic Potential of Gel Matrices with the Rat Aortic Ring Model"
- 17.6. – 19.6.2004 International Conference "Strategies in Tissue Engineering" in Würzburg, Germany, 2004:
Vogel T., Lieb E., Volk B., Hacker M., Göpferich A., Schulz M.B.:
"Dose-dependent Effects of TGF- β 1 Supplementation on Bone Formation in 3-D Culture of Rat Marrow Stromal Cells"

AWARDS

- 4.12.1992 FAG Kugelfischer Foundation (Germany)
- 4.2.2001 CRS German Chapter Annual Meeting, Saarbrücken (Germany): Poster Award
- 21.5.2004 SFB Biomaterials World Congress, Sydney (Australia): Poster Award

7. Acknowledgements

An dieser Stelle möchte ich all jenen meinen herzlichen Dank aussprechen, die zum Gelingen dieser Arbeit und zu der unvergesslichen Zeit am Lehrstuhl beigetragen haben.

Herrn Prof. Dr. Achim Göpferich danke ich sehr herzlich für die Überlassung des Themas, seine kontinuierliche Unterstützung bei dessen Bearbeitung und die Möglichkeit zur freien Entfaltung der wissenschaftlichen Arbeiten. Die zahlreichen Diskussionen und Anregungen waren immer sehr hilfreich für mich. Auch für die vielfältigen Möglichkeiten, die durchgeführten Arbeiten auf nationalen und internationalen Kongressen zu präsentieren, bin ich außerordentlich dankbar.

Frau Dr. Michaela Schulz danke ich für die engagierte Betreuung der Arbeit, ihr stetes Interesse am Fortgang der Experimente und für ihre Unterstützung, insbesondere bei der Niederschrift der Arbeit. Dank ihres Engagements hatte ich die Möglichkeit neue Meßmethoden bei Kooperationspartnern kennen zu lernen und anzuwenden.

Herrn Dr. Torsten Blunk danke ich für unzählige konstruktive Ratschläge, wissenschaftliche Diskussionen und die freundschaftliche Zusammenarbeit.

Für die finanzielle Förderung der durchgeführten Projekte gilt mein Dank Aventis Research & Technologies sowie dem Bundesministerium für Bildung & Forschung (BMBF).

Allen derzeitigen und ehemaligen Kolleginnen und Kollegen danke ich für das gute, oft freundschaftliche Arbeitsklima, die konstruktive Zusammenarbeit und kritische Diskussionen.

Mein herzlicher Dank gilt insbesondere:

- Prof. Dr. Horst Kessler, Claudia Dahmen und Ulrich Hersel (Organische Chemie und Biochemie, TU München) für die Synthese der RGD Peptide und die fachlichen Ratschläge.
- Dr. Michael Ringhofer und seinem Team bei der Anton Paar GmbH für die Bereitstellung eines Rheometers und der Unterstützung bei den Messungen.
- Dr. Michael Ahlers (DGF Stoess AG Ebersberg) für die Bereitstellung der Gelatine und den Informationen zu deren GFC-Analytik.
- Dr. Thomas Burgemeister für die Durchführung von NMR-Messungen.
- Angelika Kühn und Dr. Dieter Rose für die Unterstützung am Elektronenmikroskop.
- Prof. Tony Mikos, Prof. A. Göpferich und der Familie Teßmar für 2 außergewöhnliche Monate an der Rice University in Houston. Thank you Johnna, Theresa, Kathlene, Prof. John Jansen, Simon, Jeremy and Roy.

- Claudia Fischbach für die vielen hilfreichen fachlichen und privaten Gespräche und die gemeinsam verbrachte Zeit.
- Esther Lieb für die produktive Zusammenarbeit im RGD-Projekt.
- Sigrid Drotleff für die Synthese der MeO-PEG-PLAs und der aktiven Block-Copolymere.
- Angelika Maschke für ihr Know-how rund ums Insulin und viele Gespräche.
- Miriam Breunig für die Unterstützung am FACS.
- Allison Dennis für die schnelle und gewissenhafte Durchsicht zahlreicher Manuskripte einschließlich dieser Arbeit.
- Markus Neubauer für die unvergessliche, freundschaftliche Laborgemeinschaft, die vielen gemeinsamen Versuche und deren Diskussion, sowie die exzellente Zusammenarbeit im Aventis-Projekt. Danke auch für zahlreiche gemütliche und kurzweilige Abende.
- Jörg Teßmar für seine Freundschaft, die Synthese der MeO-PEG-PLAs und der aktiven Block-Copolymere, die hervorragende Zusammenarbeit im Aventis-Projekt und die Einarbeitung in die Geheimnisse von Hard- und Software am Lehrstuhl. Dani & Jörg: Vielen Dank für Alles!
- Florian Sommer, Christian Becker und Christoph Koelwel für fachliche Diskussionen und ´ne Menge Spaß bei und neben der Arbeit.
- Thomas Vogel, Hans-Jürgen Untch, Markus Pongratz, Marc Pignitter und Anton Spreitzer für die gute Zusammenarbeit im Vaskularisierungsprojekt.
- Thomas Vogel und Breda Volk für Kost & Logis in Graz.
- Bernhard Appel und Hatem Sarhan für die Unterstützung bei der Chondrozyten-Zellkultur.
- Bernhard Appel, Jörg Teßmar und Florian Sommer für die engagierte Zusammenarbeit im Bits&Bytes-Team.
- Allen „Doktoranden der ersten Generation“ für die freundliche Aufnahme und die gemeinsamen Unternehmungen.
- Andrea Blaimer für ihre vielfältige technische Unterstützung und die Durchführung der Viskositätsmessungen.
- Edith Schindler, Christine Niel, Albert Weingart und Stefan Kolb für die technische Unterstützung.
- Lydia Frommer und Liane Öttl für deren Hilfe bei allen Verwaltungsangelegenheiten.
- ... und der Schafkopf-Runde.

Vielen Dank, Andrea, für deinen Beistand und deine Geduld!

Abschließend gilt mein tiefer Dank allen Freunden und insbesondere meinen Eltern und Schwestern, die mir diesen Weg ermöglicht und mich auf ihm bestärkt und unterstützt haben.

VIELEN DANK!